



ARNO JANSSEN

TRANSCRANIAL MAGNETIC STIMULATION

Measuring and Modeling in Health and Disease

ARNO JANSSEN

TRANSCRANIAL MAGNETIC STIMULATION

Measuring and Modeling in Health and Disease

COLOFON

The research presented in this thesis was carried out at the Department of Neurology, Donders Institute for Brain Cognition and Behaviour, Radboud University Medical Center, Nijmegen, The Netherlands. The research was funded by the BrainGain Smartmix program of the Dutch government. Printing of this thesis was financially supported by the Radboud University Medical Center, Donders Institute for Brain, Cognition and Behaviour.

Cover & book design: Ilse Schrauwers – www.isontwerp.nl

Printing: Gildeprint Drukkerijen, Enschede, The Netherlands

ISBN: 978-94-92303-05-9

Copyright © Arno M. Janssen, 2016, Nijmegen, The Netherlands

All rights reserved. No part of this work may be reproduced or transmitted in any form or by any means without the permission of the author.

TRANSCRANIAL MAGNETIC STIMULATION

Measuring and Modeling in Health and Disease

Proefschrift

ter verkrijging van de graad van doctor
aan de Radboud Universiteit Nijmegen
op gezag van de rector magnificus,
volgens besluit van het college van decanen
in het openbaar te verdedigen op donderdag 2 juni 2016
om 12.30 uur precies

door

Arno Marin Janssen
geboren op 27 juli 1985
te Eindhoven

Promotoren

Prof. dr. ir. D.F. Stegeman (Vrije Universiteit Amsterdam)

Prof. dr. B.R. Bloem

Copromotor

Dr. T.F. Oostendorp

Manuscriptcommissie

Prof. dr. W.P. Medendorp

Prof. dr. O. Dössel (Karlsruher Institut für Technologie, Duitsland)

Prof. dr. L. Timmermann (Uniklinik Köln, Duitsland)

CONTENTS

List of abbreviations	7
-----------------------	---

PART I

1. Outline Thesis	13
2. Introduction to Transcranial Magnetic Stimulation	17

PART II

3. Parkinson's disease, Freezing of Gait and TMS	29
4. Cerebellar theta burst stimulation improves gait speed in Parkinson's disease patients with freezing of gait	37
5. Short rapid steps to provoke freezing of gait in Parkinson's disease	53

PART III

6. Modeling Transcranial Magnetic Stimulation	65
7. The influence of sulcus width on simulated electric fields induced by transcranial magnetic stimulation	73
8. The effect of local anatomy on the electric field induced by TMS: evaluation at fourteen different target sites	95
9. The coil orientation dependency of the electric field induced by TMS for M1 and other brain areas	115
10. Appendices	135

PART IV

11. Summary and General Discussion	155
12. Nederlandse Samenvatting	167

PART V

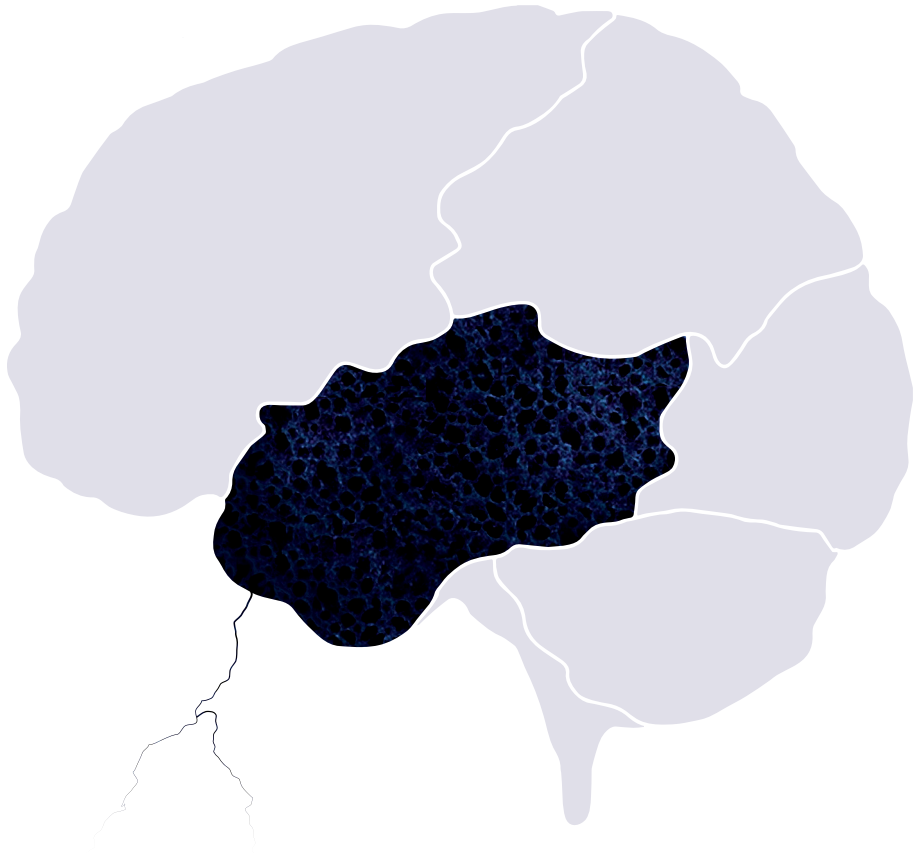
181

13.	Dankwoord	183
14.	Biography	187
15.	Publications	189
16.	Dissertations of the disorders of movement research group, Nijmegen	193
17.	Bibliography	197

LIST OF ABBREVIATIONS

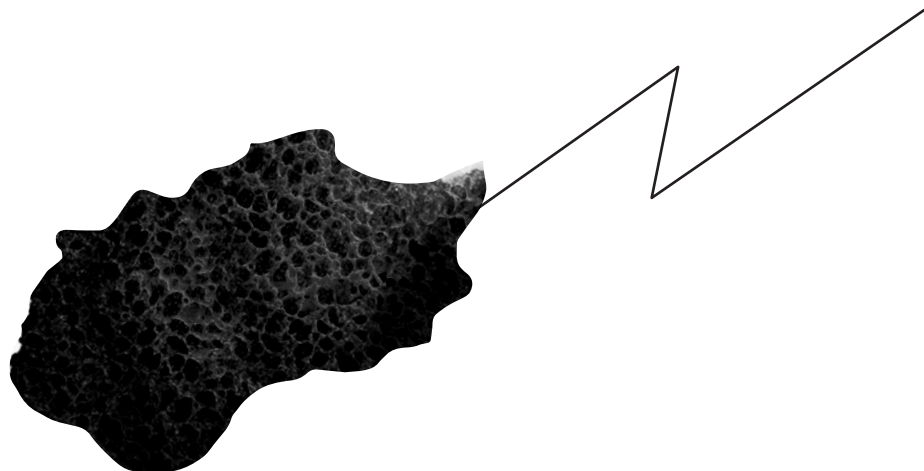
AMT	active motor threshold
APA	anticipatory postural adjustment
BEM	boundary element method
BG	basal ganglia
CBI	cerebellar brain inhibition
CMCT	central motor conduction time
CSF	cerebrospinal fluid
CSP	cortical silent period
cTBS	continuous theta burst stimulation
DBS	deep brain stimulation
DLPFC	dorsolateral prefrontal cortex
DN	dentate nuclei
DTI	diffusion tensor imaging
D-waves	direct waves
DW	diffusion weighted
EC	eddy current
EEG	electroencephalography
EMG	electromyography
FAB	frontal assessment battery
FDA	Food and Drug Administration
FDI	first dorsal interosseous
FDM	finite difference method
FEM	finite element method
FOG	freezing of gait
FOUL	freezing of the upper limbs
fMRI	functional magnetic resonance imaging
GM	gray matter
GPe	globus pallidus pars externa
GPi	globus pallidus pars interna
ICF	intracortical facilitation
IFG	inferior frontal gyrus
IIM	independent impedance method
ISI	inter stimulus interval
iTBS	intermittent theta burst stimulation
I-waves	indirect waves
LID	levodopa induced dyskinesia
LTD	long-term depression

LTP	long-term potentiation
M1	primary motor cortex
MAG	magnification
MDS-UPDRS	Movement Disorders Society-Unified Parkinsons' disease rating scale
MEG	magnetoencephalography
MEP	motor evoked potential
MLR	mesencephalic locomotor region
MMSE	mini mental state examination
MRI	magnetic resonance imaging
MSO	maximum stimulator output
MT	motor threshold
NANS	normal amplitude + normal speed
NAFS	normal amplitude + fast speed
N-FOGQ	new freezing of gait questionnaire
OC	occipital cortex
PD	Parkinson's disease
PDE	partial differential equation
PET	positron emission tomography
pmRF	pontomedullary reticular formation
PPN	pedunculopontine nucleus
PSP	progressive supranuclear palsy
RDM	relative difference measure
RMT	resting motor threshold
rTMS	repetitive transcranial magnetic stimulation
SANS	small amplitude + normal speed
SAFS	small amplitude + fast speed
SEM	standard error of mean
SICI	short intracortical inhibition
SMA	supplementary motor area
SN	substantia nigra
TBS	theta burst stimulation
TCS	transcranial current stimulation
tDCS	transcranial direct current stimulation
TES	transcranial electric stimulation
TMS	transcranial magnetic stimulation
VCM	volume conduction model
WM	white matter



PART I

**OUTLINE
&
GENERAL INTRODUCTION TO
TRANSCRANIAL MAGNETIC STIMULATION**



1.

OUTLINE THESIS



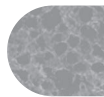
Transcranial magnetic stimulation (TMS) is a technique that enables neuroscientists, neurologists and clinicians in rehabilitation medicine to temporarily influence brain activity in healthy subjects and patients, without major discomfort. By using a rapidly changing magnetic field, an electric field is induced in the human brain, without the need for sending an electric current through the poorly conducting skull^{71,163,215}.

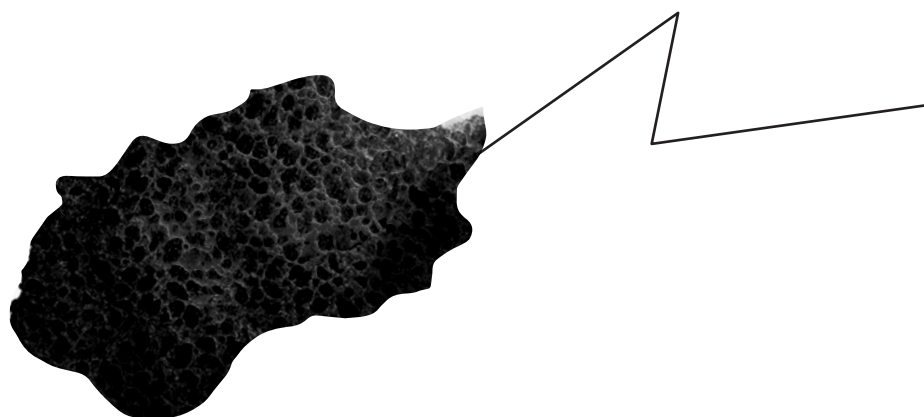
This PhD thesis, consisting of five parts, focuses on the use of TMS over the cerebellum, motor cortex and other brain areas. **Part 1** provides a brief background on TMS. The second and third parts concern research results. **Part 2** is on the application of TMS to study the phenomenon of freezing of gait in Parkinson's disease. **Part 3** is on modeling of volume conduction in the brain. **Part 4** gives a summary of the research chapters (part 2 and part 3) and a general discussion on the main findings and future perspectives. **Part 5** includes, amongst others, the bibliography and a curriculum vitae of the author. A more detailed introduction to the parts 2 and 3 is given next.

In part 2, the **chapters 4** and **5** are dedicated to the investigation of the parkinsonian symptom called 'freezing'. Freezing during gait is a highly disabling symptom, characterized by brief periods of inability of effective forward stepping^{64,138,186}. The freezing of gait phenomenon is episodic in nature and does not always occur when patients are placed in a clinical research setting. In **chapter 4** the brain mechanism behind the occurrence of freezing is addressed. A series of scientific reports have suggested that the cerebellum could be involved in the pathophysiology of Parkinson's disease in general, and possibly also in the freezing phenomenon. As TMS is able to temporarily modulate brain activity, we use this technique to alter cerebellar activity and to observe the effects in a series of gait and hand tasks. Several gait tasks are used in **chapter 4**, including rapid turning and walking with small steps. To improve future research protocols to observe freezing of gait after non-invasive brain stimulation, **chapter 5** is devoted to the question how to optimally evoke freezing during gait in a research set-up. The battery of gait tasks that was used in **chapter 4** is evaluated.

The third part of this thesis concerns the improvement of TMS protocols, such as the one used in **chapter 4**, by introducing knowledge from computational modeling. Although TMS is a widely used tool for research, therapies and diagnostics, the underlying neural mechanisms are still far from being completely understood. Most protocols, techniques and conventions are based on daily practice, trial-and-error studies and other user's experience. To improve stimulation protocols and to optimize the effects of stimulation, better understanding of the mechanisms of TMS is highly desirable. Part of such understanding concerns the estimation of the TMS-induced electric field in targeted brain structures. **Chapters 7, 8** and **9** discuss the estimation of the TMS-induced electric fields by means of volume conduction modeling. **Chapter 10** contains a series of appendices supporting these chapters.

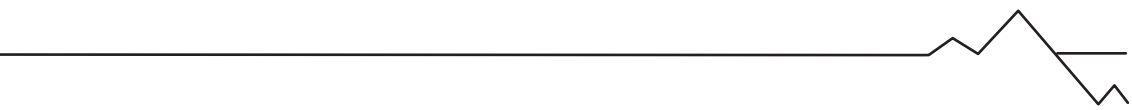
Chapter 7 is devoted to the construction of a highly realistic head model, which is an essential aspect of TMS simulations. Specifically the importance of detail in the cortical surface geometry is investigated in this chapter. The same realistic head model is used in **chapters 8** and **9** in simulations of TMS of cortical targets other than the motor cortex. It is well known that differences exist in the anatomy of different cortical regions targeted by TMS protocols. The protocols and hardware settings used for these non-motor regions are still mainly based on the conventions determined for the motor cortex. This is due to the fact that most non-motor regions lack observable outcome effects like the electromyography response elicited by motor cortex stimulation. By means of modeling one can calculate the induced electric fields for all these brain regions and compare them. In **chapter 8** this approach is used to evaluate the effect of coil-target distance and target site anatomy on the magnitude of the electric field. **Chapter 9** is dedicated to the effect of coil orientation over several different cortical regions





2.

INTRODUCTION TO TRANSCRANIAL MAGNETIC STIMULATION



2.1 HISTORY OF NON-INVASIVE MAGNETIC BRAIN STIMULATION

When one asks neuroscience researchers or a clinicians about the origin of transcranial magnetic stimulation (TMS), they will often refer to the famous short paper of Antony Barker and colleagues published in the Lancet in 1985⁸. This article was the first to present the technique of TMS to the neuroscience and neurology community. However, this moment was by far not the first time scientists and clinicians used non-invasive stimulation on the human brain. For that we have to go back at least to the time of the Greeks and Romans, where the first electric stimulation techniques were employed. The Roman physician Scribonius Largus (47 AD) described in his *Compositiones* the employment of electrical torpedo fish to treat headaches⁸³.

Although the use of electric fish remained a medical treatment of headaches throughout the centuries, a big leap towards the 18th and 19th century has to be made to find the next important developments in the scientific field of non-invasive stimulation. During these centuries, famous physicians and physicists like Luigi Galvani¹⁵⁰, Alessandro Volta^{151,200} and Giovanni Aldini¹⁴⁵ did experiments with externally applied electrical stimulation on animal and human bodies, laying the foundation of modern electrophysiology. Galvani and Volta were the first to show that the legs of dead frogs twitch when an electric current is applied externally to the nerves and muscles of the animals. Thereafter, physics professor Giovanni Aldini, who was Galvani's nephew, continued the work of electro-stimulation experiments on limbs of deceased criminals (figure 2.1). After successfully reproducing the results in animals, Aldini started to treat patients with mental disorders with electric stimulation¹⁴⁵. The discoveries of these pioneers opened a whole new field of research with electric stimulation. It should be noted that around the same time period of these experiments,

Mary Shelley's *Frankenstein; or, The Modern Prometheus* was written. In her introduction, where she tells about her inspiration to write the classic novel, Mary Shelley talks about *'Perhaps a corpse would be re-animated; galvanism had given token of such things: perhaps the component parts of a creature might be manufactured, brought together, and endued with vital warmth.'*¹⁸¹

Around the same period in which Aldini performed his experiments, the famous British scientist Michael Faraday demonstrated another crucial phenomenon for the future development of TMS. In 1831 he discovered the scientific principle of electromagnetic induction⁴⁵. In one of the most famous experiments, he wound two coils of wire on opposite sides of an iron ring (figure 2.2). When a current was switched on in one coil, it induced a brief current flow in the other (secondary) coil. This also happened when he off-switched the current. This experiment was his first inspiration to formulate the statement that a changing magnetic field produces an electric field and vice versa, which would establish the basis for electromagnetism and the important development of transformers in electric power engineering.

The findings of Faraday inspired physicians and physicists around the end of the 19th century, like Jacques Arsene d'Arsonval³² and Sylvanus Thompson¹⁹⁷, to start experiments with electromagnetic induction on the human body. These researchers discovered that people observed light flashes and experienced vertigo when their head was placed inside a large coil with rapidly alternating currents, which produced time-varying magnetic fields. It should be noted that this was in fact not due to cortical stimulation, but the result of direct stimulation of the retina and the vestibular system. For direct cortical stimulation stronger and more rapidly changing currents appeared to be needed.

In the 1970's hardware was developed that could produce the required strong and rapidly changing currents to obtain the time-varying magnetic fields that are required, but brain stimulation was not the first application. The hardware was first used for magnetic stimulation of the peripheral nervous system¹⁵⁶. It was only after the introduction of transcranial electric stimulation (TES)¹¹¹ that researchers began to think about transcranial magnetic stimulation (TMS). By combining the availability of peripheral magnetic stimulation and the concept of TES, the first electromyographic (EMG) response in the hand muscle after TMS over the primary motor cortex was reported in the already mentioned paper by Barker and colleagues in 1985⁸. An advantage of TMS over TES was the characteristic to bypass the skin and the highly resistive skull and thereby causing substantially less discomfort. Especially this minimum discomfort is of crucial importance in the preference of TMS over TES in brain stimulation.



The introduction of TMS by Barker and colleagues showed that it is possible to non-invasively stimulate cortical neurons without causing severe discomfort. Since the technique was non-invasive and fairly easy to apply, it swiftly became popular in the field of clinical neurophysiology and somewhat later in neuroscience. New hardware and stimulation protocols were developed. Major improvements were the introduction of a figure-of-eight coil, which made stimulation more focal, and the introduction of multi pulse protocols that enables the modulation of brain activity for a longer period. These improvements fueled successive developments, such as targeting non-motor brain areas and the treatment of neurological disorders. Nowadays, TMS is a widely used tool in the field of neuroscience, neurology and rehabilitation medicine.

2.2 PRINCIPLES OF TRANSCRANIAL MAGNETIC STIMULATION

Although the term *magnetic stimulation* suggests that the magnetic field is responsible for evoking a response in the brain, the magnetic field is merely a transporter of energy from the stimulation coil, through the scalp and skull, into the brain. The actual stimulation of neurons is electric in nature. A very brief and high-current pulse is sent through a coil, which consist of multiple windings of copper wire. The time-varying current will produce a time-varying magnetic field, which in strength is proportionally dependent on the strength of the current. In turn the time-varying magnetic field will produce an electric field in a nearby conductor, the human brain in the case of TMS. The induced electric field is directed roughly parallel and opposite to the current in the stimulation coil and may excite neurons. The physics and mathematics that specify these relationships can be found in **part 3** of this thesis.

Various coil designs exist, but the oldest and the most easy to use is the circular coil (figure 2.3A). The strongest induced electric field exists under the circumference of the coil and the field decreases in strength with increasing distance. For a circular coil, the electric field strength is zero at the axis through the center of the coil (figure 2.3C). A figure-of-eight coil (figure 2.3B), which consists of two round coils, produces the maximal electric field strength directly under the intersection of the two coils (figure 2.3D). This makes the figure-of-eight coil a tool for more focal stimulation and consequently a highly popular investigatory tool. The decrease in strength with distance also implies that only superficial brain areas can be stimulated with TMS. Deeper brain areas can be reached in theory, but everything between the coil and the target region is stimulated with even higher electric field strengths. More sophisticated coil-designs with complex windings, such as the H-coil²²⁵, are developed to permit a slower decay with distance of the field strength in

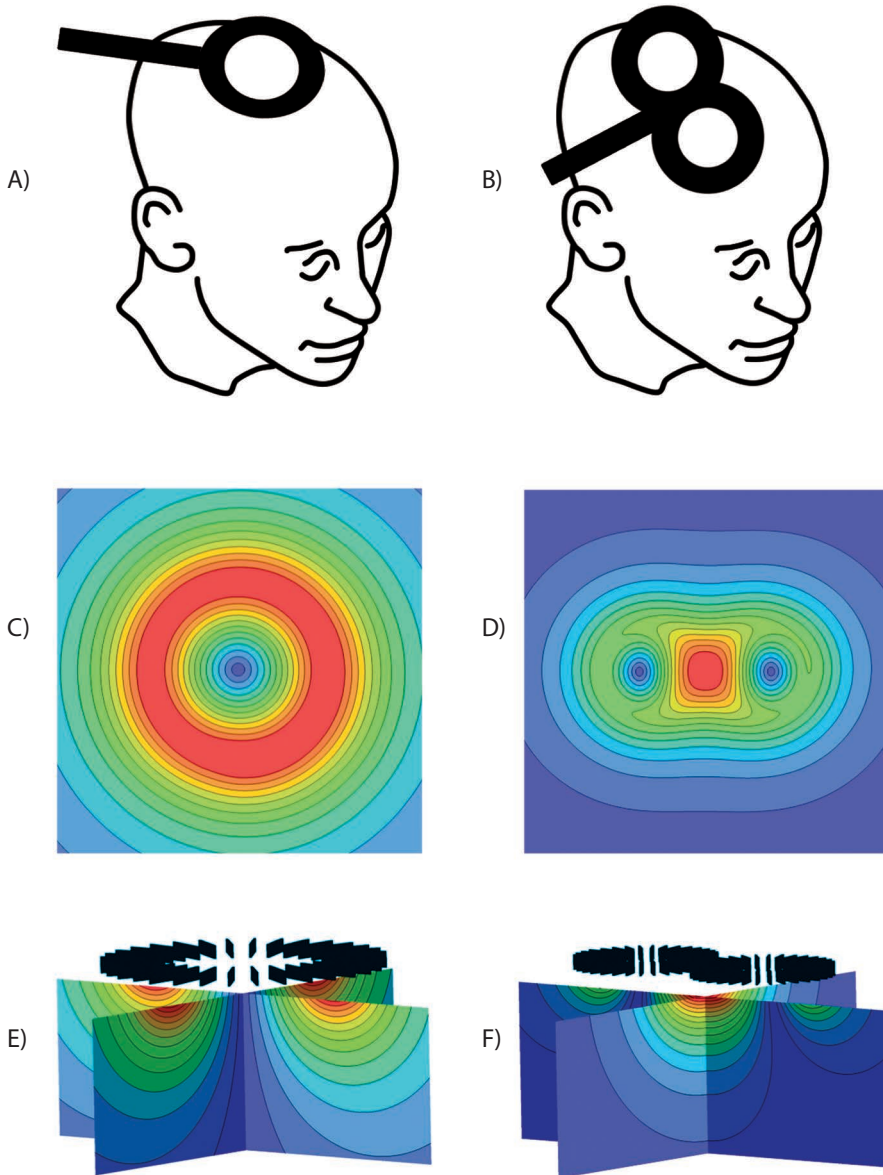


FIGURE 2.3. (A) A schematic drawing of a round coil, placed with the circumference over the right hemispheric motor cortex. The center of the coil is placed on top of the head. (B) A schematic drawing of a figure-of-eight coil, placed with the intersection of the two coils over the right hemispheric motor cortex. (C) The primary electric field strength in a parallel plane below a round coil and (D) below a figure-of-eight coil. (E) The primary electric field strength in a three-dimensional grid produced by a round coil and (F) by a figure-of-eight coil. In subfigures C-F the strongest electric field is represented in red and the weakest in blue. Illustrations in A and B are adapted from Munneke 2014¹²⁷.

order to reach deeper brain areas. First results are promising^{170,189}. However, these coils are still in a developmental stage and are not widely used in daily research or clinical applications.

When the circumference of a round TMS coil, or the intersection of the two round coils in the figure-of-eight coil, is placed above the primary motor cortex, the induced electric field is able to excite cortical motor neurons. The TMS pulse will evoke a corticospinal activation volley. Subsequently, an electrophysiological response in the accompanying contralateral muscle can be measured, which is called the motor evoked potential (MEP) (figure 2.4). The MEP is interpreted as a measure of cortical excitability of the motor cortex. The magnitude of the MEP response depends on the stimulation intensity and an MEP will only be evoked if at least certain minimal stimulation intensity is used, called the stimulation threshold. The resting motor threshold (RMT) is defined as the minimum intensity to elicit small MEP's (usually above 50 μ V) in a target muscle at rest in at least half of the trials¹⁶⁷. This threshold has to be determined individually, as it will differ between individuals due to anatomical and physiological differences. The active motor threshold (AMT) is defined as the minimum intensity to elicit small MEP's (usually above 50 μ V) in a voluntary contracted target muscle at least half of the trials. The difference is related to the fact that when a muscle is contracting, MEPs are larger and easier to evoke³⁶.

Not only the intensity, but also the orientation of the coil is important for the effectiveness of the stimulation. The direction of the electric field is (primarily) determined by the orientation of the coil. Several studies have shown the influence of coil orientation on the output of the motor cortex^{7,23,114}. In general, the largest MEPs are measured when the electric field in the brain is oriented perpendicular to the central sulcus of the individual subject and the current in the brain structure is flowing in a posterior-anterior direction.

Although the precise mechanism of neuronal stimulation with TMS is still under debate, the evidence from epidural spinal cord recordings suggest an indirect activation of the corticospinal neurons⁹⁹. The earliest MEP responses evoked by stimulus intensities just above the individual threshold are due to indirect waves (I-waves). These I-waves reflect indirect activation of the corticospinal pyramidal neurons in layer V of the cortex through stimulation of excitatory interneurons in more superficial cortical such as layers II and III⁹⁷. Corticospinal neurons in layer V can be stimulated directly, but only with relatively high stimulation intensities⁹⁹.

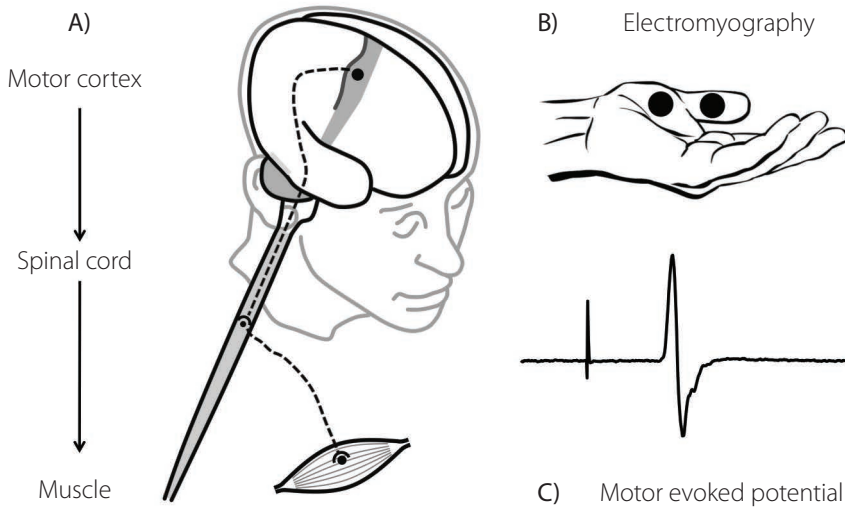


FIGURE 2.4. (A) Schematic and simplified representation of the corticospinal pathway. The primary cortex is a long strip located just in front of the central sulcus. The cortical neurons project to the spinal cord directly and give direct control of the α -motor neurons that activate the muscle. When the motor cortex is stimulated with an intensity above the motor threshold an evoked response (C) can be measured with (B) EMG over the contralateral muscle. The placement of the EMG electrodes indicated here is used for measurements of the first dorsal interosseous (FDI). This illustration is adapted from Munneke 2014¹²⁷.

2.3 REPETITIVE TRANSCRANIAL MAGNETIC STIMULATION AND OTHER MULTI-PULSE PROTOCOLS

The most common form of TMS is a single-pulse protocol, in which an alternating current is sent through the coil only during a short pulse (rise time 100 – 200 μ s, total duration ~ 500 μ s) resulting in a single instance of a rapidly changing magnetic field. This type of TMS is used in many applications. However, there are also multi-pulse protocols and an important category herein is the repetitive transcranial magnetic stimulation (rTMS) protocols.

Repetitive TMS protocols are not aimed at determining cortical excitability, but are applied to modulate brain activity for a period that outlasts the stimulation period. In rTMS protocols a train of multiple pulses is applied over the targeted cortex area. Depending on the repetition frequency of the train the cortical area will be inhibited or facilitated. In general, low frequencies, between 0.2 and 1 Hz, will inhibit the brain excitability³⁰, as determined by a subsequent single pulse TMS. Frequencies of 5 Hz and higher will boost brain excitability¹⁴⁸. One specific kind of rTMS, called theta burst stimulation (TBS), combines a short

stimulation period (40-190 seconds) with consistent, long lasting (up to 1 hour), inhibitory (continuous TBS) or facilitatory (intermittent TBS) effects on cortical excitability⁷⁵.

The ability to alter brain activity of a targeted brain region for a time span that outlasts the stimulation period, suggest that rTMS is able to evoke a form of brain plasticity. For inhibitory protocols, long-term depression (LTD) will be induced, and for facilitatory protocols long-term potentiation (LTP). This ability of rTMS makes it an extremely interesting research and therapeutic tool. Especially the TBS protocols that have a short stimulation period are considered suitable for patient studies and potential candidates for therapy.

In addition to the single-pulse and repetitive TMS protocols, other multi-pulse protocols have been developed. An example is the so-called paired-pulse protocol, which consists of two pulses that are separated by an inter-stimulus-interval (ISI) and are used to study intracortical connections. The influence of interneurons in the cortex is estimated by determining the effect of a conditioning pulse on a second pulse, called the test pulse. Similar to the frequency effects in rTMS protocols, depending on the ISI and the pulse strengths of both pulses, different neuronal mechanisms can be evoked. An ISI less than 5 ms will cause inhibition and at intervals between 8 and 30 ms facilitation will occur. With a sub-threshold conditioning pulse and a supra-threshold test pulse after a short ISI, short intracortical inhibition (SICI) and intracortical facilitation (ICF) can be elicited^{92,226}.

2.4 APPLICATIONS

Transcranial magnetic stimulation has evolved from a simple single-pulse stimulation technique for the motor cortex to a technique that is applied over all areas of the cerebral cortex and cerebellar cortex. Stimulation targets include, but are certainly not limited to, dorsolateral prefrontal cortex (DLPFC)^{13,59}, occipital cortex¹²⁴, supplementary motor area (SMA)^{3,72,80}, inferior frontal gyrus (IFG)¹⁵⁵ and cerebellum^{88,95,203}. The technique is applied in all kinds of neuroscience research and clinical studies.

In healthy subjects, most studies are aimed at fundamental research questions and no long-lasting effects are expected in these kinds of studies, although performance enhancement with brain stimulation is a topic of scientific debate⁷³. A general subdivision into online and offline protocols can be made for TMS approaches. In the online protocols, the stimulation is given during a task or is used as quantification tool to measure local brain or network properties. This requires stimulation intensities strong enough to produce a direct output. In such applications mostly single pulse or paired pulse protocols, rather than rTMS, are used. The offline protocols are basically the rTMS protocols. In

these offline protocols the effects of the stimulation are measured (shortly) after the stimulation.

TMS is also used as a tool in fundamental research questions in patient populations. Almost every neurological disorder is, or has been, a topic of brain stimulation research. These neurological disorders range from stroke³⁴, amyotrophic lateral sclerosis¹²⁶, multiple sclerosis¹⁷⁹, epilepsy⁵, tinnitus⁵², depression⁵⁹ to Parkinson's disease^{13,72,88}. The same online and offline approaches are used in patient populations and in healthy subjects. In many studies healthy subjects are used as a control group where the effects of stimulation are compared between groups.

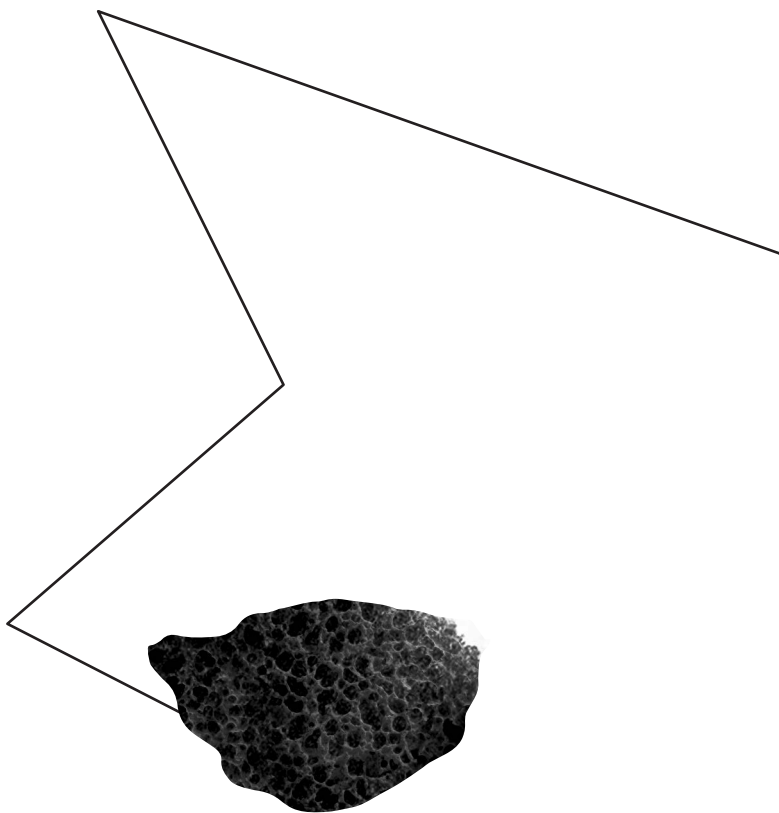
In addition to fundamental research, TMS is also widely used as a diagnostic tool in clinical settings⁸⁷. For example, the technique can be used to measure central motor conduction time (CMCT). This is the time interval between stimulation of the primary motor cortex and the arrival of the corresponding MEP in the contralateral muscle. A delay in CMCT can be an indication for demyelinating injuries in the corticospinal tract⁸⁷. Also MEP amplitude can be used in diagnostic procedures. After a stroke, the absence of a TMS-evoked MEP predicts a poor prospect for recovery⁴⁰.

The last class of applications in patients is therapy. As mentioned previously in section 2.3, the repetitive protocols can be used to temporarily inhibit or facilitate a certain brain area. In therapy the goal is to prolong the effects of rTMS, or even make it permanent. In neurological diseases this (relatively) long-term effect can be used to restore activity in hypo- or hyperactive of brain areas to a normal level, or it can be used to boost compensational activity. Several attempts have been made to apply TMS as a therapeutic tool, but until now only single-pulse stimulations for migraine headaches (FDA approval K130556) and rTSM for depression have received approval from the Food and Drug Administration (FDA) office (FDA approval K061053).



PART II

**PARKINSON'S DISEASE, FREEZING OF GAIT
&
CEREBELLAR THETA BURST STIMULATION**



3.

PARKINSON'S DISEASE, FREEZING OF GAIT AND TMS

3.1 GENERAL INTRODUCTION TO PARKINSON'S DISEASE

Parkinson's disease (PD) is the second most common neurodegenerative disorder of the central nervous system, affecting about 1 percent of people over 60 years of age in industrialized countries⁹⁶. The disease is named after the British medical practitioner James Parkinson, who was the first to publish a clinical description of the disorder in his 'An Essay of the Shaking Palsy' in 1817¹⁴⁶. The disorder he described included motor symptoms that we still associate with PD, such as rest tremor, festination (involuntary quickening of gait), bradykinesia (slowing down of movements) and rigidity. Nowadays, the clinical description of the disease includes several other motor symptoms, like postural instability²⁰, freezing of gait¹³⁸, and non-motor dysfunctions, such as olfactory problems¹¹², sleep problems¹⁴¹ and cognitive decline⁷⁴. The disease is asymmetrical in nature, as motor symptoms typically start on one side of the body; although the contralateral side becomes inevitably affected as well, this initially involved side remains the most prominently affected during the entire course of the disease³⁷. Of all neurological diseases, PD is associated with the highest risk of falling¹⁹¹, with of course an enormous impact on the quality of life.

The symptoms and signs of the disease are, to large extent, caused by a loss of dopaminergic neurons in the substantia nigra (SN), which is one of the major substructures of the basal ganglia (BG), anatomically located in the mesencephalic locomotor region (MLR) of the brain. The BG include the striatum (caudate nucleus and putamen), the globus pallidus (pars interna (GPi) and pars externa (GPe)), the subthalamic nucleus, the nucleus accumbens and the SN. The SN consists of the pars compacta and the pars reticula. The pars compacta serves as an input drive of the BG complex by providing the striatum, especially the putamen, with dopamine. Specifically the loss of neurons in the pars compacta causes a dopaminergic deficiency in the striatum and thereby functional problems for the

remainder of the BG and their connected circuitries. As the BG are involved in multiple processes (figure 3.1), such as movement control, working memory and emotion, the loss of dopaminergic neurons in the SN affects both motor and non-motor circuits¹⁶⁴. The neurological problems in the BG manifest themselves in the symptoms classified as parkinsonian.

The cause underlying the degeneration of dopaminergic neurons in the SN remains unknown, and no cure or protective medication is currently available to slow down (let alone arrest) the disease progression¹⁸⁵. Nevertheless, several symptomatic treatments are available to reduce or cope with the symptoms, such as dopaminergic medication^{18,31}, deep brain stimulation (DBS)^{49,216,217} or physiotherapy^{67,85} and other allied health interventions. The most commonly used symptomatic treatment is L-DOPA medication^{18,31}. L-DOPA is a precursor of dopamine that can pass the blood-brain barrier, in contrary to dopamine itself. After the drug passes this barrier, it is converted into dopamine by the enzyme dopa-decarboxylase. Through this mechanism the lost dopamine can be replenished. Unfortunately, long-term intake of L-DOPA will lead to the development of involuntary movements (dyskinesia)⁴¹ and fluctuations in motor function⁸¹, due to a narrowing of the effective medication dosage window with disease progression. When motor fluctuations occur, the patients' state can change between few PD symptoms during the effective dosage window ('on' state) and significant PD symptoms during a shortage of dopamine ('off' state).

3.2 FREEZING OF GAIT

Gait impairments are often present in PD and are characterized by slowness of walking, irregular step timing and shortened step length. Within the class of gait impairments, a distinction can be made between continuous gait impairments that consistently affect the gait pattern, and episodic phenomena that are transient and unpredictable⁶². One of the most remarkable episodic phenomena is freezing of gait (FOG). A patient who experiences FOG has the subjective feeling of the feet 'being glued to the floor'. Three different manifestations of FOG can be distinguished: (1) trembling in place (this is the most common phenotype), (2) shuffling forward and (3) complete akinesia¹³⁸. Commonly episodes last only a few seconds, or even shorter than one second, but sometimes they are longer than thirty seconds¹⁷⁶. It is a phenomenon that negatively impacts mobility, affects the quality of life in PD patients¹¹⁸ and is highly associated with falling and resultant injuries¹⁹. Around fifty percent of patients with PD will suffer from FOG at a certain time point during the disease⁶⁵ and the probability increases with progression of the disease. Levodopa treatment is able to decrease FOG in PD patients that suffer from 'off' state FOG⁹.

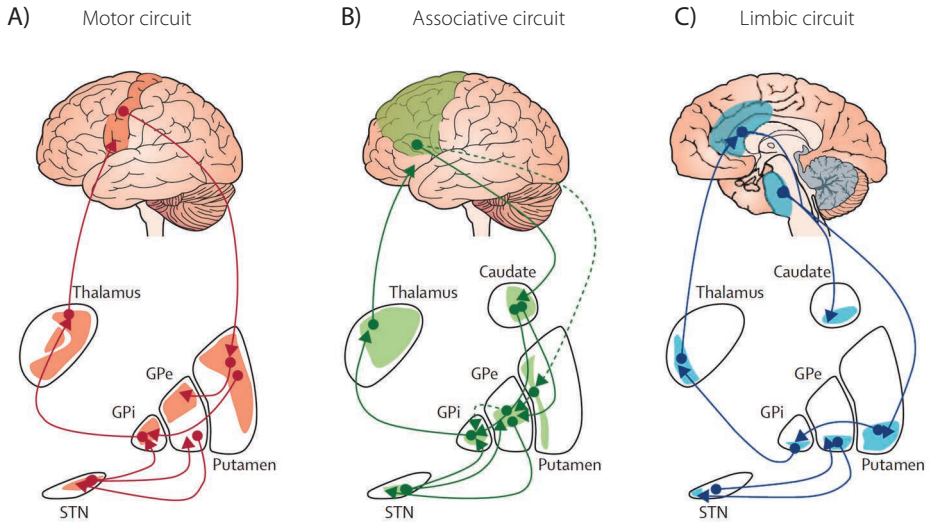


FIGURE 3.1. The functional organization of the basal ganglia. The basal ganglia are divided into motor (A), associative (B), and limbic (C) subregions, which are topographically segregated, as highlighted by areas colored in red (motor cortex), green (prefrontal cortex), and blue (anterior cingulate cortex). Figure reprinted from Obeso and colleagues¹³⁹. GPe = globus pallidus pars externa, GPi = globus pallidus pars interna, STN = subthalamic nucleus.

The formal definition of FOG is a 'brief, episodic absence or marked reduction of forward progression of the feet, despite the intention to walk'¹³⁸. Due to its episodic character, it is difficult to examine FOG in a clinical or scientific environment. Nevertheless, it is known that several factors affect the amount of freezing. Compared to normal straight-line walking, patients typically freeze more during gait initiation¹⁷⁶, while turning^{176,186} and when a decreased step length is required²⁸. Overall, increasing the motor or cognitive load during walking will increase the likelihood of FOG appearance^{131,138}.

Although FOG only refers to a phenomenon in the lower extremities, specifically during walking, similar phenomena can be observed in the upper extremities and during speech¹²⁰. There are several examples of PD patients that are unable to execute a motor task with their upper extremities, such as the occurrence of 'manual motor blocks' during finger tapping²²⁷ and 'freezing of the upper limbs' during a repetitive finger flexion-extension task¹³³. The latter appeared correlated with patients' gait abnormalities. To describe all these episodic phenomena - during which the patient cannot execute a movement, irrespective of the type of movement and the effectors involved - Giladi et al. proposed the general term 'motor blocks' in 1992⁶³. However, the overlap between clinical and epidemiological characteristics of non-gait freezing motor problems and FOG is still a matter of debate²⁰⁵.

During the last few decades, the clinical picture for FOG has become much clearer, but the neuronal circuitries and pathophysiological mechanisms underlying FOG are still largely unexplained. It has been proposed that generally FOG is caused by a dysfunction of a complex neural circuitry that involves brain areas, such as the supplementary motor area (SMA)¹⁸⁷, the MLR in the brainstem^{138,187} and the cerebellar locomotor region^{47,48}. Following this idea FOG is once reported as the 'ultimate break in the frontal lobe – basal ganglia – cerebellar – brainstem network that controls gait'²⁴. Several theories about the pathogenesis of FOG have been suggested, which range from a problem with general pattern generators in the spinal cord to deficits in the perceptual processing¹³⁸, but no decisive answer has been found to determine which theory is most probable.

3.3 PARKINSON'S DISEASE AND TRANSCRANIAL MAGNETIC STIMULATION

Since its introduction, transcranial magnetic stimulation (TMS) has been used as a technique to study PD. Although PD is known to be a degenerative substantia nigra disease, the disease affects many cortical brain areas. This property makes the neurological disorder interesting for TMS research. As the motor system is most applicable to TMS research and PD has clear motor symptoms, several aspects of cortical excitability have been a topic of investigations, such as the motor evoked potential (MEP) amplitude or short intracortical inhibition (SICI). These investigations provided information about the cortical excitability within the motor cortex, caused by the problems with the dopaminergic neurons in the SN. For example, PD patients showed abnormally large MEP amplitudes compared to healthy subjects in rest, but reduced amplitudes were observed during voluntary contractions²⁰⁴. In addition, the normally observed increase in cortical excitability in preparation of a voluntary movement begins earlier and rises slower in PD patients¹⁴⁷. Furthermore, SICI is reduced¹⁰⁷, and the cortical silent period (CSP), a period of 100-200 ms of rest in the electromyography (EMG) after a pulse, is shortened in PD patients^{15,158}. These are only some of the findings of TMS studies at the level of the motor cortex. Multiple other studies have been performed with TMS over other brain areas. This shows that TMS can be a valuable tool to study neurological disorders, although they cannot reach the deeper brain areas such as the SN. It is interesting to know that most of the observed (pathological) changes in the excitability of the motor cortex in PD patients are in fact partly driven to a normal healthy state by brain stimulation or dopaminergic therapy¹⁰¹.

Transcranial magnetic stimulation is not only used as a diagnostic investigation tool, but is also considered as a possible new treatment strategy for neurological or psychiatric patients. As mentioned in sections 2.3 and 2.4, repetitive TMS has the ability to alter brain

activity of a targeted brain region for a time span that outlasts the stimulation period. This possibility has been used to study the neural mechanisms in PD²⁶, but might also be used to restore activity in hypo- or hyperactive of brain areas to a normal level. Moreover, it could be used to boost compensational activity in intact brain areas that take over functions of areas that are originally involved in maintaining particular functions. All cortical cerebral and cerebellar areas are potential targets for non-invasive brain stimulation techniques.

Currently, the standard treatment of PD is substitutive dopaminergic medication therapy. But as the disease progresses, this type of treatment starts losing its effectiveness, in particular because of the development of dose-limiting side effects. Specifically, after several years of treatment, dopaminergic treatment is associated with shorter effective periods with minimum discomfort of the disease symptoms. Several strategies are available to combat these so-called response fluctuations, including a drug dosage increase. This drug dosage increase, in turn, can lead to a worsening of drug-induced dyskinesia and other drug-induced symptoms. When the standard treatment finally fails to alleviate the parkinsonian symptoms (or when it produces too many negative side effects), a next therapeutic option is DBS. This is the implantation of an electric stimulator device that injects pulsed currents with a high frequency in a subcortical brain structure, such as the thalamus, GPe or GPi, pedunculopontine nucleus (PPN) or subthalamic nucleus. This type of treatment can be very effective in treating PD symptoms^{49,216,217}, but is an option for only a limited group of well-selected candidates. Moreover, this deep brain surgery carries risks of complications. So, other (and less invasive) therapies such as repetitive transcranial magnetic stimulation (rTMS) remain worth studying. Of course, the clinical studies on DBS treatment provide us with useful information on the neural circuitries underlying PD. This can guide decisions where and how to apply non-invasive brain stimulation.

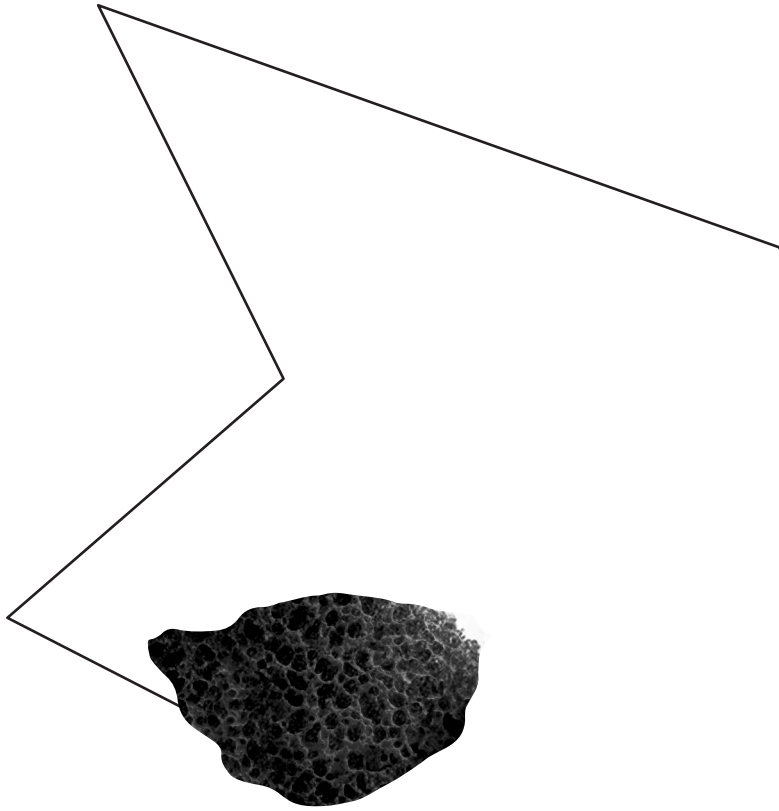
Already multiple rTMS studies have been performed with the aim to find a therapeutic value for PD patients. An advantage of rTMS is that, at least theoretically, specific symptoms can be treated as specific cortical areas can be targeted. Examples are the use of cerebellar theta burst stimulation (TBS) to treat levodopa induced dyskinesia (LID)⁸⁸, rTMS applied over the primary motor cortex (M1) and the dorsolateral prefrontal cortex (DLPFC) to improve mood in PD^{13,53}, or rTMS applied over M1 and DLPFC to treat bradykinesia¹⁰⁴. Most of these studies are still in a research phase, but some are promising (see Benninger & Hallett 2015¹⁴ for an overview). However, one should keep in mind that most symptoms are probably caused by a dysfunction in a network of brain areas, which means that for treatment of one specific symptom multiple stimulation sites are possible. Moreover, one specific brain area can be linked to multiple parkinsonian symptoms and therefore a single stimulation site probably affects more than one parkinsonian symptom.

3.4 THE FOLLOWING CHAPTERS IN THIS PART OF THE THESIS

In the following chapters of this part of the thesis the clinical PD symptom freezing of gait (FOG) will be the topic of research. As already mentioned in section 3.2, FOG is an episodic phenomenon that is difficult to study in an experimental setting, and the underlying brain mechanisms and responsible circuitries are still largely unknown. To develop a more effective treatment, this debilitating feature of PD has to be studied in much more detail. In **chapter 4**, we will focus on one specific brain mechanism that is possibly involved in the generation of FOG. Specifically, we studied the effect of repetitive TMS applied over the cerebellum, in the context of a presumed involvement of the cerebellum in the neurological mechanism of FOG. The cerebellum of PD patients that manifest FOG was temporarily inhibited or facilitated, and the effect on the amount of freezing was measured in consecutive motor tasks.

In **chapter 5**, the focus will be on the FOG task battery that was used in the protocol of **chapter 4**. Not all tasks in the FOG task battery are equally good in provoking FOG. To improve the protocol for future studies, gait tasks have to be selected that are best in evoking FOG. Previous research has already shown that 360-degree rapid turns on the spot¹⁸⁶ and small step gait tasks²⁸ are both effective in eliciting FOG. In **chapter 5**, these two tasks will be compared. Also the small step gait executed *as fast as possible* is added to the comparison.





Submitted as:

Janssen AM, Munneke MAM, Nonnekes J, Van der Kraan T, Nieuwboer A, Toni I, Snijders AH, Bloem BR, Stegeman DF.

Cerebellar theta burst stimulation improves gait speed in Parkinson's disease patients with freezing of gait.

Submitted

4.

CEREBELLAR THETA BURST STIMULATION IMPROVES GAIT SPEED IN PARKINSON'S DISEASE PATIENTS WITH FREEZING OF GAIT

ABSTRACT

In Parkinson's disease (PD), freezing of gait (FOG) most likely results from dysfunction within a complex neural gait circuitry involving multiple brain regions. Herein, cerebellar involvement has been proposed to be compensatory. We hypothesized that patients with FOG are less able to recruit the cerebellum to compensate for dysfunction in other brain areas. Cerebellar activity was modified unilaterally by either facilitatory or inhibitory theta burst stimulation (TBS), applied during two separate sessions. The stimulated side was the ipsilateral cerebellar hemisphere that corresponded to the body side most affected by PD. Seventeen patients with PD showing 'off' state FOG participated. The presence of gait freezing was objectively verified upon inclusion. Before and directly after TBS, gait and bimanual rhythmic upper limb movements were monitored. Gait was evaluated with a FOG-provoking protocol, including rapid 360-degree turns and a 10-meter walking test with small fast steps. Upper limb movement performance was evaluated with a repetitive finger flexion-extension task. Facilitatory TBS increased gait speed when walking with small steps, but did not affect the amount of freezing during walking or finger tapping. Inhibitory stimulation decreased gait speed while walking with normal step size, and had no effect on either hand- or gait freezing. The changes in gait speed were not accompanied by changes in corticospinal excitability of M1. We suspect that the increase in gait speed following facilitatory stimulation is due to an increase in cerebellar activity and a corresponding strengthening of cerebello-cortical connectivity, suggesting a compensatory role of the cerebellum in PD.

4.1 INTRODUCTION

Freezing of gait (FOG) is a most disabling feature in Parkinson's disease (PD), resulting in mobility problems and frequent falls^{19,84}. FOG is an episodic phenomenon, characterized by brief periods of inability to step effectively⁶⁴. It is usually experienced during step initiation or during turning in tight quarters^{138,176}. FOG is not present in all patients, but becomes more common in advanced PD⁶⁵. Although the clinical presentation and the factors that provoke FOG are becoming better defined, the mechanism behind its occurrence is still not clear.

We focus on the possible role of the cerebellum in PD, and specifically on its role in the pathophysiology underlying FOG. Although lesions in a single brain area can occasionally induce FOG¹⁰⁸, it has become clear that FOG generally does not result from a single lesion, but rather from widespread dysfunction within a neural gait circuitry involving the supplementary motor area (SMA)¹⁸⁷, the mesencephalic locomotor region (MLR)^{138,187} and the cerebellar locomotor region^{47,48}. Recent work has emphasized the tight interplay between the cerebellum and the basal ganglia^{172,221}. Cerebellar activity is increased in PD patients compared to healthy subjects^{2,222}. This hyper-activation in the cerebellum may be an adaptive mechanism that compensates for the defective basal ganglia^{2,144,161,221,224}.

We hypothesize that compared to patients without FOG, patients with FOG are less able to recruit the cerebellum to compensate for dysfunction of other brain circuitries, such as the brain areas mentioned above. This hypothesis is supported by the fact that FOG is common in patients with progressive supranuclear palsy (PSP)⁴², who also have lesions in brainstem areas that are connected with the cerebellum¹⁴⁹.

To investigate the possible compensatory role of the cerebellum in PD patients with FOG, we intended to up-regulate cerebellar activity with transcranial magnetic stimulation (TMS)^{8,87}, and to measure the resulting effect on freezing and movement performance in general using a specific set of tasks. The tasks included a FOG-provoking gait protocol, including rapid 360-degree turns¹⁸⁶ and a 10-meter walking test with small fast steps^{28,136}, as well as a repetitive finger flexion-extension task, which can evoke upper limb freezing (FOUL)^{133,207}. The severity of FOUL correlates with FOG scores, but not with disease severity, which supports the hypothesis that a generic motor control problem partially underlies freezing in both the upper and the lower extremities²⁰⁵.

Theta burst stimulation (TBS), a specific type of repetitive TMS (rTMS)⁸⁷, is a suitable stimulation protocol for patient studies. It combines a short stimulation period (40-190 seconds) with long lasting (up to 1 hour) effects on cortical excitability that are either inhibitory

or facilitatory⁷⁵. Following the rationale of previous studies^{26,88,90}, we used an facilitatory TBS form (intermittent TBS, iTBS) to stimulate the cerebellum, and hypothesized that this should both improve general gait and upper limb performance, including a reduction in freezing episodes. As a control condition, we stimulated the cerebellum with a protocol that aimed to achieve the opposite effect, i.e. inhibitory continuous TBS (cTBS). Part of the hypothesis is that when the increased cerebellar activity is indeed compensatory, this control condition should either worsen or (in case of ceiling effects) not affect freezing episodes in the upper and lower limbs.

4.2 METHODS

4.2.1 Subjects

Fifteen patients (12 men) were included in all analyses and two additional patients (1 man) only in gait, pegboard and corticospinal excitability analyses. Three additional patients were included in the study, but could not be included in any analyses. Two of them dropped out during the first session TBS, because of uncomfortable co-activation of neck muscles during TBS. The other patient experienced the protocol as stressful and did not participate in the second session.

Patients had moderate PD (Hoehn and Yahr stage 2-3) and objectively verified FOG. FOG was objectified by expert raters during routine clinical consultations, or when patients participated in previous clinical studies, using standardized and established FOG-provoking methods^{136,186}. Exclusion criteria were neurological disorders other than PD, presence of deep brain stimulation, a Mini Mental State Examination (MMSE)⁵⁰ score under 24, and exclusion criteria for TMS experiments¹⁶⁶. All subjects gave written informed consent prior to participation. The ethics committee of the Radboud University Medical Centre approved the study, which was performed in accordance with the Declaration of Helsinki.

4.2.2 Experimental design

Testing occurred while patients were in a practically defined 'off' state; i.e. after withholding all anti-parkinsonian medications for at least 12 hours. To create a homogeneous patient group, we included only patients with 'off' state FOG (i.e. when dopaminergic medication effects have worn off), as this is the most common type of FOG^{137,188}. Prior to testing, clinical data were collected including the new freezing of gait questionnaire (N-FOGQ)¹³², MMSE⁵⁰, frontal assessment battery (FAB)³⁸ and the Movement Disorder Society Unified Parkinson's disease rating scale (MDS-UPDRS) part 3⁶⁶. Subjects were stimulated with iTBS and cTBS over one cerebellar hemisphere, in separate sessions. The stimulated side was the ipsilateral cerebellar hemisphere that corresponded to the body side

most affected by PD, based on the MDS-UPDRS part 3 (i.e. the body side with the highest scores). During the first session, patients were stimulated with cTBS or iTBS; during the second session they received the opposite TBS protocol, always in a counterbalanced manner. Patients were kept blinded with respect to the nature of the stimulation and the nature of the expected effects. The sessions were at least one week apart to ensure a sufficient washout period for the preceding TBS. Before and after TBS, subjects had to perform a gait protocol and rhythmic upper limb task to measure the effect on movement performance and freezing duration. In addition to these primary outcome measures, cortical excitability was measured with motor evoked potentials (MEPs) and patients performed a pegboard dexterity task, to objectively quantify upper limb bradykinesia^{69,70}. The entire protocol, including all parts of one session, is shown schematically in figure 4.1.

4.2.3 Theta burst stimulation

TBS⁷⁵ was administered using a MagPro figure-of-eight coil (C-B60, MagVenture A/S, Farum, Denmark) connected to a MagPro X100 (MagVenture) stimulator. The ipsilateral cerebellum (1 cm below and 3 cm lateral toinion), corresponding to the most affected side, was stimulated. The coil was placed tangentially to the scalp with the handle pointing upwards. To ensure anatomically identical coil positioning during and over sessions, location and orientation of the coil target position were saved using a stereotactic image guidance system (Localite TMS Navigator, Localite GmbH, Sankt Augustin, Germany). Cerebellar TBS was administered with an intensity of 70% of resting motor threshold (see *Methods, Corticospinal excitability, subsection 4.2.7*). The stimulation period for cTBS was 40 seconds and for iTBS 192 seconds. Both protocols consisted of 600 TMS pulses.

4.2.4 Gait protocol

Occurrence of FOG was measured using a protocol that is known to elicit FOG. This protocol included eight 360-degree turns (as fast as possible, four times clockwise, four times counter-clockwise)¹⁸⁶ and a 10-meter gait trajectory (including gait initiation and gait termination while reaching a destination (stripes on the floor)), using different velocities (self-selected speed = normal; and as fast as possible) and different stride lengths (self-selected stride length = normal steps; and 20% of leg-length = small steps)^{28,136}. Visual guidance for the small steps was provided with stripes on the floor for three steps at the beginning and at the end of the gait trajectory.

The entire gait protocol was videotaped, allowing for offline assessment of FOG. Two independent, experienced and fully blinded raters scored the videos for the presence and duration of FOG. The definition used to score FOG was an obvious episode with ineffective stepping and the characteristic FOG phenotype. When raters disagreed, trials were sent back for consensus. FOG seen when turning after the 10-meter gait trajectory was

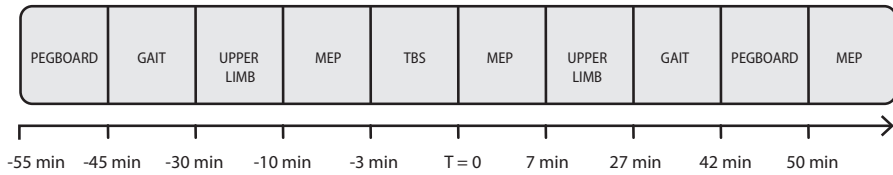


FIGURE 4.1 Protocol-design for a session. All post TBS measurements were performed in 30 to 60 minutes, depending on the patients' performance. The added timeline is a rough indication (in minutes, and the moment directly after the TBS set to 0). Not included are N-FOGQ, MMSE, FAB and MDS-UPDRS part 3, for which the scores were determined prior to this protocol in session one.

not included in the analysis. If it was not clear whether there was FOG or just 'walking with small steps', no FOG was rated.

The time to complete each task (execution time) was determined to measure general gait performance. A decrease in execution time may be due to increased gait speed as walking is easier and less likely to be driven to the threshold for FOG¹⁵⁴. Therefore, a decreased execution time was interpreted as increased gait speed and as improvement of performance.

4.2.5 Upper limb task

To elicit FOUL, the instruction was to make anti-phase rhythmic flexion and extension movements using both index fingers, as described previously^{133,206,207}. Two different amplitudes (45° [normal] or 30° [small]) and two different movement frequencies (normal [100%] or fast [133%]) were used. "Normal frequency" was defined as the patients' specific comfortable movement speed, determined for each subject individually at the beginning of the first session. The four different conditions were: normal amplitude + normal speed (NANS), normal amplitude + fast speed (NAFS), small amplitude + normal speed (SANS) and small amplitude + fast speed (SAFS). Earlier it was found that SAFS proved the most sensitive condition to elicit FOUL²⁰⁷. Each condition was repeated three times (both pre- and post- TBS). Auditory pacing guided the first six movement cycles to enable the pre-set movement frequency at the beginning of each trial. After auditory pacing stopped, the subjects had to maintain the rhythm for 25 seconds. Both hands were covered to prevent visual feedback. Angular finger displacement was registered with single axis goniometers (Type F35, Biometrics Ltd., Newport, United Kingdom), which were placed over metacarpophalangeal joint of the index fingers. A calibration measurement for the goniometers was performed before each *pre* and *post* measurement within a session. The data were calibrated off-line with the individual calibration files.

The data of the goniometers were processed and analyzed with MATLAB^a. For each condition the peak-to-peak amplitude and frequency values were calculated per movement cycle. In order to define each movement cycle, the turning points in movement direction (positive to negative, and vice versa) in the signal were detected. A peak had to meet three criteria: (1) the time derivative changes sign; (2) the difference in absolute value between two consecutive peaks had to be at least one degree and (3) for positive peaks, the value had to be higher than the preceding and following peak. For negative peaks, the value had to be lower than the preceding and following peak. A single cycle was defined as the period between a maximum peak value and the subsequent maximum peak value.

For each *pre* and *post* measurement, the mean duration of freezing during a complete trial (per task condition, per stimulation (cTBS or iTBS), per hand) was defined. In accordance with Vercruysse and co-workers²⁰⁷, the beginning of a freezing episode was determined as “the onset of abnormally small motion cycles (<50% of the initial amplitude) accompanied by an irregular cycle frequency”, which proved a reliable procedure. The end was defined as the moment where movement cycles with regular amplitude and frequency were resumed, or when the trial ended. A semi-automatic detection was used, which was visually checked and corrected by two independent raters.

4.2.6 Pegboard dexterity test

The pegboard dexterity test^{69,70} was used to determine upper limb bradykinesia at the start and end of each session, as a brief surrogate test to estimate overall treatment effects and disease state. This test strongly correlates with the overall MDS-UDPRS part 3 score^{69,70} and repeating the entire MDS-UDPRS part 3 was considered to be too cumbersome for patients. The time needed to turn four wooden pegs upside down using one hand, from one hole into the next, was recorded four times for each hand. The average over the four trials was taken for each hand separately.

4.2.7 Corticospinal excitability

With single pulse TMS corticospinal excitability of the primary motor cortex (M1) was determined. The pulses were administered using the MagPro figure-of-eight coil connected to the MagPro X100 stimulator. The optimal location of the coil for eliciting MEPs in the resting first dorsal interosseous (FDI) muscle of the most affected hand was tracked (hotspot).

To ensure identical coil positioning during and over sessions, the location and orientation of the coil over the hotspot were also saved using the stereotactic image guidance system.

a MathWorks, Natick, Massachusetts, USA

The resting motor threshold was determined, defined as the minimum stimulator intensity required to obtain MEPs with an amplitude of at least 50 μ V in at least 5 out of 10 trials in the relaxed FDI of the most affected hand. Last, the minimum stimulator intensity was determined to obtain single pulse MEPs of on average 1 mV over 10 trials (SI_{1mV}). Directly before (*pre*) TBS, directly after TBS (*post 1*) and at the end of the session (*post 2*), 20 single pulses at SI_{1mV} were applied to measure the corticospinal excitability.

4.2.8 Statistical analyses

All statistical analyses were performed in IBM SPSS Statistics 20. The data for the upper limb task, the gait protocol and the pegboard dexterity test, were all separately analyzed using the ANOVA with random factor '*patient*' and fixed factors '*stimulation*' (cTBS or iTBS) and '*time*' (*pre* or *post*). The fixed factor '*task*' was added for the analyses of the upper limb task (NANS, NAFS, SANS or SAFS) and for the gait protocol (*normal*, *fast*, *small steps* or *small fast steps*). The analyses for the upper limb task and the pegboard dexterity test were performed separately for the most and least affected hand, as the difference between hands was not a research question.

The main variables of interest were the mean FOG duration (per trial) in the gait protocol and the mean FOUL duration (per trial) in the upper limb task. We used the mean freezing duration per trial, instead of the mean freezing duration per period or the number of episodes, because this measure reflected that a single 5-second freezing episode was considered worse than three 1-second episodes¹²¹.

In addition to freezing duration, the mean execution time in the gait protocol, and the mean peak-to-peak amplitude and mean frequency in the upper limb task (calculated over the complete trials) were evaluated. The variable for the pegboard dexterity test was execution time. In case the fixed factors '*stimulation*', '*time*' or an interaction between factors, had a significant effect on the tested variables, *post hoc* analyses were performed using paired sample t-tests.

A change in corticospinal excitability was tested comparing the MEP amplitudes of all three *time points* (*pre*, *post 1*, *post 2*) using a repeated measurements test and for two time points (*pre* and *post 1*) a paired sample t-test. These comparisons for MEP amplitudes were done for cTBS and iTBS separately.

For all analyses, a *p-value* < 0.05 was considered significant. All data are shown as means \pm standard error of mean (SEM).

4.3 RESULTS

4.3.1 Subjects

Clinical and demographic characteristics of all 17 included patients are listed in table 4.1. One adverse event was reported, in which the patient developed temporary nausea at the end of the iTBS session (*second session*). Follow-up reports one week and three weeks after this session showed no long-term effects.

4.3.2 Gait: FOG

The gait protocol successfully provoked FOG in 12 patients (out of 17 patients: 71%). The other five patients did not show any FOG during the experiments, although they had showed unequivocal FOG-episodes during earlier assessments. From the 12 patients who did show FOG, five showed only one or two episodes during the baseline gait measurements. The FOG duration per trial varied from less than 1 second in some patients to a maximum of 357.5 seconds in one patient.

No significant effect of stimulation (*cTBS* vs. *iTBS*), time (*pre* vs. *post*), task or interaction between factors was found for FOG duration when all turn and gait conditions were included as separate tasks, nor when all turns were combined and all gait trajectory conditions (normal, fast, small steps, small fast steps) were combined (table 4.2). Because of the lack of a significant effect, only the FOG duration results for the turns are shown (figure 4.2), as this is the most FOG provoking task^{136,186}. No post hoc analyses were performed for FOG duration.

4.3.3 Gait: Speed

When comparing the gait speed for all turns and gait conditions separately with the ANOVA, a significant main effect of task was found, but not for stimulation or time. The interaction of factors time and task also showed a significant effect (table 4.2).

Post hoc analyses showed a significant decrease in execution time between *pre* and *post* for iTBS in the small steps condition (figure 4.3A, *34.2 s pre-iTBS versus 25.9 s post-iTBS*; $p = 0.014$). A small, but also significant increase in execution time between *pre* and *post* for cTBS in normal walking (*12.4 s pre-cTBS versus 13.4 s post-cTBS*; $p = 0.020$) and fast walking (*8.5 s versus 10.1 s*; $p = 0.001$) was found (figure 4.3B). All other combinations of stimulation and gait conditions did not show significant effects.

TABLE 4.1. Clinical and demographic characteristics of 17 Parkinson's disease patients.

PARAMETER	MEAN	RANGE
Age (years)	61.2	46 - 76
Parkinson's disease duration (years)	8.5	1 - 25
FOG duration (years)	3.4	1 - 12
Hoehn & Yahr stage		2 - 3
MDS-UPDRS part 3	33.4	12 - 68
NFOGQ	16.5	3 - 28
FAB	16.0	12 - 18
MMSE	28.5	24 - 30
Resting motor threshold (%MSO)	43	34 - 60

MDS-UPDRS: Movement Disorder Society – Unified Parkinson's disease rating scale part 3 (score 0 - 132), N-FOGQ: New Freezing of Gait Questionnaire (score 0 - 28), Hoehn and Yahr stage (score 0 - 5), MMSE: Mini Mental State Examination (score 0 - 30), FAB: Frontal Assessment Battery (score 0 - 18). For MDS-UPDRS, N-FOGQ and Hoehn and Yahr stage, higher scores indicate worse functioning. For both FAB and MMSE, lower scores indicate worse functioning. The scores were evaluated 'off' medication.

TABLE 4.2. Statistics gait task.

	TIME	STIMU- LATION	TASK	STIMU- LATION x TIME	STIMU- LATION x TASK	TIME x TASK	STIMU- LATION x TIME x TASK
FOG duration [combined]	[0.867; n.s.]	[0.874; n.s.]	[0.865; n.s.]	[1.032; 0.326]	[0.971; n.s.]	[0.735; n.s.]	[0.152; n.s.]
FOG duration [separate]	[0.840; n.s.]	[0.901; n.s.]	[1.078; 0.379]	[0.974; n.s.]	[1.074; 0.382]	[1.180; 0.326]	[0.997; n.s.]
Mean execution time [separate]	[4.005; 0.062]	[1.142; 0.301]	[10.058; 0.000]	[1.903; 0.186]	[1.045; 0.398]	[3.214; 0.011]	[0.826; n.s.]

The factors are 'time' (pre or post), 'stimulation' (cTBS or iTBS) and task (normal, fast, small steps, small fast steps, turning clockwise or turning counter-clockwise). Factor task and interactions with factor task in separate [$F_{5,16}$; p]. All other factors and interactions [$F_{1,16}$; p]. FOG duration was analyzed for all gait tasks [separately, 6 task conditions] and for turns and gait trajectory [combined, 2 task conditions] combined. Significant results are indicated in bold.

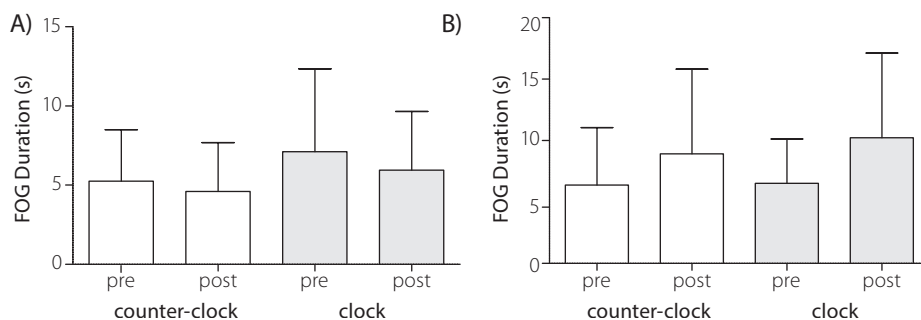


FIGURE 4.2. The mean freezing (FOG) duration during turning, before and after stimulation, for the (A) facilitatory iTBS and (B) inhibitory cTBS in seconds. The error bars signify the SEM.

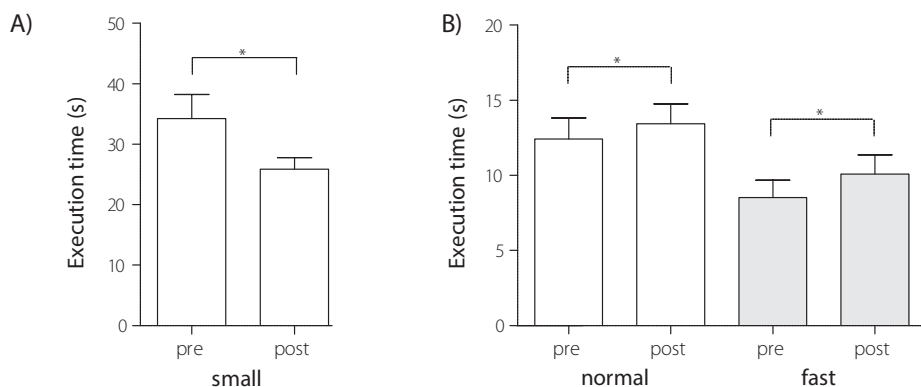


FIGURE 4.3. The mean task execution times for the gait protocol (only shown for significant differences) before and after stimulation for the (A) facilitatory iTBS and (B) inhibitory cTBS in seconds. The error bars signify the SEM. The asterisks indicate a significant difference between pre and post measurements.

4.3.4 Upper limb

The upper limb task successfully provoked FOUL at least once in all patients at baseline. The FOUL duration varied strongly from 0.2 to 37.9 seconds and was 3.1 seconds on average. In 42% it was shorter than 1 second and in 66% shorter than 2 seconds. The average duration is shorter than in previous reports^{206–208}. In total 271 trials showed freezing during baseline (both sessions combined), with 54% bilateral, 31% unilateral most affected and 15% unilateral least affected side.

The main factors time and stimulation showed no significant effect, nor did any of the interactions between factors (table 4.3). The factor task (NANS, NAFS, SANS or SAFS) showed a significant effect. The tasks with small amplitudes evoked more freezing than the normal

TABLE 4.3. Statistics upper limb task.

	TIME	STIMU- LATION	TASK	STIMU- LATION x TIME	STIMU- LATION x TASK	TIME x TASK	STIMU- LATION x TIME x TASK
FOUL duration [most]	[3.218; 0.073]	[3.287; 0.070]	[19.158; 0.000]	[0.671; n.s.]	[0.442; n.s.]	[0.565; n.s.]	[0.017; n.s.]
FOUL duration [least]	[0.348; n.s.]	[3.801; 0.052]	[5.883; 0.001]	[0.697; n.s.]	[1.162; 0.323]	[0.860; n.s.]	[0.657; n.s.]
Ampli- tude [most]	[0.009; n.s.]	[1.760; 0.185]	[60.733; 0.000]	[0.942; n.s.]	[0.302; n.s.]	[0.699; n.s.]	[0.250; n.s.]
Ampli- tude [least]	[0.661; n.s.]	[1.271; 0.260]	[87.445; 0.000]	[0.139; n.s.]	[0.354; n.s.]	[0.437; n.s.]	[0.005; n.s.]
Fre- quency [most]	[1.772; 0.184]	[2.472; 0.116]	[11.317; 0.000]	[2.746; 0.098]	[0.033; n.s.]	[0.285; n.s.]	[0.191; n.s.]
Fre- quency [least]	[0.709; n.s.]	[0.052; n.s.]	[17.049; 0.000]	[0.591; n.s.]	[0.139; n.s.]	[0.381; n.s.]	[0.043; n.s.]

The factors are 'time' (pre or post), 'stimulation' (cTBS or iTBS) and task (NANS, NAFS, SANS or SAFS). Factor task and interactions with factor task [$F_{3,14}$; p]. All other factors and interactions [$F_{1,14}$; p]. Significant results are indicated in bold.

amplitudes, and the fast speed tasks evoked more freezing than the normal speed tasks. Figure 4.4 shows the mean FOUL duration calculated over all tasks combined, for both stimulation protocols and both hands.

Similar to the result for FOUL, only the fixed factor task showed a significant effect on amplitude and frequency (table 4.3).

4.3.5 Pegboard

The pegboard dexterity test did not show a difference in execution time between *pre* and *post* stimulation for both TBS protocols (cTBS and iTBS) in both the most and least affected hand.

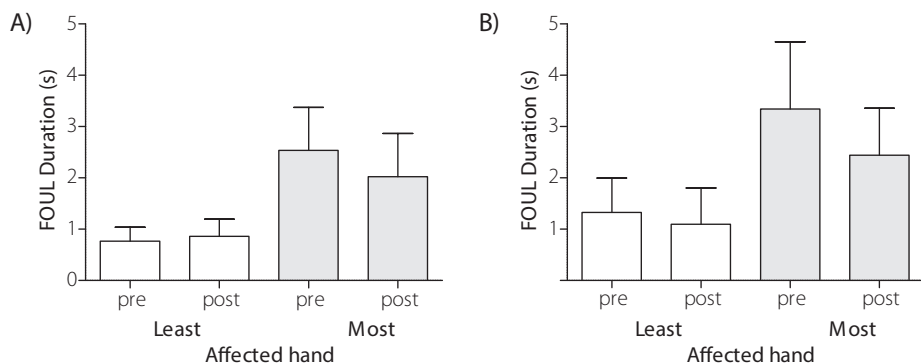


FIGURE 4.4. The results on the mean freezing (FOUL) duration of the upper limb task, before and after stimulation, for the (A) facilitatory iTBS and (B) inhibitory cTBS in seconds. TBS stimulated the ipsilateral cerebellum of the most affected hand. The white bars show the results of the least affected hand and the gray bars of the most affected hand. The error bars signify the SEM.

4.3.6 Corticospinal excitability

Both cTBS and iTBS did not have a significant effect on the corticospinal excitability over time, measured over the M1 contralateral to the most affected side, when taking all three time points into consideration (*pre*, *post 1*, *post 2*) (factor time: $F_{2,32} = 1.181$; $p = 0.320$, factor stimulation: $F_{1,16} = 0.518$; $p = n.s.$). Neither was a significant effect measured, for both cTBS ($p = 0.820$) and iTBS ($p = 0.130$), when only *pre* and *post 1* were taken into consideration.

4.4 DISCUSSION

4.4.1 Gait speed

We tested the hypothesis that PD patients with FOG, who may have reduced cerebellar compensatory drive for motor function, would benefit from repetitive transcranial magnetic stimulation of the cerebellum. The main conclusion is that both TBS protocols (facilitatory iTBS and inhibitory cTBS) did not significantly alter freezing duration in the upper limbs, nor during gait. However, an increase in overall gait speed when walking with small steps was found after iTBS (decreased execution time), while gait speed during normal and fast walking decreased after cTBS.

We stimulated the cerebellum, because previous studies suggested that the role of the cerebellum in the motor control of PD is compensatory^{2,144,161,221,224}. Although our hypothesis about compensatory cerebellar activity preventing freezing in PD has not been confirmed, the results do suggest that an improvement in gait performance is possible after cerebellar iTBS.

4.4.2 Gait effects and FOG

In PD patients with FOG, an increased functional connectivity between the SMA on the one hand, and the cerebellum and the MLR on the other hand, was found during rest⁴⁸. This emphasizes the importance of the cerebellum in this specific PD patient population. Because the increase in functional connectivity was correlated with objective ratings of freezing, it was proposed that it reflects a maladaptive compensation in FOG. However, this correlation did not necessarily reflect causality and the increase in functional connectivity could also indicate an increase in compensational strength of the network with increasing severity of FOG.

The importance of cerebellar activity in PD patients with FOG was confirmed in this study as the gait protocol showed significant changes in the execution times, i.e. gait speed. However, the hypothesized changes in FOG duration were not found. A possible reason for the latter is the sensitivity to detect changes. In line with previous experiments, FOG proved difficult to elicit¹⁸⁸. More repetitions in the gait protocol, especially the most FOG provocative tasks, could have increased the statistical power.

Another reason could be that cerebellar iTBS is not able to sufficiently improve the complex neural circuitry that is involved specifically in the occurrence of FOG. For example, the brainstem motor regions also have been associated with FOG^{180,182,187}. Moreover, pedunculopontine nucleus (PPN) stimulation, which is a form of deep brain stimulation, successfully reduced the number of FOG episodes¹⁹³, albeit not consistently. Possibly, stimulation of specific regions is necessary and global cerebellar stimulation lacks such specificity.

4.4.3 FOUL

Not only the effects of cerebellar TBS on freezing during gait were evaluated in this study, but also the effects on upper limb freezing. Similar to the results on FOG, no changes in FOUL duration were found after cerebellar TBS nor in pegboard performance.

Verduyck and colleagues identified the neural correlates of motor blocks or “freezing episodes” during a bimanual motor task in PD patients with FOG²⁰⁸. Using functional MRI (fMRI) they found that FOUL episodes were associated with increased cortical (right SMA, dorsal premotor and M1, and left prefrontal cortex) brain activity, while subcortical activity in the bilateral pallidum and putamen was decreased. Previous fMRI studies of upper limb motion in PD patients without FOG have consistently shown increased activation in premotor-parietal and cerebellar regions. The increase in the cerebellar regions was interpreted as a compensatory shift for the dysfunctional striato-supplementary motor loop^{223,224} and thought to influence the activity in the M1 through cerebellar-motor connections. The present results do not confirm the compensatory role of the cerebellum in upper limb motor control.

4.4.4 Corticospinal circuitry

The changes in gait speed were not accompanied by changes in MEP amplitude, measured after cerebellar TBS. This lack of effect on corticospinal excitability is in agreement with previous measurements in PD²⁷. This suggests that the cerebellar TBS does not affect the direct output from M1 of PD patients. In contrast to PD patients, healthy subjects did show an excitability decrease after cerebellar cTBS and an increase after iTBS⁸⁹, although such effects were not always observed¹⁵⁷.

In addition to measuring MEPs reflecting direct M1 output, cerebellar-motor connectivity can be measured with a TMS technique that induces cerebellar brain inhibition (CBI)^{152,203}. By application of CBI an alteration of the cerebello-cortical connectivity after cerebellar rTMS was found for PD patients^{26,90}, but again not always²⁷. It could be that the increased gait speed after iTBS was accompanied by an alteration of cerebello-cortical connectivity. For example, in PSP patients cerebellar iTBS improved dysarthria, which was accompanied by an increased CBI and increased activity in the caudate nucleus bilaterally, as shown with resting-state fMRI²⁶.

In conclusion, it could be that cerebello-cortical connectivity, and not motor cortex activity itself, is altered after cerebellar TBS.

4.4.5 Future perspectives

The results from this exploratory study provide more insight in the involvement of the cerebellum in gait mechanisms of PD patients with FOG. The hypothesis about compensatory cerebellar activity preventing freezing in PD has been strengthened, but not confirmed.

This study does provide multiple leads for future research. Although the lateral cerebellum has been shown to be involved in gait¹⁹⁸, the medial cerebellum could possibly be a better target location for future stimulation protocols. The medial cerebellum has been shown to be very important in balance and gait control^{79,122}, and patients with medial cerebellar atrophy have gait and stance problems¹⁹⁸.

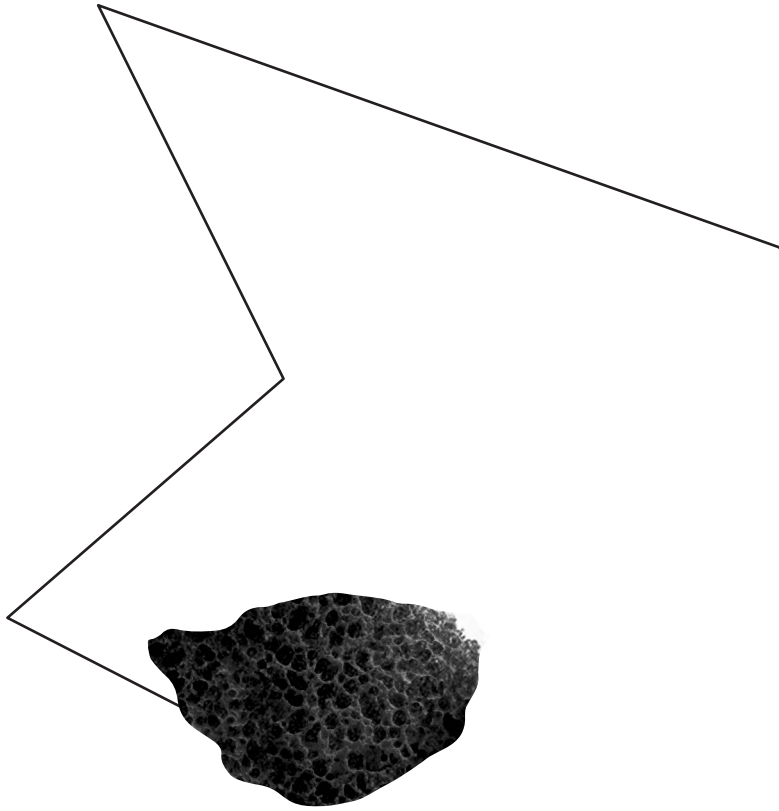
Also the unilateral instead of bilateral stimulation could have had an influence. Bilateral stimulation may be needed to compensate for freezing in both legs, although the dominant view is that reducing the asymmetry of gait parameters improves FOG⁴⁶. Bilateral stimulation should include an asymmetry, wherein the least affected side is stimulated less than the most affected side⁴⁶.

To identify the cerebellar and cerebral effects of the TBS that accompany the gait effects, future studies can combine stimulation sessions with fMRI or positron emission tomog-

raphy (PET)²⁵. This would also help to establish how and to what extent activity in the cerebellum and the connected circuitries is affected by TBS.

A limitation of our study was the absence of a sham stimulation condition. We decided to minimize the burden for the patients and only include a cTBS and an iTBS session (such that the contrast in facilitatory effects and direction of the effect for both active conditions could serve as control for the opposite condition). Patients had to be tested 'off' medication to increase the possibility to observe FOG, which has a high impact on mobility^{19,84} on the days of testing. As a consequence placebo effects cannot be fully ruled out. But if present, the placebo effects must have been the same for both conditions, as the patients were blinded with respect to the nature of the stimulation and conditions were randomized. Positive placebo effects could partly be responsible for the positive effects after iTBS and cancel out the negative effects on freezing after cTBS. On the other hand, it should be considered that effects of fatigue and time after last medication intake for the *post* compared to *pre* measurement could have dampened the positive effects of iTBS. They could also be the reason for the decrease in gait speed after cTBS. Nevertheless, because iTBS and cTBS affect performance differently in the gait protocol, the results still show an involvement of the cerebellum in gait for PD patients with FOG. To test the hypothesized compensational mechanism of the cerebellum, future studies should include a sham condition.

Finally, stimulation of the cerebellum with TBS and other techniques will only become clinically relevant for future therapies when accompanied by a substantial decrease in freezing, not only by changes in gait speed. Therefore, new studies in larger patient populations would be welcomed, with the aim of achieving an effect on freezing duration by increasing stimulation strength or by patient-specific targeting of the cerebellum. To compensate for the transient effect of rTMS, cerebellar transcranial direct current stimulation (tDCS) could be used instead⁵⁶. An advantage of that technique is the possibility to stimulate the cerebellum during execution of the freezing evocative tasks.



Published as:

Nonnekes J, **Janssen AM**, Mensink SHG, Oude Nijhuis LB, Bloem BR, Snijders AH.

Short rapid steps to provoke freezing of gait in Parkinson's disease.

Journal of Neurology, Vol. 261(9), p. 1763-1767, 2014

5.

SHORT RAPID STEPS TO PROVOKE FREEZING OF GAIT IN PARKINSON'S DISEASE

ABSTRACT

Freezing of gait (FOG) is both common and debilitating in patients with Parkinson's disease (PD). Due to its episodic nature, it is a challenge to provoke FOG in clinical practice and in the research setting. Turning is most sensitive to provoke FOG, particularly when performed as rapidly as possible. Walking with short steps is an alternative approach to provoke FOG. Here, we assessed a modified version of this test, consisting of the instruction to make short steps as rapidly as possible. We evaluated what the diagnostic value of this new test is compared to rapid turning. Twenty-eight patients with PD participated, who all had objective FOG. Patients performed the following tasks two times: (1) normal walking, (2) walking as rapidly as possible, (3) walking with short steps, (4) walking with short steps as rapidly as possible and (5) making full rapid turns in both directions. FOG was provoked in twenty subjects (71%). The most effective test to provoke FOG was rapid full turns (64% of subjects). FOG occurred more often when patients walked with rapid short steps (50%) compared to walking with short steps at normal speed (18%). The combination of 'full rapid turns' and 'walking with short steps rapidly' yielded the highest sensitivity of provoking FOG (0.71, CI: 0.51-0.86). The most sensitive way to provoke FOG is by asking patients to make full rapid turns, but if negative, walking with short steps as rapidly as possible can identify further subjects with FOG.

5.1 INTRODUCTION

Freezing of gait (FOG) is both common and debilitating in patients with Parkinson’s disease and atypical parkinsonism^{19,125}. It is characterized by sudden, relatively brief episodes of inability to step or by extremely short steps that typically occur on gait initiation or on turning while walking¹³⁸. However, due to its episodic nature, it is often a challenge to provoke FOG¹³⁴. This not only hinders the objective classification of freezing, but also the follow up of freezing severity in clinical practice, as well as in a research setting. Turning is the most sensitive clinical test to provoke FOG¹⁸⁶. The sensitivity of turning to provoke FOG increases when patients are instructed to make narrow turns as rapidly as possible compared to turning at self selected speed¹⁸⁶. In addition to turning, walking with short steps has been proposed as an alternative test to provoke FOG²⁸. Here, we assessed a modified version of this test, consisting of the instruction to make short steps as rapidly as possible. We investigated whether this new test increases the FOG occurrence in ‘definite freezers’¹⁸⁶ compared to walking with short steps at a self-selected speed. Moreover, we investigated what the value of walking with short steps rapidly is compared to rapid turning. We hypothesized that adding ‘walking with short steps as rapidly as possible’ to ‘full rapid turns’ improves the sensitivity of provoking FOG.

TABLE 5.1. Clinical characteristics.

PARAMETER	MEAN (SD)
Age (years)	62 (9)
Gender	8 F, 20 M
MDS-UPDRS-part III	38 (14)
N-FOGQ	18 (7)
HY-stage	2.6 (0.5)
Disease duration (years)	9 (6)
FAB-score	16 (2)

Data are mean (SD). MDS-UPDRS = Movement Disorders Society-Unified Parkinson’s disease rating scale part III (score 0-132). N-FOGQ = New Freezing of Gait Questionnaire (score 0-33). For both MDS-UPDRS and N-FOGQ, higher scores indicate worse functioning. HY-stage = Hoehn and Yahr-stage. FAB = Frontal Assessment Battery (score 0-18). For FAB, lower score indicate worse functioning.

5.2 METHODS

5.2.1 Patient characteristics

We included 28 patients with idiopathic Parkinson's disease (table 5.1), who all had a previous history of FOG that was objectified by previous studies or seen by a specialized neurologist ('definite freezing'). FOG was assessed subjectively using the New Freezing of Gait Questionnaire (N-FOGQ)³². Twenty-one patients reported more FOG during OFF-phases compared to ON-medication, whereas seven patients reported no difference in freezing during ON or OFF. Patients were diagnosed according to the UK Brain Bank criteria⁷⁷, and assessed clinically with the motor subsection (Part III) of the Movement Disorders Society–Unified Parkinson's Disease Rating Scale (MDS-UPDRS)⁶⁶. Additionally, global executive function was assessed with the Frontal Assessment Battery (FAB). Exclusion criteria were other causes for gait impairment (such as severe arthrosis or neuropathy). All subjects gave their written informed consent prior to the experiment, and the experiment was performed in accordance with the declaration of Helsinki and with local ethical guidelines.

Patients were measured in an OFF-state, for 12 patients when they experienced an end-of-dose effect prior to intake of their next medication dose, and for 16 patients after at least 12 hours of dopaminergic medication withdrawal. The pattern of results as reported in the results section (5.3) is comparable for both groups.

5.2.2 Protocol

Patients performed the following tests twice:

- Normal walking; patients walked 10 meters at self-selected speed.
- Walking rapidly; patients walked 10 meters as rapidly as possible, however, running was not allowed.
- Walking with short steps; patients walked 10 meters with short steps (approximately 25% of step length).
- Walking with short steps rapidly; patients walked 10 meters with short steps (approximately 25% of step length), but now as rapidly as possible.
- Rapid full turns; patients were instructed to make 360° axial turns from standstill on the spot, as rapidly as possible, and in both directions.

The order of the conditions was balanced across patients. Every test condition was practiced once.

5.2.3 Data analysis

The entire experiment was videotaped for offline visual analysis. Two independent and experienced raters (JN and AS) scored the videos for the presence of FOG. The raters were blinded for the instruction given to the patients, although they could of course see the difference between performance of conditions. The videos of the conditions were mixed. FOG was defined as an unintentional and temporary phenomenon where the feet failed to progress¹⁷⁶. If the raters disagreed, trials were sent back to them for consensus. FOG seen when turning after the 10-meters walking trials was not included in the analysis. If it was not clear whether there was FOG seen or just 'walking with small steps', no FOG was rated.

5.2.4 Statistical analysis

Using the data-values prior to consensus between both raters, inter-rater reliability was assessed using Cohen's kappa for the rating of presence of FOG in each trial. Using Wilcoxon's signed rank test for related samples we explored the effectiveness of the conditions in evoking FOG in the patients. We specifically explored the following predefined contrasts: 1) normal walking versus walking with short steps, and 2) walking with short steps at self selected speed versus walking with short steps as rapidly as possible. The alpha level was set at 0.025 to correct for multiple comparisons (Bonferroni). Furthermore, we determined the most sensitive test to provoke FOG. Finally, we investigated which combination of tests is most sensitive to provoke FOG.

5.3 RESULTS

5.3.1 Inter-rater reliability

Prior to consensus, the raters reached a high degree of agreement for presence of FOG within each trial (agreement 92%, Cohen's kappa =0.85).

5.3.2 Best way to provoke FOG

All patients understood the test instructions without any problems. FOG was observed in 20 of the 28 patients (71%). One patient was not able to perform the turning task due to severe balance problems. Both normal walking and walking rapidly provoked FOG in 5 patients (18% of patients; Wilcoxon's $Z = 0.00$, $p=1.00$; see figure 5.1). Walking with short steps rapidly provoked FOG in 14 patients compared to 6 patients when walking with short steps at a self selected speed (50% versus 21% respectively; Wilcoxon's $Z = -3.00$, $p=0.003$). The average number and duration of FOG-episodes is shown in table 5.2.

Full rapid turns were most effective in provoking FOG, with a sensitivity of 0.64 (CI 0.44-0.81). A combination of 'rapid full turns' with 'short steps rapidly' yielded the highest sensi-

tivity to detect FOG (0.71, CI: 0.51-0.86). Two patients, who did not freeze during rapid full turns, did so when asked to walk with short steps rapidly. Combining ‘rapid full turns’ with ‘short steps’ or ‘walking rapidly’ yielded a sensitivity of 0.68 (CI 0.48-0.83). The combination of ‘rapid full turns’ with ‘normal walking’ did not yield a higher sensitivity than ‘rapid full turns’ alone. Combining three or more tests together did not result in a higher sensitivity than the combination of ‘rapid full turns’ and ‘short steps rapidly’.

TABLE 5.2. Mean number and duration of FOG-episodes.

TASK	MEAN NUMBER FOG-EPISODES	MEAN DURATION OF FOG (s)
Normal walking	1 (1-2)	1.5 (1-3)
Walking rapidly	1 (1-2)	1 (1-4)
Short steps	2 (1-6)	4 (1-13)
Short steps rapidly	2 (1-8)	2.5 (1-94)
Turning	4 (1-7)	27 (1-193)

Data are mean for the two trials combined (range). For calculation of means only patients were included in which FOG was provoked in that specific task.

Provocation of FOG (% of included patients)

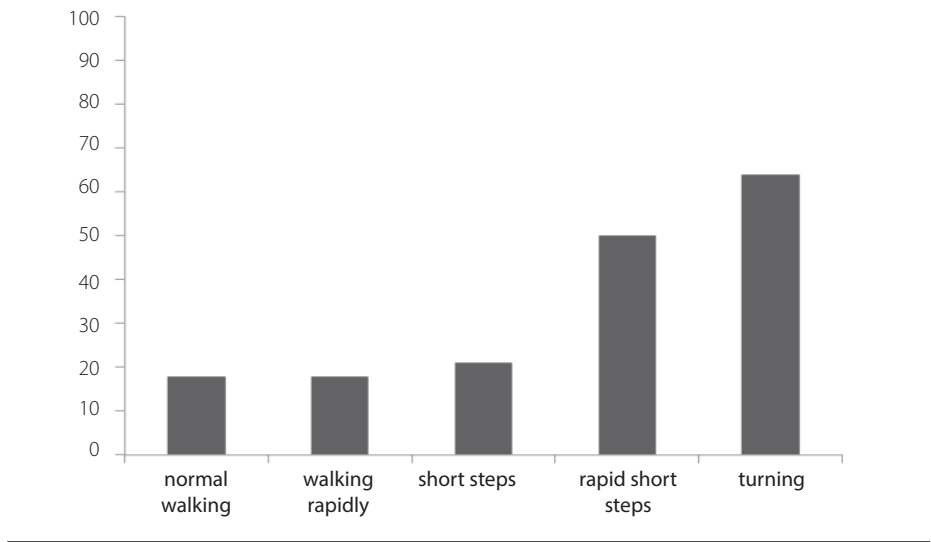


FIGURE 5.1. Provocation of FOG by different tests.

5.4 DISCUSSION

Here, we examined walking with short steps rapidly as a simple clinical measure to evoke FOG in known freezers. Our results demonstrate that FOG is more often provoked when patients walk with short steps as rapidly as possible compared to walking with short steps at normal speed. Full rapid turns were most sensitive to provoke FOG. However, the combination of 'full rapid turns' and 'walking with short steps rapidly' yielded more FOG than full rapid turns alone.

Chee and colleagues reported that FOG is more often detected when patients walk with short steps compared to normal walking²⁸. Here we did not replicate that finding. Interestingly, in the study of Chee *et al.*, FOG was observed in a higher percentage of patients compared to our study, both in the normal walking condition (44% versus 18%) and in the walking with short steps condition (69% versus 21%). The fact that Chee *et al.* used four trials per condition in contrast to two trials in the present study could have contributed to a higher occurrence of FOG in each condition¹⁸⁶. In addition, it suggests that the patient group included by Chee *et al.* was more severely affected, which is supported by a lower Hoehn and Yahr stage in our group (3.88 versus 2.61). The scores on the MDS-UPDRS and FOG-questionnaires could not be directly compared because different versions were used. Thus, walking with short steps may be more effective in evoking FOG in severely affected freezers compared to less affected freezers. We showed that FOG during walking with short steps was more often provoked when the command 'as rapidly as possible' was given. Hence, walking with short rapid steps is an effective test to provoke FOG, even in mildly affected patients.

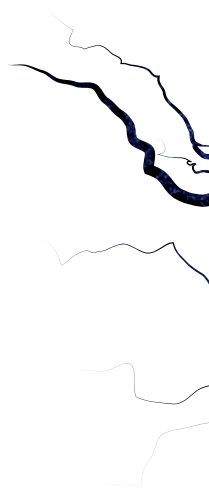
In the present study we evaluated the sensitivity of walking with short steps to provoke FOG in known freezers. The combination of rapid full turns with a gait trajectory involving dual tasking has been reported to increase the sensitivity of detecting FOG compared to rapid full turns alone (increase from 61% to 72%)¹⁸⁶. Here, we show that the sensitivity of detecting FOG is also increased when walking with short steps rapidly is added to full rapid turns. The disadvantage of a gait trajectory involving dual tasking is that the latter might evoke the 'stops walking when talking' phenomenon¹⁰⁶, which could result in a false-positive classification rate¹⁸⁶. This 'stops walking when talking' phenomenon is not expected when patients walk with short steps rapidly. Moreover, walking with short steps rapidly is easier and less time consuming than a gait trajectory involving dual tasking. However, similar to the 'stop walking when talking', it was sometimes difficult to distinguish walking with short steps rapidly from a true FOG-episodes. Possibly, objective assessment using accelerometry can help in this matter¹¹⁹. Future studies may examine whether the combination of a dual task and walking with short steps rapidly further increases the FOG yield.

It should be noted that we did not include PD patients without freezing of gait. Thus, whether the short-steps are specific enough to differentiate freezers from non-freezers, should be a subject of future study. A limitation of the present study is the fact that we did not standardize the step length, for example using visual cues, although it does make it easier to implement the present findings in future studies and clinical assessment. Another disadvantage is that we did not collect gait data, to evaluate the actual step length. These disadvantages make the comparison with other studies, such as the study of Chee *et al.*²⁸ more difficult, but do not influence our main finding that walking with short steps rapidly is more effective in provoking FOG than walking with short steps at a self selected speed.

Several potentially co-existing hypotheses exist concerning the pathogenesis underlying FOG¹³⁸. The observation that FOG is more often seen when patients walk with short steps rapidly compared to short steps at self-selected speed, could be interpreted in three ways. First, it might underscore the importance of gait rhythmicity and gait cycle coordination. Gait rhythmicity is probably coordinated by central pattern generators in the spinal cord¹³⁸. Disordered supraspinal input on these central pattern generators might result in high-frequency oscillations during FOG-episodes. When walking with small steps rapidly gait rhythmicity and gait cycle coordination is challenged, possibly resulting in FOG-episodes. Secondly, our results could be explained by abnormal coupling between anticipatory postural adjustments (APAs) and subsequent stepping movements. The pontomedullary reticular formation (pmRF) and pedunculopontine nucleus (PPN) are likely involved in the integration of APAS with subsequent steps¹⁷⁸. When walking with short steps rapidly, the coupling between APAs and stepping movements is further challenged. This will likely increase the computation load on the PPN and the pmRF, which could subsequently result in FOG^{135,187}. Finally, the effect of the instruction to walk with short steps as rapidly as possible may suggest stress as a provoking factor for FOG. Especially stress associated with timing, like ringing of a telephone or the doorbell, has been reported as a provoking factor for FOG⁶¹. Hypothetically, emotional input may overload the system, due to cross-talk between the normally segregated basal ganglia circuitries¹⁰². Future work has to further explore these hypotheses. These studies should take into account the role of executive dysfunctioning in the pathogenesis of FOG. PD patients may compensate for their gait deficits by increasing their attention or executive load. When this executive compensation fails, FOG might develop⁶¹. In the present study, all of the included patients understood the test instructions without any problems. Hence, we do not think that cognitive impairments directly influenced the differences between the test conditions.

5.5 CONCLUSION

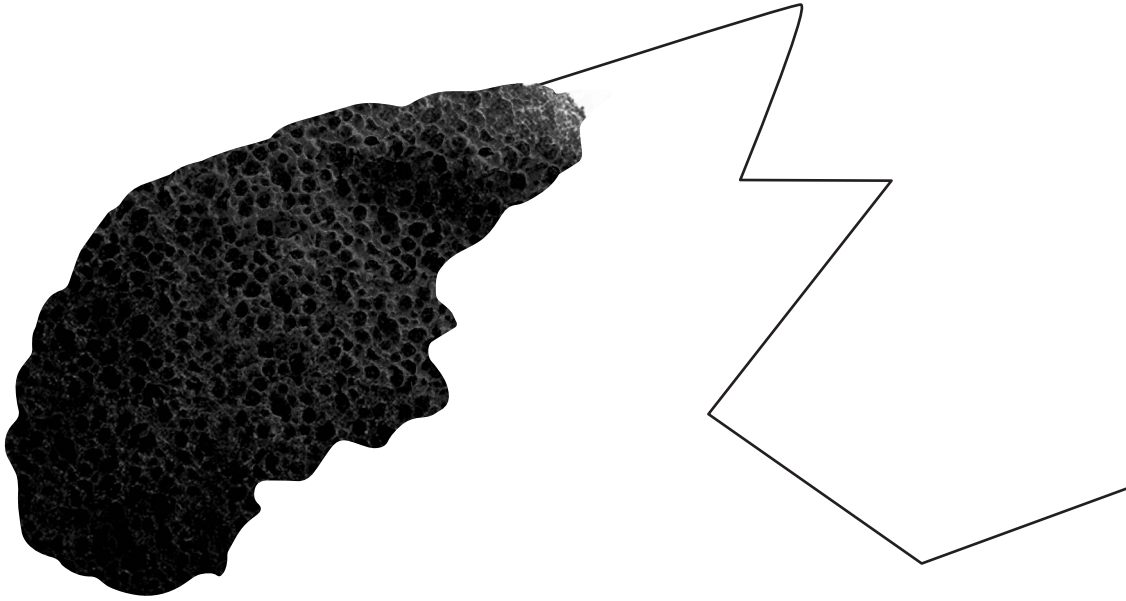
As described previouslyⁱ⁸⁶, full rapid turns into each direction are most effective when aiming to objectify FOG in clinical practice or in the research setting. If these tests do not evoke FOG, we suggest to add walking with short steps as rapidly as possible. For both turningⁱ⁸⁶ and walking with short steps, the instruction to perform the test 'as rapidly as possible' is essential for evoking more FOG.





PART III

TRANSCRANIAL MAGNETIC STIMULATION
&
THE FINITE ELEMENT METHOD



6.

MODELING TRANSCRANIAL MAGNETIC STIMULATION



6.1 WHY VOLUME CONDUCTION MODELING?

Despite the wide application of transcranial magnetic stimulation (TMS), the effects of stimulation at the cortical level are only partially understood. This is largely because *in vivo* measurements are problematic due to ethical issues and hardware problems. Computational models are the only non-invasive alternative without these problems. Such models can be very useful to estimate the effects induced by TMS. Furthermore, it is relatively inexpensive to test new scientific hypotheses with computational models, for example to improve stimulation protocols with new coil designs³⁵. In this thesis, a highly detailed computational model is employed to study the TMS-induced electric fields at a macroscopic level (i.e. at the cortical level, but not at the level of individual neurons).

An appropriate method to determine the induced electric fields throughout the scalp, skull and brain is to use a volume conduction model (VCM). In this type of modeling the human head is described as a volume conductor with electromagnetic properties for different tissue types. The different tissues are separated by geometrically accurate boundaries. Based on the general laws of physics, the electric fields induced by TMS can be determined throughout the VCM. This type of modeling has already proven to be valuable in studying electrophysiological phenomena in transcranial current stimulation (TCS)^{117,159,210,213} and TMS^{17,143,196}. It will be used in the studies to investigate several properties of the TMS-induced electric fields described in the following **chapters 7-9**.

6.2 ELECTROMAGNETIC FIELDS

Electromagnetism is one of the fundamental forces in nature and lays at the basis of TMS. The knowledge about the physical laws of electromagnetism can be used to calculate the magnetic and electric fields induced in the human brain by TMS. The English physicist James Clerk Maxwell introduced a set of differential equations that describe the interactions between electric and magnetic fields¹⁰⁹:

$$\nabla \cdot \vec{E} = \frac{\rho}{\epsilon_0} \quad (6.1) \quad \nabla \cdot \vec{B} = 0 \quad (6.2)$$

$$\nabla \cdot \vec{E} = -\frac{\partial \vec{B}}{\partial t} \quad (6.3) \quad \nabla \times \vec{B} = \mu_0 \left(\vec{J} + \epsilon_0 \frac{\partial \vec{E}}{\partial t} \right) \quad (6.4)$$

Herein, \vec{E} is the electric field [V m⁻¹], ρ the charge density [C m⁻³], ϵ_0 the permittivity of free space [F m⁻¹], \vec{B} the magnetic field [T], μ_0 the permeability of free space [N A⁻²] and \vec{J} the current density [A m⁻²]. The nabla symbol ∇ denotes the three-dimensional gradient operator ($\frac{\partial}{\partial x}, \frac{\partial}{\partial y}, \frac{\partial}{\partial z}$), $\nabla \cdot$ describes the divergence of the electric (eq. 6.1) and magnetic field (eq. 6.2), and $\nabla \times$ describes the curl of the electric (eq. 6.3) and magnetic field (eq. 6.4).

For the modeling work presented in this thesis (**chapters 7 till 9**), the volume conductor is assumed to be purely resistive, and consequently no net transport of charge is assumed. In this quasi-static approach¹⁵³ the electric field and current density within the volume conductor at any moment in time depend only on the value of $\partial \vec{B} / \partial t$ at that particular moment. Previous reports have justified the quasi-static approach for the TMS frequency range [~1-10 kHz]^{195,214}. This allows a simplification from the Maxwell equations for TMS.

Maxwell-Faraday's equation (eq. 6.3), which states that a time-varying magnetic field produces an electric field, is the most important for TMS. To calculate the induced electric field for TMS, it is practical to use the magnetic vector potential \vec{A} instead of the magnetic field \vec{B} . The relationship between these two is defined as:

$$\vec{B} = \nabla \times \vec{A} \quad (6.5)$$

When we combine this with the Maxwell-Faraday equation (eq. 6.3), the following can be stated:

$$\nabla \times \left(\vec{E} + \frac{\partial \vec{A}}{\partial t} \right) = 0 \quad (6.6)$$

This shows that the curl of the part between brackets is zero, and can consequently be

described as the gradient of a scalar field ϕ : the electric potential. This helps to define the electric field as a summation of two components:

$$\vec{E} = -\frac{\partial \vec{A}}{\partial t} - \nabla \phi \quad (6.7)$$

Herein, $\frac{\partial \vec{A}}{\partial t}$ is a time-dependent magnetic vector field directly caused by the TMS coil and it is called the primary component \vec{E}_{primary} . The susceptibility of biological tissues is negligible¹⁷⁷ and therefore the primary component is independent of the head anatomy as specified in the VCM. The second term $\nabla \phi$ is the gradient in the electric potential within the head. The conductivity of a tissue type is its ability to conduct electric current. If the conductivity is isotropic the electric current is conducted equally well in all directions. Many tissues in the body, however, have anisotropic conductivity, which need to be incorporated in the VCM. The $\nabla \phi$ term is also called the secondary component $\vec{E}_{\text{secondary}}$ and describes the effect of the presence of the volume conductor on the electric field. The term \vec{E} on the left side of this equation is the total induced electric field. In volume conduction modeling of TMS, equation 6.7 is used to describe the electric field and is thereby the most important equation for all the following research chapters.

The electromagnetic law of Biot-Savart states that a time-varying current will produce a time-varying magnetic field, the strength of which is proportional to the current strength. To determine the magnetic vector potential \vec{A} , an adaptation of the traditional Biot-Savart law is used, which converts a time-varying current into a time-varying magnetic vector potential:

$$\vec{A}(\vec{r}, t) = \frac{\mu_0 I(t)}{4\pi} \int_c \frac{d\vec{l} \times \hat{r}}{|\vec{r} - \vec{r}'|} \quad (6.8)$$

Herein, \vec{A} is the magnetic vector potential [V s m^{-1}], μ_0 the permeability of free space [N A^{-2}] and $I(t)$ the time-dependent current in the coil [A]. The integral describes the contribution of the TMS coil to the magnetic vector potential. The strength of the magnetic vector potential is proportional to the current strength. As it is the change over time in the magnetic vector potential that produces the electric field within the head (eq. 6.7), the induced electric field strength is proportional to the change in the current through the TMS coil.

The secondary component $\nabla \phi$ in equation 6.7 is the result of discontinuities in the electrical conductivity σ at the boundaries between different tissue types. Because electric fields produce current densities following Ohm's law (quasi-static approach), and the current density perpendicular to tissue boundaries is continuous, a jump in the total electric field \vec{E} occurs across boundaries. As the primary component of the electric field is independent of the volume conductor, this jump in the electric field is completely deter-

mined by the secondary component. Finding an analytical expression for the secondary component, and hence the total electric field, for a VCM with highly complex geometric boundaries is difficult, if not impossible. However, it can be approximated with a numerical method. In this thesis the finite element method (FEM) is used. **Chapter 7** (7.2.3 *Finite Element Method*) describes in detail the implementation of FEM.

6.3 THE FINITE ELEMENT METHOD

Numerical methods, such as the FEM, are widely applied to determine solutions to (bio)-physical problems that are difficult, time-consuming or (as for most volume conductors of realistic shape) impossible to obtain analytically. The solutions of these methods are approximations up to a predefined error. To determine a solution with the FEM, the domain for which a problem has to be solved is discretized into small subdomains, called elements. Each element consists of a set of nodes that are connected by edges. In most cases these elements are hexahedral or tetrahedral (figure 6.1A and 6.1B). Specific properties are assigned to all elements, depending on the problem at hand. The advantage of the FEM over other numerical methods is the possibility to easily include numerous inhomogeneities, anisotropic conductivities and complex geometric boundaries between subdomains within the VCM.

For each element within the VCM a separate partial differential equation (PDE) is defined, based on the electromagnetic properties and the boundary conditions of that element. The complete set of all PDEs can be written as a single matrix equation describing the problem for the complete domain. In combination with specific boundary conditions, an initial solution for the problem at hand, the solution to the problem can be approximated iteratively with FEM software until the desired residual error or maximum number of iteration steps is reached.

Because one equation has to be solved for each element, the quality of the final solution for the total VCM is also determined by the choice of element sizes. The solution can be interpolated throughout a large element to determine the electric field at any point within the VCM, but this is not as accurate as solving the equation for multiple elements that cover that same volume in space. Especially when the conductivity or the anisotropy changes within the larger element. However, by increasing the number of elements the computational time will also increase. Consequently, it is important to determine the appropriate element size for each tissue type in combination with the question where results are most relevant. This can be based on position, shape and electrical properties of the anatomical and physiological structure. As mentioned in section 6.2, for TMS the

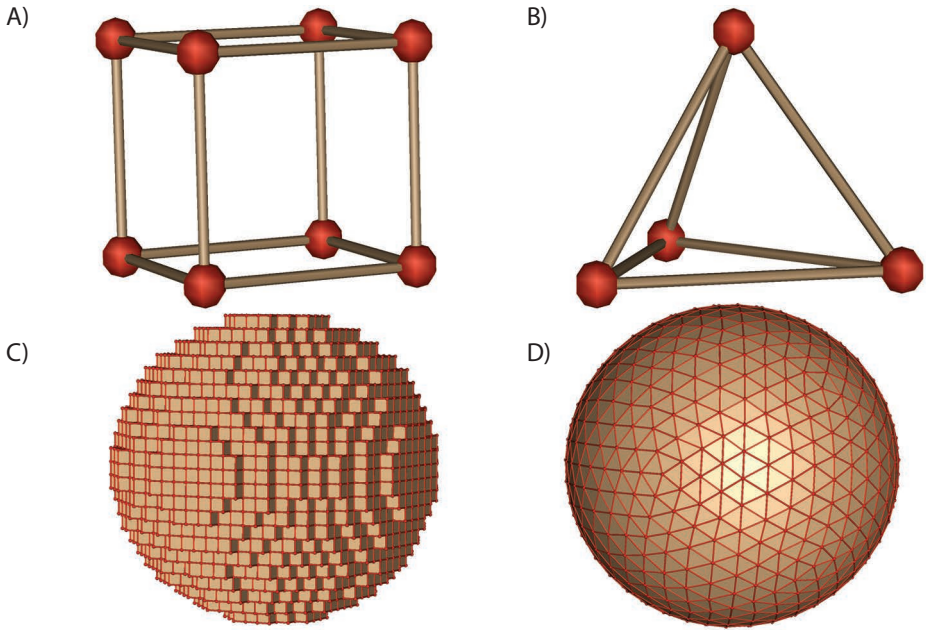


FIGURE 6.1. (A) Hexahedral element. (B) Tetrahedral element. (C) A spherical volume mesh constructed out of hexahedral elements. (D) A spherical volume mesh constructed out of tetrahedral elements.

primary field can be determined independently of the VCM and the FEM is not needed to calculate this part of equation 6.7. The FEM is used to compute the secondary field of equation 6.7. In case of TMS the PDE of each element in the VCM is a version of equation 6.7 with its own electrical conductivity and the precomputed primary field at the center of the element.

6.4 CONSTRUCTION OF REALISTIC HEAD MODEL

The construction of a realistic head model is of utmost importance in TMS modeling. Throughout the last decade, computational VCMs have reached a high standard. This is due to increasing computational power, but also to the increasing interest in TMS by the scientific and clinical community.

The first VCMs were simplified homogenous spherical models that provided researchers with the first information on the electric field produced by a TMS coil^{68,162}. However, the modeled electric fields provided only crude approximations of the induced electric fields within the head, mostly due to the neglect of the secondary field components caused

by discontinuities in the electrical conductivities at tissue boundaries (the second term in eq. 6.7). Therefore, modeling the human head as an inhomogeneous spherical conductor with multiple compartments with different conductivities was already an improvement¹¹⁶. Thereafter, several studies showed the importance of incorporating accurate descriptions of tissue boundary geometries, which significantly differed in shape from spherical boundaries. The geometry of these realistic head models can be derived from (individual) magnetic resonance images (MRI)^{17,29,195}.

The first step in constructing a VCM from MRI data is the identification of different tissue types, which is called segmentation. This can be done manually, which is very time consuming, or (semi-) automatic. The more tissue types are segmented, the more accurate the model will be, but also the more time consuming the segmentation process will be.

As mentioned for the FEM, the most common MRI-derived VCM's are constructed from hexahedral^{94,220} or tetrahedral elements^{29,195} (figure 6.1). Models consisting of hexahedral elements are easy to construct, because the mesh can directly derived from the MRI voxels. Based on the segmentation, the voxels can be assigned to a certain tissue type. However, these hexahedral models generally lack detail about the cortical surface geometry. Models consisting of tetrahedral elements are more difficult and time-consuming to construct, but they incorporate smoother boundaries between tissue types. To obtain tetrahedral models, the segmentation is used to construct three-dimensional triangular surfaces for each boundary between different tissue types. Subsequently, the spaces between triangular surfaces are filled with tetrahedral elements using specific software.

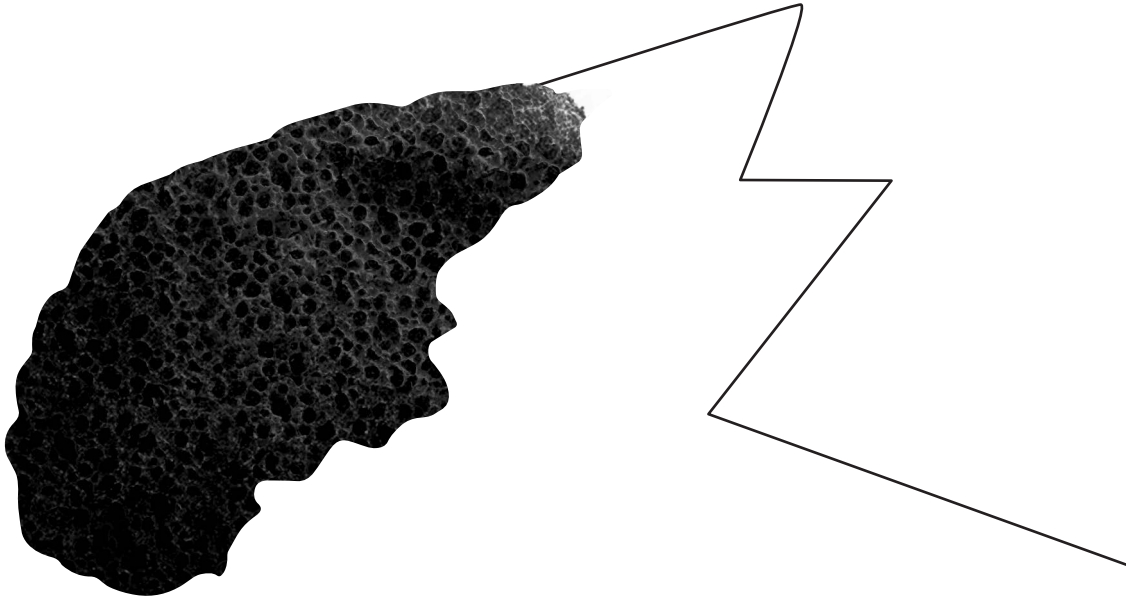
In the last step, the assignment of appropriate tissue properties is handled, which for TMS are the proper electric conductivity values. Common practice is to determine the bulk conductivity values from literature on experimental *in vitro* data⁵⁴. The conductivity values are in most cases assumed to be isotropic for the majority of tissue types. The FEM allows incorporating anisotropic conductivity values. In the human brain, the conductivity along neuronal fiber bundles is higher than the conductivity perpendicular to the fibers^{57,130}. For this reason, anisotropic conductivity values for the brain should be included. In the most widely applied method to determine brain conductivity anisotropy, the conductivity tensors are assumed to have the same eigenvectors as the diffusion tensors determined in the MRI system²⁰². These diffusion tensors can be acquired with diffusion tensor MRI imaging (DTI). The most recent models are now based on MRI and incorporate brain anisotropy based on DTI^{105,143}.

6.5 THE FOLLOWING CHAPTERS IN THIS PART OF THE THESIS

In the following chapters the FEM will be used to study the electric fields induced with TMS. To do this, a highly realistic VCM of a human head is constructed. This model consists of several millions of tetrahedral elements and is based on MR images and DTI measurements. An elaborate description of the VCM construction is included at the end of **part 3**, as appendix A (section 10.1).

Chapter 7 describes a so-called “*modeling to improve modeling*” study. The importance of a highly accurate description of the cortical surface that includes gyri and sulci in a VCM is evaluated. The information gained from such a study can help us in the accurate, but efficient, development of future models. This is important in studies where multiple patient-specific models are required and the minimum amount of time has to be spend on producing the models.

Chapters 8 and 9 concern practical research questions that can be answered with VCM modeling. In the daily application of TMS stimulation protocols that are designed for motor cortex stimulation are also used over brain areas other than the motor cortex. As most other brain areas have no clear measurable output similar to the motor cortex, it is not clear whether the stimulation strength based on motor cortex stimulation is appropriate in these areas. VCM can possibly help to improve these protocols by computing and studying the induced electric field. In this thesis, the influences of intra-individual differences in local brain anatomy (**chapter 8**) and coil orientation relative to the targeted brain area (**chapter 9**) will be studied.



Published as:

Janssen AM, Rampersad SM, Lucka F, Lanfer B, Lew S, Aydin U, Wolters CH, Stegeman DF, Oostendorp TF.

The influence of sulcus width on simulated electric fields induced by transcranial magnetic stimulation.

Physics in Medicine and Biology, Vol. 58, p. 4881-4896, 2013

7.

THE INFLUENCE OF SULCUS WIDTH ON SIMULATED ELECTRIC FIELDS INDUCED BY TRANSCRANIAL MAGNETIC STIMULATION

ABSTRACT

Volume conduction models (VCMs) can help in acquiring knowledge about the distribution of the electric field induced by transcranial magnetic stimulation (TMS). One aspect of a detailed model is an accurate description of the cortical surface geometry. Since its estimation is difficult, it is important to know how accurate the geometry has to be represented. Previous studies only looked at the differences caused by neglecting the complete boundary between the cerebrospinal fluid (CSF) and gray matter (GM)^{17,195}, or by resizing the whole brain²¹¹.

However, due to the high conductive properties of the CSF, it can be expected that alterations in sulcus width can already have a significant effect on the distribution of the electric field. To answer this question, the sulcus width of a highly realistic head model, based on T1-, T2- and diffusion-weighted magnetic resonance images (MRI), was altered systematically.

This study shows that alterations in the sulcus width do not cause large differences in the majority of the electric field values. However, considerable overestimation of sulcus width produces an overestimation of the calculated field strength, also at locations distant from the target location.

7.1 INTRODUCTION

Transcranial magnetic stimulation (TMS) is a non-invasive technique that is used in a wide range of neurophysiologic and clinical studies to measure or change the excitability of specific brain areas. To do this, a very brief and strong electric current is sent through a coil, which causes a time-varying magnetic field. This magnetic field consequently induces an electric field in the human head as described by Faraday's law of induction. This current may generate neural excitation.

Although nowadays TMS is a widely used research tool, most of our knowledge is still based on experimental experience. The underlying biophysical mechanisms are not well understood yet. To adjust and improve TMS protocols, it is important to have a clear understanding of the (neural) mechanisms behind TMS. To gain insight into these mechanisms, an estimate of the induced electric field in the brain can be made with the use of computational model simulations. In the last decade several numerical models using the finite element method (FEM)^{105,143}, the boundary element method (BEM)¹⁷⁴, the independent impedance method (IIM)⁵⁸ or the finite difference method (FDM)¹⁹⁹ have been introduced to study the spatial distribution of the induced electric field. The earliest models made use of spherical meshes^{116,162} and are still used today in TMS navigation devices.

Although spherical models are still in use, more realistic head models have been developed in the last couple of years to study TMS-induced electric field^{29,143}. One of the most important aspects of a realistic head model is the inclusion of a highly accurate description of the boundary between cerebrospinal fluid (CSF) and gray matter (GM)^{17,195,211}. The studies with spherical models already demonstrated the importance of tissue heterogeneity^{116,162}, but studies using realistic head models revealed the importance of proper tissue boundary geometries¹⁹⁵.

The question addressed in this study is: *how precise has the cortical surface geometry to be modeled to get an accurate estimate of the induced electric field*. In previous model studies only differences caused by neglecting the complete boundary between the CSF and GM^{17,195}, or by resizing the whole brain and including only one sulcus²¹¹ have been investigated. However, due to the high conductive properties of the CSF, it can be expected that even small changes in the geometry of the cortical surface will have a significant effect on the distribution of the electric field. This has already been shown to be the case in electroencephalography (EEG) source localization⁷⁸ and to our knowledge not yet been studied for TMS.

In this study we alter the cortical sulcus width of a highly realistic tetrahedral head model in a systematic manner to verify if subtle changes in the cortical geometry have an effect on the TMS-induced electric field. There are mainly two reasons for choosing the sulcus width as our primary variable and not (for example) resizing the whole cortical surface. Firstly, by only altering the sulcus width, the coil-target distance is kept constant and thereby the calculated differences are solely due to a change in cortical surface curvature. Secondly, by using this specific alteration we can study the effects of the presence of highly conductive CSF deep in the sulci, on the strength of electric fields in deeper parts of the cortex. As a by-product, the effect of the relative distribution of the CSF layer thickness, between the gyri and neighboring sulci, can also be observed.

The insights gained by this study will help to understand the importance of correctly incorporated gyri and sulci in the cortical surface and more generally the geometrical accuracy of the cortical surface needed for TMS modeling. This information is relevant for building new individual realistic head models and setting up pipelines to construct volume conduction models for TMS simulations. The creation of a realistic head model comprises several processing steps including segmentation and possibly smoothing. Previous studies demonstrated that different software packages (FSL^a, SPM5^b and FreeSurfer^c) produced suboptimal GM and white matter (WM) segmentations^{86,183}. All three packages produce GM and WM volumes that deviate up to 10 percent from a reference template, depending on the method and image quality⁸⁶. Both FSL and FreeSurfer reach a very high specificity for segmentation of GM and WM (almost 100 percent), but reach a much lower sensitivity (approximately 70 percent)¹⁸³. This means that the cortical surface can still differ several millimeters, for example in sulcus width, from reality. These segmentation errors can partially be solved with manual corrections, but this is a time consuming process. Hence, it is important to know how precise the cortical surface has to be modeled to get an accurate estimate of the induced electric field.

To answer the scientific question at hand, a highly realistic head model was constructed that contains multiple tissues and brain anisotropy. To our knowledge, this model is one of the most accurate head models produced for TMS modeling, whereby it largely makes use of freely available software. An elaborate description of the construction can be found in appendix A (section 10.1). Furthermore, a precise description of the stimulation coil is included as well. The electric field generated by the TMS coil depends on the conductive medium underneath the coil and it determines the main part of the total induced field. The importance of a realistic coil description over a simplified coil description¹⁰⁵ has

a (FLIRT - FMRI's Linear Image Registration Tool, <http://www.fmrib.ox.ac.uk/fsl/flirt/index.html>)

b <http://www.fil.ion.ucl.ac.uk/spm/>

c <http://surfer.nmr.mgh.harvard.edu/>

already been shown in earlier studies^{174,194}. The methods and head model developed for this sensitivity study can be used in future TMS investigations and can therefore be considered as valuable results in themselves.

7.2 METHODS

7.2.1 Head model

A highly realistic head model was constructed using three-dimensional boundaries of eight different tissue types (skin, skull spongiosa, skull compacta, neck muscle, eye, CSF, GM and WM), which were based on T1 and T2 magnetic resonance images (MRI) scans of a healthy 25-year old male subject with 1 mm³ resolution. The construction of this standard model can be split up in five steps, namely MRI (figure 7.1(A)) and diffusion tensor image (DTI) acquisition, automatic segmentation of different tissues with manual corrections (figure 7.1(B)), extraction of high resolution triangular surface meshes, construction of a volume mesh with linear tetrahedral elements (figure 7.1(C)) and inclusion of anisotropic conductivity tensors. A detailed description of the standard model is added in appendix A (section 10.1). As also explained in appendix A (subsection 10.1.1), in this study the WM surface was not used in the construction of the volume mesh, but afterwards to assign the resulting tetrahedrons within the brain compartment to either GM or WM. Also the cerebellum was not included in the head model.

An important aspect of a realistic head model in TMS simulations is brain anisotropy^{105,116,143}. For adult human subjects, the effect of brain anisotropy on the induced electric field is mainly significant for the white matter (WM), but some smaller effects can be found for the GM as well¹⁴³. Therefore, brain anisotropy was also included in the standard and altered models used in this study (figure 7.1(D)). The brain anisotropy was based on the diffusion tensors from DTI data, using the volume-normalized approach as described in¹⁴³. The bulk conductivity values for all tissues can be found in table 7.1.

7.2.2 Cortical geometry alteration

To study the effects of changes in the cortical surface geometry on the electric field, the GM surface mesh used in the standard model was altered by a process of either erosion or expansion of the gyri. The triangular surface meshes of other tissues were kept the same. For the construction of the altered surfaces, the nodes of the standard GM surface were shifted along their normal vectors relative to the surface (inward for erosion and outward for expansion). They were shifted 0.5, 1.0 and 1.5 mm in positive or negative direction. Because this alteration was applied to the whole surface and therefore also to both walls of one sulcus, the total change would be comparable to an incorrect segmentation of 3

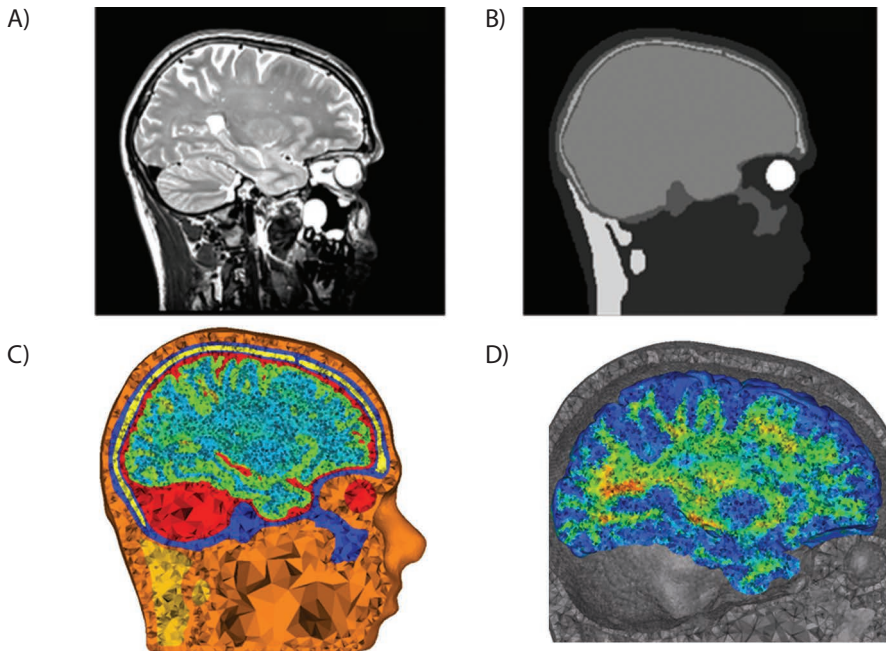


FIGURE 7.1. (A) A sagittal cut plane of the T2w MRI showing the different skull layers. (B) The same sagittal cut plane of the manually corrected segmentation including skin, skull compacta, skull spongiosa, neck muscle, eyes and one compartment for inner skull (CSF, GM and WM, before segmentation with Free-surfer). (C) Sagittal cut plane of the final tetrahedral volume mesh. The different tissue types are represented with different colors. The corresponding bulk conductivities are given in table 7.1. (D) Sagittal cut plane of the brain mesh with the fractional anisotropy on a scale from 0 (blue) to 1 (red). The maximal fractional anisotropy value in the brain is 0.99 and the minimum is 0.

TABLE 7.1. The bulk conductivity values ($S\ m^{-1}$) for all the tissue types used in the standard model.

	BULK CONDUCTIVITY VALUES
Skin	0.465^{214}
Skull compacta	0.007^1
Skull spongiosa	0.025^1
CSF	1.65^{214}
Neck muscle	0.4^{43}
Eyes	1.5^{128}
GM	0.276^{214}
WM	0.126^{214}

sulci voxels in an MRI scan with 1 mm resolution. The spatial effect of 1.5 mm erosion or expansion on a specific sulcus is illustrated in figure 7.2. Intersections caused by shifting the nodes were solved using open source software MeshFix⁴. The expanded surface meshes had less nodes and triangles because of disappearing sulci. To avoid differences in the electric field caused by a change in CSF thickness between the top of the gyri and the skull^{17,211} and the distance of the cortical surface to the TMS coil, the altered surfaces were up- or down-scaled to fit the dimensions of the standard GM surface again. The cortical TMS target location was set at the same location as in the standard model. This way only the differences in width of the sulci distinguish the altered models from the standard model. The altered surfaces were incorporated in new tetrahedral models and the final volume meshes had between 3.50M and 4.04M elements.

The anisotropic brain conductivity tensors were mapped from the hexahedral MRI mesh onto the altered models in the same way as for the standard model (subsection 10.1.7). The additional elements in the expanded models were assigned the conductivity tensors from the nearest elements in the hexahedral MRI mesh.

7.2.3 Finite element method

The finite element method is widely used to compute the spatial distribution of the electric field and current distributions that arise from electromagnetic phenomena in three-dimensional models. For the application of TMS we used the simplification of the full Maxwell's equations by a quasi-static system wherein we neglect the displacement currents. Neglecting the displacement currents was justified in an earlier study²¹⁴.

Consequently the total electric field \vec{E} induced by the TMS coil is described by:

$$\vec{E} = -\frac{\partial \vec{A}}{\partial t} - \nabla \varphi \quad (7.1)$$

with $\frac{\partial \vec{A}}{\partial t}$ being the time-derivative of the magnetic vector field and φ the electrical scalar potential. The first term, also called the primary component, is completely determined by the TMS coil and can be calculated at the center of each element in the tetrahedral volume mesh. The second term, called the secondary component, describes the charge accumulation at conductivity discontinuities in the volume mesh and needs to be computed with the FEM. The primary component is computed by:

$$\frac{d\vec{A}}{dt} = \frac{\mu_0 N dI/dt}{4\pi} \int \frac{d\vec{l}}{|\vec{r} - \vec{r}_0|} \quad (7.2)$$

with μ_0 the permeability of free space, N the number of windings in the TMS coil, $\frac{dI}{dt}$ the time dependent coil current, $d\vec{l}$ an infinitesimal vector representing an element of the

wire through which the current passes and $|\vec{r} - \vec{r}_0|$ the distance between a point in space and that coil element. The spatial distribution of the primary electric field component thus fully depends on the geometry of the coil. Therefore, an accurate description of the coil should be used¹⁷⁴.

Because the figure-of-eight coil can be considered the standard coil in fundamental TMS research, such a coil was simulated. The position and orientation of the coil with respect to the head were based on experimental data measured using the Localite^d neuronavigational system. This coil position showed the highest motor evoked potential (MEP) in the first dorsal interosseous (FDI) muscle of the healthy 25-year old male subject and is therefore called the 'FDI hotspot' position.

The resulting relative spatial distribution of the field is independent of the absolute coil current. For simulations, the field distribution was scaled such that the maximum primary field strength was 300 V m⁻¹. This is approximately 45% of the maximum intensity of a biphasic pulse measured for the simulated figure-of-eight coil¹⁷⁴. This intensity evoked the MEP mentioned earlier with a mean amplitude of 1.0 mV in the subject on whom the standard model is based.

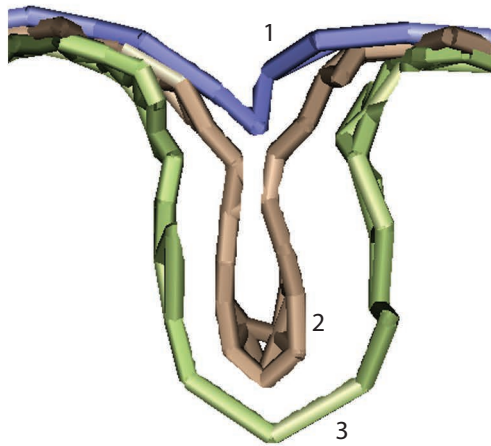


FIGURE 7.2. *The effect of erosion and expansion on a sulcus. In the middle a sulcus of the standard model is shown (2), at the bottom the sulcus of a 1.5 mm eroded surface (3) and at the top the sulcus of a 1.5 mm expanded surface (1). All other alterations lie between these two boundaries.*

The secondary component of the induced electric field is caused by the discontinuities in the conductivity σ . The induced electric field causes a current density \vec{J} following Ohm's law:

$$\vec{J} = \vec{E} \sigma \quad (7.3)$$

Perpendicular to the boundary between elements, this induced current is continuous, which yields the following constraint across boundaries:

$$\vec{J}_1 \cdot \vec{n} = \vec{J}_2 \cdot \vec{n} \quad (7.4)$$

When the medium is inhomogeneous, a discontinuity in the electric field occurs at the boundary between tissues with different conductivities¹¹⁶. Because the magnetic vector field is determined only by the properties of the TMS coil, this change is caused by a difference in potential gradient at the tissue boundaries.

To acquire the potential gradient in equation 7.1 we make use of the fact that in the quasi-static limit the divergence of the induced current has to be zero:

$$\nabla \cdot \vec{J} = 0 \quad (7.5)$$

By combining equations 7.1, 7.3 and 7.5 the continuity equation under quasi-static condition follows:

$$\nabla \cdot \left(-\sigma \frac{\partial \vec{A}}{\partial t} - \sigma \nabla \varphi \right) = 0 \quad (7.6)$$

The Neumann boundary condition states that no current leaves the volume conductor, so at the outer boundary we have:

$$\vec{J} \cdot \vec{n} = 0 \quad (7.7)$$

This equation combined with equations 7.1 and 7.3 yields:

$$\left(\sigma \frac{\partial \vec{A}}{\partial t} \right) \cdot \vec{n} = -(\sigma \nabla \varphi) \cdot \vec{n} = 0 \quad (7.8)$$

The potential φ , solved by the FEM, is then used in combination with the primary field $\frac{\partial \vec{A}}{\partial t}$ to calculate the total electric field for each element inside the volume conductor using equation 7.1.

The construction of the coil geometry and the placement over the models was performed with custom written MATLAB^e code. The calculation of the magnetic vector field was done with a custom written C++^f program for each model individually following a discretized version of equation 7.2. The total number of wire elements (184k) was determined by doubling the number of elements step by step until the resulting magnetic vector field, calculated on the standard model, differed less than 1 percent compared to the magnetic vector field of the previous step. For the FEM calculations the freely available SCIRun^g software was used. The system of linear equations was solved with a preconditioned Jacobi conjugate gradient method with residuals $< 10^{-15}$. It took approximately 2.5 minutes to solve the system of linear equations with SCIRun on a Mac Pro, 2.66 GHz Quad-Core Intel Xeon with 16 GB memory.

The cortical erosion process can produce a very small number of elements which are less shape-regular. For example, in TetGen^h, the ratio of $Q=R/L$ is used for determining shape-regularity with R the radius of the outer circumsphere and L the length of the shortest edge of an element. Numerical convergence properties (Braess 2007²², *Theorem 7.3*) depend on the shape regularity of the elements. Less shape-regular elements (larger Q) lead to larger convergence constants that might result in less numerically accurate potential values within or close to the deformed elements. Furthermore, the secondary component (*equation 1*) is calculated by taking the gradient of the potential. The diminished accuracy of the potential values at the nodes of large- Q elements then propagates into a diminished accuracy of the potential gradient vectors. For these reasons the maximum field strength is not the best comparison measure and we have used the more robust median of the 1 percent highest electric field values instead. The few badly shaped elements that possibly lead to a few outliers do not influence this median value of the 1 percent highest electric field values.

7.2.4 Comparison methods

The induced electric fields predicted for the altered head models were compared with the results from the standard model in two ways, namely in a cross section of the volume meshes through a sulcus near the hotspot and over the whole cortical surface. For generalization of the results found for optimal stimulation of the FDI hotspot on the left hemispheric motor cortex (M1), the whole procedure was repeated for three more coil orientations (90, 180 and 270 degree turn compared to optimal) and three other brain areas (right hemispheric motor cortex, left hemispheric inferior frontal gyrus and left hemispheric visual cortex).

e MathWorks, Natick, Massachusetts, USA

f The C++ programming Language, Addison-Wesley, 1986. A general purpose programming language.

g The freely available SCIRun 4.5 (Scientific Computing and Imaging Institute, Salt Lake City, UT)

h TetGen: A Quality Tetrahedral Mesh Generator and a 3D Delaunay Triangulator, <http://tetgen.berlios.de/>

For the whole cortical surface comparisons, the electric field on the GM side of the CSF-GM boundary was used. In this way the effects of alterations in the cortical geometry on the induced field just beneath the cortical surface are compared. This is important because there is sufficient evidence that the TMS-induced activation occurs mostly at the interneurons in the GM⁹⁹. The surfaces after expansion had less nodes and triangles because of the disappearing sulci. For this reason, only the nodes in the altered model for which the original node could be located in the standard model were used in the surface comparison.

For the quantification of the difference between two models the relative difference measure (RDM)¹⁰ and the magnification (MAG) factor¹⁰ were used:

$$RDM = \sqrt{\frac{\sum_{i=1}^M |\vec{E}_{a_i} - \vec{E}_{std_i}|^2}{\sum_{i=1}^M |\vec{E}_{std_i}|^2}} \quad (7.9)$$

and

$$MAG = \sqrt{\frac{\sum_{i=1}^M |\vec{E}_{a_i}|^2}{\sum_{i=1}^M |\vec{E}_{std_i}|^2}} \quad (7.10)$$

Here \vec{E}_a is the electric field on a node i in the altered model and \vec{E}_{std} the electric field on the same node i in the standard model.

TABLE 7.2. The median of the top 1 percent highest electric field values (V m⁻¹), for each tissue type in the standard model and all altered models.

TISSUE TYPE	MEDIAN OF THE TOP 1 % HIGHEST ELECTRIC FIELD VALUES						
	1.5 mm expansion	1.0 mm expansion	0.5 mm expansion	Standard model	0.5 mm erosion	1.0 mm erosion	1.5 mm erosion
Skin	159	159	159	159	159	159	159
Skull compacta	185	183	182	182	182	182	182
Skull spongiosa	142	142	142	142	142	142	142
CSF	119	117	115	117	116	113	116
Neck muscle	7	7	7	7	7	7	7
Eyes	7	7	7	7	7	6	7
GM and WM	94	92	92	97	100	105	113

7.3 RESULTS

7.3.1 Cortical geometry alteration

The electric field throughout the whole volume mesh was computed. Table 7.2 shows the median of the top 1 percent absolute field strength values in the different tissue types of all models. All models show the highest and almost identical values for the electric field in the skin and the skull compacta. The relatively small distance to the coil causes these high values within the skin. The even higher values inside the skull compacta are caused by its relatively low conductivity compared to the neighboring tissue types (skin, skull spongiosa and CSF). Here the secondary field has its main effect. The alterations to the cortical surface do not affect the maximum field strength in the skin, skull spongiosa, neck muscle and eyes. For the skull compacta the maximum field strength increases slightly with cortical expansion.

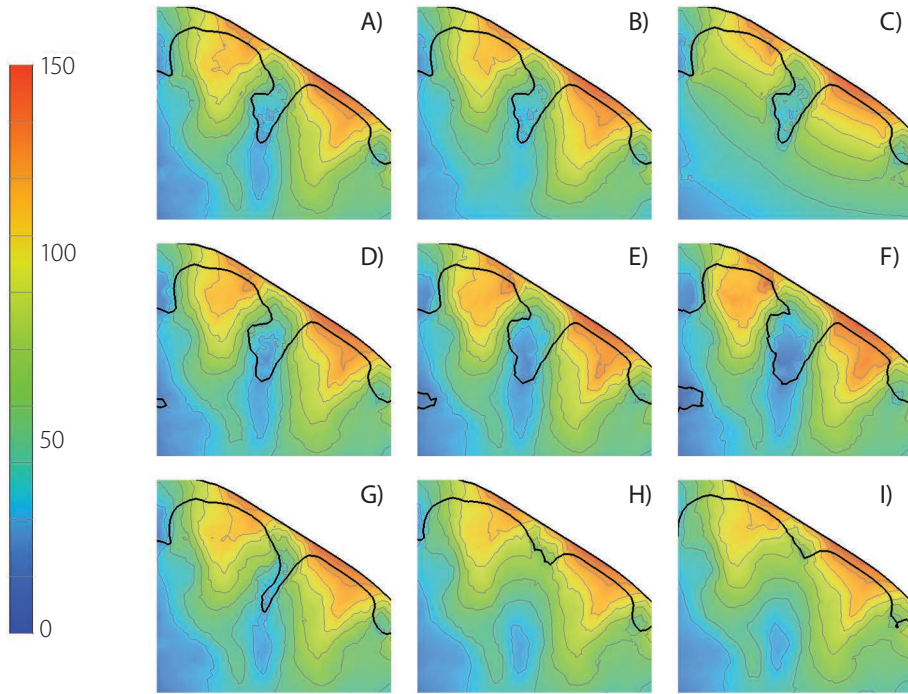


FIGURE 7.3 (A) The electric field distributions ($V m^{-1}$) in a cross section of the standard model with brain anisotropy. The black lines show the boundaries between the CSF and the skull and the CSF and GM. (B) The same cross-section for an inhomogeneous brain with the bulk conductivity for GM and WM and (C) for a homogeneous brain with the GM bulk conductivity. Subsequently the cross-section for the anisotropic brain with (D) 0.5 mm erosion, (E) 1.0 mm erosion, (F) 1.5 mm erosion, (G) 0.5 mm expansion, (H) 1.0 mm expansion and (I) 1.5 mm expansion. In all panels the field strength is displayed on a scale from 0 to $150 V m^{-1}$.

Although it is relevant to know the intensities induced in other tissue types, our main interest of course concerns the field in the brain. The alterations have an opposite effect on the electric field in the brain compared to that in the skull compacta. The maximum field strength increases with cortical erosion. A slight decrease can be seen for the brain tissue with expansion. No clear effect can be seen in the CSF.

Figure 7.3A shows a cross-section around a sulcus in the standard model. The black lines show the boundaries between the CSF and the skull and the CSF and GM. The electric field in the CSF of the sulcus is relatively low (blue color) compared to the electric field in the brain structures (orange). The locations where the CSF is thinnest, between the cortex and the skull, have the highest field strengths. This is in accordance with previous reports¹⁷. Figure 7.3B shows the electric field in the standard model with an inhomogeneous isotropic brain to illustrate the effect of the inclusion of brain anisotropy on the electric field. The differences (compared to figure 7.3A) are small and can mostly be found in the WM, confirming previous reports^{105,143}. The electric field in the standard model with a homogeneous isotropic brain is shown in figure 7.3C, to illustrate the effect of tissue inhomogeneity. In a homogeneous model the electric field in the deeper brain regions consists almost exclusively of the primary field, because there are no conductivity boundaries. Tissue inhomogeneity (present in figures 7.3A and 7.3B) introduces additional boundaries inside the brain because of the change in bulk conductivity for the WM region. The tissue inhomogeneity causes an increase in field strength in the gyri and in the WM beneath the gyri. The field strength decreases in the brain region beneath the sulci.

In figure 7.3D-F, the effects of erosion of the cortical surface (of the standard model in figure 7.3A) are shown. When the cortical surface is eroded, more CSF is introduced and the tops of the gyri become narrower. An increase in sulcus width causes the electric field to become more focal on top of the gyri and to increase in absolute field strength at these locations. The overall effects of the alterations are mainly present in the areas close to the cortical surface. The part of the volume mesh that is distant to the CSF shows only minor or no differences compared to the standard model.

In figure 7.3G-I the effects of expansion are shown. As expected the decrease in sulcus width by expansion causes an increase in the electric field between the original gyri.

TABLE 7.3. The median of the top 1 percent of (1) the highest electric field values (V m^{-1}) and (2) the highest differences in the electric field values (V m^{-1}).

MODEL	MEDIAN VALUE 1% HIGHEST:	
	Electric field values (V m^{-1})	Differences in electric field values (V m^{-1})
1.5 mm erosion	131	25
1.0 mm erosion	123	16
0.5 mm erosion	119	8
Standard	117	0
0.5 mm expansion	112	9
1.0 mm expansion	113	13
1.5 mm expansion	116	14

All values are based on the cortical surface of the standard model and all altered models.

7.3.2 Cortical surface

The experimentally identified 'FDI hotspot' was located at the top of a gyrus of the hand area of the motor cortex (figure 7.4A, *black dot*). At this location the electric field is maximal (figure 7.4A). In addition to the motor cortex, also parts of the pre-motor and sensory cortex appear to be stimulated with a similar intensity. In most cases the highest values for the electric field are located at the crowns and lips of the gyri, which is in accordance with earlier reports^{17,195}. The median of the top 1 percent electric field values just below the cortical surface are given in table 7.3.

An increase of the sulcus width increases the area for which the induced field strength is above a certain threshold (figure 7.4B). This means that the electric field is less focal in a human brain with wide sulci compared to a brain with narrower or no gyri. Figure 7.4B shows the area with an induced field above 123 (V m^{-1}). Expansion of the cortical surface has an opposite effect to erosion, but the effect is smaller.

In the eroded brain surface (figure 7.4C) the maximum field strength is increased and other peaks in the field occur at gyral lips. The wider sulci cause an increase in electric field strength at the gyral crowns and lips and a larger dispersion of high intensity field peaks. These other peaks especially occur at the new sharp gyral lips that lie distal from the FDI hotspot. Figure 7.4D shows the difference in the electric field strength at the cortical surface level between the eroded and standard model. The difference between the models is especially found at the gyral lips over a widespread area. The majority of the electrical field values differ less than 13 (V m^{-1}), which is 10 percent of the maximum value in the standard model.

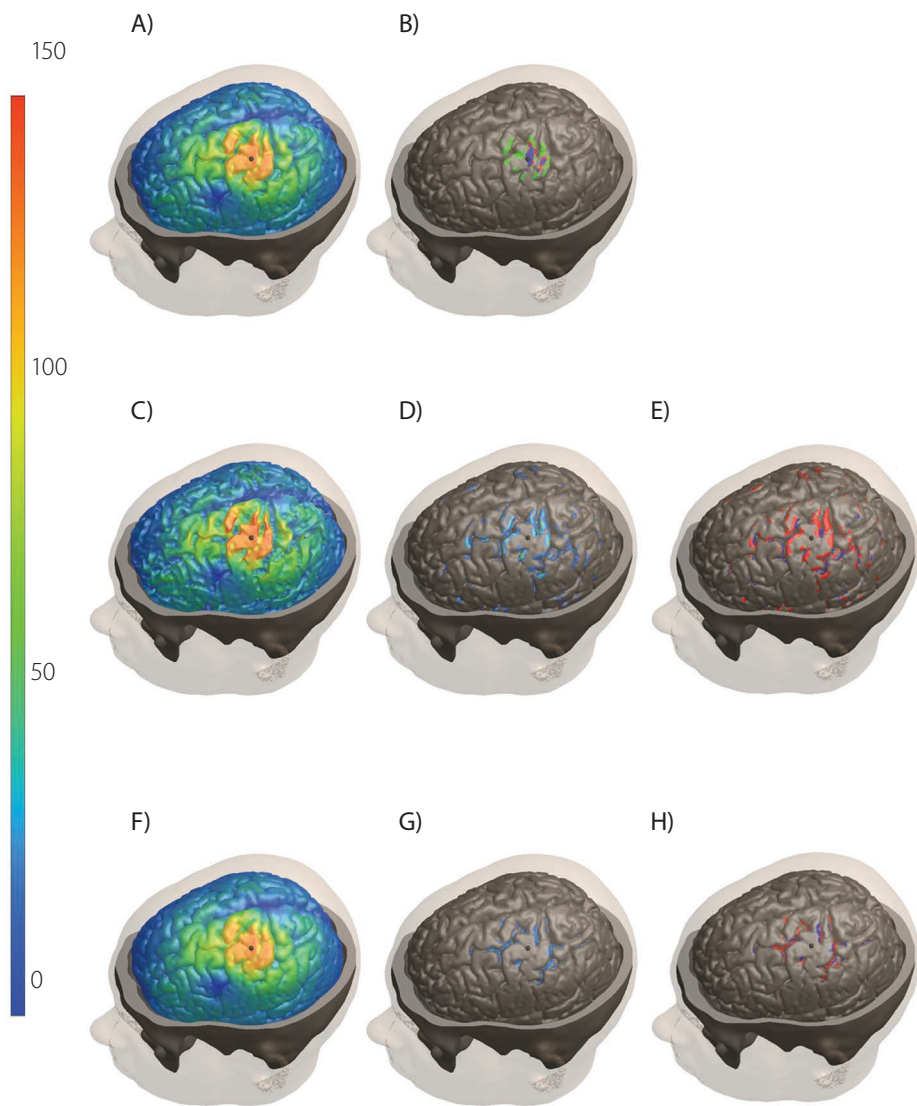


FIGURE 7.4. Top row: (A) The induced electric field (V m^{-1}) just below the cortical surface of the standard model and (B) the areas stimulated with more than 123 (V m^{-1}) for the 1.5 mm expanded model (blue), the standard model (red) and the 1.5 mm eroded model (green). Middle row: For the 1.5 mm eroded model, (C) the induced electric field (V m^{-1}), (D) the magnitude of the differences with the standard model and (E) the direction of the differences (red, the altered model has a higher electric field strength, blue the altered model has a lower electric field strength). Bottom row: For the 1.5 mm expanded model, (F) the induced electric field (V m^{-1}), (G) the magnitude of the differences with the standard model and (H) the direction of the differences. The differences in panels D, E, G and H are projected on the standard model surface. In panels (A, C, D, F & G) the field strength is displayed on a scale from 0 to 150 (V m^{-1}).

Figure 7.4E provides information about the direction of the change in the electric field. The electric field in the eroded model is higher at the top of the gyri (*red*) and lower in the sulci (*blue*).

As was expected, expansion of the cortical surface has an opposite effect to erosion (figure 7.4F-H). The expanded brain surface shows a wide dispersion of the electric field and overall lower values on top of the gyri and higher in the (former) sulci. The median of the top 1 percent electric field values differs only moderately from the standard model (table 7.3), but there are clear differences in field strength locally.

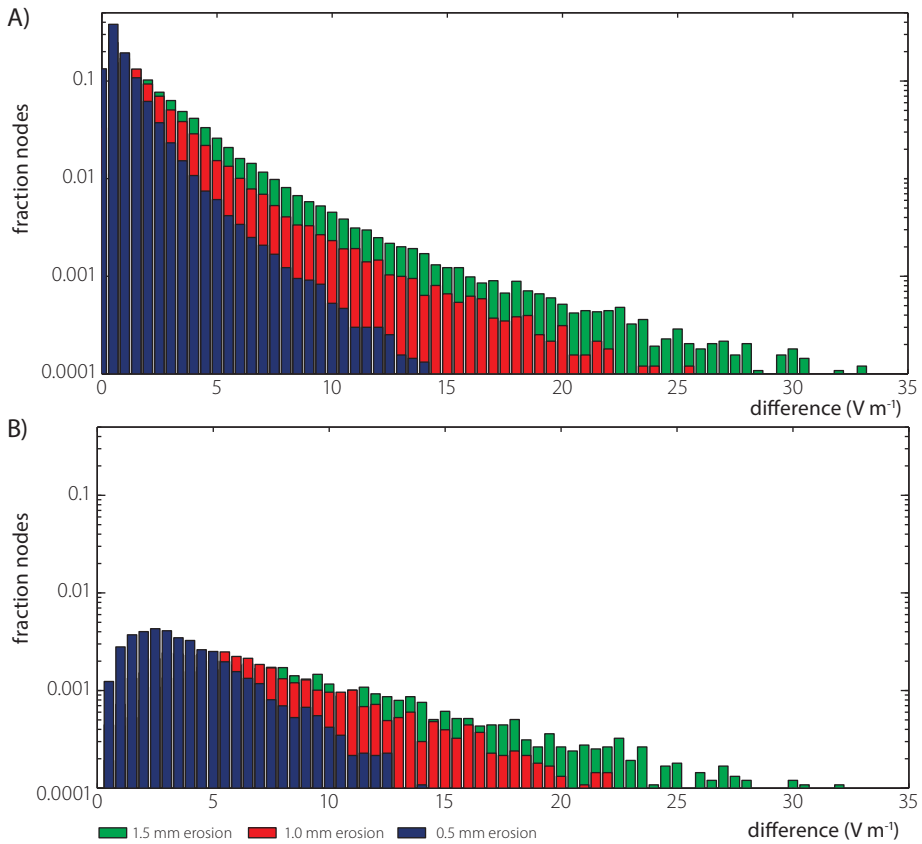


FIGURE 7.5. Two logarithmic histogram plots that show the differences in electric field strength for the nodes of the cortical surface with eroded sulci compared to the standard cortical surface. Only differences up to 35 V m⁻¹ (the far majority) are shown. (A) The differences between all comparable nodes in the standard model and the nodes in a model with 0.5 mm erosion, 1.0 mm erosion and 1.5 mm erosion. (B) The same comparison, but only for the nodes that are within a 30 mm radius of the cortical FDI hotspot.

TABLE 7.4. RDM and MAG value.

ALTERATION	LEFT M1				RIGHT M1		LEFT IFG		LEFT OC	
	Optimal orientation		+90 deg		Optimal orientation		Optimal orientation		Optimal orientation	
	RDM	MAG	RDM	MAG	RDM	MAG	RDM	MAG	RDM	MAG
1.5 mm erosion	0.22	1.11	0.20	1.09	0.21	1.10	0.20	1.09	0.19	1.09
1.0 mm erosion	0.14	1.06	0.13	1.05	0.13	1.06	0.13	1.05	0.12	1.05
0.5 mm erosion	0.08	1.03	0.07	1.02	0.07	1.03	0.07	1.02	0.07	1.02
0.5 mm expansion	0.08	0.99	0.08	0.99	0.07	0.98	0.07	0.99	0.07	0.98
1.0 mm expansion	0.11	0.97	0.10	0.97	0.10	0.97	0.10	0.97	0.10	0.97
1.5 mm expansion	0.10	0.96	0.10	0.96	0.09	0.96	0.09	0.97	0.09	0.96

The RDM (equation 7.9) and MAG (equation 7.10) values calculated over the cortical surface between the altered models and the standard model. The calculations are repeated for stimulation over 4 different brain areas (left hemispheric M1, right hemispheric M1, left hemispheric inferior frontal gyrus (IFG), and left hemispheric visual cortex (OC)). For the left hemispheric M1, 2 coil orientations are represented.

7.3.3 Alteration magnitude

The degree of alteration in the cortical surface has an effect on the differences in the electric field compared to the standard model. A higher degree of erosion induces larger changes in the electric field compared to the field in the reference model (figure 7.5A-B). When only a small alteration of 0.5 mm is applied to the cortex, the change in field strength is less than 15 V m^{-1} for almost all locations. However, an increase in erosion to 1.0 mm or 1.5 mm introduces a large number of surface nodes whose fields differ far more than 15 V m^{-1} from the standard model. Most of these larger differences apply to the nodes within a range of 30 mm to the cortical hotspot (figure 7.5B).

The RDM is a measure for the difference over all surfaces nodes. The value for the cortical surface demonstrates the dependency on the degree of alteration. Table 7.4 shows that for the eroded model the RDM value of the cortical surface can go up to 0.22 for an alteration of 1.5 mm. The RDM value has a clear correlation with the magnitude of the alteration: the bigger the erosion, the bigger the value.

The comparison between the standard model and the expanded models shows a less strong dependency. The reason is that the nodes in the sulci are removed after expansion and only the nodes at the top of the gyri can be compared. This causes a ceiling effect in the differences between the expanded and standard model. The MAG values show that

the field strength increases with erosion, while the strength decreases with expansion. Similar RDM and MAG values are found for three more TMS coil orientations and for three different brain areas. Only two coil orientations are shown in table 7.4, because turning the TMS coil 180 degrees and from -90 to +90 degrees produced the same RDM and MAG values, as would be expected.

7.4 DISCUSSION

7.4.1 Global versus local changes in electric field

The results from this study show that most of the changes in the simulated electric field caused by a slight alteration to the cortical surface are small and rather patchy. Alterations in sulcus width up to 1.5 mm do not drastically change the electric field distribution globally, as has been shown before⁹⁴. These results would indicate that for a global approximation of the electric field the incorporation of an accurate description of the sulci (+/- 3 mm in width) is not highly important. However, incorporation of wide sulci (and consequently thin gyri) will cause high electric field values at gyri more distant from the stimulation target. This means that for estimations about the maxima in the electric field, these alterations may be relevant.

7.4.2 The effects of alteration on the electric field

In all model versions, the electric field is highest at the top and lips of the gyri, which is in accordance with the results of previous studies^{17,195}. As the distance between the skull-CSF and CSF-GM boundary decreases, the electric field strength at these boundaries increases. This effect causes the highest peaks in electric field to occur at the gyral crowns and lips (figure 7.3). Locations with lower electric field values can be found in the sulci. The largest differences caused by the cortical alterations can be found at the gyral lips. An effect was found both on field strength and on field distribution. Overall, the cortical alterations do not affect deeper brain areas. The alterations to the cortical geometry change the thickness of the gyral tops and thereby alter the length of the narrow passages between the cortex and the skull. In the case of erosion the gyral crowns decrease in width and thereby the maximum electric field strength increases at the gyral lips and at the top of the gyri as well. The opposite effect can be seen in the case of expansion. These results suggest that especially the ratio between the volume of CSF on top of a gyrus and in the neighboring sulci has an effect on the electric field strength.

The simulations with the eroded surfaces show that a cortical surface with narrow gyri can have multiple peaks in the electric field. These can be distant from the targeted FDI hotspot (figure 7.4B-C). Most of the peaks can again be found on the crown or lips of gyri.

7.4.3 Neuron models

The precisely studied differences in field strength caused by the alterations may not be relevant for a global estimation of the induced electric field, but are relevant for the future combination with neuron models. For a complete understanding of TMS effects at a neuronal level, volume conduction models must be combined with neuron models¹⁷⁵. But for neuron models to be of value, realistic field estimations are a *condicio sine qua non*.

There is evidence that the first neuronal activation by TMS, presented as I-waves in subdural recordings, takes place at the level of the interneurons in the GM⁹⁹. Only with high stimulation intensities the direct activation of the neuronal axons is achieved, presented as direct waves (D-waves), generated in or close to the WM. The effects of cortical alteration are mainly found near the CSF-GM boundary and will therefore probably only affect the electric field that produces the indirect waves (I-waves).

There is also evidence that the actual activation of neurons is directly related to the electric field (i.e. the gradient in the potential) along the axon¹⁶⁸. This means that cortical sites that have high electric field strength parallel to an axon are the most likely locations to become activated. Previous model studies already concluded that the sites of neuronal activation are gyral crowns with neurons that are aligned with the primary field and axon collaterals and terminations in the lip of the gyrus^{175,184}. These are also the locations with the highest electric field strength in our simulations. The effect of cortical alterations on the neurons in the gyral crowns is minimal (figure 7.4D) and figure 7.4F). For the axon collaterals and terminations in the gyral lips the effects are largest.

7.4.4 Limitations of the presented study and future model studies

A previous study showed that the resolution needed for TMS simulations is 2 mm⁹⁴. In that particular study, the effects of different hexahedral grid resolutions on the calculated average TMS field strength within a specified analysis volume were reported. The authors observed no changes in the electric field due to increase in grid resolution from 0.25 mm to 2.00 mm. Our study is partially in agreement with these previous results, because globally no large differences are observed. However, our results provide additional information about local changes in the electric field that are possibly relevant for future studies with neuron models.

This study primarily looked at the influence of the effect of sulcus width in the cortical surface. To isolate the effects of erosion and expansion, we corrected the model versions for the large effect of a change in CSF thickness^{17,211}. This way also the distance of the cortical surface to the TMS coil was the same for all models.

The comparison between an isotropic and anisotropic brain was already made in earlier studies which showed that the differences caused by anisotropy were mainly present in the WM¹⁴³. The average difference was around 8 percent in the WM and could rise up to 40 or 50 percent locally. In the GM the authors only found less than 1 percent difference between an isotropic and anisotropic brain. The sulcus width as considered in this study has its main effect on the electric field near the CSF-GM boundary, so no strong effects of brain anisotropy was to be expected. To verify that brain anisotropy has no effect on the main conclusions of this study, all comparisons have been repeated with an isotropic brain (gray and white matter). The RDM values for these comparisons are similar to the ones produced with an anisotropic brain (0.22 for 1.5 mm erosion and 0.10 for 1.5 mm expansion, table 7.4) for the optimal orientation.

Permittivity has also an influence on the effective conductivity of several tissues⁵⁸. This would imply a scaling of some conductivities in our quasi-static model. We verified that this would not influence the main message of this study.

The WM surface was not included in the construction of tetrahedral models, because it caused too many intersections in the triangular surface meshes after the cortical alterations. Instead the WM surface was used to assign WM labels to elements in the final tetrahedral volume meshes and give them the corresponding bulk conductivity. In other studies that used a realistic head model, this WM surface was included in the construction¹⁴³. The segmentation and construction of the WM surface with the standard software packages is subject to the same errors and difficulties as the GM surface^{86,183}. Therefore, the assumption can be made that alteration of this surface can also have an influence on the induced electric field. However, in this study we decided to focus only on the alterations in the GM surface, because it has the most prominent conductivity jump and is closer to the TMS coil.

A different option for a volume conductor model is a hexahedral model directly derived from the measured MRI data¹⁰⁵. This approach allows for an easy and automated FEM mesh generation without the manual work steps involved in the construction of tetrahedral head models. However, the tissue boundaries in this kind of volume mesh will contain geometrical imperfections. This study showed that even small differences to the cortical geometry could locally induce relevant differences in the electric field distribution. A possible way to overcome imperfections of a hexahedral model could be the use of partial volume CSF modelling⁷⁸ or geometry-adapted hexahedral meshes²²⁰.

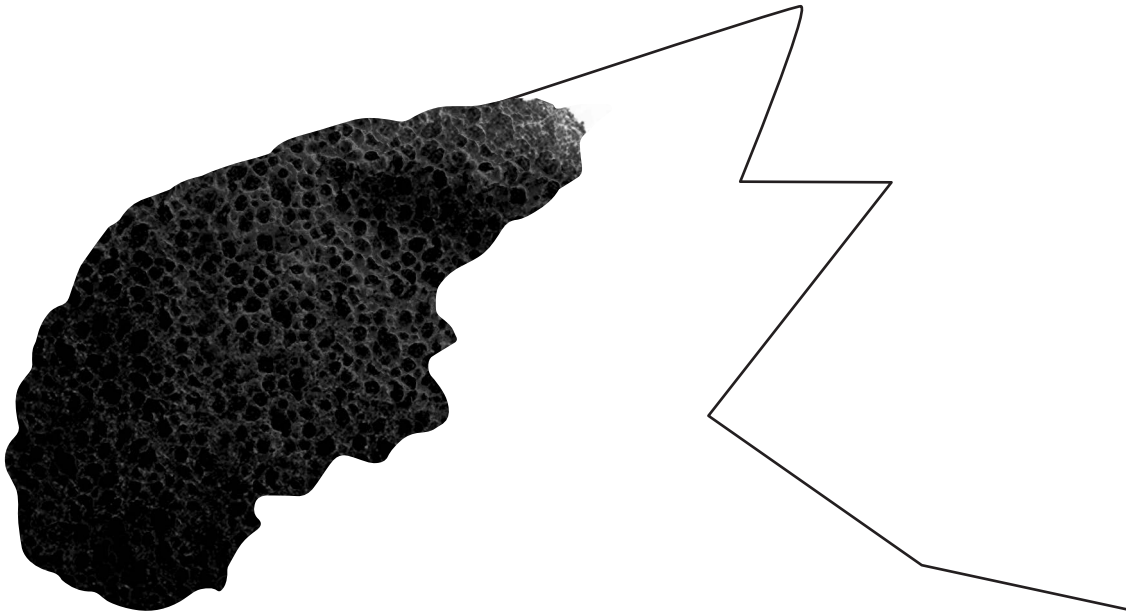
Finally, the results from this study could have consequences for future patient specific models. Several brain diseases, like Alzheimer's disease and stroke are caused by real

geometrical changes in the cortex. The induced field caused by TMS in these diseased brains will therefore have a specific effect. This was found in a first simplified brain model for stroke²¹², but the present study shows that even small alterations can induce relevant effects.

7.5 CONCLUSION

In a highly realistic head model, alterations in sulcus width (up to 3 mm) do not cause large differences in the calculated electric field values for most areas of the brain. For a global approximation of the electric field, the incorporation of an accurate description of the sulci is not highly important. However, considerable overestimation of sulcus width produces an overestimation of the local field strength, also at locations distant from the cortical hotspot. This means that for estimations about the maxima in the electric field and (future) combinations with neuron models, an accurate description of the sulcus width is advisable.





Published as:

Janssen AM, Oostendorp TF, Stegeman DF.

The effect of local anatomy on the electric field induced by TMS: evaluation at 14 different target sites.

Medical & Biological Engineering & Computing, Vol. 52, p. 873-883, 2014

8.

THE EFFECT OF LOCAL ANATOMY ON THE ELECTRIC FIELD INDUCED BY TMS: EVALUATION AT FOURTEEN DIFFERENT TARGET SITES

ABSTRACT

Many human cortical regions are targeted with transcranial magnetic stimulation (TMS). The stimulus intensity used for a certain region is generally based on the motor threshold (MT) stimulation intensity determined over the motor cortex (M1). However, it is well known that differences exist in coil-target distance and target site anatomy between cortical regions. These differences may well make the stimulation intensity derived from M1 sub-optimal for other regions.

Our goal was to determine in what way the induced electric fields differ between cortical target regions. We used finite element method (FEM) modeling to calculate the induced electric field for multiple target sites in a realistic head model. The effects on the electric field, due to coil-target distance and target site anatomy have been quantified.

The results show that a correction based on the distance alone does not correctly adjust the induced electric field for regions other than M1. Also a correction based solely on the TMS-induced electric field (primary field) does not suffice. A precise adjustment should include coil-target distance, the secondary field caused by charge accumulation at conductivity discontinuities and the direction of the field relative to the local cerebro-spinal fluid – gray matter (CSF-GM) boundary.

8.1 INTRODUCTION

Transcranial magnetic stimulation (TMS) is a powerful tool in the neurosciences to study brain functions by non-invasively depolarizing groups of neurons. A strong electric current is briefly sent through a coil, which produces a time-varying magnetic field. When the coil is placed on top of a subject's head, this magnetic field consequently induces an electric field in the head as described by Faraday's law of induction. TMS can be used as a tool to investigate causal relationships in the brain and also to study the relation between cognitive processes and their neural substrates in combination with functional magnetic resonance imaging (fMRI)¹⁰³. Since its introduction⁸, most protocols have been designed for the motor cortex (M1). This is mainly due to the fact that the outcome can be objectified by measuring motor evoked potentials (MEPs) in the targeted muscles. For clinical use and research purposes, TMS has a substantial advantage over transcranial electrical stimulation (TES)¹¹¹, because it causes little to no pain. The minimal intensity to evoke an MEP is called the motor threshold (MT) and it has to be determined for each subject individually, due to large inter-individual differences in brain anatomy.

Protocols to stimulate other cortical regions have been developed as well^{3,13,72,80,95,124,155}, but none of these regions have an easily observable outcome measure like the MEP. The intensity used for stimulation of these brain regions is therefore generally based on the MT found over M1. However, this intensity is probably sub-optimal for other regions due to the large intra-individual differences in coil-target distance and target site anatomy. One can therefore argue that, in order to optimize TMS protocols, the intra-individual differences between cortical regions should be included in the determination of the stimulation intensity. Applying a coil-target distance related correction factor, as done in previous reports^{190,201}, is a logical first step. However, these correction factors were all determined with experiments performed over the same cortical location and thereby ignore intra-individual differences in target site anatomy. A different approach is to determine the primary electric field at the cortical level, using a neuronavigation system (*The primary and secondary fields together constitute the total induced electric field, Methods 8.2.3*). Knowledge of the primary field can be used to adjust the stimulation intensity before starting stimulation¹⁶⁵, or to correlate the measured outcome to the primary electric field intensity at the cortical level post-intervention¹⁴⁰. Unfortunately, this approach ignores the secondary field and the effect of electric field direction relative to the underlying cortical surface.

In this study we tried to estimate how the (1) coil-target distance and (2) target site anatomy influence the stimulation intensity at the target site. The target site anatomy has an impact on the stimulation intensity in two different ways, namely (1) the secondary field is influenced by charge accumulation at conductivity discontinuities and (2) the effectiveness of

stimulation depends on the direction of the electric field relative to the cortical surface of the target site. We state that both components of target site anatomy influence the effective electric field in such a way that they have to be included for a proper adjustment of the TMS stimulation intensity. A correction for the coil-target distance, or solely the primary electric field, is not sufficient. To verify this argument, we used computer modeling to compare calculated induced electric fields for multiple target sites. We have quantified the effects in coil-target distance as well as target site anatomy.

We used a realistic finite element method (FEM) head model to simulate the induced electric fields over fourteen target locations that are commonly used in clinical and cognitive research. The induced field strength in M1 will be considered as a reference, as in usual practice. We used orientations that induced the strongest electric field perpendicular to the cerebrospinal fluid – gray matter (CSF-GM) boundary. Most probably, the gradient of the component of the induced electric field that is parallel to the neuronal axon is the determining factor whether an action potential is evoked¹⁶⁸. At least for M1 stimulation, the effective part of the electric field is cortical column-aligned⁵¹, i.e. perpendicular to the CSF-GM boundary⁹³, and the orientation of the TMS coil relative to the underlying cortical structure is as important as is the intensity^{23,114}.

Several numerical models using the boundary element method (BEM)¹⁷³, the FEM^{105,143,195}, the independent impedance method (IIM)⁵⁸ or the finite difference method (FDM)¹⁹⁹ have been used in the past to study the spatial distribution of the TMS-induced electric field. Although studies have described the effect over regions other than M1^{17,143}, there are no modeling studies that compare the effects between these regions with M1 as a reference.

8.2 METHODS

8.2.1 Overview

To simulate the electric fields induced by TMS, a mathematical problem has to be solved for a volume that realistically represents a human head in terms of volume conduction properties. Because of the complicated geometrical tissue boundaries we used the FEM. First the construction of realistic head model will be described shortly and thereafter a delineation of the FEM for TMS will be given. Finally, the cortical sites used in this study and the methods of analysis will be presented.

8.2.2 Volume conduction model

A realistic head model was constructed, including eight different tissue types (skin, skull spongiosa, skull compacta, neck muscle, eye, cerebrospinal fluid (CSF), gray matter (GM)

and white matter (WM)), based on T1 and T2 magnetic resonance image (MRI) scans of a healthy 25-year old male subject with 1 mm³ resolution. T1-, T2- and diffusion weighted (DW) MRI image scans were measured on a 3T MR scanner (Magnetom Trio, Siemens, Munich, Germany) with a 32-channel head coil. Written informed consent was obtained prior to scanning. The T1-weighted (T1w) image was acquired with an MP-RAGE pulse sequence (TR = 2300 ms, TE = 3.03 ms, TI = 1100 ms, flip angle = 8 degrees, FOV = 256 x 256 x 192 mm, voxel size = 1 x 1 x 1 mm) with fat suppression and GRAPPA parallel imaging (acceleration factor = 2). The T2-weighted (T2w) image was acquired with an SPC pulse sequence (TR = 2000 ms, TE = 307 ms, FOV = 255 x 255 x 176 mm, voxel size = 0.99 x 1.0 x 1.0 mm interpolated to 0.498 x 0.498 x 1.00 mm). The construction of the model can be split up in five steps, namely MRI and diffusion tensor imaging (DTI) acquisition, automatic segmentation of different tissues with manual corrections, extraction of high resolution triangular surface meshes, construction of a volume mesh with linear tetrahedral elements using TetGen^a and inclusion of anisotropic conductivity tensors. A detailed description of the construction of the head model can be found in appendix A (section 10.1).

An important aspect of a realistic head model in TMS simulations is the structural brain anisotropy^{105,116,143}. To include brain anisotropy in our head model the diffusion tensors from DTI data were used, using the volume-normalized approach as described in Opitz et al. 2011¹⁴³. The DW images were acquired with the standard Siemens pulse sequence ep2d_diff (TR = 7700 ms, TE = 89 ms, b-value = 1000 s/mm², bandwidth = 2000 Hz/pixel, FOV = 220 x 220 x 141 mm, voxel size = 2.2 x 2.2 x 2.2 mm) in 61 directions equally distributed on a sphere, and 7 images were acquired with flat diffusion gradient (DW factor b = 0 (B₀-)). Additionally, seven images with flat diffusion gradient (DW factor b = 0 (B₀+)) with reversed phase and frequency encoding gradients were acquired. The bulk conductivity values for all tissues are based on previous reports and can be found in table 8.1.

8.2.3 Finite element method

The mathematical problem for TMS can be described by a simplification of the full Maxwell equations. It is described by a quasi-static system wherein we neglect displacement currents²¹⁴:

$$\vec{E} = -\frac{\partial \vec{A}}{\partial t} - \nabla \varphi \quad (8.1)$$

With \vec{A} being the magnetic vector potential, φ the electrical scalar potential and the \vec{E} the induced electric field. Equation 8.1 consists of two semi-independent parts, namely the primary field $\frac{d\vec{A}}{dt}$ (or \vec{E}_p), which is completely determined by the TMS coil and the

a TetGen: A Quality Tetrahedral Mesh Generator and a 3D Delaunay Triangulator, <http://tetgen.berlios.de/>

TABLE 8.1 The bulk conductivity values (S m^{-1}) for all the tissue types used in the standard model.

TISSUE TYPE	BULK CONDUCTIVITY (S m^{-1})
Skin	0.465 ²¹⁴
Skull compacta	0.007 ¹
Skull spongiosa	0.025 ¹
CSF	1.65 ²¹⁴
Neck muscle	0.4 ⁴³
Eyes	1.5 ¹²⁸
GM	0.276 ²¹⁴
WM	0.126 ²¹⁴

secondary field $\nabla\phi$ (or \vec{E}_s), which describes the charge accumulation at conductivity discontinuities in the volume mesh.

The spatial distribution of \vec{A} fully depends on the geometry of the coil, so first of all an accurate description of the coil is essential^{82,174}. We modeled a figure-of-eight coil (inner radius 30 mm, outer radius 45 mm, height 10 mm, wire width 1.5 mm, 10 turns), as this is the standard coil in fundamental TMS research. The results from this study are only applicable to the figure-of-eight coil described here and new simulations will be needed if different shaped TMS coils are studied. The construction of the coil geometry and the placement over all locations was done with custom written MATLAB^b code. The calculation of the magnetic vector field was performed with a custom written C++^c program. The time derivative of the field distribution for \vec{A} was scaled such that the maximum field strength was 300 V m^{-1} . This is approximately 45% of the maximum intensity of a biphasic pulse measured for the simulated figure-of-eight coil¹⁷⁴. This intensity evoked an MEP with 1.0 mV mean amplitude in the first dorsal interosseous (FDI) muscle of the subject on whom the model is based.

The secondary field $\nabla\phi$ depends on the magnetic vector potential, the geometry and the conductivity of the volume mesh and needs to be computed with the FEM. To determine the value of ϕ throughout the whole volume mesh, we use four properties: 1.) the induced electric field follows Ohm's law ($\vec{J} = \sigma\vec{E}$), 2.) in the quasi-static limit the divergence of the induced current density is zero ($\nabla \cdot \vec{J} = 0$), 3.) no current leaves the head

^b MathWorks, Natick, Massachusetts, USA

^c The C++ programming Language, Addison-Wesley, 1986. A general purpose programming language.

($\vec{J} \cdot \vec{n} = 0$) (Neumann boundary condition) and 4.) the induced current density is continuous ($\vec{J}_1 \cdot \vec{n}_1 = \vec{J}_2 \cdot \vec{n}_2$). Due to different conductivities σ (table 8.1) on both sides of a tissue boundary (for example CSF-GM), the secondary field is imposed by the combination of property 1 and 4. The Neumann boundary condition imposes a restriction to the outermost boundary of the head model, where the conductivity outside the head model is equal to zero (vacuum). For the FEM calculations the freely available SCIRun^d software was used. The gradient in ϕ was then used in combination with the primary field to calculate the total electric field for each element inside the head model using equation 8.1.

8.2.4 Cortical regions other than M1

As mentioned, fourteen cortical sites were selected, commonly used in clinical and cognitive studies (figure 8.1A-C & table 8.2). The coordinates for eleven out of these fourteen locations were acquired from the subject on whom the head model is based with the Localite^e neuronavigational system. The coordinates for the three other cortical sites were based on visual inspection of the model (1st column, table 8.2, indicated by *visual*). In the rest of this paper the target sites are coded (2nd column, table 8.2).

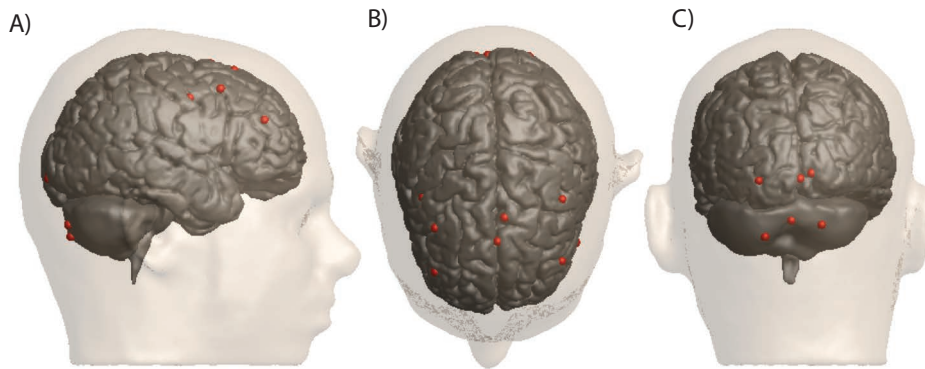


FIGURE 8.1. (A-C) The 14 stimulation target sites used in this study projected on the cortical surface of the head model. All tetrahedral brain elements inside the 3 mm radius to the cortical target were used in the analyses.

^d The freely available SCIRun 4.5 (Scientific Computing and Imaging Institute, Salt Lake City, UT)

^e <http://www.localite.de>

TABLE 8.2. The cortical target sites based on neuronavigational data or visual inspection of the model (as indicated).

CORTICAL LOCATION	CODE
M1 right hemisphere	MR
Lateral cerebellum left ⁹⁵	CL
Medial cerebellum ⁹⁵	CM
Lateral cerebellum right ⁹⁵	CR
O1 (occipital lobe left hemisphere) ¹²⁴	OL
Oz (medial occipital lobe) ¹²⁴	OM
O2 (occipital lobe right hemisphere) ¹²⁴	OR
Dorsolateral premotor cortex left hemisphere ⁸⁰	PML
Dorsolateral premotor cortex right hemisphere ⁸⁰	PMR
Dorsolateral prefrontal cortex left hemisphere ¹³ (<i>visual</i>)	PFL
Dorsolateral prefrontal cortex right hemisphere ¹³ (<i>visual</i>)	PFR
Supplementary motor area 30 mm anterior to Cz ^{3,80}	SM1
Supplementary motor area 50 mm anterior to Cz ⁸⁰	SM2
Inferior frontal gyrus ¹⁵⁵ (<i>visual</i>)	IL

The stimulation locations are based on studies indicated with the reference numbers.

8.2.5 Coil orientation and electric field direction

The electric field component perpendicular to the cortical surface is most likely to activate the cortical neurons, because it is aligned with the cortical-column structures⁵¹. The cortical target sites in table 8.2 were placed in the sulcal walls, because at those locations the field component perpendicular to the CSF-GM boundary is strongest. On top of the gyri the field is mostly parallel, and thereby likely less effective^{51,93}. The orientation of the TMS coil has a large influence on the direction of the electric field and thereby its effectiveness^{23,114}. We chose to use TMS coil orientation that induces the strongest electric field perpendicular to the CSF-GM boundary for each individual target site.

8.2.6 Analysis volume

Although TMS can also induce effects distant from the intended stimulation location¹⁷, the intention of the experimenter is to induce the largest electric field amplitude at a specific cortical target site. For a quantitative comparison of the induced electric field between different target sites, an outcome measure has to be used that is similar for all sites. There is evidence that the first neuronal activation by TMS takes place at GM level⁹⁹. Therefore, we chose to use the GM elements within a 3 mm distance from each individual cortical surface target (*red spheres in figure 8.1*). By using a fixed radius for each target site, a similar volume (*spherical*) is taken. To get an estimate of the field values within this volume, the mean field strength \bar{E} and the mean field strength in the direction perpendicular to the CSF-GM boundary \bar{E}_\perp are calculated. The value for \bar{E}_\perp is calculated as $\bar{E}_\perp = \bar{E} \cdot \vec{n}$, where \bar{E} is the electric field and \vec{n} the normal vector for the nearest boundary surface triangle.

8.2.7 Distance correction

Previous reports recommended an inverse proportional correction¹⁹⁰ for the coil-target distance. To compare the field computed by using such a correction factor to the actual induced electric field \bar{E} , we calculated the expected electric field following a distance correction based on inverse proportionality:

$$\tilde{E}_R = \frac{R^{MR}}{R} \bar{E}^{MR} \quad (8.2)$$

with \tilde{E}_R the expected electric field for target site x based on the coil-target distance, R the distance between the center of the TMS coil (for stimulation of target site x) and the target site x , R^{MR} the distance between the center of the TMS coil (for MR stimulation) and the motor reference site (MR), and \bar{E}^{MR} the mean electric field value \bar{E} (*equation 8.1*) for MR.

8.2.8 Primary field correction

The difference between \tilde{E}_R (*equation 8.2*) and the eventual FEM modeled \bar{E} (*equation 8.1*) both for site x , can be partially due to the fact that the analyzed volumes differ between target locations because the local anatomy in a 3 mm radius from each individual cortical target differs. Also the orientation of the coil is not taken into count with \tilde{E}_R , whereas we know that it is a relevant factor^{23,114}. To correct for these discrepancies, an outcome measure has been calculated that does not use the coil-target distance, but the mean primary electric field distribution over the volume instead. In formal terms:

$$\tilde{E}_A = \frac{\bar{E}_p}{\bar{E}_p^{MR}} \bar{E}^{MR} \quad (8.3)$$

with \tilde{E}_A the expected electric field for target site x based on the mean primary field strength, \bar{E}_p the mean primary field strength for the area within the 3 mm radius of the

target site x , \bar{E}_p^{MR} the mean primary field strength for the area within the 3 mm radius of the M1 reference site (MR), and \bar{E}^{MR} the mean electric field value \bar{E}_\perp (equation 8.1) for MR after FEM modeling. For the comparison with \bar{E}_\perp the same equation 8.3 is used, only with the components perpendicular to the cortical surface of \bar{E}_p , \bar{E}_p^{MR} and \bar{E}^{MR} . The outcome measure \tilde{E}_A is similar to the fields calculated and used to correct the stimulation intensity in previous studies^{140,165}. The difference between \tilde{E}_A and \bar{E} is due to the influence of the target site anatomy on the field (secondary electric field). The difference between $\tilde{E}_{A\perp}$ and \bar{E}_\perp also includes the direction relative to the CSF-GM boundary.

8.3 RESULTS

8.3.1 The induced electric field

Using the same stimulation strength, the total electric field has been calculated throughout the whole volume mesh, for all the target sites listed in table 8.2. In figure 8.2, the corresponding induced electric field distributions, just within the cortex, are shown. This figure demonstrates that the field distribution and its strength can differ considerably between target sites. The results show that indeed the field also depends on the local curvature of the cortex. The field is mostly stronger for the lateral hemispheric areas (for example IL) than for the posterior areas (for example OR). All locations display multiple gyri with high field amplitudes, except for the cerebellum. For the majority of the locations the highest field amplitude values are near the target site. In the case of cerebellar stimulation (CL, CR & CM) the largest field amplitude is systematically found more superior. With these cerebellar stimulation sites, the occipital cortex is stimulated as well.

8.3.2 Field over right M1

The total electric field \bar{E} over the right M1 (MR) will be used as a reference for the other locations and thus deserves special attention. Figure 8.3 shows the total electric field amplitude induced just below the cortical surface induced by the usual stimulation of MR. The highest electric field values are located at the crowns and lips of the gyri, which is in accordance with earlier reports^{17,195}. The \bar{E} value near the target site at the anterior bank of the central sulcus is 85 V m⁻¹ (table 8.3, MR) and the \bar{E}_\perp value is 76 V m⁻¹ (table 8.3, MR). This indicates that the total field is highly perpendicular to the CSF-GM boundary at our site of analysis. In addition to MR, the pre-motor and sensory areas are also stimulated with a relative high intensity (figure 8.3, red and orange).

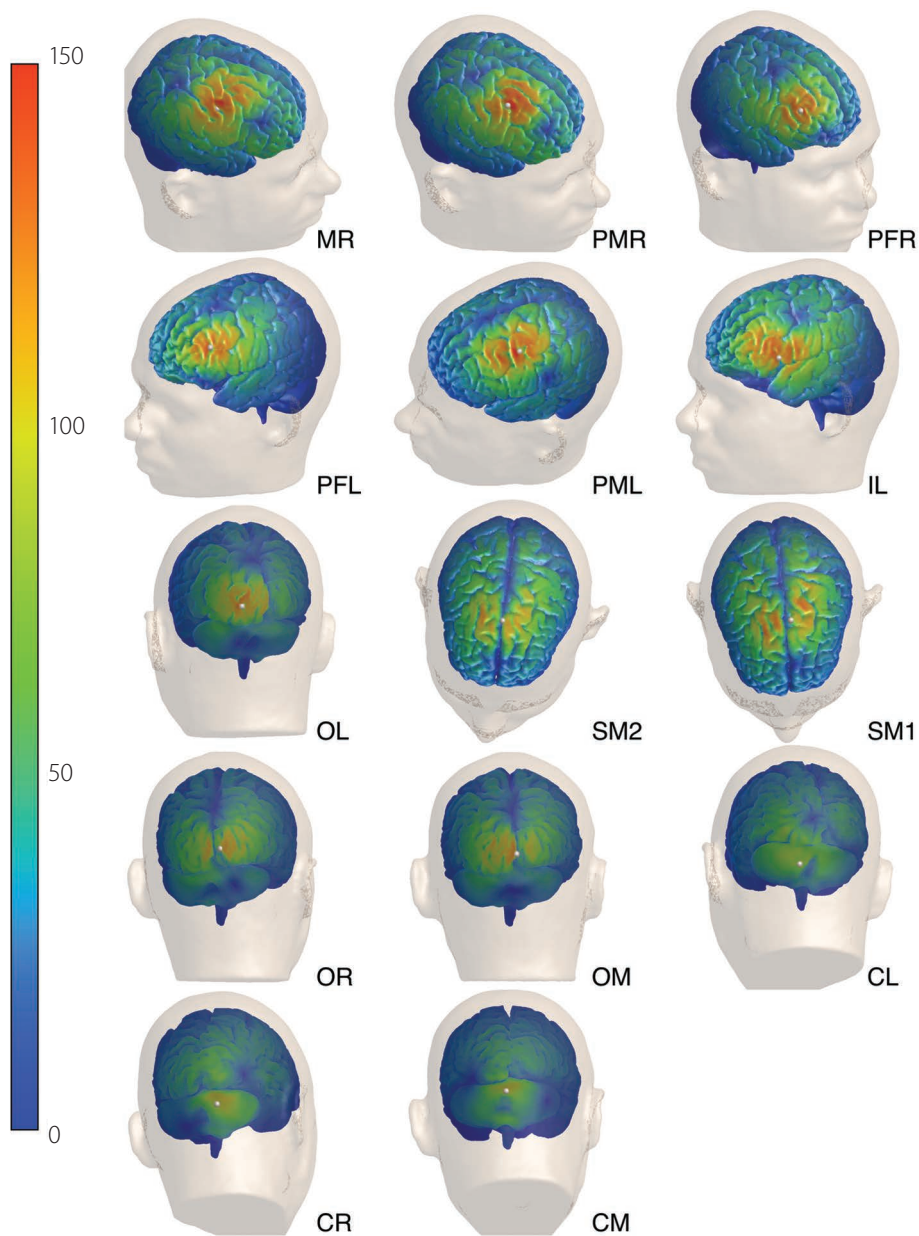


FIGURE 8.2. The electric field \vec{E} strength distributions, just within the cortex for all 14 cortical target sites as listed in table 8.2. The cortical target site code from table 8.2 is shown in every right bottom corner. The field strength is displayed on a scale from 0 to 150 V m^{-1} for clarity. Locations with field strength above 150 V m^{-1} are shown with the same color as 150 V m^{-1} . The cortical target sites are shown as small white dots on the cortical surface.

8.3.3 Primary field

In figure 8.4A-E, we have ordered the target sites used in this paper (table 8.2) according to their coil-target distance (figure 8.4A). The distance for the reference site (MR) is almost central in this ordering. To quantify the effects of intra-individual differences in coil-target distance as well as the secondary field (one aspect of the target site anatomy), the outcome measures \tilde{E} (from FEM modeling, figure 8.4B, *circles*, equation 8.1), \tilde{E}_R (distance based, figure 8.4B, *squares*, equation 8.2) and \tilde{E}_A (primary field based, figure 8.4B, *triangles*, equation 8.3) have been calculated.

Although \tilde{E}_A (figure 8.4B, *triangles*) does not exactly conform to the relation expected from the inverse distance to the center of the coil \tilde{E}_R , it is assuring that it shows a similar trend with a decrease in field strength based on increasing distance (figure 8.4B, *triangles*). As explained in the methods section, the differences between the two outcome measures \tilde{E}_R and \tilde{E}_A stem from the fact that in the computation of \tilde{E}_A the local anatomy in a 3 mm radius from each target site is included, whereas in \tilde{E}_R it is not.

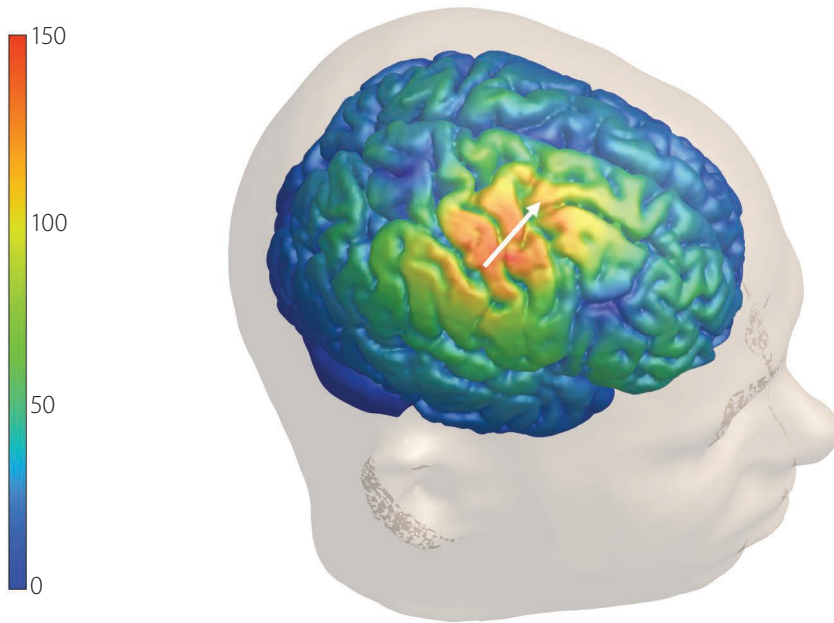


FIGURE 8.3. The electric field \tilde{E} strength distribution, just below the cortical surface, for the stimulation over MR. The field strength is displayed on a scale from 0 to 150 V m⁻¹ for clarity. Locations with field strength above 150 V m⁻¹ are shown with the same color as 150 V m⁻¹. The direction of the induced electric field (equation 8.1) under the coil midline is represented with a white arrow.

TABLE 8.3. Mean electric field strength [$V\ m^{-1}$] and correction factors.

LOCATION CODE	MEAN ELECTRIC FIELD STRENGTH		CORRECTION FACTOR		
	\bar{E}	\bar{E}_{\perp}	\tilde{E}_R	\bar{E}	\bar{E}_{\perp}
MR	85	76	1.00	1.00	1.00
PMR	135	139	0.78	0.63	0.55
PFR	112	85	0.86	0.75	0.90
PFL	120	77	0.86	0.70	0.99
PML	111	78	0.94	0.76	0.97
IL	107	53	0.94	0.79	1.43
OL	102	67	0.96	0.82	1.14
SM2	87	65	1	0.98	1.17
SM1	77	56	1	1.10	1.37
OR	83	66	1.06	1.02	1.15
OM	99	51	1.10	0.86	1.48
CL	70	19	1.15	1.20	4.1
CR	79	9	1.17	1.06	8.2
CM	89	45	1.58	0.95	1.69

Per cortical target site, the mean electric field strength \bar{E} ($V\ m^{-1}$), the mean field strength in the direction perpendicular to the CSF-GM boundary \bar{E}_{\perp} ($V\ m^{-1}$) and the three correction factors according to the inverse of the distance, mean electric field strength and the mean field strength in the direction perpendicular to the CSF-GM boundary.

8.3.4 Electric field over targets other than M1 & correction factors

The computed induced electric field \bar{E} (figure 8.4B, *circles*) has overall a higher mean value than those estimated on basis of \tilde{E}_R or \tilde{E}_A (figure 8.4B, *squares, triangles*). Only in five cases the \bar{E} value is similar to what was expected from \tilde{E}_A and \tilde{E}_R (SM1, SM2, OR, CL and CR). To distinguish the effect of the secondary field from the coil-target distance effect, the comparison between \bar{E} (figure 8.4B, *circles*) and \tilde{E}_A (figure 8.4B, *triangles*) has been used. This clearly shows the substantial effect of the secondary field.

The calculated \bar{E} values show that a correction primarily based on the distance between the target site and the center of the coil is often not sufficient to induce a similar electric field at the target site as for M1. In most situations the distance correction measure \tilde{E}_R underestimates the induced electric field and a calculated correction factor will be too large (figure 8.4C, *squares*). The result is that a stronger stimulation than intended will be used.

8.3.5 Electric fields perpendicular to the CSF-GM boundary

An important aspect for the effectiveness of TMS is the direction of the electric field. Based on previous reports^{51,93}, we assume the effective part of the electric field is directed perpendicular to the CSF-GM boundary. The magnitude of the field perpendicular to the CSF-GM boundary is influenced by the target site anatomy. By including the electric field direction in the analyses, the results change drastically (figure 8.4D, *triangles and circles*). In almost all cases the component of the primary field perpendicular to the GM-CSF (*equation 8.3* is lower than expected from solely the distance, *equation 8.2*). This is due to the fact that for MR the total electric field is almost completely perpendicular to the GM-CSF boundary, which is not the case for most other locations (table 8.3 & figure 8.4D, *triangles*). Only the locations SM2, OR and OM show a similar result.

Not surprisingly, the results for the mean strength of the total electric field perpendicular to the CSF-GM boundary (*equation 8.1*) also differ from what would be expected solely based on the distance (table 8.3 & figure 8.4D, *squares versus circles*). For most target sites the value is lower than expected from the distance. They are also different than expected from the primary field figure 8.4D, *triangles versus circles*). In contrast to the results without direction (subsection 8.3.4), here only the PMR target site has a mean electric field strength value higher than expected from the distance. There are also two sites (CL and CR) with a very low value (less than 20 V m^{-1}), which means that the electric field is mostly tangentially orientated at these locations. As a result the correction factors calculated from these values are different from the previous ones (table 8.3 & figure 8.4E). The values based on \bar{E}_{\perp} for CL and CR are not displayed in figure 8.4E, because they are high and would scrimp the y-axis of that figure.

8.4 DISCUSSION

8.4.1 Correction for distance and target site anatomy

The aim of this study was to evaluate whether the geometry of the underlying tissues influences the electric field in such a way that this has to be accounted for in proper adjustment of the TMS stimulation intensity. First of all, the results for the total electric field (figure 8.4B & 8.4D, *circles, equation 8.1*) show that for a proper adjustment the differences in target site anatomy (its influence on the secondary electric field and on the magnitude of the field perpendicular to the CSF-GM boundary) should indeed be considered. In most cases, a simple correction based on the inverse of the distance does not correctly adjust the induced electric field for regions other than M1 (figure 8.4B & 8.4D, *circles versus squares*). Also, a correction based solely on the primary field does not suffice (figure 8.4B & 8.4D, *circles versus triangles*). The secondary electric field is the result of the considerably

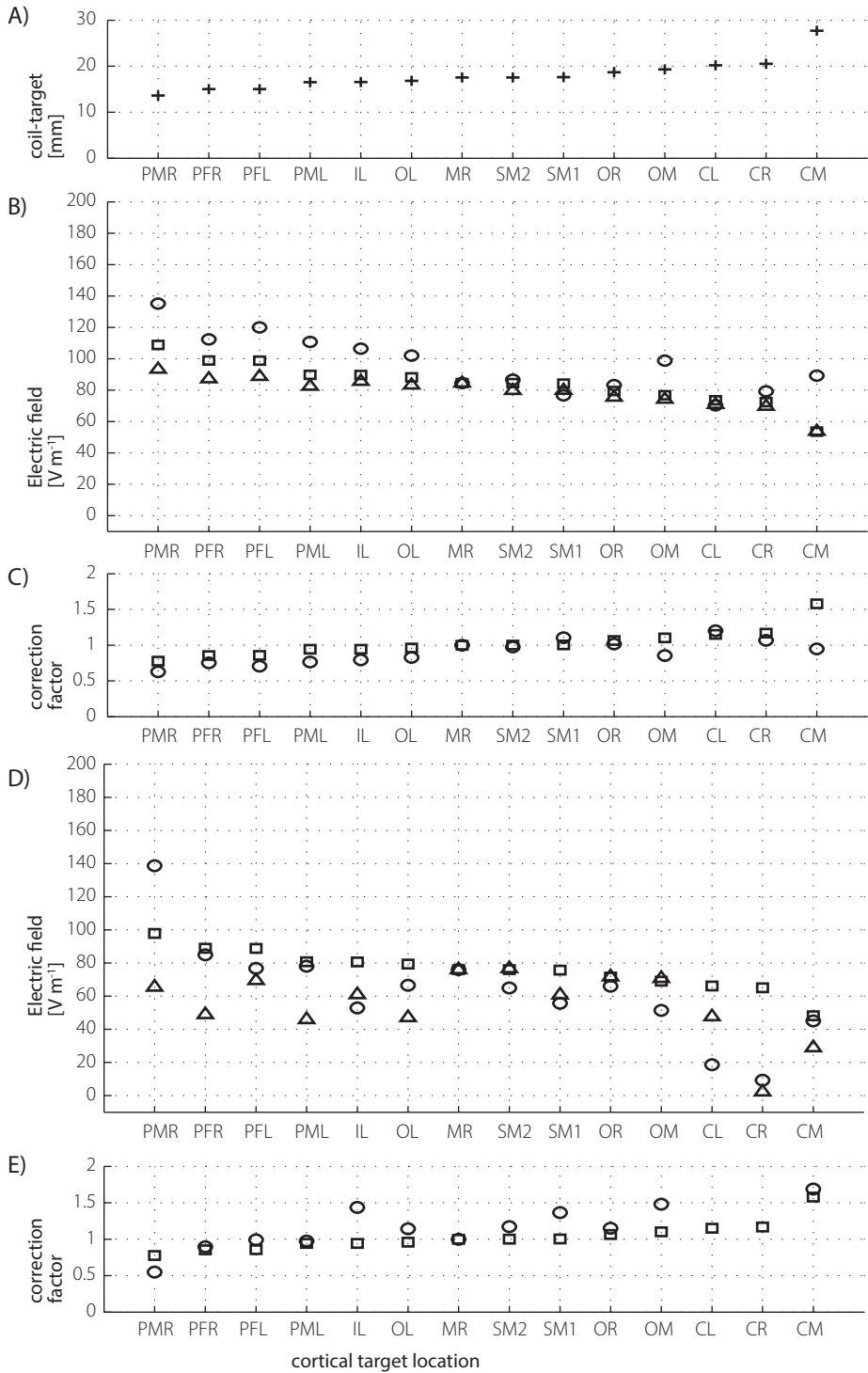
difference in conductivity between the CSF and the GM (by a factor of 15–30 at 4 kHz⁵⁵), which causes a major discontinuity in conductivity at the CSF-GM boundary. The impact of this secondary field is influenced by the local thickness of the CSF layer. Where the CSF layer thins out, the induced electric currents become largely concentrated resulting in high electric fields on the CSF-GM boundary¹⁷. As a result, large secondary electric field values are primarily found in gray matter regions adjacent to areas where the CSF layer is thinner. The differences in local GM-CSF boundary geometry cause differences in the secondary field between targeted cortical regions.

When we only consider the mean strength of the electric field, and do not include its direction relative to the CSF-GM boundary, almost all locations showed a field strength that was stronger than would be expected on the basis of distance correction (figure 8.4B). When we analyzed the field perpendicular to the CSF-GM boundary, the mean electric field strength was weaker than would be expected (figure 8.4D). Because the direction of the induced electric field has an effect on the effectiveness of stimulation^{23,114}, it should be included.

Although the results are based on a single subject, they include many target sites within that subject. They do show consistently that correction derived from a distance correction does not yield the correct field strength. For a different subject, details of the results will be different, but the principle statement that the expected field, based on distance or solely on the primary field, can differ from the actually induced electric field is a most relevant conclusion. This unfortunately means that although an adjustment of stimulation intensity is certainly advisable for stimulation other than M1, it should be based on both the coil-target distance as well as the target site anatomy. Herein, both the secondary electric field, due to charge accumulation at conductivity discontinuities, and the direction of the field relative to the CSF-GM boundary should be taken into account.

FIGURE 8.4. (A) The distance between the center of the TMS coil and the cortical target site. The targets are ordered according to this distance. (B) Per cortical target site, the mean electric field strength \bar{E} (O, equation 8.1) and the estimated fields based on the inverse of the distance \tilde{E}_R (□, equation 8.2) and on the primary electric field \tilde{E}_A (Δ, equation 8.3). (C) Per cortical target site, the correction factor to produce a similar electric field as is induced over the right hemispheric M1 (MR), based on \bar{E} (O) and on the inverse of the distance \tilde{E}_R (□). (D) Per cortical target site, the mean field strength in the direction perpendicular to the CSF-GM boundary \bar{E}_\perp (O) and the estimated fields based on the inverse of the distance \tilde{E}_R (□, equation 8.2) and on the primary electric field in the direction perpendicular to the CSF-GM boundary $\tilde{E}_{A\perp}$ (Δ, equation 8.3). (E) Per cortical target site, the correction factor to produce a similar electric field as is induced over the right hemispheric M1 (MR), based on \bar{E}_\perp (O) and on the inverse of the distance \tilde{E}_R (□). In all five subfigures, the target sites are coded according to table 8.2.

page 105 >>



8.4.2 Stimulation intensity

All the simulations in this study were based on approximately 45% of the maximum stimulator output (MSO) for a biphasic pulse for a simulated figure-of-eight coil¹⁷⁴ (see subsection 8.2.3). The induced electric fields over cortical locations other than M1 were compared to the induced field over M1. Based on this comparison, correction values have been calculated (figure 8.4C & E, *circles*). These correction values range from 0.63 (PMR) to 1.69 (CM, cerebellar locations CL and CR excluded), which in this study would correspond to stimulation intensities between 28% MSO and 76% MSO. From practical experience it is known that a 10% MSO stimulation intensity adjustment will have a large effect²¹.

The exact nature of the influence of target geometry on the induced field might differ between subjects due to the inter-individual differences in head anatomy. The correction factors found in this study, which were based on a single subject, are of course not one-to-one applicable to other subjects. A proper solution to determine appropriate stimulation intensity for target locations other than M1 would therefore need subject-based simulations. These simulations should include a detailed description of the CSF-GM boundary surface for a proper estimation of the secondary electric field (caused by the target site anatomy). When subject-based simulations are not possible, due to the time-consuming process of constructing a model, one should realize that the magnitude of the effective electric field at the target site cannot be determined properly.

8.4.3 Quantitative comparison

In this study the mean electric field, within a 3 mm range of the target, was used as an outcome measure. The size of this region of interest was based on the fact that in experimental studies a shift of 5 mm will commonly still produce an MEP for stimulation of M1²¹⁸ and this area is within that range. To confirm that the results do not strongly depend on the size of the region of interest, the analyses were also done for a radius of 5 mm. This produced similar results (appendix B (section 10.2)). When the radius is increased to a large 10 mm sphere (more than 35 times larger volume than the 3 mm sphere), the results did change substantially (appendix B (section 10.2)). However, the statement that the electric field still depends not only on distance, but also direction and secondary field, still stands.

8.4.4 Limitations of the presented study

The results of this study are based on several assumptions about neuronal activation. The most important one, usual in this field, is that the mode of neuronal activation is assumed to be similar for different cortical regions and that the preferred direction of the electric field for activation is the same. This assumption is based on the fact that a similar basic columnar structure can be found all over the cerebral cortex^{76,123}. However, the gray matter layer differs in thickness between locations and the distribution or type of neurons

may also differ. The best example is the cerebellum, where the neuronal structures are quite different with the Purkinje cell population. Nevertheless, we think that as long as no knowledge is available about the differences in activation mechanisms due to TMS, it is reasonable to assume that the same intensity and direction relative to the CSF-GM boundary is needed to stimulate neurons in the motor cortex as for other cortical regions.

The results of this study would suggest that cerebellar TMS stimulation is not possible due to the low electric field perpendicular to the CSF-GM boundary, although we know from studies that the cerebellum can be stimulated^{95,152}. A possible reason indeed is that the Purkinje cell population might be stimulated in a quite different way. Another reason could be the absence of cerebellar gyri in this model. This is due to the fact that the model is based on 3-Tesla MR images in which the cerebellar gyri are too small to be discerned reliably on the MR images. Nonetheless, the results for the cerebellar targets without direction (figure 8.4C) do give information about the stimulation strength over these regions and why they should not solely be adjusted according to distance.

8.4.5 Validation

In this study we compared the electric field induced with TMS over M1 to the electric fields induced in other cortical regions. The FEM simulations are based on well-established laws of physics (*Methods* 8.2.3) and the calculated fields are therefore trustworthy. In addition, FEM simulations have been validated for M1¹⁴². The general conclusion that coil-target distance and target site anatomy should both be included in stimulation intensity adjustment for cortical regions outside M1 is therefore most-likely true. To verify if these are the only factors that have to be taken into account validation experiments should be performed. In this way assumptions about the mode of neuronal activation, which is assumed to be similar for different cortical regions, can be verified.

Unfortunately, validation of FEM simulations has proven to be utmost difficult, because the possibilities are limited for noninvasively measuring the electric field distribution *in vivo*. This makes complete validation of our results impossible. Only for the motor cortex, FEM simulations have been validated by correlating physiologically observed MEP amplitude with simulated electric field strength¹⁴². This approach cannot be used outside M1, due to a lack of an objective outcome like the MEP.

The effect of coil-target distance has already been shown in previous studies^{190,201}. However, these studies only measured MEP amplitudes over one cortical region. To verify if an adjustment should be included for local anatomy, one could measure the resting motor threshold (RMT) for multiple muscles, for example, the leg, the tongue and the FDI muscle, and test if these results correlate with simulated electric fields for the corre-

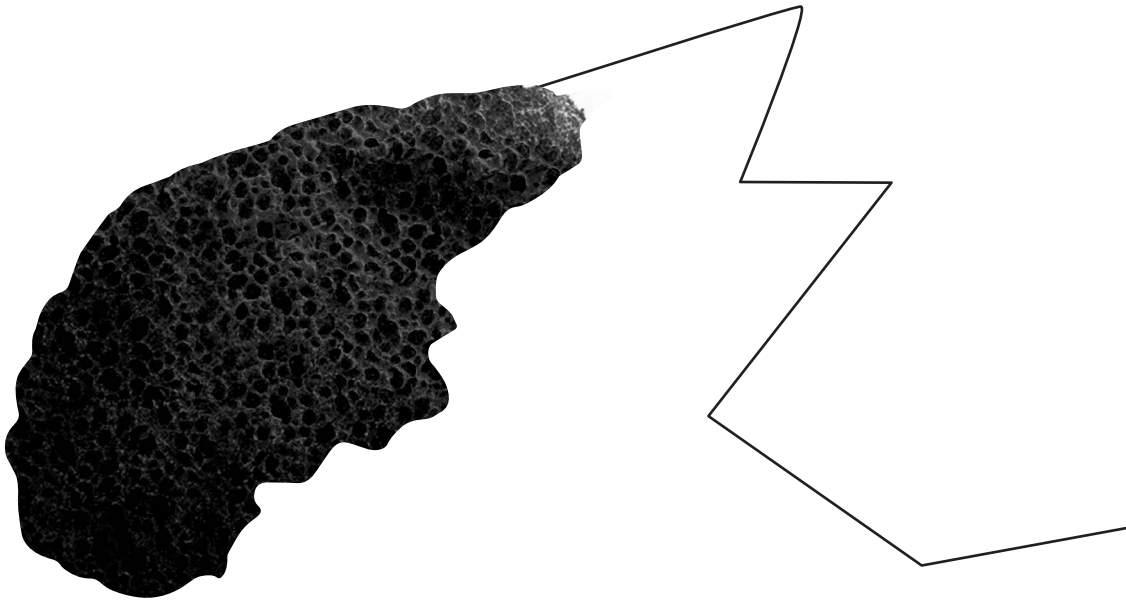
sponding cortical regions. These cortical regions should differ in coil-target distance and local anatomy, so that the influence of local anatomy on the induced electric field can be verified. To increase the number of areas, the other hemisphere could be included. However, the results will still be based on only the motor cortex and not on non-motor regions. A different approach to measure the effect of local anatomy would be the use of a conductive phantom head with multiple compartments. However, simplified geometry and impedance profile, and, therefore, the measured electric field can never be more than an approximation of the *in vivo* field.

Both approaches will not completely validate our conclusion that stimulation intensity adjustment is needed for non-motor regions and neither will it test the statement that the mode of neuronal activation is similar for different cortical regions. The only way to validate the results for non-motor regions is by finding an objective outcome measure that is similar for all cortical regions, which can be used to correlate with the simulated electric fields. At this moment such a method is not yet available, but maybe concurrent TMS-fMRI¹⁶ or TMS-EEG¹⁵ techniques can be of use in future studies.

8.5 CONCLUSIONS

The stimulation intensities used for stimulating cortical target sites other than M1 are generally based on the MT determined over M1. However, due to the differences in coil-target distance and target site anatomy, the stimulation intensity needs to be adjusted for these other cortical target sites. This study has showed that the adjustment should take into account the differences in coil-target distance, the secondary field caused by charge accumulation at conductivity discontinuities and the direction of the field relative to the local CSF-GM boundary. An adjustment of the stimulation intensity based solely on the distance to the cortical target, or only the primary electric field, is not sufficient.





Published as:

Janssen AM, Oostendorp TF, Stegeman DF.

The coil orientation dependency of the electric field induced by TMS for M1 and other brain areas.

Journal of NeuroEngineering and Rehabilitation, Vol. 12(47), p. 1-13, 2015

9.

THE COIL ORIENTATION DEPENDENCY OF THE ELECTRIC FIELD INDUCED BY TMS FOR M1 AND OTHER BRAIN AREAS

ABSTRACT

The effectiveness of transcranial magnetic stimulation (TMS) depends highly on the coil orientation relative to the subject's head. This implies that the direction of the induced electric field has a large effect on the efficiency of TMS. To improve future protocols, knowledge about the relationship between the coil orientation and the direction of the induced electric field on the one hand, and the head and brain anatomy on the other hand, seems crucial. Therefore, the induced electric field in the cortex as a function of the coil orientation has been examined in this study. The effect of changing the coil orientation on the induced electric field was evaluated for fourteen cortical targets. We used a finite element model to calculate the induced electric fields for thirty-six coil orientations (10 degrees resolution) per target location. The effects on the electric field due to coil rotation, in combination with target site anatomy, have been quantified. The results confirm that the electric field perpendicular to the anterior sulcal wall of the central sulcus is highly susceptible to coil orientation changes and has to be maximized for an optimal stimulation effect of the motor cortex. In order to obtain maximum stimulation effect in areas other than the motor cortex, the electric field perpendicular to the cortical surface in those areas has to be maximized as well. Small orientation changes (10 degrees) do not alter the induced electric field drastically. The results suggest that for all cortical targets, maximizing the strength of the electric field perpendicular to the targeted cortical surface area (and inward directed) optimizes the effect of TMS. Orienting the TMS coil based on anatomical information (anatomical magnetic resonance imaging data) about the targeted brain area can improve future results. The *standard* coil orientations, used in cognitive and clinical neuroscience, induce (near) optimal electric fields in the subject-specific head model in most cases.

9.1 INTRODUCTION

9.1.1 Coil orientation effects

Transcranial magnetic stimulation (TMS)⁸ is a non-invasive brain stimulation technique that is used in a wide range of neurophysiologic and clinical studies to measure or change the excitability of specific brain areas. Although the popularity of TMS is growing, the mechanism by which the induced electric field affects neuronal excitability is not clear. This holds particularly for the effect of the direction of the induced field relative to the cortical structures. It already has been proven that the effectiveness of the stimulation depends highly on the coil orientation relative to the tissue distribution below the coil^{10,23,114}. Many non-motor brain areas are studied with TMS nowadays^{13,72,80,95,124,155} and general rules about optimal coil orientation, applicable all over the cortex, would help future studies.

A suitable method to obtain knowledge about the induced field and its direction is volume conduction modeling^{17,82,143,195}. Although several TMS modeling studies have been published in the past 2 decades^{116,162,174,195,214}, the effect of coil orientation on the electric field distribution has not been studied extensively, except for the motor cortex (M1)⁹³. Because we are interested in generalizations about coil orientation, the present study concerns the effect of coil orientation also for cortical areas other than M1. For this, the finite element method (FEM) was used. On the basis of agreed optimality for M1^{51,93}, the aim was to determine the effect of coil orientation for multiple cortical target sites and the importance of an optimal coil orientation. Generalizations for all cortical areas about the effects of coil orientation were made and the optimality of ‘standard’ TMS coil orientations, used in several cognitive and clinical neuroscience studies, were considered for our subject-specific volume conduction model.

9.1.2 Optimality and the cortical cosine model

For M1 there is already ample evidence for the importance of coil orientation^{7,10,23,114}. The optimal orientations for this cortical area were determined by finding the highest or most stable motor evoked potential (MEP) amplitude per individual. In general, the optimal coil orientation for M1 induces a primary electric field directed at an angle of approximately 45 degrees to the medial-sagittal plane of the subjects head^{23,114}. This orientation induces a posterior-anterior (P-A) directed electric field perpendicular to the central sulcus.

The most logical explanation for the coil orientation preference of M1 stimulation is given by the theoretical *cortical column cosine model of TMS efficacy (C³-model)*⁵¹. This model is based on the cortical column^{76,123} as the functional unit. The authors state that the cortical-column aligned electric field (perpendicular to and directed into the cortical surface) contributes most to the TMS-induced brain activation, due to the fact that the field will be

longitudinal and orthodromic to the greatest possible number of cortical neurons at the site of interest. The C^3 -model is supported by volume conduction modeling⁹³, supported with TMS-positron emission tomography (PET) experiments^{51,91}, and is nicely in agreement with the orientation specificity found for M1^{23,114}.

Due to a lack of an outcome measure like the MEP for cortical target areas outside M1, the optimal orientation cannot easily be obtained experimentally. Nevertheless, several brain structures have been studied with TMS in the course of years^{13,72,80,95,124,155}. The C^3 -model can possibly contribute in determining the optimal coil orientation for these brain areas and improve experimental TMS studies. If the *theoretical* model is applicable to M1, it could be argued that it could as well be applicable to other cortical areas, due to the fact that a similar basic columnar structure can be found all over the cerebral cortex^{76,123}. This statement is supported by the orientation specificity found for the supplementary motor area (SMA)³. The coil orientation over the SMA that optimally affects the motor output measured with electromyography (EMG) over M1, induces an electric field directed perpendicular to the midsagittal plane and thus perpendicularly into the underlying cortical surface. This TMS coil orientation preference for SMA was verified in a TMS-PET study¹²⁹.

Based on the premise that the C^3 -model is applicable to all cortical areas, we determined the effect of coil orientation for thirteen cortical target locations outside M1 in a realistic head model. From the results, generalizations about coil orientation applicable to all cortical target areas are made to predict the optimal orientations.

9.2 METHODS

9.2.1. Overview

In order to study the induced electric field in the brain, a highly realistic head model with intricate geometrical tissue boundaries was constructed. Herein, fourteen cortical target locations were selected, including M1 (*table 9.1*). The cortical locations were based on clinical and cognitive studies (*references table 9.1*). The coordinates for eleven out of these fourteen locations were acquired with the Localite^a neuronavigational system from the subject on whom the head model is based. The coordinates for the three other cortical sites were based on visual inspection of the model. For each cortical target location the coil was rotated systematically in steps of 10 degrees (thirty-six orientations in total), while keeping the horizontal plane of the TMS coil at the same level and the center at the same location.

a <http://www.localite.de>

TABLE 9.1. The cortical target locations commonly used in clinical and cognitive studies, based on neuronavigational data and visual inspection of the model (as indicated).

CORTICAL LOCATION	CURRENT DIRECTION IN BRAIN FOR 'STANDARD' ORIENTATION	CODE
M1 right hemisphere	Experimentally determined (highest MEP amplitude)	MR
Lateral cerebellum left ^{95,203}	rostral (upwards)	CL
Medial cerebellum ^{95,203}	rostral (upwards)	CM
Lateral cerebellum right ^{95,203}	rostral (upwards)	CR
O1 (occipital lobe left hemisphere) ¹²⁴	medial-lateral	OL
Oz (medial occipital lobe) ¹²⁴	medial-lateral leftwards	OM
O2 (occipital lobe right hemisphere) ¹²⁴	medial-lateral	OR
Dorsolateral premotor cortex left hemisphere ^{60,80}	antero-medial	PML
Dorsolateral premotor cortex right hemisphere ^{60,80}	antero-medial	PMR
Dorsolateral prefrontal cortex left hemisphere ¹³ (visual)	antero-medial	PFL
Dorsolateral prefrontal cortex right hemisphere ¹³ (visual)	antero-medial	PFR
Supplementary motor area 30 mm anterior to Cz ^{3,72}	medial-lateral leftwards	SM1
Supplementary motor area 50 mm anterior to Cz ^{3,80}	medial-lateral leftwards	SM2
Inferior frontal gyrus ¹⁵⁵ (visual)	antero-medial	IL

The stimulation locations are based on studies indicated by the references. All cortical target locations are situated in the sulcal wall.

An extensive description of the head model is provided in appendix A (section 10.1), and the theoretical background of TMS can be found in subsection 7.2.3. The construction of the model will only be described briefly in subsection 9.2.2. The induced electric field was computed for all combinations of cortical target site and coil orientation using the FEM (subsection 9.2.3). The FEM was used, because it has been proven to calculate the TMS-induced electric field relatively fast and accurately in a highly realistic anisotropic head model^{105,143,195}. At each target location the fields for all coil orientations were compared, as described in subsection 9.2.4.

9.2.2 Volume conduction model

A prerequisite for studying the effect of coil orientation are realistically described tissue boundaries, and especially the boundary between cerebrospinal fluid (CSF) and gray matter (GM), as introduced in the latest models^{82,195}. Spherical volume conduction models^{116,162} lack cortical curvature that make it impossible to describe the electric field in the sulci. We therefore incorporated precise geometrical detail and specifically a highly realistically described CSF-GM boundary. Other important factors are tissue heterogeneity¹¹⁶ and brain anisotropy¹⁴³.

The realistic head model includes eight different tissue types (skin, skull spongiosa, skull compacta, neck muscle, eye, CSF, GM and white matter (WM)) and is based on T1 and T2 magnetic resonance images (MRI) of a healthy 25-year old male subject, with 1 mm³ resolution. The corresponding bulk conductivity values were assigned to different tissue types as previously described⁸²: $\sigma_{\text{skin}} = 0.465$, $\sigma_{\text{spongiosa}} = 0.025$, $\sigma_{\text{compacta}} = 0.007$, $\sigma_{\text{neck muscle}} = 0.400$, $\sigma_{\text{eye}} = 1.500$, $\sigma_{\text{csf}} = 1.650$, $\sigma_{\text{gm}} = 0.276$, $\sigma_{\text{wm}} = 0.126$. The head model includes diffusion tensor imaging (DTI) based brain anisotropy, using the volume-normalized approach as described in Opitz et al. 2011¹⁴³.

9.2.3 Theoretical background of TMS

For each combination of cortical target site (table 9.1) and coil orientation the induced electric field follows in the quasi-static approach from a subset of the Maxwell equations:

$$\vec{E} = -\frac{\partial \vec{A}}{\partial t} - \nabla \varphi = -\vec{E}_p - \vec{E}_s \quad (9.1)$$

with \vec{A} being the magnetic vector potential, φ the electrical potential and the \vec{E} the induced electric field. In the quasi-static approach displacement currents are neglected, which is justified for the stimulation frequency range of TMS (~1–10 kHz). Within this frequency range, the permittivity values for healthy human tissue (within the head) are approximately between $10^3 \epsilon_0$ and $10^5 \epsilon_0$ ^{54,55}, with ϵ_0 the permittivity for free space. Previous FEM simulations already demonstrated that permittivity values between $10^2 \epsilon_0$ and $10^4 \epsilon_0$ had negligible effects on the distribution of the induced electric field and only permittivity values in the range of $10^7 \epsilon_0$ had an effect on the electric field distributions²¹⁴.

Equation 9.1 consists of two semi-independent parts. The first part $\frac{d\vec{A}}{dt}$, which is completely determined by the geometry of the TMS coil and the current strength passing through the coil, is called the primary field (\vec{E}_p). The second part $\nabla \varphi$, which describes the charge accumulation at conductivity discontinuities in the volume mesh, is called the secondary field (\vec{E}_s).

The calculation of \vec{E}_p was performed with a custom written C++^b program, using an accurate description of a figure-of-eight coil geometry^{82,174}. The field distribution of \vec{E}_p was scaled for each combination of target site and coil orientation, such that the maximum field strength just beneath the coil center was 300 V m⁻¹. The secondary field (\vec{E}_s) depends on the primary field (\vec{E}_p), the geometry of the volume conductor and its conductivities, and is computed by using the FEM. The FEM is able to rapidly compute the induced electric field for a realistic head model with complicated geometrical tissue boundaries (approx. 2.5 minutes with SCIRun^c on a Mac Pro, 2.66 GHz Quad-Core Intel Xeon with 16 GB memory). To determine the value of ϕ throughout the whole volume mesh, four properties were used: 1.) The induced currents follow Ohm's law ($\vec{J} = \sigma \vec{E}$). 2.) In the quasi-static limit the divergence of the induced current density is zero ($\nabla \cdot \vec{J} = 0$). 3.) No current leaves the head ($\vec{J} \cdot \vec{n} = 0$) (Neumann boundary condition). 4) The induced current density is continuous throughout the volume conductor ($\vec{J}_1 \cdot \vec{n}_1 = \vec{J}_2 \cdot \vec{n}_2$). The resulting system of linear equations was solved with a preconditioned Jacobi conjugate gradient method yielding residuals $< 10^{-15}$. The gradient of ϕ was used in combination with the primary field \vec{E}_p to calculate the total electric field for each element inside the head model using equation 9.1.

9.2.4 Data analysis

For each combination (target site & orientation), the induced electric field was calculated throughout the whole head model. As we are interested in the TMS-induced effects at the cortical level, the fields at the CSF-GM boundary have been visualized. To quantify the effects of coil orientation on the TMS-induced field, we used the electric field strength $|\vec{E}|$ and the field strength perpendicular to the CSF-GM boundary E_{\perp} . As stated earlier, the stimulation is probably most effective when the field is perpendicular to the cortical column. This choice was based on the *C³-model*, which can be expected to be applicable to all cortical areas, due to the fact that a similar basic columnar structure can be found all over the cerebral cortex^{76,123}. The value for E_{\perp} is calculated as $E_{\perp} = \vec{E} \cdot \vec{n}$, where \vec{E} is the induced electric field and \vec{n} the normal vector for the nearest boundary surface triangle.

The target regions, which are used for analysis, are chosen to be spherical (3 mm radius) with their centers located on the cortical surface. By using a fixed radius for each target region, a similar volume is taken for each location. For all targets, except the cerebellar ones, the center of the target region was located in a sulcal wall. They were located in the sulci, because there the field is mostly perpendicular and consequently more likely to be first affected by the stimulation (subsection 9.4.4; *I-waves and the perpendicular electric field*). Within the target region only the GM elements are used to determine $|\vec{E}|$ and E_{\perp} , because there is evidence

b The C++ programming Language, Addison-Wesley, 1986. A general purpose programming language.

c The freely available SCIRun 4.5 (Scientific Computing and Imaging Institute, Salt Lake City, UT)

that the first neuronal activation by TMS takes place at GM level⁹⁹. The optimal orientation is defined as the one inducing the highest mean value for E_{\perp} .

9.3 RESULTS

9.3.1 The electric field for standard coil orientations

In figure 9.1, the electric fields at the cortical level are visualized for three locations and their corresponding *standard* coil orientations reported in literature (MR: left column, PML: middle column & SM1: right column, table 9.1). The electric field strength ($|\vec{E}|$, top row) and the field strength perpendicular to the CSF-GM boundary (E_{\perp} , bottom row) are shown. The black arrow indicates the direction of the primary electric field directly beneath the coil center (*black dot*).

All target locations have multiple gyri with high field amplitudes near the target site (figure 9.1, top row, *red*). The highest electric field values are located at the crowns and lips of the gyri, which is in accordance with earlier reports^{17,195}. High field values can be found for multiple gyri anterior and posterior to the target site following the midline of the coil (figure 9.1, top row, *red and pink*).

The highest field values for the perpendicular component (*cortical column aligned*) were found in the sulci and almost never on top of the gyri (figure 9.1, bottom row). A distinction can be made visually between the inward (*red*) and outward (*blue*) directed electric field. The maximum field values for all fourteen target locations and their *standard* coil orientations, determined over the complete cortical surface, are listed in table 9.2. The maximum values for E_{\perp} are always lower than the maximum values of $|\vec{E}|$, as expected. However, the maximum values for E_{\perp} are still between 45 and 80 percent of their corresponding maximum value for $|\vec{E}|$.

9.3.2 Change in coil orientation for M1 stimulation

In figure 9.2 the results are presented for 5 coil orientations over M1, namely (1) the *standard* from literature, (2) the *standard* + 40 degrees, (3) + 90 degrees, (4) + 150 degrees and (5) + 180 degrees of clockwise rotation. The induced electric field strength ($|\vec{E}|$, top row) and the field strength perpendicular to the CSF-GM boundary (E_{\perp} , bottom row) are shown. The black arrow again indicates the direction of the primary electric field directly under the coil center (*black dot*). Both rows in figure 9.2 show the effect of coil orientation on the electric field distribution. The highest electric field values are always located at the crowns and lips of gyri for all orientations (figure 9.2, top row). However, no clear orientation dependency can be observed in the field strength on top of the precentral gyrus (M1, *around black dot*).

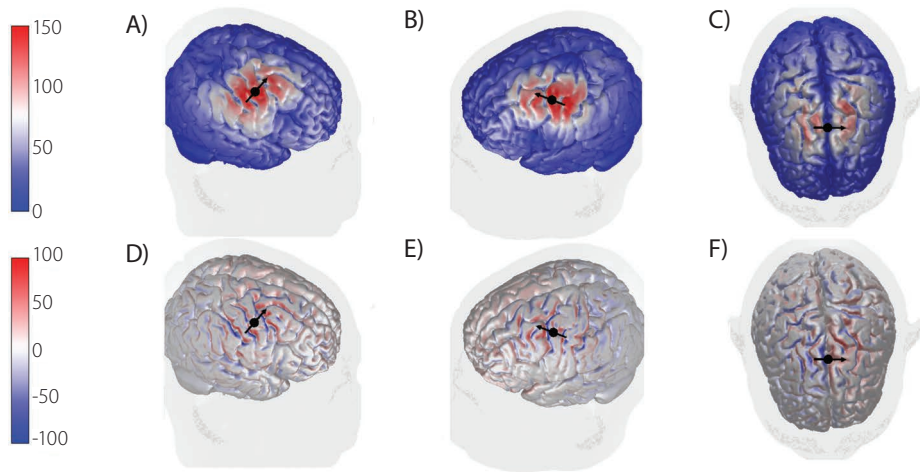


FIGURE 9.1. The electric field distribution ($V m^{-1}$), just within the cortex for three locations. On the top row the field strengths $|\vec{E}|$ for (A) the right motor cortex (MR), (B) the left premotor cortex (PML) and (C) the supplementary motor area 3 cm anterior to Cz (SM1) are displayed. In the bottom row the field strengths perpendicular to the CSF-GM boundary E_{\perp} are shown for (D) MR, (E) PML and (F) SM1. For the later scale, a positive value means directed inward and a negative means directed outward. The black dot indicates the location of the center of the TMS coil. The direction of the primary electric field directly under the coil center is indicated with the black arrow.

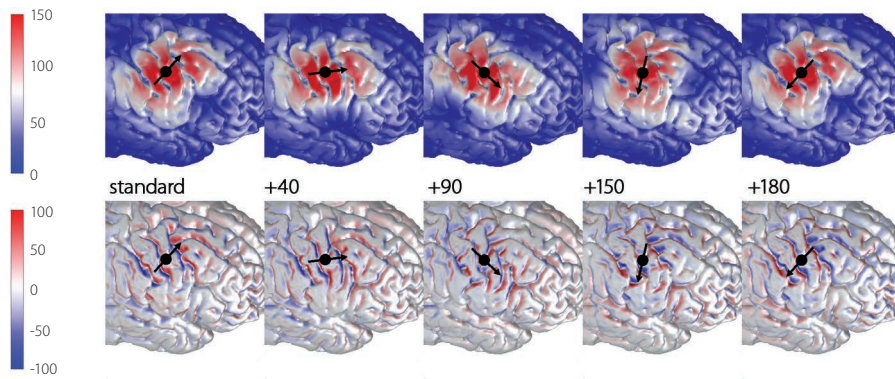


FIGURE 9.2. The electric field distribution ($V m^{-1}$), just within the cortex, for M1 stimulation with the standard coil orientation (1st column) and 4 other orientations (+40 (2nd column), +90 (3rd column), +150 (4th column) and +180 (5th column) degrees of clockwise rotation). The field strength $|\vec{E}|$ (top row) and the field strength perpendicular to the CSF-GM boundary E_{\perp} (bottom row) are shown. For the later scale, a positive value means directed inward and a negative means directed outward. The black dot indicates the location of the center of the TMS coil. The direction of the primary electric field directly under the coil center is indicated with the black arrow.

The component perpendicular to the cortical surface shows no high field values on top of the gyri, but always inside the sulci (figure 9.2, bottom row). The field clearly differs between orientations. The consistency of the calculations is expressed by the fact that the absolute strength of the electric field becomes the same for the *standard* orientation and the 180 degrees rotation of the coil; only the direction of the field reverses from inward to outward (*red turns blue and vice versa*). The *standard* orientation induces the strongest E_{\perp} values directed into the cortex at the anterior sulcal wall of the central sulcus. This is in accordance with earlier findings^{51,91,93}.

TABLE 9.2. Maximum electric field strength [V m⁻¹].

	\vec{E}	E_{\perp}
MR	157.7	86.1
PMR	163.5	101.3
PFR	150.4	81.9
PFL	142.3	100.9
PML	170.7	96.7
IL	142.7	96.6
OL	130.5	82.2
SM2	117.9	93.4
SM1	130.2	104.9
OR	114.8	73.6
OM	124.3	74.2
CL	101.0	49.1
CR	101.9	47.2
CM	95.5	62.3

The maximum values for the electric field strength $|\vec{E}|$ and the field strength perpendicular to the CSF-GM boundary E_{\perp} for all fourteen target locations with the *standard* coil orientations found in literature. The cortical target location coding can be found in table 9.1. The values are based on the complete cortical surface.

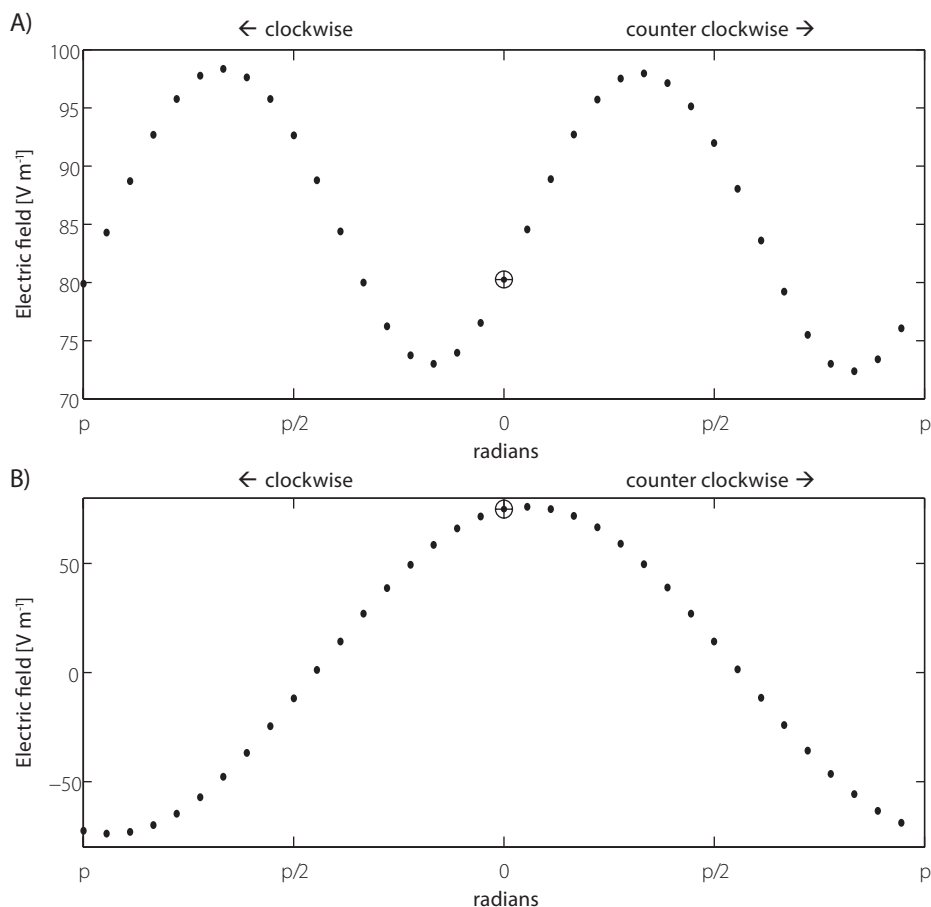


FIGURE 9.3. The mean electric field values for (A) $|\vec{E}|$ and (B) E_{\perp} within the target region M1. The standard coil orientation from literature is indicated separately in both panels (circle with cross). The coil is rotated in steps of 10 degrees.

The results from figure 9.3 show that coil orientation has an effect on the TMS-induced electric field distribution and therefore probably also on the TMS-induced activation of neuronal structures. In figure 9.3 the mean values for $|\vec{E}|$ and E_{\perp} within the target region MR are shown for all thirty-six orientations. The *standard* coil orientation from literature is indicated in both panels of figure 9.3 (circle with cross). The results again show that for M1, the orientation dependency of the mean field strength is small (figure 9.3A), especially compared to the dependency of the perpendicular electric field (figure 9.3B). Based on the mean field strength the *standard* coil orientation induces an electric field far from optimal (figure 9.3A, circle with cross). However, the *standard* coil orientation induces almost the highest possible perpendicular electric field, directed into the cortex (figure 9.3B circle with cross).

It is known from earlier reports that a coil rotation of 90 degrees (compared to the most optimal orientation) will induce the least effective electric field¹¹⁴. The results from this study show that the field perpendicular to the cortical surface is almost equal to zero with both a clockwise or an anti clockwise rotation of 90 degrees. The results presented in figure 9.3 are clearly in favor of the argument that the optimal field is directed perpendicular and into the cortical surface as found in previous studies^{51,91,93}.

9.3.3 Optimization of stimulation at other locations

Following the same procedure as for M1, the mean values for $|\vec{E}|$ and E_{\perp} within the target region for all thirty-six orientations over the other thirteen cortical surface targets have been calculated. The mean values for the *standard* coil orientation and the optimal orientation are listed in table 9.3 (*per target location*). The results for all other coil orientations can be found in appendix C (section 10.3). The optimal orientation for the outcome measures $|\vec{E}|$ and E_{\perp} are determined separately (table 9.3). Also for the other locations the optimal

TABLE 9.3. The mean electric field values for $|\vec{E}|$ and E_{\perp} within the target region[V m⁻¹].

LOCATION	MEAN ELECTRIC FIELD VALUES			
	\bar{E} standard	\bar{E} optimal (% standard)	\bar{E}_{\perp} standard	\bar{E}_{\perp} optimal (% standard)
MR	80.3	98.3 (122)	74.9	76.1 (102)
PMR	131.5	138.0 (105)	119.0	138.7 (117)
PFR	111.7	112.4 (101)	83.8	84.9 (101)
PFL	123.7	127.3 (100)	76.2	76.7 (100)
PML	107.7	114.3 (106)	40.6	73.6 (181)
IL	106.5	115.7 (109)	52.9	52.9 (100)
OL	100.6	102.9 (102)	65.0	66.6 (102)
SM2	86.7	109.7 (127)	64.9	64.9 (100)
SM1	74.4	89.8 (121)	54.2	55.7 (103)
OR	80.2	87.0 (108)	64.3	66.6 (104)
OM	98.9	99.2 (100)	51.4	51.4 (100)
CL	68.6	71.2 (104)	4.9	18.7 (382)
CR	81.8	82.2 (100)	-7.2	9.3 (-129)
CM	88.4	89.8 (101)	42.7	45.0 (105)

For each location the value for the standard coil orientation and the optimized coil orientation are given. The optimized values are determined for both outcome measures ($|\vec{E}|$ and E_{\perp}) individually. The cortical target location coding can be found in table 9.1.

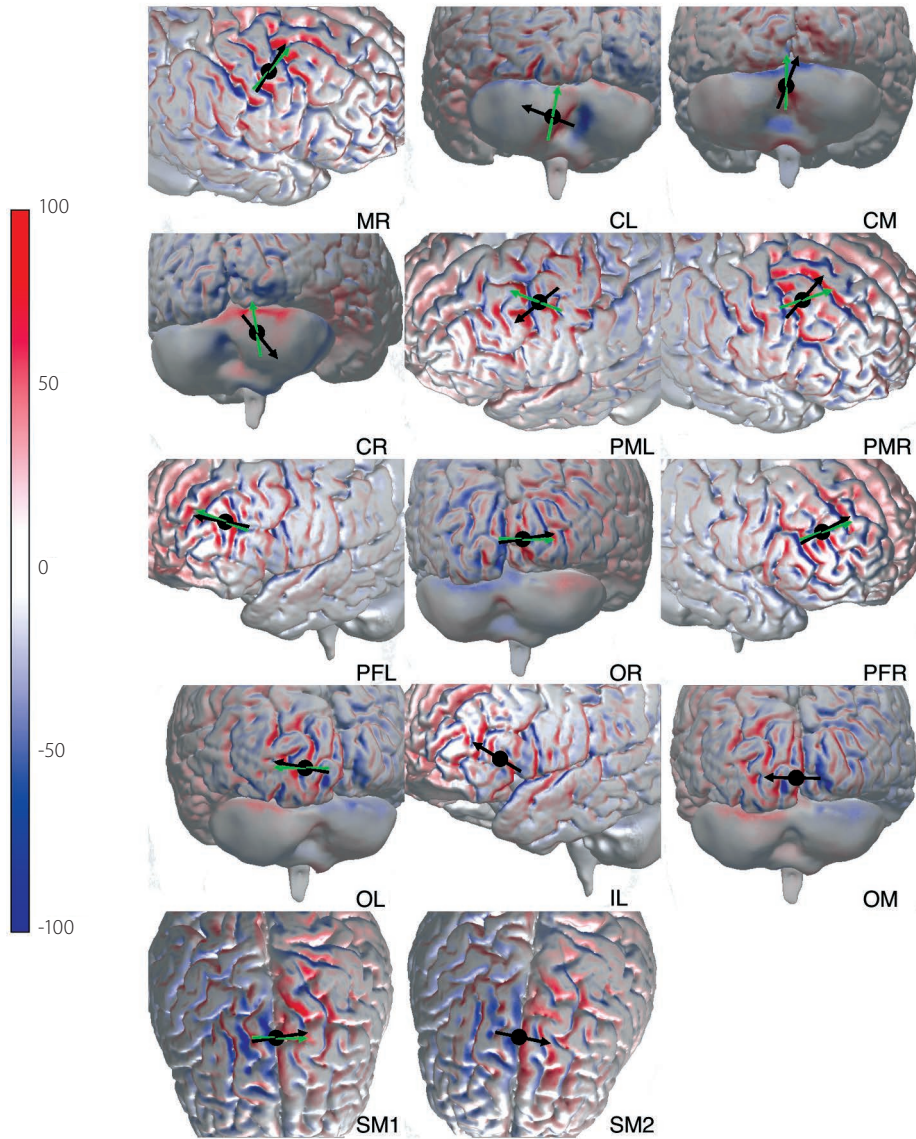


FIGURE 9.4. The optimized electric field perpendicular to the CSF-GM boundary E_{\perp} (V m^{-1}), just within the cortex, for all fourteen cortical target locations (table 9.1). The cortical location index from table 9.1 is shown in every right bottom corner. A positive value means directed inward and a negative means directed outward. The black dot indicates the location of the center of the TMS coil. The direction of the primary electric field directly under the coil center is indicated with the black arrow for the optimized coil orientation. The green arrow indicates direction of the primary electric field for the standard coil orientation.

orientation can differ between outcome measures (*appendix C, section 10.3*). This means that it is important to choose the optimal orientation, based on the correct outcome measure. Here we decided to use the C^3 -model (E_{\perp})⁵¹ as well, because this theory best explains orientation dependency.

Most of the *standard* orientations found in literature can be considered almost optimal for inducing the strongest perpendicular fields in nearby sulcal walls in our subject-specific model. Only four out of fourteen target locations could possibly be improved with more than 5 percent (PMR, PML, CL and CR). A generalization of the results will be discussed in the subsections *Simulation outside M1* (9.4.2) & *Generalization* (9.4.3). Because of their distinctive results, the cerebellar targets will be discussed separately in more detail in the subsection *Cerebellum* (9.4.5). The electric field distribution per target location for the optimal coil orientation, which induces the strongest perpendicular field directed into the cortex, is shown in figure 9.4.

9.4 DISCUSSION

9.4.1 Motor cortex

The variation in the induced electric field for M1, caused by a change of coil orientation, has been visualized and quantified. Although the strongest electric field can be found on top of the precentral gyrus for all coil orientations, no clear orientation dependency can be observed in the field strength at this cortical location (figure 9.2, top row, *around black dot*). The electric field on top of the gyrus is primarily parallel to the cortical surface and never perpendicular. According to the C^3 -model, the electric field has to be perpendicular and directed into the cortical surface (orthodromic to the underlying cortical neurons¹⁶⁰).

In the central sulcus, the strength of the perpendicular component varies strongly with coil rotation (figure 9.2, bottom row & figure 9.3B). The coil orientation dependency of the mean field strength is small in the sulcal wall (figure 9.3A). For M1, the strongest perpendicular fields (*positive and negative*) are produced by a coil orientation of 45 degrees relative to the medial-sagittal plane. A 90-degree coil rotation compared to the optimal orientation, which aligns the figure-of-eight midline with the central sulcus, produces a weak perpendicular component (figure 9.3B). The results from this study are nicely in agreement with experimental findings^{23,114} and previous modeling results of Laakso et al. 2014⁹³. They confirm that the field in the sulcal wall (and orthodromic to the cortical neurons¹⁶⁰), is highly susceptible to coil orientation changes and most probably a primary location for neuronal activation.

9.4.2 Stimulation outside M1

The local anatomy of the areas outside M1 are different compared to M1 and therefore the optimal orientation of the TMS coil has to be determined per target location (table 9.1). In general, all locations display multiple gyri with high electric field strengths near the targeted cortical location for all coil orientations. The highest field values are located on top of the gyri, which is similar to the results of M1 and earlier reports^{17,82,143,195}. Similar to M1, the electric field on top of the gyri is mainly parallel to the cortical surface and therefore probably not susceptible to coil orientation changes. Considerable field values are also found in the sulcal walls, where it is considered to be highly effective due to its direction (*perpendicular to the cortical surface*) (figure 9.1 & figure 9.4).

To determine whether the *standard* TMS coil orientations (*references table 9.1*) can be improved for the subject model at hand, we calculated the field perpendicular to the cortical surface in target regions located in the nearest sulcal walls (subsection 9.2.4). For almost all cortical target regions chosen in this study the *standard* TMS coil orientations are inducing an (near) optimal electric field (figure 9.4 & table 9.3). This was not the case for the locations PMR, PML, CL and CR. For PMR and PML a simple coil rotation (-30 and +40 degrees) could be applied to direct the field perpendicular to the sulcal wall in the target region and make it optimal. The results for CR and CL deserve some more attention and are discussed in more detail in the section *Cerebellum* (9.4.5).

For the cerebellar (CL, CR & CM) and the DLPMC locations (PMR & PML) the choice of orientation was based on physiological outcome measures. For the SMA locations (SM1 & SM2) the choice of orientation was validated by physiological outcome measures. For the other locations the *standard* TMS coil orientations could be based on the theory that the induced field should be perpendicular to the underlying cortical gyrus. Therefore, one could say that it is not surprising that these coil orientations produce the electric fields with almost the strongest perpendicular component. However, most experimental studies still determine their coil orientation on general landmarks, for example an angle relative to the sagittal midline. The standard orientations used in this study are also not based on anatomical MRI data, but on these general landmarks. It is therefore reassuring that the orientations, based on these general landmarks, also produce electric fields with a strong perpendicular field in our subject-specific head model.

9.4.3 Generalization

Of course, due to the inter-individual differences in head and brain anatomy, the optimal coil orientations found in our model can be sub-optimal for other individuals. Nevertheless, there are still several important conclusions that can be drawn from the results presented. First and most important, the general rule that the figure-of-eight TMS coil

has to be oriented perpendicular to the underlying sulcal wall and has to induce an inward directed electric field is also valid for areas outside M1. This means that orienting the coil based on anatomical information about the targeted brain area (for example with anatomical MRI data) can improve the results of the study. Elaborate computational modeling might not be needed to determine the optimal orientation, although it can provide much information about the induced electric field. Secondly, it can be considered reassuring that the *standard* TMS coil orientations appear near optimal for the head model used in this study. This could imply that the inter-individual differences in curvature are small enough to not drastically changing the induced electric field (perpendicular to the cortical surface). However, the specific results for the locations PMR and PML lessen this statement. Third and lastly, the results show that a coil rotation of 10 degrees (*from the optimal orientation*) does not change the electric field much (*figure 9.3, appendix C (section 10.3)*). This means that small orientation errors (for example due to improper placement of the coil by the experimenter) will probably not affect the TMS-induced effects much. An orientation error of 90 degrees will definitely minimize the TMS effect, but this kind of error is highly improbable with the neuronavigational tools commonly used today.

9.4.4 I-waves and the perpendicular electric field

The cortical response to TMS depends on a complex interaction between the applied electric field distribution and the neural elements and networks in the cortex. Herein, the orientation of the electric field is essential, as shown in this study, but also aspects like the type of coil, stimulation (single, paired-pulse or repetitive) and pulse waveform are important.

A generally accepted theory to explain the mechanisms of cortical activation in M1 is based on the generation of the direct (D) and the indirect (I) waves. Stimulation of M1 with a figure-of-eight TMS coil, a monophasic waveform and a posterior-anterior (P-A) field direction, produces several I-waves, reflecting the indirect activation of the layer V pyramidal neurons (P5)⁹⁹. With higher intensities direct activation of the P5 neurons is accomplished as well, generating a D-wave. The corticospinal wave with the lowest TMS threshold for this specific type of stimulation is called the I1-wave. The generation of this wave has an orientation preference of the electric field (electric field directed PA to the hand-knob)⁹⁸. The indirect stimulation of layer V pyramidal neurons (P5) in this TMS set-up is probably due to the activation of excitatory pyramidal neurons in layers II (P2) and III (P3) in the cortex⁹⁷ (figure 9.5).

The P2 and P3 axonal connections to the P5 neurons lie within a cortical column, along the direction of the cortical column axis. This means that an electric field perpendicular to the cortical surface is likely to produce an I1-wave. Because the direction of the induced elec-

tric field is predominantly parallel to the plane of the TMS coil, the field in the sulci is mostly perpendicular to the cortical surface. At the top of the gyri the TMS-induced electric field is mostly parallel to the cortical surface. This would mean that the I1-wave following TMS stimulation originates in the sulcal wall. The later I-waves are produced by complex circuits, higher stimulation intensities and possibly by other electric field components⁹⁸. This could mean that the electric field direction preference is most applicable to the I1-wave and that the effects of coil orientation are most prominent at low stimulation intensities.

The results for stimulation of M1 with a figure-of-eight TMS coil, a monophasic waveform and a P-A field direction are nicely in agreement with the argument stated above. However, there are also other protocols and TMS hardware set-ups. For example, stimulation with a figure-of-eight coil and a biphasic waveform produces less homogeneous descending cortical volleys compared to stimulation with a monophasic waveform^{97,99}. This could mean that also other neural elements are activated by such stimulation. Still, the anterior-posterior-posterior-anterior (AP-PA) orientation produces a similar pattern of recruitment of D and I waves with increasing stimulation intensities as the monophasic PA stimulation^{97,99}.

The above argument is based on the assumption that cortical activation occurs through stimulation of neural elements aligned with the axis of the cortical column. However, this is certainly not the only possible mechanism of cortical activation. For a detailed discussion about the possible mechanisms of cortical activation and neural elements that can be stimulated by TMS, see for example⁷⁵.

9.4.5 Cerebellum

The results in table 9.3 and figure 9.4 suggest that the *standard* coil orientation for CR and CL stimulation, which induce an electric field with a caudal-rostral direction, cannot be considered optimal. The optimal orientations found in this study would induce a medial-lateral directed field. In addition, the results from table 9.3 suggest that lateral cerebellar stimulation is highly unlikely due to the low values for the perpendicular field. However, it is known from previous studies that the cerebellum can be stimulated^{95,152}.

There are two possible explanations for the discrepancies. The first reason could be that the neuronal structures in the cerebellum are quite different with their Purkinje cell population. These cells might be stimulated in a different way and more susceptible to an electric field that is directed parallel to the cerebellar surface. A different reason could be the absence of cerebellar gyri and sulci in this particular model. This is due to the fact that the model is based on 3-Tesla MRI in which the cerebellar gyri are too small to be discerned reliably on the MR images. Therefore, we cannot determine a perpendicular component

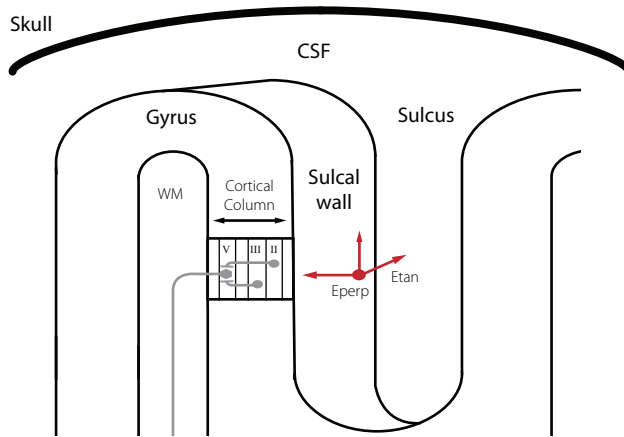


FIGURE 9.5. A simplified schematic representation of the cortical column in the sulcal wall. Included are neural elements (PII, PIII, PV) that are possibly stimulated by the electric field component aligned with the axis of the cortical column. The electric fields perpendicular (E_{perp}) and tangential (E_{tan}) to the sulcal wall are represented by red arrows.

of the electric field in the sulcal walls of the cerebellum. For future modeling studies that particularly focus on the cerebellum, it would be important to include cerebellar gyri in the model construction process.

9.4.6 Limitations and Validation

The C^3 -model is highly suitable to explain the effect of coil orientation on the activation of neuronal populations, but it is still a simplification of the mechanism responsible for the neural activation by TMS. The parallel component of the electric field might also contribute to the activation of neurons in the cortex. As mentioned earlier in the subsection *I-waves and the perpendicular electric field* (9.4.4), at higher intensities late I-waves are produced by more complex circuits and possibly other electric field directions⁹⁸. The notion that other electric field directions possibly also contribute to the generation of MEPs is strengthened by the study of Opitz et al. 2013¹⁴². Within a specified area of M1, correlations were found between the MEP amplitude and both the mean strength of the perpendicular component as well as the mean tangential component of the electric field. Although these findings appear to be in contrast to the assumption that the perpendicular component is the most important for coil orientation dependency, this is not necessarily the case. The correlations were determined for the variation in MEP amplitude due to coil position and not specifically for coil orientation. The strengths of both electric fields components are likely to depend on the distance to M1, as does the MEP amplitude. It could therefore still be that both electric field components contribute to the generation of MEPs, but that only the strength of the perpendicular component contributes to the orientation dependency.

The results of this study are also based on assumptions and simplifications about neuronal activation for different cortical areas. The most important ones are the similar mode of neuronal activation and the preferred direction of the electric field for all cortical areas. Nonetheless, the distribution or type of neurons may differ and also the preference of direction for activation by the induced electric field (see subsection 9.4.5; *Cerebellum*). However, the assumptions are justified by the fact that a similar basic columnar structure can be found all over the cerebral cortex^{76,123}. We think that as long as no knowledge is available about the differences in activation mechanisms between cortical areas due to TMS, it is reasonable to assume that the same intensity and direction relative to the CSF-GM boundary is needed to stimulate neuronal populations in all cerebral areas.

The presented FEM simulations are based on well-established laws of physics (subsection 9.2.3) and the calculated fields are valid. However, the results still have to be verified with careful validation experiments. In these experiments the dependence of the coil orientations should be tested for non-motor brain areas, for example with concurrent TMS-fMRI¹⁶, TMS-EEG¹⁵, phosphene threshold (*occipital cortex*) or with two coil - paired pulse protocols (*cortical areas connected to M1*). Such experiments have already been performed, for example for the SMA^{3,129} of which the physiological measurements are in agreement with the results presented here. Nevertheless, to validate the general rules that the induced electric field should always be directed perpendicular to the underlying gyrus and that small orientation changes do not have a large effect on the outcome measures, new validation experiments should be performed. In these experiments, the exact cortical target location should be verified with for example fMRI and the coil orientation should be varied in small 10-degree steps. This way the exact orientation relative to the cortical target can be determined. With these experiments also the justification of the previous mentioned simplifications about neural activation can be tested.

9.4.7 Future volume conduction models

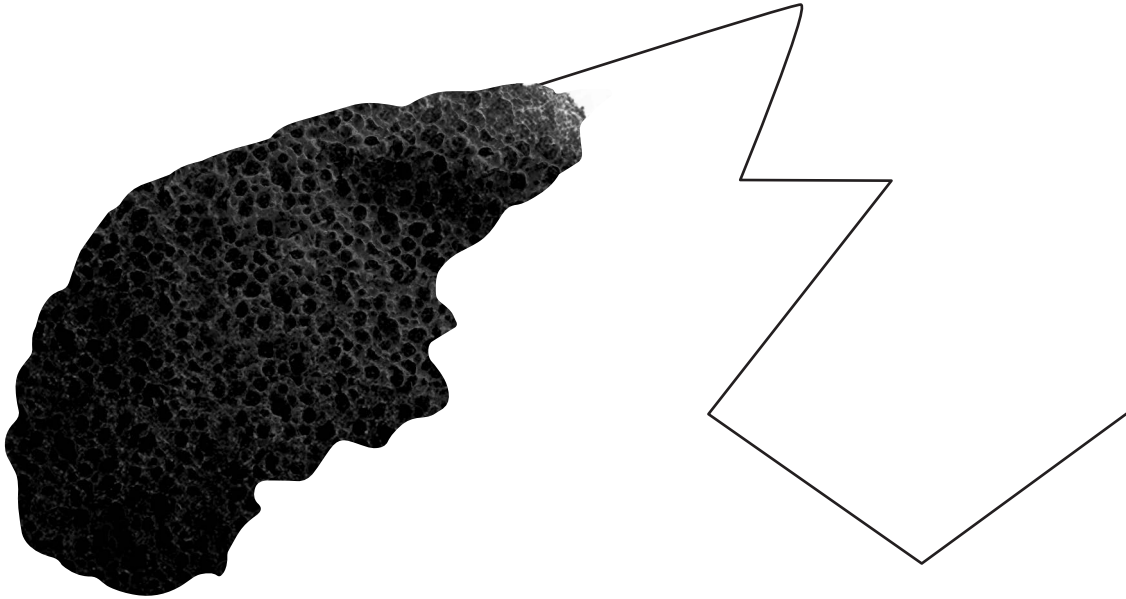
Previous reports mainly directed their attention on the strength of the electric field and did hardly address the electric field direction^{17,195}. Other studies did include direction, but focused only on one sulcus^{175,184}. We here want to make an argument for focusing on direction relative to the underlying cortical structures. In this study we decided to focus on the field perpendicular to the cortical surface, based on the *C³-mode*^{51,93}. A related approach would be to focus on the field direction guided by the first eigenvector of the DTI at the GM-WM interface¹⁴².

Producing complex and realistic finite element models is time-consuming and requires a significant amount of computational power. It is therefore that often spherical or low-resolution models are used instead. However lack of cortical curvature, as in the first spherical

models^{116,162}, makes it impossible to study the electric field within sulci and thereby underestimate the field perpendicular to the cortical surface. It can be concluded that modeling studies should include a realistic CSF-GM boundary to properly answer questions about the induced electric field at the cortical level.

9.5 CONCLUSIONS

The effect of coil orientation for multiple cortical target sites was determined and generalizations for all cortical areas were made. In addition, the optimality of ‘*standard*’ TMS coil orientations used in some example cognitive and clinical neuroscience studies were considered for our subject-specific volume conduction model. The results for M1 are nicely in agreement with experimental findings^{23,114} and confirm previous modeling results⁹³. For all cortical targets, the electric field perpendicular to the sulcal walls is considered to be the most effective and most susceptible to coil orientation changes. Small coil orientation changes do not alter the induced electric field drastically. We suggest that the general rule to optimize the effect of TMS should be that the strength of the electric field perpendicular to the targeted cortical surface area (and inward directed) has to be maximized. Therefore, orienting the coil based on anatomical information about the targeted brain area can improve future study results (for example with anatomical MRI data). The *standard* TMS coil orientations, based on previous studies, also seem to be near optimal for some cortical target areas in the subject-specific individual head model. This last finding has to be replicated with more than one subject model and the general rules about coil orientation should be validated with experimental studies.



Appendix A

Based on supplementary material

Janssen AM, Rampersad SM, Lucka F, Lanfer B, Lew S, Aydin U, Wolters CH, Stegeman DF, Oostendorp TF. The influence of sulcus width on simulated electric fields induced by transcranial magnetic stimulation.

Physics in Medicine and Biology, Vol. 58, p. 4881-4896, 2013. **To chapters 7, 8 and 9.**

Appendix B

Based on supplementary material

Janssen AM, Oostendorp TF, Stegeman DF. The effect of local anatomy on the electric field induced by TMS: evaluation at 14 different target sites.

Medical & Biological Engineering & Computing, Vol. 52, p. 873-883, 2014. **To chapter 8.**

Appendix C

Based on supplementary material

Janssen AM, Oostendorp TF, Stegeman DF. The coil orientation dependency of the electric field induced by TMS for M1 and other brain areas.

Journal of NeuroEngineering and Rehabilitation, Vol. 12(47), p. 1-13, 2015. **To chapter 9.**

10.

APPENDICES

10.1 APPENDIX A: MODEL CONSTRUCTION

10.1.1 Introduction

The research presented in **chapters 7-9** was performed with a volume conduction model (VCM) that represents a human head. The model included eight different tissue types, namely skin, skull spongiosa, skull compacta, neck muscle, eye, cerebrospinal fluid (CSF), gray matter (GM) and white matter (WM). An elaborate description of the construction process and a framework for creating a similar model can be found in the following subsections (10.1.2 – 10.1.7).

In the VCM of **chapter 7**, the GM-WM surface was not included explicitly in the construction of the volume mesh. First the volume mesh of the whole brain was constructed on the basis of the brain-CSF boundary. Subsequently the resulting tetrahedrons within the brain compartment were assigned to either GM or WM, based on their location according to the MRI segmentation (subsection 10.1.6). Tetrahedrons that cross the GM-WM segmentation boundary were assigned to the compartment that contained the largest volume fraction of that element. This was necessary because inclusion of the WM surface in construction of the tetrahedral mesh would cause too many intersections between the triangular surface meshes after the cortical alterations (subsection 7.2.2). For this same reason the cerebellum was not included in the construction of the head model. For the head model that was used in **chapters 8 and 9** the GM-WM surface and the cerebellum surface as obtained by the segmentation were incorporated explicitly in the VCM.

10.1.2 MRI acquisition

T1-, T2- and diffusion weighted (DW) magnetic resonance image (MRI) scans of a healthy 25-year old male subject were measured on a 3T MR scanner (Magnetom Trio, Siemens, Munich, Germany) with a 32-channel head coil. Written informed consent was obtained prior to scanning. The T1-weighted (T1w) image was acquired with an MP-RAGE pulse sequence (TR = 2300 ms, TE = 3.03 ms, TI = 1100 ms, flip angle = 8 degrees, FOV = 256 x 256 x 192 mm, voxel size = 1 x 1 x 1 mm) with fat suppression and GRAPPA parallel imaging

(acceleration factor = 2). The T2-weighted (T2w) image was acquired with an SPC pulse sequence (TR = 2000 ms, TE = 307 ms, FOV = 255 x 255 x 176 mm, voxel size = 0.99 x 1.0 x 1.0 mm interpolated to 0.498 x 0.498 x 1.00 mm). The T2w sequence was adjusted such that it gives a high contrast between the different layers of the skull (figure 10.1A). The field of view of both scans captured the complete head and was cut as low as the chin.

10.1.3 DTI acquisition

To estimate the anisotropic conductivity tensors for the brain, we used the assumption that the conductivity tensors share eigenvectors with the measured diffusion tensors¹¹. Modeling of the eigenvalues will be described below. The DW images were acquired with the standard Siemens pulse sequence ep2d_diff (TR = 7700 ms, TE = 89 ms, b-value = 1000 s/mm², bandwidth = 2000 Hz/pixel, FOV = 220 x 220 x 141 mm, voxel size = 2.2 x 2.2 x 2.2 mm) in 61 directions equally distributed on a sphere, and 7 images were acquired with flat diffusion gradient (DW factor b = 0 (B₀-)). Additionally, seven images with flat diffusion gradient (DW factor b = 0 (B₀+)) with reversed phase and frequency encoding gradients were acquired.

10.1.4 Segmentation

The T2-MRI was registered onto the T1-MRI using a rigid registration approach and mutual information as a cost-function as implemented in FSL^a. The compartments skin, skull compacta and skull spongiosa were then segmented from the registered T1w and T2w images using gray-value based active contour model²⁰⁹ and thresholding techniques. These segmentations were carefully checked and corrected manually to ensure the highest possible agreement with the MR images and make sure that the different tissues form closed surfaces (figure 10.1B). Eye, neck muscle and vertebrae segmentations were added manually. The vertebrae were connected to the skull compacta. The foramen magnum and the two optic canals were correctly modeled as skull openings. The segmentation of GM and WM was extracted from brain parcellation data of the T1w image created with the freely available Freesurfer^b software.

10.1.5 Triangular surface meshes

The software package CURRY^c was then used to extract high resolution triangular surface meshes of skin, eyes, skull compacta, skull spongiosa and muscle from the voxel-based segmentation volumes. The surfaces were smoothed using Taubin smoothing¹⁹² to remove the blocky structure which results from the fine surface sampling of the voxels. Triangular

a FLIRT - FMRIB's Linear Image Registration Tool, <http://www.fmrib.ox.ac.uk/fsl/flirt/index.html>

b <http://surfer.nmr.mgh.harvard.edu/>

c CURRent Reconstruction and Imaging (CURRY), <http://www.neuroscan.com/>

surface meshes of all brain parcellations were made in MATLAB^d and refined using the package iso2mesh^{e,44} (figure 10.1C). As Freesurfer produces separate segmentations for each hemisphere, the hemispheres had to be attached whereby (self-)intersections were removed with custom MATLAB code. The WM surface that crossed out of the GM surface especially in the inferior brain region was identified and corrected to remain inside of the GM surface. At some locations in the segmentation the brain touches the skull. To avoid resulting intersections between the GM and compacta surfaces, the complete brain was scaled down by 2% and flattened at remaining intersections.

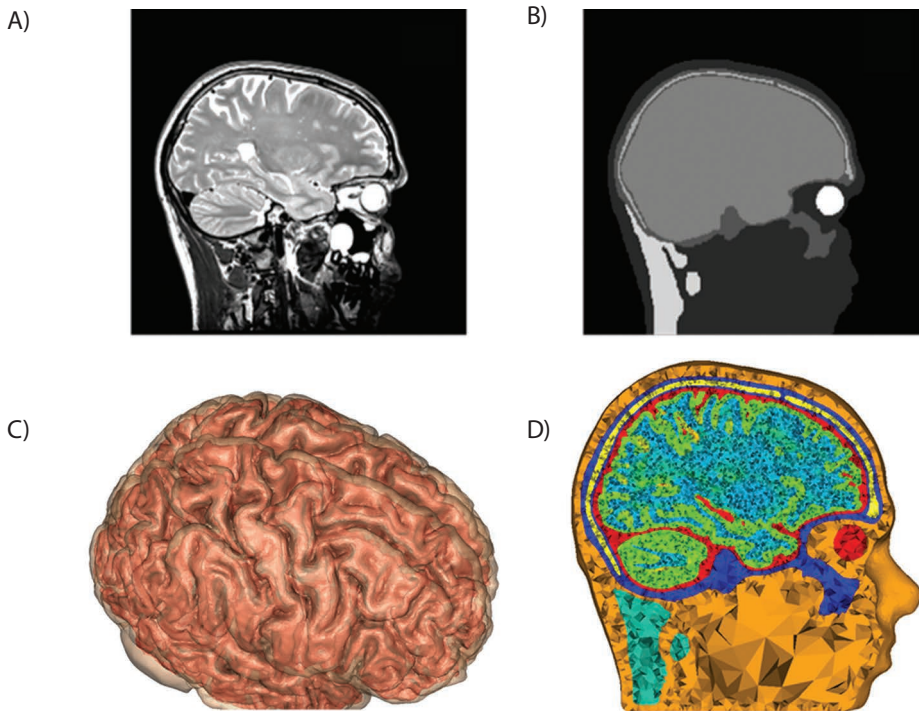


FIGURE 10.1. (A) A sagittal cut plane of the T2w MRI showing the different skull layers. (B) The same sagittal cut plane of the manually corrected segmentation including skin, skull compacta, skull spongiosa, neck muscle, eyes and one compartment for inner skull (CSF, GM and WM, before segmentation with Freesurfer). (C) High resolution triangular meshes of GM (transparent) and WM (red), constructed with Freesurfer. (D) Sagittal cut plane of the final tetrahedral volume mesh created with TetGen. The different tissue types are represented with different colors. The corresponding bulk conductivities are given in table 10.1. This illustration is adapted from Janssen et al. 2013⁸².

^d MathWorks, Natick, Massachusetts, USA

^e <http://iso2mesh.sourceforge.net/cgi-bin/index.cgi>

10.1.6 Tetrahedral volume meshes

The smoothed surfaces (skin, compacta, spongiosa, GM, WM, left eye, right eye, muscle) were then used to create a high quality 3D Delaunay triangulation via TetGen^f. This resulted in a mesh consisting of 672k nodes and 4.12M linear tetrahedral elements (figure 10.1D) (575k nodes and 3.54M tetrahedral elements for the mesh used in **chapter 7**). The element size in the brain was restricted to 1 mm³. Due to the use of detailed surfaces, the elements of the skull and CSF are very small as well. A tissue index was assigned to all elements in the space between two surfaces, or inside a closed surface. We used an additional closed skull surface to label all elements within the skull surface that are not part of the brain compartments as CSF.

10.1.7 Anisotropic conductivity tensors

An important aspect of a realistic head model is tissue anisotropy¹¹⁶. For adult human subjects, the effect of brain anisotropy is mainly significant for the WM, some smaller effects can be found for the GM as well¹⁴³.

The DW MR images were corrected for eddy current (EC) artifacts by registering each directional image to the average B_0+ image using the FSL routine FLIRT. After EC correction, the gradient directions were reoriented by multiplying them with the rotational part of the transformation matrix¹⁰⁰. Other main error sources for DTI analysis are the susceptibility artifacts. In order to correct for susceptibility artifacts, we used a reversed gradient approach that uses the averaged B_0+ and B_0- images to compute, using a problem-adapted multi-scale nonlinear image registration procedure, smooth and diffeomorphic geometric transformations¹⁷¹. This approach is implemented in the freely available FAIR toolbox^g. The EC and susceptibility corrections then allowed a simple rigid registration of the artifact-corrected averaged B_0 image to the T2w image (which was already registered to the T1w image in a previous step) using FLIRT. The transformation matrix obtained in this step was then used to also register the directional images to the T2w image (which is in T1 space). At this step, the corresponding gradient directions were also reoriented accordingly. From the artifact-corrected and registered DW images the diffusion tensors were then calculated using the FSL routine DTIFIT¹². In a last step, conductivity tensors were calculated from these diffusion tensors using the volume-normalized approach as described in Opitz et al. 2011¹⁴³. Next, the conductivity tensors were mapped from the MRI voxels onto the GM and WM elements of the tetrahedral head mesh described above. The normalized eigenvectors were multiplied with the conductivities of the tissues for WM and GM separately¹⁴³. The bulk conductivity values and the literature sources for all tissues can be found in table 10.1.

f TetGen: A Quality Tetrahedral Mesh Generator and a 3D Delaunay Triangulator, <http://tetgen.berlios.de/>

g Flexible Algorithms for Image Registration (FAIR), <http://www.siam.org/books/fa06/>

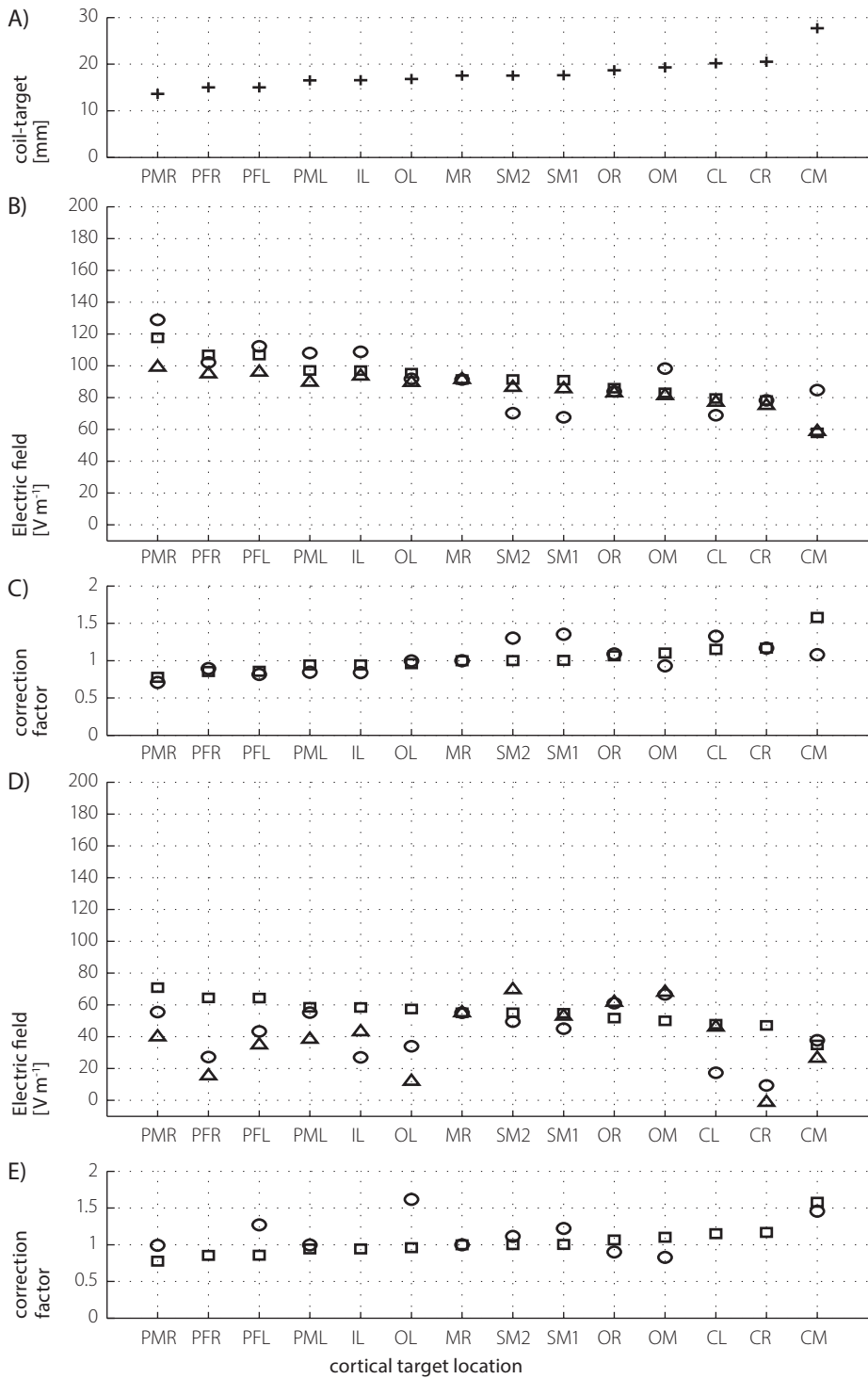
TABLE 10.1. The bulk conductivity values ($S\ m^{-1}$) for all the tissue types used in the standard model.

TISSUE TYPE	BULK CONDUCTIVITY ($S\ m^{-1}$)
Skin	0.465^{214}
Skull compacta	0.007^1
Skull spongiosa	0.025^1
CSF	1.65^{214}
Neck muscle	0.4^{43}
Eyes	1.5^{128}
GM	0.276^{214}
WM	0.126^{214}

10.2 APPENDIX B: SIZE EFFECT OF REGION OF INTEREST IN THE ANALYSES OF CHAPTER 8

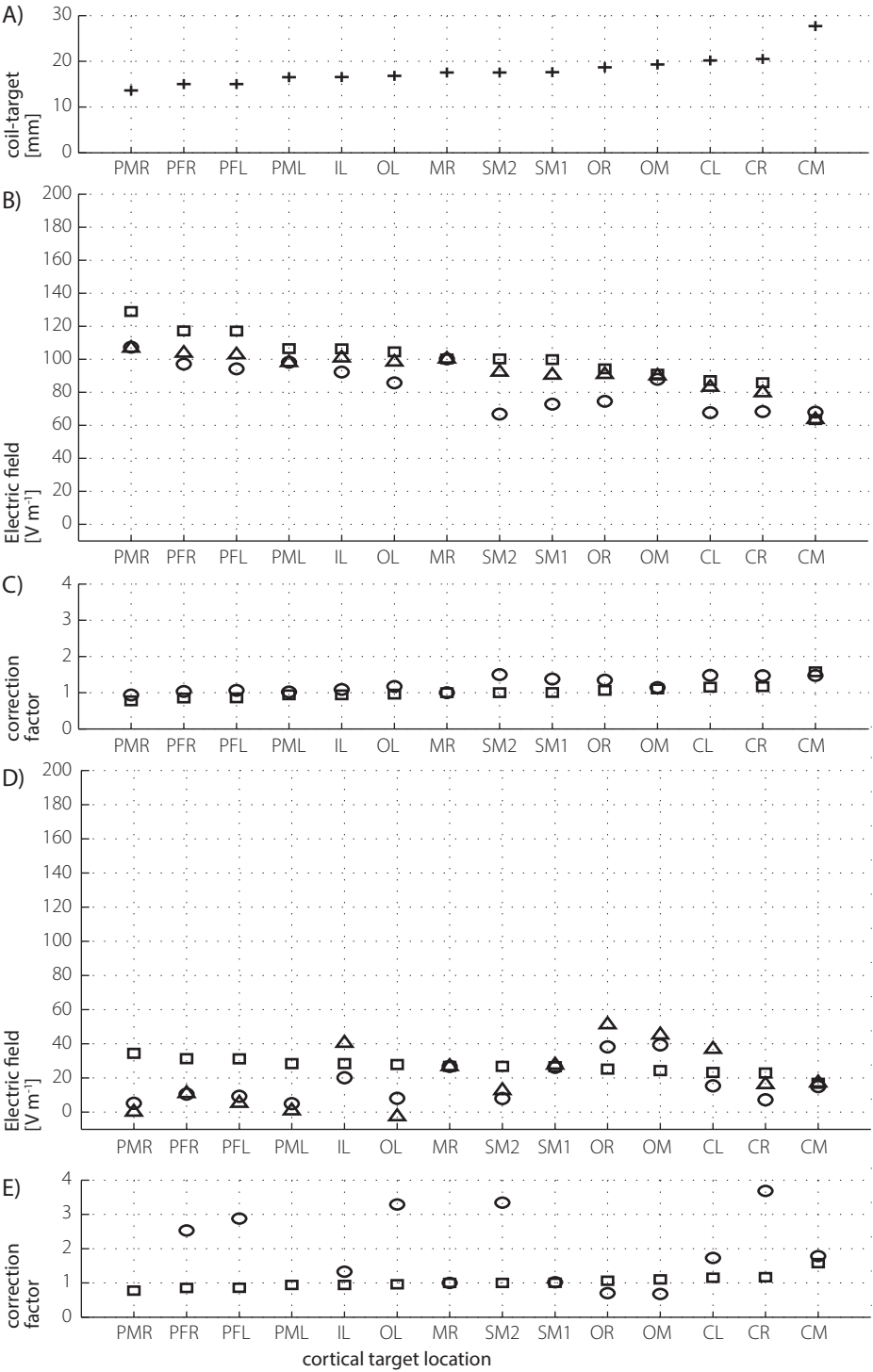
The analyses for all gray matter elements within a radius of 5 mm of the cortical target location.

FIGURE 10.2. (A) The distance between the center of the TMS coil and the cortical target location. (B) Per cortical target location, the mean electric field strength \bar{E} (○, equation 8.1) and the estimated fields based on the inverse of the distance \tilde{E}_R (□, equation 8.2) and on the primary electric field \tilde{E}_A (Δ, equation 8.3). (C) Per cortical target location, the correction factor to produce a similar electric field as is induced over the right hemispheric M1 (MR), based on \bar{E} (○) and on the inverse of the distance \tilde{E}_R (□). (D) Per cortical target location, the mean field strength in the direction perpendicular to the CSF-GM boundary \bar{E}_\perp (○) and the estimated fields based on the inverse of the distance \tilde{E}_R (□, equation 8.2) and on the primary electric field in the direction perpendicular to the CSF-GM boundary $\tilde{E}_{A\perp}$ (Δ, equation 8.3). (E) Per cortical target location, the correction factor to produce a similar electric field as is induced over the right hemispheric M1 (MR), based on \bar{E}_\perp (○) and on the inverse of the distance \tilde{E}_R (□). In all five subfigures, the locations are coded according to table 8.2. Page 137 >>



The analyses for all gray matter elements within a radius of 10 mm of the cortical target location.

FIGURE 10.3. (A) The distance between the center of the TMS coil and the cortical target location. (B) Per cortical target location, the mean electric field strength \bar{E} (○, equation 8.1) and the estimated fields based on the inverse of the distance \tilde{E}_R (□, equation 8.2) and on the primary electric field \tilde{E}_A (Δ, equation 8.3). (C) Per cortical target location, the correction factor to produce a similar electric field as is induced over the right hemispheric M1 (MR), based on \bar{E} (○) and on the inverse of the distance \tilde{E}_R (□). (D) Per cortical target location, the mean field strength in the direction perpendicular to the CSF-GM boundary \bar{E}_\perp (○) and the estimated fields based on the inverse of the distance \tilde{E}_R (□, equation 8.2) and on the primary electric field in the direction perpendicular to the CSF-GM boundary $\tilde{E}_{A\perp}$ (Δ, equation 8.3). (E) Per cortical target location, the correction factor to produce a similar electric field as is induced over the right hemispheric M1 (MR), based on \bar{E}_\perp (○) and on the inverse of the distance \tilde{E}_R (□). In all five subfigures, the locations are coded according to table 8.2. Page 139 >>



10.3 APPENDIX C: THE EFFECT OF COIL ROTATION FOR 13 CORTICAL LOCATIONS

For all figures: The mean electric field values for (A) $|\vec{E}|$ and (B) E_{\perp} within the target regions (see subsection 9.2.4) defined in table 9.1. The standard coil orientation from literature is indicated in both panels (circle with cross). The coils are rotated in steps of 10 degrees.

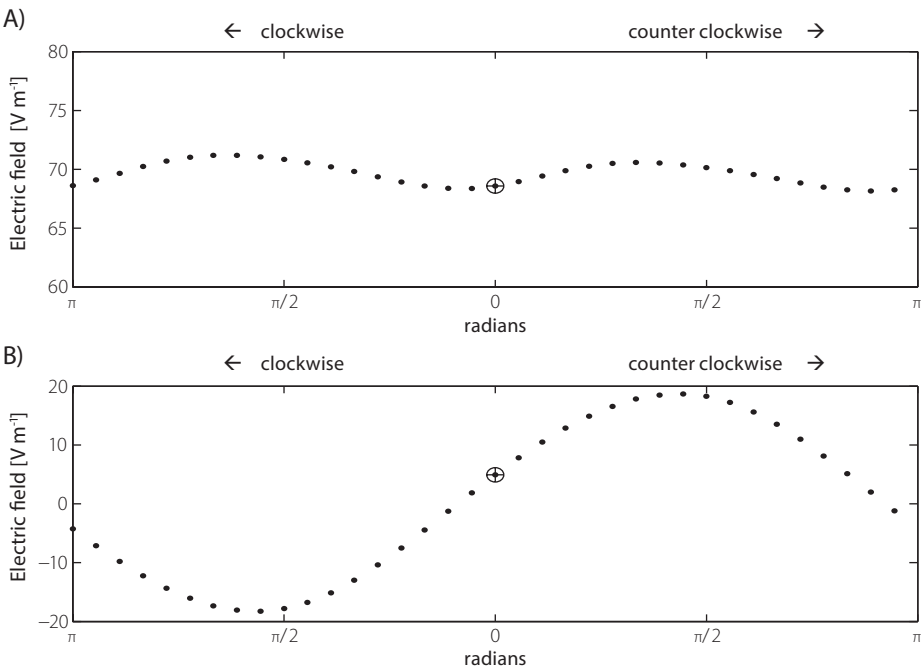


FIGURE 10.4.1. Lateral cerebellum left (CL)

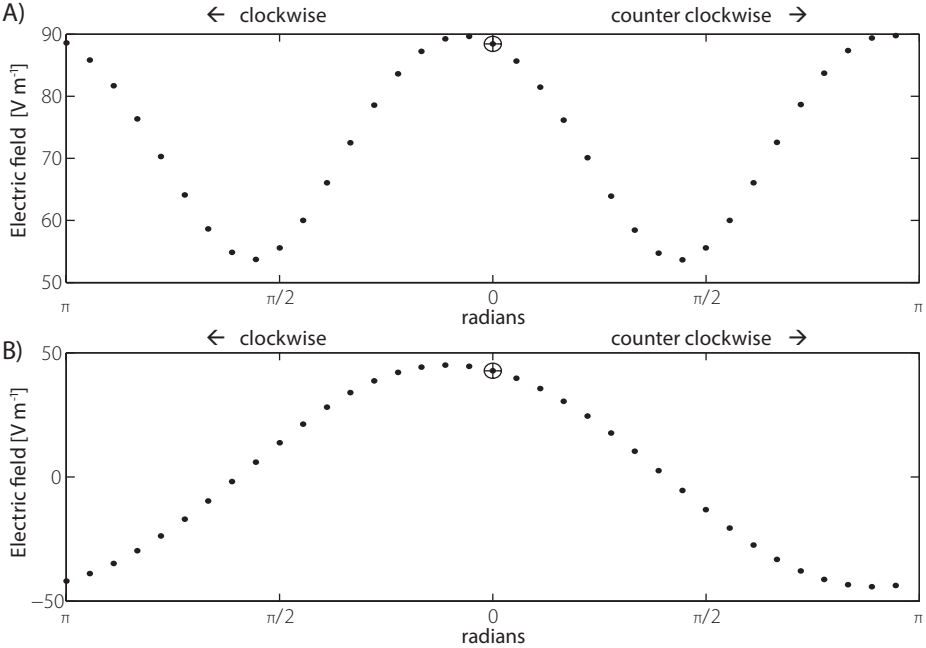


FIGURE 10.4.2. Medial cerebellum (CM)

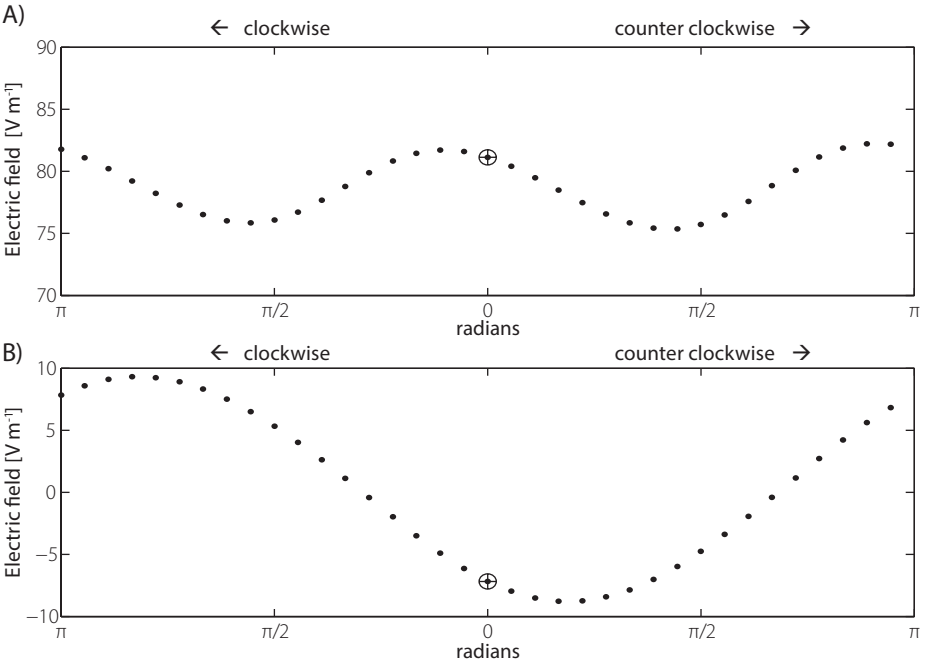


FIGURE 10.4.3. Lateral cerebellum right (CR)

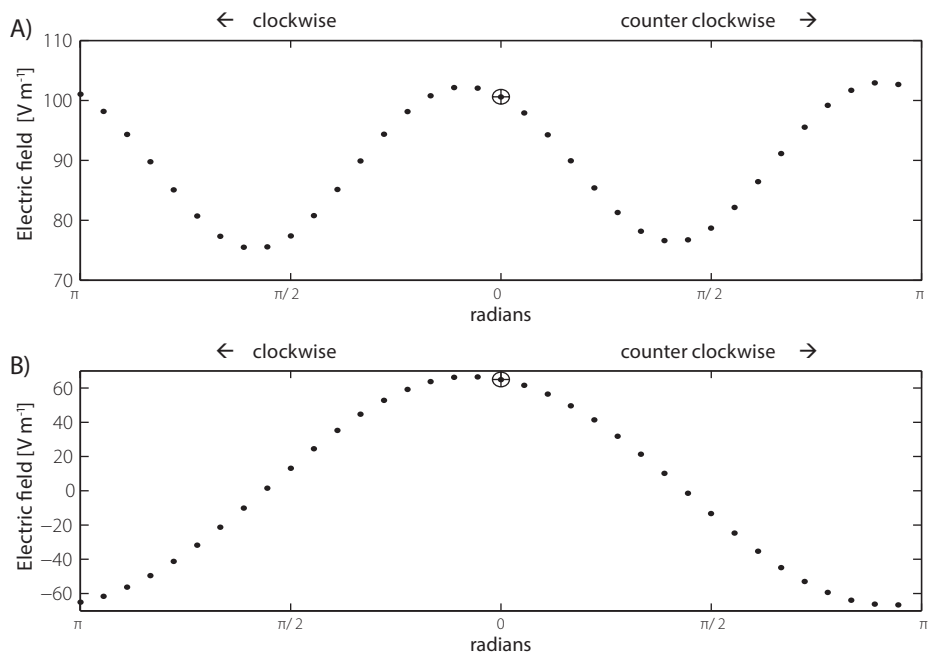


FIGURE 10.4.4. Occipital lobe left hemisphere (OL)

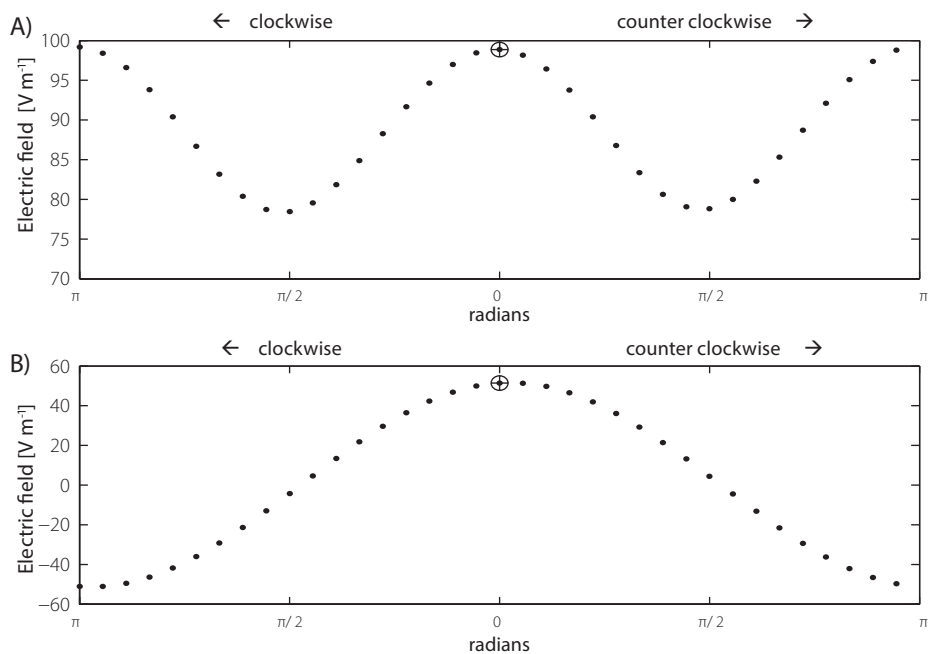


FIGURE 10.4.5. Medial occipital cortex (OM)

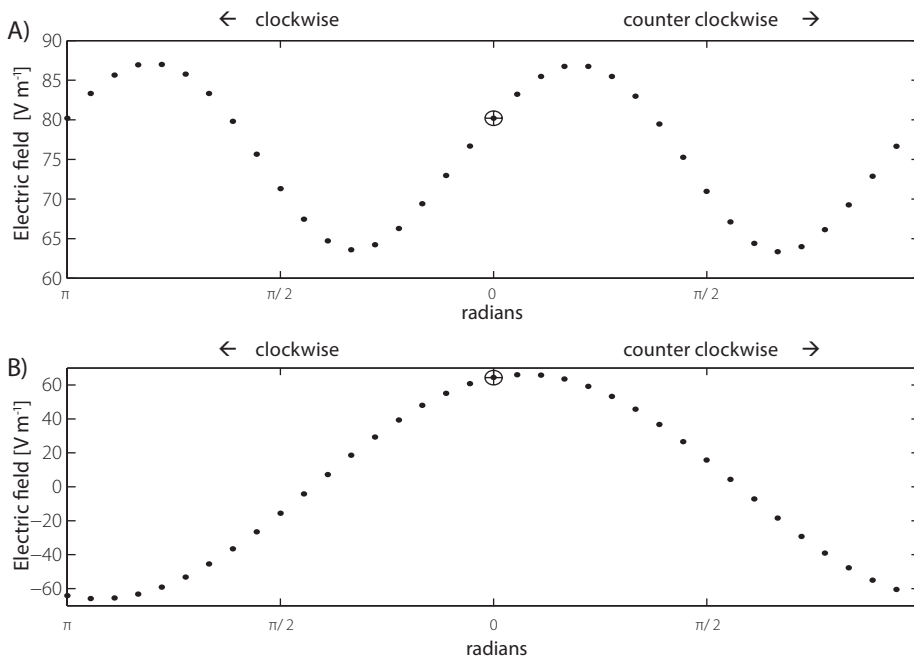


FIGURE 10.4.6. Occipital lobe right hemisphere (OR)

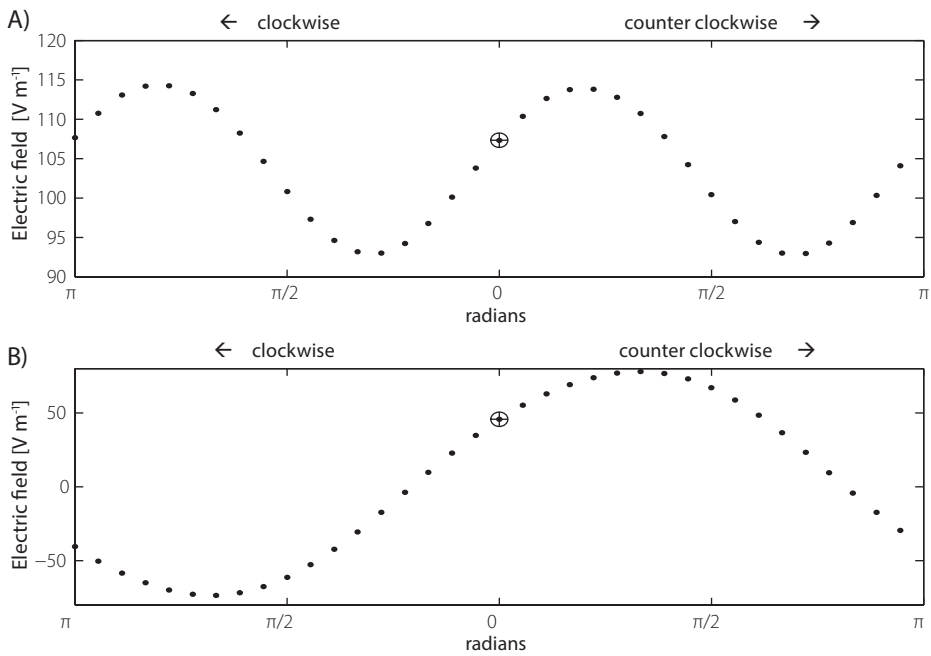


FIGURE 10.4.7. Dorsolateral premotor cortex left hemisphere (PML)

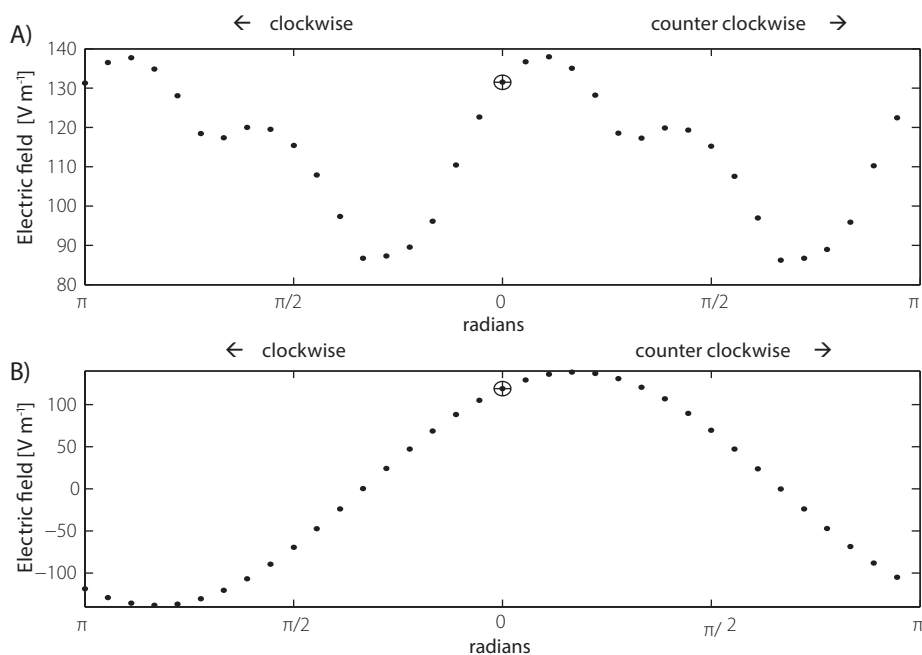


FIGURE 10.4.8. *Dorsolateral premotor cortex right hemisphere (PMR)*

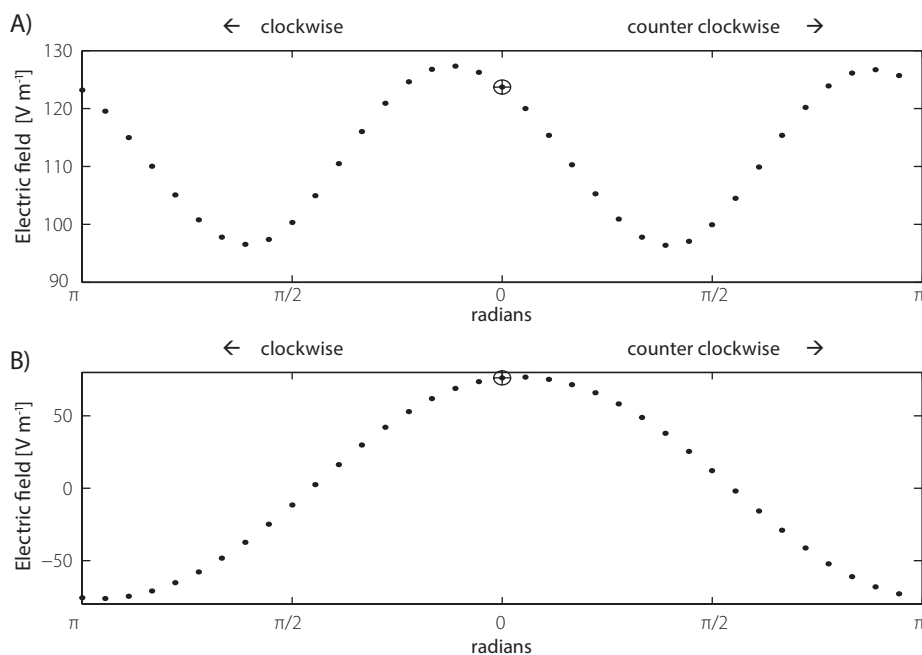


FIGURE 10.4.9. *Dorsolateral prefrontal cortex left hemisphere (PFL)*

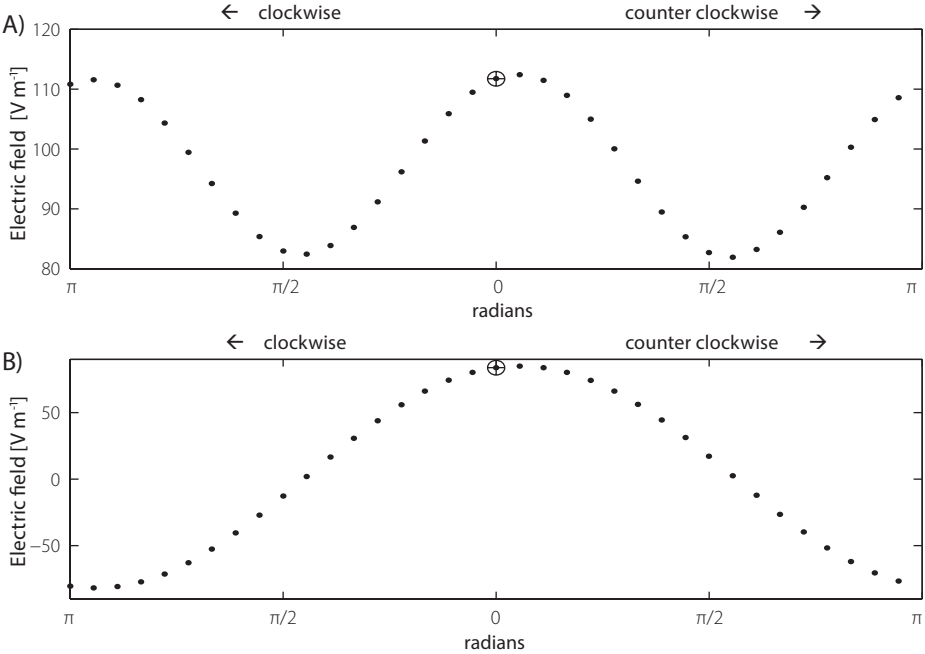


FIGURE 10.4.10. Dorsolateral prefrontal cortex right hemisphere (PFR)

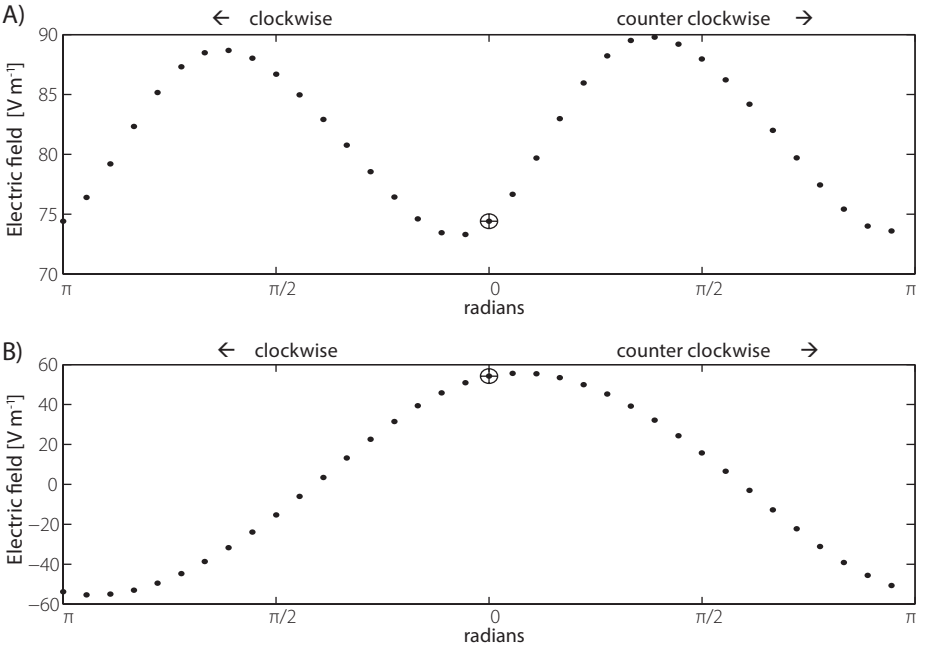


FIGURE 10.4.11. Supplementary motor area 30 mm anterior to Cz (SM1)

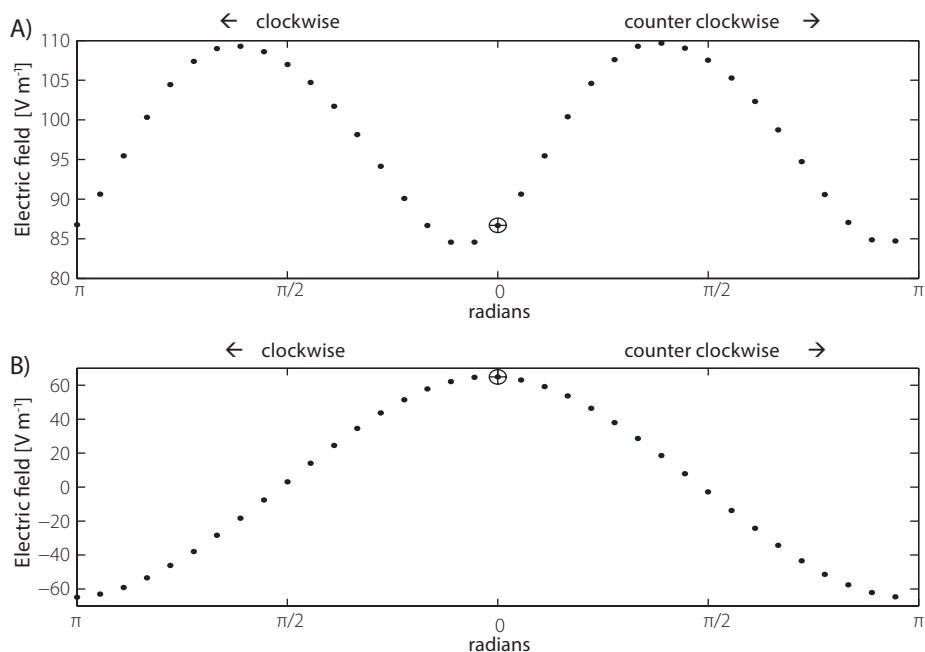


FIGURE 10.4.12. *Supplementary motor area 50 mm anterior to Cz (SM2)*

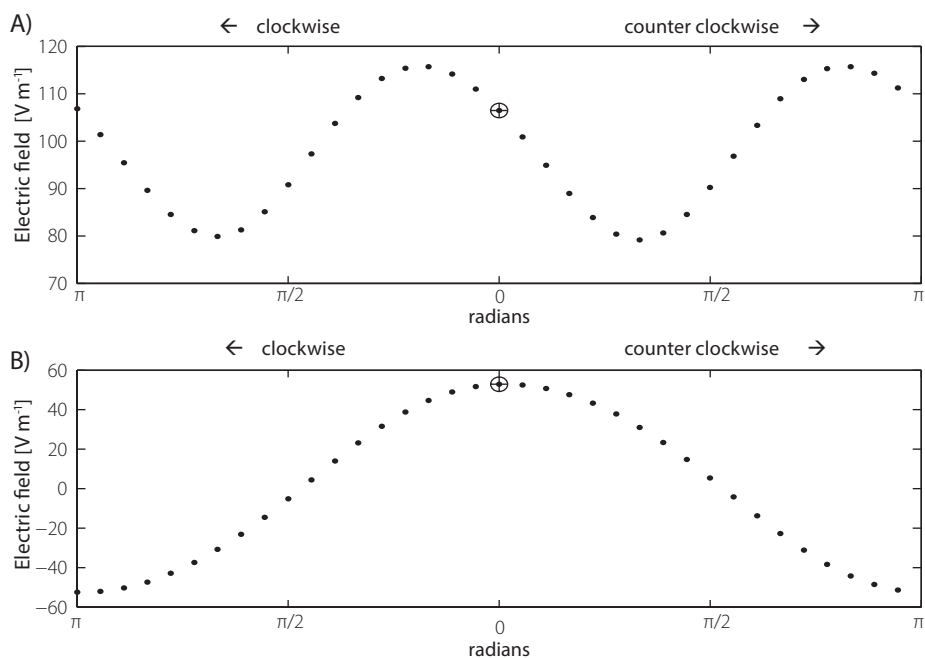
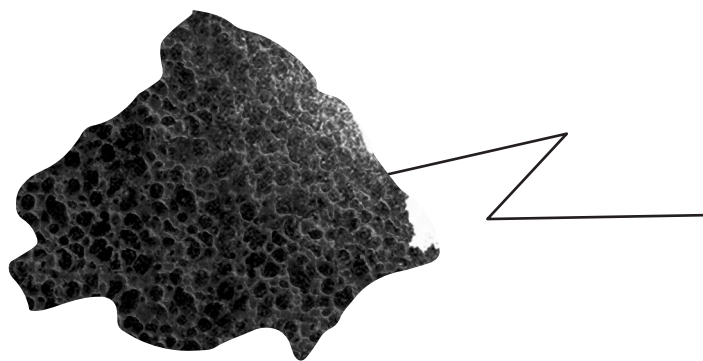


FIGURE 10.4.13. *Inferior frontal gyrus (IL)*



PART IV

SUMMARY & GENERAL DISCUSSION



11.

SUMMARY & GENERAL DISCUSSION

A decorative line graphic consisting of a horizontal line with a jagged, mountain-like peak on the right side.

11.1 OUTLINE CHAPTERS

In this thesis five scientific studies were presented. After the introductory **part 1** (**chapters 1 - 2**) and the first chapter of **part 2** (**chapter 3**), **part 2** of this thesis described two studies on freezing of gait (FOG) in patients with Parkinson's disease (PD). In **chapter 4**, transcranial magnetic stimulation (TMS) was used as an investigatory tool to study the effect of cerebellar theta burst stimulation (TBS) on freezing. **Chapter 5** was devoted to the evaluation of the gait tasks that were used in **chapter 4**, with the goal to improve future gait protocols that aim at evoking freezing during gait in a research set-up. In **part 3**, volume conduction modeling was used to explore the electric field in the brain induced by TMS. The goal was to examine the induced electric fields for areas other than the motor cortex and to use the information thus obtained to improve future stimulation protocols. Now follows a summary of the main findings (11.2 & 11.3). Subsequently, the findings are reviewed in a general discussion (11.4) that places the chapters in a broader perspective and discusses future perspectives.

11.2 PARKINSON'S DISEASE, FREEZING OF GAIT & CEREBELLAR THETA BURST STIMULATION

11.2.1 Cerebellar theta burst stimulation improves gait speed

FOG is common in patients with PD. Although the clinical presentation and the factors that provoke FOG are becoming better defined, the mechanism behind its occurrence is still not fully understood. In **chapter 4**, we focused on the possible role of the cerebellum in the pathophysiology underlying FOG. In PD, FOG most likely results from dysfunction within a complex neural gait circuitry involving multiple brain regions. Previous studies suggested that the role of the cerebellum in the motor control of PD is compensatory^{2,144,161,221,224}. We therefore tested if PD patients with FOG could benefit from repeti-

tive TMS of the cerebellum, as a means to non-invasively stimulate cerebellar functioning and thereby boost its compensatory function. In 17 PD patients with objectively verified FOG, cerebellar activity was modified unilaterally by either facilitatory iTBS or inhibitory cTBS, applied during two separate sessions. The lateral cerebellum corresponded to the side that was most affected. Before and directly after the stimulation, gait and bimanual rhythmic upper limb movements were monitored and freezing episodes were quantified. Gait was evaluated with the task battery, including full rapid turns and walking with short steps. Upper limb movement performance was evaluated with a repetitive finger flexion-extension task. The main conclusion was that both TBS protocols (facilitatory iTBS and inhibitory cTBS) did not significantly alter the amount of gait freezing, nor the amount of hand freezing, but did change gait speed. An increase in overall gait speed when walking with small steps was found after iTBS, while gait speed during normal and fast walking decreased after cTBS. Although alteration of cerebellar activity with TBS did not decrease the amount of FOG, the results do suggest that an improvement in gait performance is possible after cerebellar iTBS. We suspect that the increase in gait speed following facilitatory stimulation is due to an increase in cerebellar activity and a strengthening of cerebello-cortical connectivity, suggesting a compensatory role of the cerebellum in PD.

11.2.2 Short rapid steps to provoke freezing of gait

Due to its episodic nature and suppression by anxiety or attention, it is a challenge to provoke FOG both in clinical practice, and even more so in a research setting. In **chapter 5** the effectiveness of walking with short steps to provoke FOG was compared to rapid turning. Previous investigations had shown that turning is suited best to provoke FOG, particularly when performed as rapidly as possible¹⁸⁶. However, walking with short steps has been used as an alternative²⁸. We evaluated what the diagnostic value of a short steps task, especially when performed as rapidly as possible, is compared to rapid turning. Twenty-eight PD patients with objectively verified FOG performed the following tasks: (1) normal walking, (2) walking as rapidly as possible, (3) walking with short steps, (4) walking with short steps as rapidly as possible and (5) making full rapid turns in both directions. All tasks combined provoked FOG in 20 subjects (71%), with rapid full turns being the most effective test to provoke FOG (64% of subjects). FOG occurred more often when patients walked with rapid short steps (50%) compared to walking with short steps at normal speed (18%). The combination of full rapid turns and walking rapidly with short steps yielded the highest sensitivity of provoking FOG (71%). This study confirmed previous findings about full rapid turns being the most effective clinical test to provoke FOG in clinical or research settings¹⁸⁶. If negative, walking with short steps as rapidly as possible can further identify subjects with FOG. For both turning¹⁸⁶ and walking with short steps, the instruction to perform the test 'as rapidly as possible' is essential.

11.3 TRANSCRANIAL MAGNETIC STIMULATION & THE FINITE ELEMENT METHOD

11.3.1 Modeling sulcus width

A detailed volume conduction model (VCM), using a finite element method (FEM) approach, was employed to acquire knowledge about the TMS-induced electric fields at a macroscopic level in the brain (i.e. at the cortical level, but not at the level of individual neurons). In this VCM a highly realistic representation of the cortical surface geometry was included. It is important to know how accurate the cortex should be represented in the cortical surface geometry. In **Chapter 7**, the importance of properly represented sulci and gyri in the cortical surface geometry was investigated. Due to the high conductive properties of the cerebrospinal fluid (CSF), it can be expected that alterations in the sulcus width of the cortical surface geometry can have a significant effect on the distribution of the TMS-induced electric field. To quantify the impact of such alterations, the sulcus width of the cortical surface geometry in the VCM was altered systematically. The simulated electric fields showed that a slight alteration to the cortical surface causes small, rather patchy changes. This means that for a global approximation of the electric field, the incorporation of an accurate description of the sulci is not highly important. However, considerable overestimation of sulcus width produces an overestimation of the calculated local field strength. This means that for estimations about the maxima in the electric field and (future) combinations with neuron models, an accurate description of the sulcus width is important.

11.3.2 Local anatomy and coil-target distance

In **Chapter 8**, the detailed volume conduction model was used to determine in what way the induced electric fields differ between cortical target regions. Many human cortical regions are targeted with TMS and the stimulus intensity used for a certain region is generally based on the motor threshold (MT) determined over the motor cortex (M1). It is well known that differences exist in coil-target distance and target site anatomy between cortical regions. These differences may well make the stimulation intensity derived from M1 sub-optimal for other regions. To examine the differences in the induced electric field for multiple target sites, the effects on the electric field, due to coil-target distance and target site anatomy have been quantified. The results show that a simple correction based on the inverse of the distance, as often used, does not correctly adjust the induced electric field for regions other than M1. A better adjustment should indeed take into account the coil-target distance, but also the local anatomy of the cortical target site. A secondary field is caused by charge accumulation at the conductivity discontinuities, such as the CSF - brain boundary. Because the local anatomy is variable, this secondary field is unique for each targeted region. This unfortunately means that an adjustment of stimulation intensity for should not only be based on the coil-target distance, but also on target site anatomy for stimulation other than M1.

11.3.3 Coil orientation

The effectiveness of TMS has proven to depend highly on the coil orientation relative to the subject's head^{7,23,114}. This implies that the efficiency of TMS is largely dependent on the direction of the induced electric field. Knowledge about the relationship between the coil orientation and the direction of the induced electric field on the one hand, and the head and (local) brain anatomy on the other hand, seems essential. In **Chapter 9**, the induced electric field in the cortex as a function of the coil orientation has been examined. The induced electric field was calculated for fourteen cortical targets and thirty-six coil orientations per target location. The effect of coil rotation in combination with target site anatomy on the electric field has been quantified. The electric field perpendicular to the anterior sulcal wall of the central sulcus is determined to a large degree by the coil orientation. This has also been found in previous research⁹³. We showed that the electric fields for areas other than the motor cortex also depend on the coil rotation. According to the assumption that the electric field should be perpendicular to the cortical surface, an optimal coil orientation can be determined for these areas as well. Small orientation changes (10 degrees) do not alter the induced electric field drastically. The results from the fourteen cortical targets in this study can be extrapolated to all cortical areas, and generalizations can be made. We suggest that the general rule to optimize the effect of TMS should be that the strength of the electric field perpendicular to the targeted cortical surface area (and inward directed) has to be maximized. This means that future experimental protocols can be improved by orienting the TMS coil based on anatomical information about the targeted brain area (for example with structural magnetic resonance imaging (MRI) data).

11.4 GENERAL DISCUSSION

11.4.1 Non-invasive brain stimulation and freezing of gait

Freezing of gait is an episodic phenomenon that causes serious discomfort in a patient's daily life. It is a parkinsonian symptom that is not present in all PD patients. To effectively treat PD patients with FOG, it is important to unravel the neural mechanism responsible for this symptom. In **chapter 4** we investigated the role of the cerebellum, which has been proposed to be compensatory^{2,144,161,221,224}, and tested whether an intervention with cerebellar TBS could be beneficial. No significant effects on FOG were found, but changes in gait speed were observed after stimulation. This suggests that the cerebellum does play a role in the neural circuits responsible for gait that are affected in PD patients with FOG. It has not (yet) been proven if cerebellar TBS boosts a compensatory activity or hampers a pathological activity.

To further investigate the question about compensatory or pathological activity in the cerebellum, future neuroimaging studies with techniques such as functional magnetic resonance imaging (fMRI), magnetoencephalography (MEG), EEG or PET are necessary. Such studies should first focus on the question which parts of the cerebellum are actually affected by the stimulation and how they are affected. It would be interesting to know whether the superficial Purkinje system is stimulated, or whether the deeper structures of the dentate nuclei (DN) are reached as well. Previous studies on cerebellar stimulation suggest that TMS targets the Purkinje system^{33,95}, which has an inhibitory projection to the DN. Facilitatory stimulation would thereby have inhibitory effects on the DN. However, with direct stimulation of the DN, the effect would be facilitatory. A previous report about inhibitory cerebellar TBS suggests that also the DN and cerebellar vermis are affected directly by stimulation²⁵.

It would require neuroimaging studies to reveal how the stimulation affects neuronal networks further down the line, as the DN exerts a tonic facilitatory drive through the ventral lateral thalamus to the motor cortex. It has been suggested that this facilitatory drive can be altered in magnitude by cerebellar repetitive transcranial magnetic stimulation (rTMS)^{39,113}. Also, facilitatory cerebellar TBS increases activity in the caudate nucleus bilaterally of progressive supranuclear palsy (PSP) patients²⁶. In combination with clinical measures, neuroimaging can therefore help to answer the question if cerebellar TBS boosts or hampers cerebellar activity.

Despite the unknown effects, facilitatory TBS did increase gait speed. The increased gait speed could imply an improvement in gait performance, which suggests that a beneficial effect can be obtained from non-invasive brain stimulation. This provides directions for future research and possible therapeutic purposes. However, the effects of cerebellar TBS should be improved in order to prolong and intensify the effects, in order to make this a clinically relevant and feasible intervention. Volume conduction modeling can help to design protocols that might achieve such prolonged and stronger effects. In subsections 11.4.3 and 11.4.4 it will be discussed how the results of the volume conduction modeling studies (**chapters 7-9**) may improve TMS protocols for brain areas other than the motor cortex.

Although no effects of the cerebellar TBS on FOG were found, the increased gait speed suggests that (positive) effects on FOG are possible. To increase the chance of finding such an effect on FOG, not only the stimulation protocol should be improved in future studies, but the gait protocol as well. The protocol should be focused more on FOG provoking tasks and not include tasks that evoke only a few episodes. In **chapter 5**, we evaluated the gait task battery that was used in **chapter 4**. We will now discuss the implications of the results.

11.4.2 Improving the gait task battery

In order to unravel the underlying neural mechanisms, FOG has to be evoked as reliably as possible in a clinical or research setting. Not every task evokes FOG equally well and due to its episodic character the same task does not always provoke freezing at every trial. In **chapter 4**, a battery of tasks was tested before and after the cerebellar TBS. In **chapter 5** we examined this battery to determine which tasks did actually provoke FOG best. Turning had already proven to be effective in provoking FOG⁸⁶, but also walking with short steps had been advocated before²⁸. In future studies these tasks should be used as much as possible with the instruction to perform them 'as rapidly as possible'. Turning is still the best choice of task to evoke FOG, but a protocol that also includes short rapid steps increases the likelihood of observing FOG. Normal walking, rapid walking with a normal stride length, and walking with short steps but at a normal pace, appeared not useful in a protocol, as these tasks have a much smaller chance of evoking FOG. When walking in a straight line is required, short steps as rapidly as possible is the best choice of task. In all situations, repetition of the task is highly important, as even turning does not provoke FOG in every trial.

11.4.3 Improving stimulation

The ultimate goal of the volume conduction modeling research in this thesis (**chapters 7-9**) was to improve TMS protocols for areas other than the motor cortex. It is common practice, also for cerebellar stimulation, to use TMS protocols designed for the motor cortex for other cortical brain areas. Differences in anatomy and physiology are ignored. The stimulation intensities in the TMS protocols are the same as used for the motor cortex. The coil placement for these areas is usually based on anatomical landmarks on the scalp and coil orientation is determined relative to the midsagittal plane. The results of **chapters 8 and 9** show that all these aspects result in an unknown, probably suboptimal, electric field strength at the cortical level. It would certainly be an improvement if stimulation protocols were adapted to the targeted brain region with respect to at least two aspects.

Firstly, to improve stimulation protocols, coil position and orientation have to be optimized. Using individual anatomical information from MRI scans to position the coil above the cortical target would already be an improvement. This will ensure that the same cortical structure is stimulated in each individual patient. Information from fMRI, transferred to individual anatomical coordinates, will even further improve coil placement. Anatomical information can possibly also help to optimize coil orientation. The optimal TMS coil orientation in the volume conduction modeling of this thesis was based on the assumption that cortical activation occurs through stimulation of neural elements aligned with the axis of the cortical column. This assumption currently best fits the existing experimental data and theories about coil orientation. This means that the component of the induced

electric field perpendicular to the cortical surface should be maximized. The best way to achieve this is to determine the coil orientation that produces the optimal electric field according to volume conduction modeling. However, when this is not available, orienting the coil based on anatomical information from MRI scans is the second best choice. In this case, the coil should be oriented in such a way that the primary electric field (see section 6.2) is directed perpendicular to the sulcal wall of the targeted brain region.

Secondly, the coil-target distance has an impact on the strength of the induced electric field. If stimulation intensity is not adjusted, stimulation of brain areas other than the motor cortex will not result in similar electric field strengths in the target area (figures 8.3 & 8.5). For stimulation to be equally effective as in motor cortex stimulation, stimulation intensity has to be changed for areas with a different coil-target distance. Unfortunately, this will not always solve the problem as the local anatomy also has a large impact on the electric field distribution and strength. Adjusting the stimulation intensity purely on the coil-target distance will produce an unknown (suboptimal) electric field strength that may cause unwanted side effects because it might be much stronger than intended. The only way to correct the stimulation intensity properly is again using a (personalized) VCM to calculate the local field strength. In that way, the stimulation intensity can be optimized to induce the 'best' electric field at the cortical target.

11.4.4 Patient specific modeling

As mentioned for both aspects discussed in the previous subsection, the future of TMS computational modeling is the construction of patient-specific models. Inter-individual differences in (brain) anatomy cause substantial differences in the induced electric field distributions, similar to intra-individual differences (**chapters 8 and 9**). These differences in electric field distribution are manifest in the observed variation in individual motor thresholds and coil orientations for the motor cortex. Patient-specific models can help experimental studies in optimizing the effects of TMS by calculating the stimulation intensity and coil orientation needed to induce a certain electric field distribution.

For patient-specific models to be feasible, fast procedures to produce realistic VCMs are required. The inclusion of a realistic cortical surface geometry is important, as this has a large effect on the computed electric fields. **Chapter 7** showed that the inclusion of sulci and gyri within this cortical surface geometry is necessary, as they have a large impact on the local field strength. The least complicated method to quickly produce a VCM directly derived from MRI is by using hexahedral elements based on the MRI voxels. However, as the direction relative to the cortical surface is an important factor in the effectiveness of the stimulation, tetrahedral elements are the preferable choice for the VCM. In square hexahedral models the cortical boundary can only be represented realistically smooth

enough by an inhibitory large number of elements. Geometry-adapted hexahedral models²²⁰ might contain sufficient detail, but a comparison with tetrahedral models has to be made first. The scientific community is already able to produce VCMs with tetrahedral elements that realistically represent a human head, and automated pipelines exist that are able to produce reasonable patient-specific models from MR images²¹⁹. Consequently, the implementation of patient-specific volume conduction modeling into experimental studies may well be achievable within the coming years.

11.4.5 Neuronal models

Although patient-specific volume conduction modeling can already provide valuable information about the TMS-induced electric fields and thereby help to improve experimental protocols, future computational models should incorporate neuronal (network) models. The neuronal (network) models are essential in further improvement of TMS protocols as they provide the connection between the induced electric fields and the resulting neuronal processes. This interaction of the electric field with neurons is at least as important as the (local) field strength and orientation. The optimal TMS coil orientation is currently based on the assumption that cortical activation occurs through stimulation of neural elements aligned with the axis of the cortical column⁵¹. However, this is certainly not the only mechanism to activate the relevant cortical networks¹⁷⁵. This assumption is also derived from experiences in motor cortex stimulation, and although it is in agreement with experimental findings for other brain areas^{3,129}, it is conceivable that the mechanisms of activation differ between cortical areas. Therefore, for TMS simulations to reach a higher level of realism, adequate neuronal network models should be incorporated in future computational frameworks.

11.4.6 Improving the results of cerebellar stimulation in PD patients with FOG

The cerebellum is a deviant structure in many respects compared to the other cortical areas. As cerebellar stimulation plays the central role in **chapter 4**, adaptations to the motor cortex “gold standard” is even more relevant when cerebellar stimulation should be optimized. As for all other cortical areas, the best way to improve the TMS protocol for cerebellar stimulation is by using patient-specific models. The inclusion of cerebellar gyri and sulci in the cerebellar surface geometry is essential to calculate the most realistic induced electric fields here as well. Incorporation of the cerebellar neuronal structure and activity models (including the Purkinje cells) would help to improve the models even further, especially in determining the optimal electric field direction. But as the incorporation of such neuronal models still needs to be developed, also here the optimal orientation of the electric field can be based on the assumption that activation occurs through the electric field perpendicular to the CSF-brain boundary. Furthermore, patient-spe-

cific VCMs can already provide valuable information about the differences in electric field distribution due to coil-target distance and local anatomy.

For example, based on the results of **chapter 8**, one can already conclude that the stimulation intensity has to be increased for cerebellar stimulation in order to be as effective as standard motor cortex stimulation. This conclusion can be made, even without the incorporation of the cerebellar gyri and sulci and Purkinje cells into the model. Unfortunately, the standard figure-of-eight coil will cause uncomfortable stimulation of the neck muscles, which induces muscle twitches. Especially with repetitive protocols, these twitches can cause patients to withdraw from experimental clinical studies, and possibly from future therapies with rTMS. A solution could be the use of novel coil designs, such as the H-coil^{169,170,225}. This type of coil has already been used for repetitive motor cortex stimulation in PD patients¹⁸⁹. These coils are able to stimulate deeper brain areas without extreme stimulation of structures between the coil and the target. So, new protocols with novel coil designs can help to improve the possibilities of cerebellar stimulation. However, new coils should be introduced with caution, as deeper structures such as brainstem areas might be stimulated as well.

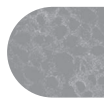
In future research the cerebellar TBS protocol as used in **chapter 4** could be customized to each individual PD patient with FOG. The patient-specific VCM should be created with anatomical MRI and DTI data, preferably with an automated pipeline that creates a tetrahedral model with an accurate cortical surface representation. Functional MRI could provide data about the area in the cerebellum involved in the neural circuitry of FOG that should be targeted with the TBS. A gait task specifically designed for MRI experiments^{6,187} would be a possible way to obtain the necessary fMRI data. A gait task with small steps executed rapidly on a treadmill would be best, as turning is impossible to perform in an MRI scanner. The optimal coil position, orientation and stimulation intensity can be determined for each individual patient, also for a novel coil design such as the H-coil. The effect of the stimulation on FOG should be measured with the best FOG provoking tasks that followed from the study in **chapter 5**. This means turning as rapidly as possible, possibly with an additional task wherein patients walk rapidly with small steps.

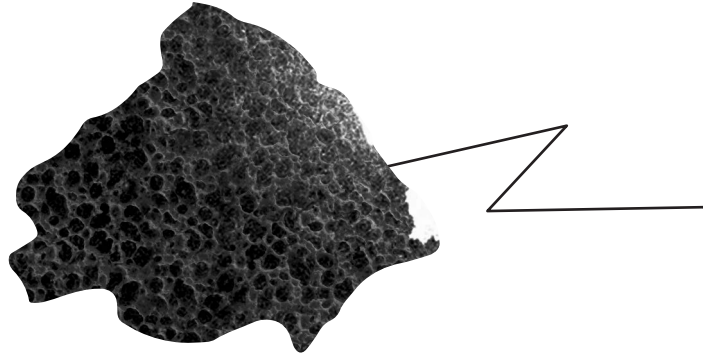
11.4.7 Questions for the future

This thesis included two different forms of TMS research: TMS as an investigatory tool (**chapter 4**) and computational modeling of TMS (**chapters 7-9**). These two types of research both come to their own conclusions and each approach poses new questions. However, more essential is that modeling results can help to improve the experimental results, and the experimental studies can pose new questions and challenges for modeling. For example, which part of the cerebellum was actually stimulated in the indi-

vidual PD patients in **chapter 4**? And can we improve the results by making patient-specific models to adjust the stimulation protocol accordingly? Furthermore, is the assumption about the optimal direction of the electric field correct, or do we need the information from advanced neuronal (network) models? In addition, it is important to validate whether new protocols, based on computational modeling, do result in better and stronger effects of stimulation.

It can be concluded that TMS is a valuable tool in the study, and possibly the therapy, of neurological diseases such as Parkinson's disease. Computational modeling can help to approach the full potential use of this stimulation technique.





12.

NEDERLANDSE SAMENVATTING (SUMMARY IN DUTCH)

12.1 ONDERZOEK BESCHREVEN IN DIT PROEFSCHRIFT

De kern van dit proefschrift bestaat uit vijf wetenschappelijke studies met als hoofdthema de toepassing van transcraniële magnetische stimulatie (TMS). Hierbij gaan twee studies over het zogenaamde 'bevriezen van lopen' bij patiënten met de ziekte van Parkinson, in de Engelstalig literatuur *"freezing of gait"* (FOG) genoemd. In hoofdstuk 4 wordt een studie beschreven waarin TMS is gebruikt als een onderzoeksinstrument om FOG te bestuderen, en hoofdstuk 5 is gewijd aan de evaluatie van de looptaken die werden gebruikt in hoofdstuk 4. Bij de drie andere wetenschappelijke studies (hoofdstukken 7, 8 en 9) werden *volumegeleidingsmodellen* gebruikt om het door TMS veroorzaakte elektrische veld in de hersenen te bestuderen. Het doel daarbij was de elektrische velden in de cortex (hersenschors) te onderzoeken en met de verkregen informatie toekomstige stimulatieprotocollen te verbeteren. In aanvulling op de wetenschappelijke studies bevat het proefschrift een eerste deel met een algemene inleiding over TMS (hoofdstuk 2), een korte inleiding over de ziekte van Parkinson (hoofdstuk 3), en informatie over het modelleren van TMS met de zogenaamde eindige elementen methode (hoofdstuk 6). In dit hoofdstuk zal een samenvatting worden gegeven van het gehele proefschrift, inclusief de algemene informatie uit de hoofdstukken 2, 3 en 6.

12.2 ALGEMENE ACHTERGROND TRANSCRANIËLE MAGNETISCHE STIMULATIE

12.2.1 Introductie transcraniële magnetische stimulatie (hoofdstuk 2)

In 1985 introduceerde Anthony Barker met zijn collega's transcraniële magnetische stimulatie (TMS) via een korte publicatie in de *Lancet*⁸. In deze publicatie toonden zij aan dat het mogelijk is om niet invasief (dat wil zeggen: zonder een instrument in het lichaam te

brengen) pijnloos de hersenen te stimuleren. De techniek werd snel populair binnen de klinische neurofysiologie, neurologie, neurowetenschappen en revalidatiegeneeskunde vanwege het minieme ongemak, het niet invasieve karakter en *last-but-not-least* omdat het relatief eenvoudig toe te passen was.

Aan de ontwikkeling van TMS ligt een lange geschiedenis ten grondslag van (elektrische) stimulatie van het menselijk lichaam, en meer specifiek van de hersenen. De belangrijkste voorafgaande ontwikkelingen vonden plaats in de 18e en de 19e eeuw. Beroemde artsen en natuurkundigen als Luigi Galvani, Alessandro Volta, en Giovanni Aldini deden experimenten met elektrische stimulatie van dierlijke en menselijke lichamen (figuur 2.1, p. 14). De ontdekkingen van deze pioniers openden een geheel nieuw gebied van onderzoek en legden het fundament voor de moderne elektrofysiologie. Een andere belangrijke ontwikkeling was de ontdekking van het wetenschappelijke principe van elektromagnetische inductie⁴⁵ (figuur 2.2, p. 15) door de Britse wetenschapper Michael Faraday in 1831. Deze vinding zou uiteindelijk leiden tot de het natuurkundige principe dat een veranderend magnetisch veld een elektrisch veld produceert, en vice versa (Wet van Faraday). De combinatie van de bevindingen van Galvani, Volta, Aldini en Faraday, leidde tot nieuw onderzoek op het gebied van magnetische stimulatie van de hersenen^{32,197}, hetgeen uiteindelijk in de jaren '80 van de 20^{ste} eeuw zou leiden tot de introductie van TMS⁸.

Tegenwoordig wordt TMS toegepast in zeer divers neurowetenschappelijk onderzoek en in vele klinische studies. Bij gezonde proefpersonen zijn de meeste studies gericht op fundamentele onderzoeksvragen, hoewel prestatieverbetering met hersenstimulatie een actueel onderwerp is⁷³. Bij patiënten wordt TMS gebruikt om fundamentele onderzoeksvragen te beantwoorden, als diagnostisch hulpmiddel en worden inmiddels ook de therapeutische mogelijkheden bekeken. Een breed scala van neurologische aandoeningen, zoals amyotrofische laterale sclerose (ALS), epilepsie, tinnitus, depressie en de ziekte van Parkinson, zijn een onderwerp van TMS-onderzoek.

12.2.2 Principes van transcraniële magnetische stimulatie (hoofdstuk 2)

Hoewel de term 'transcraniële magnetische stimulatie' suggereert dat de reactie in de hersenen wordt veroorzaakt door een magnetisch veld, is de werkelijke stimulatie van de hersenen elektrisch van aard. Het magneetveld transporteert slechts de energie van de stimulatiespoel, door de hoofdhuid en de schedel, naar de hersenen. De techniek is gebaseerd op het eerder genoemde natuurkundige principe van elektromagnetische inductie. In het geval van TMS wordt gedurende een zeer korte periode een elektrische stroom door een spoel van koperdraad gezonden (een puls), wat een magnetisch veld genereert. Dit magnetische veld wekt op zijn beurt weer een elektrisch veld op in een nabijgelegen

geleider. In het geval van TMS vormen de hersenen van de proefpersoon of patiënt die geleider. Het elektrische veld in de hersenen is verantwoordelijk voor de stimulatie van neuronen (zenuwcellen) in de hersen. Dit zijn de belangrijkste cellen van ons zenuwstelsel die de communicatie in ons lichaam verzorgen via elektrische of chemische signalen.

Er bestaan meerdere soorten TMS-spoelen. De keuze van de juiste spoel is essentieel, omdat deze een grote invloed heeft op de verdeling en sterkte van het opgewekte elektrische veld. De twee meest gebruikte zijn de enkele ronde spoel (figuur 2.3A, p. 18) en de figuur-acht-spoel (figuur 2.3B, p. 18). De ronde spoel is het oudste type en meest eenvoudig te gebruiken, en wordt nog veelvuldig gebruikt in wetenschappelijke studies en diagnostiek. De figuur-acht-spoel bestaat uit twee ronde spoelen die tegen elkaar aan zijn geplaatst. Deze spoel heeft als eigenschap dat er gericht mee gestimuleerd kan worden. Dientengevolge is deze spoel zeer populair in neurowetenschappelijk onderzoek. Voor beide spoelen is het opgewekte elektrische veld in de hersenen het sterkste direct onder de omtrek van de spoel, ruwweg evenwijdig en tegengesteld in richting aan de stroom in de spoel. Het veld neemt in sterkte af met toenemende afstand (figuur 2.3C-F, p. 18). Die afname in sterkte met de afstand zorgt ervoor dat TMS alleen wordt gebruikt voor stimulatie van oppervlakkige hersengebieden. In theorie kunnen ook diepere hersengebieden worden gestimuleerd, maar alle structuren tussen de spoel en het doelgebied worden dan met een nog hogere elektrische veldsterkte gestimuleerd.

De cortex is de buitenste laag van de hersenen en is onderverdeeld in gebieden met verschillende functies. Een gedeelte van de cortex, de *primaire motorische cortex* (figuur 2.4A, p. 19), is verantwoordelijk voor een directe aansturing van spieren. Wanneer met TMS de neuronen in de primaire motorische cortex worden gestimuleerd, zullen deze een signaal via zenuwbanen in het ruggenmerg doorgeven aan een spier aan de andere zijde van het lichaam. Dit zal leiden tot een onvrijwillige samentrekking van de spier. De bijbehorende elektrofysiologische respons van de spier kan gemeten worden met behulp van elektromyografie (EMG) (figuur 2.4B, p. 19). Deze respons wordt de motor evoked potential (MEP) genoemd (figuur 2.4C, p. 19). De amplitude van de MEP is afhankelijk van de stimulatiersterkte en de oriëntatie van de TMS-spoel. Een MEP zal alleen worden opgewekt boven een minimale stimulatiersterkte, de zogenaamde stimulatiedrempel (motor threshold). Deze drempel moet individueel bepaald worden, omdat anatomische en fysiologische verschillen tussen personen hierop van invloed zijn. De amplitude van de MEP kan gebruikt worden als maat voor de corticale exciteerbaarheid. De corticale exciteerbaarheid geeft aan hoe makkelijk neuronen in de primaire motorische cortex worden geactiveerd bij een specifieke stimulatiersterkte. Het effect van TMS op de motor cortex is dus direct te meten. Bij delen van de cortex die niet rechtstreeks spieren activeren is dat veel moeilijker of op zijn minst indirecter.

12.2.3 Repetitieve transcraniële magnetische stimulatie (hoofdstuk 2)

Bij de meest gebruikte vorm van TMS wordt een enkele puls gegeven, bijvoorbeeld om een MEP op te wekken. Er zijn echter ook repetitieve TMS (rTMS) protocollen, waarbij meerdere pulsen achter elkaar worden toegediend. Deze protocollen zijn niet gericht op het exciteren van de cortex, maar op het veranderen van de corticale exciteerbaarheid. Deze exciteerbaarheidsverandering houdt een periode aan na het stoppen van de stimulatie. In het algemeen zal bij pulsreeksen met een frequentie tussen de 0,2 en 1 Hz (lage frequenties), de exciteerbaarheid afnemen (remmend)³⁰. Hogere pulsfrequenties vanaf 5 Hz laten de exciteerbaarheid toenemen (faciliterend)¹⁴⁸. In hoofdstuk 4 van dit proefschrift is een specifieke vorm van rTMS gebruikt, genaamd “theta burst” stimulatie (TBS)⁷⁵. Bij deze vorm van rTMS levert een korte stimulatieperiode (40-190 seconden) een consistente, langdurige (tot 1 uur) verandering van de exciteerbaarheid. Afhankelijk van het protocol is die verandering een toename of een afname.

12.3 DE ZIEKTE VAN PARKINSON, BEVRIEZEN VAN LOPEN EN THETA BURST STIMULATIE

12.3.1 De ziekte van Parkinson (hoofdstuk 3)

De ziekte van Parkinson is de op een na meest voorkomende neurodegeneratieve aandoening van het centrale zenuwstelsel. In de geïndustrialiseerde landen wordt ongeveer 1 procent van de bevolking boven de 60 jaar erdoor getroffen⁹⁶. Patiënten kunnen last krijgen van motorische symptomen, zoals tremor (trillen), loopstoornissen, balansproblemen, bradykinesie (vertraging van bewegingen) en rigiditeit (stijfheid), maar ook niet-motorische symptomen, zoals reukproblemen, slaapstoornissen, stemmingsstoornissen en cognitieve achteruitgang. De ziekte heeft een asymmetrisch karakter waarbij de motorische symptomen meestal aan één zijde van het lichaam beginnen, alhoewel de andere zijde onvermijdelijk ook wordt getroffen.

De symptomen van de ziekte worden veroorzaakt door een verlies van dopamine producerende neuronen in de substantia nigra (SN), een van de belangrijkste substructuren van de basale ganglia (BG). De BG liggen diep in de hersenen en zijn betrokken bij verschillende processen (figuur 3.1, p. 25), zoals de controle van beweging, werkgeheugen en emotie. De oorzaak die ten grondslag ligt aan de degeneratie van dopaminerge neuronen in de SN is onbekend.

Voor de behandeling van de ziekte van Parkinson worden vooral medicamenten gebruikt, zoals levodopa. Echter, ook fysiotherapie^{67,85} en diepe hersenstimulatie (*Deep Brain Stimulation*, DBS)^{49,216,217} behoren tot de behandelingsmethoden. Alle behandelingen zijn symp-

tomatisch, wat betekent dat ze de klachten onderdrukken, maar niet de degeneratie van neuronen in de SN stoppen of afremmen.

12.3.2 Het bevroren van lopen (hoofdstuk 3)

Loopstoornissen komen veel voor bij patiënten met de ziekte van Parkinson. Ze worden onder andere gekenmerkt door traagheid in beweging, irreguliere timing van het stappen en verkorte paslengte. Voor loopstoornissen kan een onderscheid worden gemaakt tussen continue problemen in het looppatroon en episodische verschijnselen. Eén van de episodische verschijnselen is het ‘bevroren van lopen’, oftewel “freezing of gait” (FOG). Bij FOG hebben patiënten het gevoel dat de voeten ‘vastgelijmd zitten aan de vloer’. Er zijn drie verschillende vormen van FOG: (1) trillen op de plaats, (2) schuifelen, en (3) complete akinesie (geen beweging)¹³⁸. Meestal duren de episodes enkele seconden, of zelfs korter dan een seconde, maar soms zijn ze langer dan dertig seconden¹⁷⁶. Er zijn verschillende factoren bekend die de mate van FOG beïnvloeden. Bijvoorbeeld, in vergelijking met ‘normaal’ lopen in een rechte lijn, bevroren patiënten doorgaans meer tijdens het starten¹⁷⁶, tijdens het keren^{176,186} en wanneer een kleinere paslengte dan normaal wordt gevraagd²⁸. Het is een fenomeen dat een behoorlijk negatieve invloed heeft op de mobiliteit en de kwaliteit van het leven¹¹⁸. Ongeveer vijftig procent van de patiënten met de ziekte van Parkinson zal uiteindelijk last gaan krijgen van FOG⁶⁵. Hoewel de term FOG verwijst naar een fenomeen in de onderste ledematen, kunnen soortgelijke verschijnselen ook worden waargenomen in de handen¹³³ en zelfs tijdens het praten¹²⁰.

12.3.3 Cerebellaire theta burst stimulatie verbetert loopsnelheid (hoofdstuk 4)

De laatste decennia is het klinisch beeld van FOG veel duidelijker geworden, maar de neurale circuits en de pathofysiologische mechanismen die er aan ten grondslag liggen zijn nog grotendeels onbekend. De algemene gedachte is dat FOG het gevolg is van het disfunctioneren van één of meer hersengebieden binnen een ingewikkeld neurale circuit. In hoofdstuk 4 van dit proefschrift hebben we ons binnen dit neurale circuit specifiek gericht op de mogelijke rol van het cerebellum, ook wel de kleine hersenen genoemd. Eerdere studies suggereren dat het cerebellum in de motorische aansturing bij de ziekte van Parkinson een compenserende rol zou kunnen spelen^{2,144,161,221,224}.

We hebben onderzocht of Parkinson patiënten met FOG symptomen zouden kunnen profiteren van stimulatie van het cerebellum met rTMS (zie 12.2.3). Bij 17 patiënten werd de activiteit van het cerebellum aan de zijde die het meest was aangedaan door de ziekte gemodificeerd met faciliterende en remmende TBS (respectievelijk iTBS en cTBS) toegepast gedurende twee afzonderlijke sessies. Direct voor en na de stimulatie werd de loopprestatie en de kwaliteit van bimanuele ritmische vingerbewegingen bepaald en daarbij

de hoeveelheid bevrozen van bewegingen gekwantificeerd. Het lopen werd geëvalueerd met een aantal taken, waaronder het zo snel mogelijk draaien op de plaats (360°) en het lopen met een verkorte paslengte. De belangrijkste conclusie was dat beide TBS protocollen (faciliterend en remmend) geen significante verandering teweeg brachten in de hoeveelheid bevrozen van zowel het lopen als de vingerbewegingen. Echter, er werd wel een significante toename van de snelheid van het lopen met verkorte paslengte gevonden na iTBS, terwijl de loopsnelheid tijdens het lopen met normale paslengte afnam na cTBS. We vermoeden dat de toename van loopsnelheid na faciliterende TBS (iTBS) het gevolg is van een toename van de neurale activiteit in het cerebellum en een versterking van de cerebello-corticale connectiviteit. En hoewel de TBS geen verandering in de hoeveelheid bevrozen teweeg bracht, suggereren de resultaten wel dat het cerebellum een compenserende rol vervult bij patiënten met FOG symptomen en dat deze kunnen profiteren van cerebellaire TBS.

12.3.4 Korte snelle stappen om FOG uit te lokken (hoofdstuk 5)

Het is moeilijk om FOG te onderzoeken in een klinische of wetenschappelijke setting vanwege de episodische (onregelmatig voorkomende) aard van het symptoom. Niet elke taak wekt FOG even goed op en vanwege het episodische karakter zal zelfs dezelfde taak niet altijd FOG opwekken bij elke uitvoering. Het is dus belangrijk taken te gebruiken die het meest effectief zijn in het opwekken van FOG. Eerder onderzoek heeft aangetoond dat draaien op de plaats het meest geschikt is om FOG uit te lokken, en dan vooral wanneer het draaien zo snel mogelijk wordt uitgevoerd¹⁸⁶. Echter, 10 meter lopen met een verkorte paslengte is in het verleden gebruikt als alternatief²⁸. In hoofdstuk 5 beschrijven we de evaluatie van de diagnostische waarde van looptaken met verkorte paslengte in vergelijking met het snel draaien. Achtentwintig patiënten met de ziekte van Parkinson en objectief geverifieerde FOG werd gevraagd de volgende taken te verrichten: (1) normaal lopen, (2) zo snel mogelijk lopen, (3) lopen met verkorte paslengte, (4) zo snel mogelijk lopen met verkorte paslengte, en (5) zo snel mogelijk 360° draaien op de plaats. De batterij aan taken wekte in 20 patiënten FOG op (71%). De meest effectieve methode was het zo snel mogelijk draaien (bij 64% van de patiënten). Wanneer patiënten zo snel mogelijk liepen met verkorte paslengte was er meer sprake van FOG dan bij lopen met verkorte paslengte op normale snelheid (50% vs. 18% van de patiënten). De combinatie van de taken snel draaien en snel lopen met verkorte paslengte leverde de hoogste gevoeligheid op (71% van de patiënten). Deze studie bevestigt de eerdere bevindingen dat zo snel mogelijk draaien de meest effectieve klinische test is om FOG op te wekken. Echter, indien deze taak geen FOG opwekt, kan een extra taak met zo snel mogelijk lopen met verkorte paslengte de kans vergroten om patiënten met FOG te identificeren en het symptoom beter te onderzoeken. Om zoveel mogelijk FOG op te wekken is voor zowel het draaien als het lopen met verkorte paslengte de instructie de taak "zo snel mogelijk" uit te voeren

essentieel. Normaal lopen, snel lopen met een normale paslengte en lopen met verkorte paslengte op normaal tempo lijken minder bruikbaar in een protocol, omdat deze taken een veel kleinere kans op het uitlokken van FOG hebben. In alle situaties is herhaling van de taak van groot belang, want ook draaien wekt geen FOG op bij iedere uitvoering.

12.4 TRANSCRANIËLE MAGNETISCHE STIMULATIE EN DE EINDIGE ELEMENTEN METHODE

12.4.1 Volumegeleidingsmodellen en de eindige elementen methode (hoofdstuk 6)

Ondanks de brede toepassing van TMS, zijn de effecten op corticaal niveau slechts gedeeltelijk bekend. Dit komt vooral doordat *in vivo* metingen in de hersenen problematisch zijn als gevolg van beperkte mogelijkheden met de huidige meetapparatuur. Computermodellen zijn een goed alternatief om wetenschappelijke vraagstukken over de effecten van TMS te beantwoorden. In dit proefschrift is een gedetailleerd volumegeleidingsmodel (VCM) gebruikt om de elektrische velden in de hersenen op een macroscopisch niveau te bestuderen (op het niveau van de cortex, maar niet op het niveau van individuele neuronen). In een dergelijk computermodel wordt het menselijke hoofd beschreven als een groot elektrisch geleidend volume met daarin verschillende weefsels die worden gescheiden door geometrisch nauwkeurig beschreven grenzen. Ieder weefsel binnen dit volume heeft zijn eigen elektrische geleidbaarheid (vermogen elektriciteit te geleiden). De hedendaagse VCM's worden meestal gebaseerd op magnetische resonantie (MR) beelden^{17,29,195}. De geleidbaarheidswaarden worden gebaseerd op experimentele data⁵⁴. Met behulp van wiskundige vergelijkingen (zie paragraaf 6.2), gebaseerd op natuurkundige wetten, kan het elektrische veld in het gehele VCM bepaald worden.

Voor een VCM met een simpele vorm, zoals een bol, kan het elektrische veld "direct" worden berekend uit (niet altijd eenvoudige) wiskundige vergelijkingen die passen bij die vorm. Voor ingewikkeldere vormen, zoals de realistische representatie van een menselijk hoofd, is dit onmogelijk. De elektrische velden kunnen wel benaderd worden met numerieke methoden, zoals de eindige elementen methode (*Finite Element Method*, FEM). Bij de FEM wordt het volume van het hoofd onderverdeeld in heel veel kleine volume-elementen. In de meeste gevallen zijn deze elementen kubussen of tetraëders (piramides met een driehoekvormig grondvlak) (figuur 6.1, p. 64). Afhankelijk van het gestelde biofysische probleem worden er eigenschappen toegekend aan alle elementen. Vervolgens wordt voor ieder element in het VCM een relatief eenvoudige afzonderlijke mathematische vergelijking opgesteld. De volledige verzameling van alle vergelijkingen kan worden geschreven als een matrixvergelijking die met daartoe geëigende software kan worden opgelost.

12.4.2 Het modeleren van de sulcusbreedte (hoofdstuk 7)

In hoofdstuk 7 wordt een “modelstudie om het modelleren te verbeteren” beschreven. Er werd onderzocht hoe nauwkeurig de beschrijving van gyri en sulci in het corticale oppervlak van een VCM moet zijn. De sulci zijn de zogenaamde hersengroeven en de gyri zijn de uitstulpingen in het oppervlak van de cortex. Door de lage weerstand (hoge geleidbaarheid) van de cerebrospinale vloeistof (CSF), die zich in de sulci bevindt, kan worden verwacht dat veranderingen in de sulcusbreedte een significant effect hebben op de verdeling van het door TMS veroorzaakte elektrische stromen en elektrische velden. Om dit onderzoek uit te voeren werd een zeer gedetailleerd en realistisch VCM met eindige elementen geconstrueerd, waarin de door TMS veroorzaakte elektrische velden werden berekend. Om de impact van veranderingen in de geometrie van het corticale oppervlak te kwantificeren, werd de sulcusbreedte (van alle sulci tegelijk) in dit oppervlak systematisch veranderd. De resultaten toonden aan dat voor een *globale* beschrijving van het elektrische veld, de inclusie van nauwkeurig gemodelleerde sulci niet van groot belang is. Echter, een overschatting van de sulcusbreedte in de geometrie van het corticale oppervlak kan er wel voor zorgen dat *lokaal* een overschatting wordt gemaakt in de berekende veldsterkte. Dit betekent dat voor de bepaling van maximale elektrische veldsterktes, en voor de (toekomstige) combinatie van de resultaten met modellen van neurale structuren¹⁷⁵, een nauwkeurige omschrijving van de sulcusbreedte wél belangrijk is. De kennis die met dit onderzoek en dergelijke onderzoeken is vergaard kan ons helpen bij het nauwkeurig, en toch efficiënt, ontwikkelen van toekomstige modellen. Deze modelstudies om het modelleren te verbeteren of te versnellen zijn vooral van belang in studies met meer patiënt-specifieke modellen, waarbij aan de constructie van de modellen details die niet of nauwelijks invloed hebben moeten worden vermeden.

12.4.3 Lokale anatomie en de afstand tussen de spoel en de hersenen (hoofdstuk 8)

In de dagelijkse toepassing van TMS worden stimulatieprotocollen die ontworpen zijn voor de primaire motorische cortex ook gebruikt voor stimulatie van andere corticale hersengebieden. Dit wordt gedaan omdat de meeste hersengebieden in tegenstelling tot de primaire motorische cortex geen rechtstreekse uitkomstmaat van de stimulatie hebben. Het is echter duidelijk dat de afstand tussen de TMS-spoel en de hersenen, maar ook de lokale anatomie, verschilt per corticaal gebied. Het is dus zeer waarschijnlijk dat de protocollen ontworpen voor stimulatie van de primaire motor cortex suboptimaal zijn voor stimulatie van andere hersengebieden. Computermodellen kunnen helpen het elektrische veld te bepalen voor hersengebieden zonder directe uitkomstmaat.

In hoofdstuk 8 hebben we het VCM gebruikt om te bepalen wat de verschillen zijn in elektrische velden bij de stimulatie van verschillende hersengebieden waarbij dezelfde stim-

ulatiesterkte wordt gebruikt. Hiertoe werden de effecten als gevolg van (1) afstand tussen spoel en cortex en (2) lokale anatomie gekwantificeerd. De resultaten tonen aan dat de elektrische veldsterktes in verschillende doelgebieden behoorlijk van elkaar verschillen wanneer dezelfde stimulatiesterkte wordt gebruikt. Wanneer men voor een willekeurig doelgebied in de hersenen eenzelfde elektrische veldsterkte op corticaal niveau zou willen als voor de primaire motor cortex dient de stimulatiesterkte hiervoor te worden aangepast. Een eenvoudige correctie van de stimulatiesterkte op basis van de afstand, zoals vaak wordt gebruikt^{190,201}, alleen is niet voldoende. Een dergelijke aanpassing van de stimulatiesterkte puur en alleen gebaseerd op de afstand zal een onbekend (mogelijk suboptimaal) elektrisch veld opwekken, met mogelijk ongewenste bijwerkingen. Voor een betere correctie, zo blijkt, dient men ook rekening te houden met de lokale anatomie van het betreffende hersengebied.

12.4.4 Oriëntatie van de TMS-spoel (hoofdstuk 9)

Experimentele studies hebben bewezen dat de effectiviteit van TMS afhankelijk is van de oriëntatie van de spoel ten opzichte van het hoofd van de proefpersoon^{23,114}. Dit betekent dat het rendement van TMS niet alleen afhankelijk is van de sterkte van het elektrische veld in de hersenen, maar ook van de richting. Kennis over de relatie tussen de spoeloriëntatie, de richting van het elektrische veld en de lokale hersenenanatomie is dus essentieel. Daarom hebben we in hoofdstuk 9 het elektrische veld in de cortex als functie van de spoeloriëntatie onderzocht. Dit is gedaan voor veertien corticale locaties die veel gebruikt worden in experimenteel onderzoek met zesendertig spoeloriëntaties per locatie (rotatie met stappen van 10°). Het effect op het elektrische veld van het roteren van de spoel, in combinatie met de unieke anatomie per locatie, is gekwantificeerd. Op basis van eerder onderzoek bestaat een hypothese dat het elektrische veld loodrecht op het corticale oppervlak zorgt voor de grootste effecten op neuronaal niveau. De resultaten laten zien dat voor alle locaties de component van het elektrische veld loodrecht op de wand van de sulcus (naar de gyrus) gevoelig is voor spoeloriëntatie. Niettemin hebben kleine veranderingen in oriëntatie (< 10°) geen drastisch effect op het elektrische veld. De resultaten zijn in overeenstemming met eerder onderzoek voor alleen de primaire motor cortex^{23,93,114}. Deze studie toont aan dat met behulp van computermodellen voor alle locaties een optimale spoeloriëntatie kan worden bepaald. Toekomstig experimentele protocollen kunnen dus worden verbeterd door de TMS-spoel te oriënteren op basis van anatomische informatie bijvoorbeeld uit structurele MRI-data.

12.5 ALGEMENE DISCUSSIE

12.5.1 Niet-invasieve hersenstimulatie van het cerebellum en FOG (hoofdstuk 11)

In hoofdstuk 4 onderzochten we het nut van een interventie met cerebellaire theta burst stimulatie (TBS) bij patiënten met de ziekte van Parkinson die last hebben van FOG. Er werden geen significante effecten van de stimulatie gevonden op de hoeveelheid FOG, maar veranderingen in loopsnelheid werden wel waargenomen na stimulatie. Dit suggereert dat het cerebellum een rol speelt bij de neurale circuits verantwoordelijk voor lopen bij patiënten met FOG. De toegenomen loopsnelheid kan wijzen op een verbetering van de loopprestaties, wat suggereert dat een gunstig effect kan worden verkregen met repetitieve TMS. En hoewel er geen effecten van de cerebellaire TBS op FOG werden gevonden, suggereert de verhoogde loopsnelheid dat (positieve) effecten op FOG mogelijk zijn. De resultaten geven in ieder geval aanwijzingen voor toekomstig onderzoek en mogelijke therapeutische doeleinden. Echter, om van de techniek een klinisch relevante en haalbare interventie te maken, dienen de effecten van cerebellaire TBS verlengd en versterkt te worden. Volumegeleidingsmodellen zoals in dit proefschrift ontwikkeld, kunnen helpen om protocollen op te stellen die mogelijk langdurigere en sterkere effecten kunnen bereiken. Hierbij is het wel van groot belang dat nieuwe protocollen die gebaseerd zijn op de resultaten van computermodellen worden gevalideerd met experimentele studies. Daarnaast dient niet alleen het stimulatieprotocol te worden verbeterd in toekomstige studies, maar ook het loopprotocol. Dit loopprotocol zou meer gericht moeten zijn op FOG opwekkende taken en niet op taken die maar enkele episoden van bevriezen oproepen.

12.5.2 Het verbeteren van stimulatie en patiënt specifieke modellen (hoofdstuk 11)

Het is gebruikelijk, ook voor cerebellaire stimulatie, om TMS-protocollen die zijn ontworpen voor de primaire motorische cortex te gebruiken voor andere corticale hersengebieden. Verschillen in anatomie en fysiologie worden hierbij genegeerd. De resultaten van de hoofdstukken 8 en 9 tonen aan dat de verschillen resulteren in een suboptimale elektrische veldsterkte op het corticale niveau. Het zou daarom zeker een verbetering zijn wanneer stimulatieprotocollen worden aangepast aan de eigenschappen van het gestimuleerde hersengebied. Hierbij kunnen bijvoorbeeld de positie en oriëntatie van de stimulatiepoel verbeterd worden op basis van anatomische informatie uit individuele MRI-scans. Echter, het is nog beter om de oriëntatie te bepalen met behulp van patiënt-specifieke VCM's, gemaakt op basis van individuele MRI-informatie. Hiermee kan ook de stimulatiesterkte aangepast worden, aangezien hier alleen goed voor gecorrigeerd kan worden met behulp van gepersonaliseerde VCM's.

Dit betekent dat de toekomst van TMS-computermodellen ligt bij het gebruik van patiënt-specifieke modellen. Interindividuele verschillen in (hersenen)anatomie veroorzaken aanzienlijke verschillen in de opgewekte elektrische velden, vergelijkbaar met intra-individuele verschillen (hoofdstuk 8 en 9). Deze verschillen in de distributie van het elektrische veld komen overeen met de gevonden variatie in individuele stimulatierempels (zie paragraaf 12.2.1) en optimale spoeloriëntaties voor de primaire motorische cortex. Patiënt-specifieke modellen kunnen helpen de effecten van TMS in experimentele studies te optimaliseren door te berekenen welke stimulatiesterkte en spoeloriëntatie nodig zijn om een bepaald elektrisch veld op te wekken. Om het gebruik van deze modellen haalbaar te maken zijn snelle procedures nodig die realistische VCM's produceren. In deze VCM's is het van belang het corticale oppervlak nauwkeurig weer te geven vanwege de grote invloed op de berekende elektrische velden. Er is geautomatiseerde software beschikbaar die op basis van MRI data patiënt-specifieke modellen met tetraëdrische elementen kan produceren²¹⁹, maar er dient onderzocht te worden of de kwaliteit hiervan voldoende is. Echter, het gebruik van patiënt-specifieke VCM's in experimentele studies lijkt met deze geautomatiseerde software haalbaar in de komende jaren.

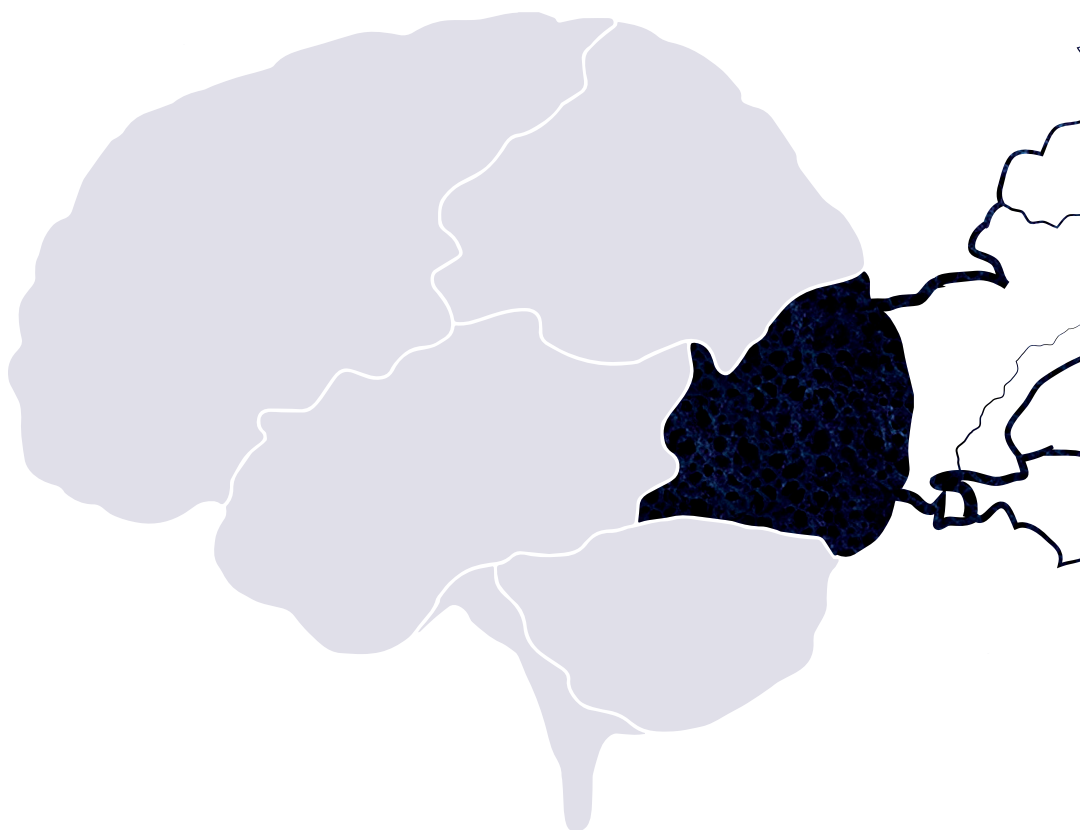
12.5.3 Het verbeteren van cerebellaire stimulatie bij patiënten met de ziekte van Parkinson en FOG (hoofdstuk 11)

De structuur van het cerebellum is in vele opzichten anders dan die van andere corticale gebieden. Op basis van de resultaten uit hoofdstuk 8 kan reeds geconcludeerd worden dat de stimulatiesterkte voor cerebellaire TMS moet worden verhoogd om deze even effectief te maken als standaard primaire motorische cortex-stimulatie. Deze conclusie kan al worden gemaakt zonder patiënt-specifieke modellen. Echter, net als voor alle andere gebieden is de beste manier om het TMS-protocol voor cerebellaire stimulatie te verbeteren gebruik te maken van patiënt-specifieke modellen. Hierin is het van essentieel belang dat de cerebellaire gyri en sulci in de geometrie van het cerebellaire oppervlak worden opgenomen om de elektrische velden zo goed mogelijk te berekenen. Incorporatie van cerebellaire neuronmodellen (inclusief de Purkinje-neuronen) zou helpen om de modellen verder te verbeteren. Uiteindelijk dienen nieuwe experimentele protocollen met sterkere stimulatie wel met enige voorzichtigheid te worden ingevoerd, aangezien hiermee bij cerebellaire stimulatie eventueel ook diepere structuren zoals de hersenstam gestimuleerd kunnen worden.

12.5.4 De toekomst (hoofdstuk 11)

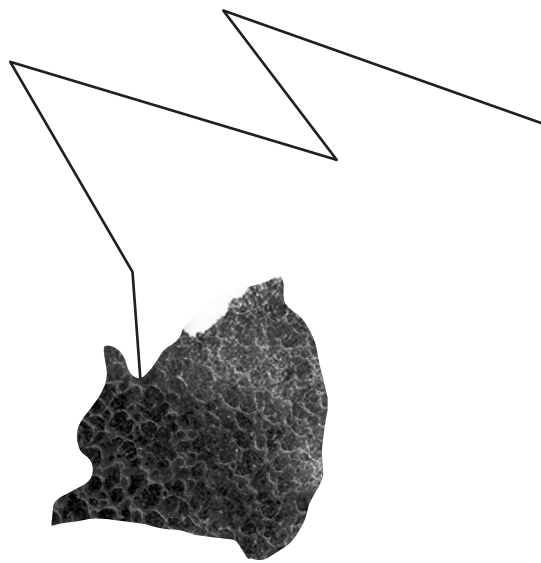
Dit proefschrift bevatte twee verschillende vormen van TMS-onderzoek: TMS als een onderzoeksinstrument (hoofdstuk 4) en onderzoek naar de werking van TMS met behulp van computermodellen (hoofdstukken 7-9). Deze twee soorten van onderzoek komen

beide met hun eigen conclusies en beide benaderingen brengen nieuwe vragen met zich mee. Maar nog belangrijker, de resultaten van studies met computermodellen kunnen helpen experimentele studies te verbeteren, en experimentele resultaten kunnen nieuwe vragen en uitdagingen opwerpen voor modelstudies. Uiteindelijk kan er geconcludeerd worden dat TMS een waardevolle onderzoekstechniek is voor neurologische ziektes zoals de ziekte van Parkinson die in de toekomst eventueel therapeutisch toepasbaar zal zijn. Computermodellen kunnen helpen om het volledige potentieel van deze stimulatietechniek te benutten.



PART V

**DANKWOORD, BIOGRAPHY, PUBLICATIONS,
PARKINSON CENTRE DISSERTATIONS
&
BIBLIOGRAPHY**



13.

DANKWOORD



Eindelijk is het dan zover! Hier ligt het resultaat van een traject waar ik in november 2009 mee ben begonnen. Er zijn mooie momenten geweest, maar zeker ook minder mooie en zware momenten. De succesvolle afronding was alleen mogelijk door de inzet en bijdrage van vele mensen, die ik daarom graag nog wil bedanken.

Dick, ik kon me geen betere promotor wensen. Jouw deur stond altijd open voor een praatje en kon ik met alle zaken bij jou terecht. Je gaf me de vrijheid en vertrouwen om mijn eigen pad in het onderzoek te kiezen. Ik kon de richting van mijn onderzoek bepalen en jij begeleidde me waar nodig. Verder bood je me de mogelijkheid om mijn onderzoek op (inter)nationale congressen te presenteren. In de afrondende fase heb ik je kritische blik op mijn manuscripten zeer gewaardeerd. Ontzettend bedankt voor de mooie tijden en de mogelijkheid die je me hebt geboden om te promoveren. Hopelijk zien we elkaar in de toekomst nog eens om bij te praten.

Thom, ik heb heel fijn met je samengewerkt. Jouw bijdrage was essentieel voor mijn onderzoek. Vaak ontving ik al binnen een halfuur een antwoord op mijn mail, en bovendien ook binnen een paar dagen een speciaal nieuw programmaatje dat me verder kon helpen. Daarnaast heb je me het afgelopen jaar nog de kans gegeven om onderzoek te doen op het gebied van de cardiologie. Want zoals we altijd zeggen, voor een fysicus maakt het niet uit of de stromen nu in het hoofd of in het hart lopen. Daarbij was het wekelijkse volleyballen nog een leuke, maar fanatieke, afwisseling.

Bas, je enthousiasme was zeer aanstekelijk. Hoe kort het overleg soms ook was, ik vertrok altijd weer met goede moed. Ook jouw kritische blik op mijn manuscripten was zeer waardevol. Je hebt me de kans gegeven om patiëntonderzoek te doen, dank hiervoor.

Vervolgens wil ik graag de patiënten bedanken die hebben meegewerkt aan de studies in hoofdstukken 4 en 5. Jullie inzet was bewonderenswaardig!

Sumientra en Moniek, als laatste lid van de brainstim support group ga ik dan ook promoveren. We waren niet alleen kamergenoten, maar als 'brain stimulation' promovendi ook een soort van lotgenoten. We konden goed tegen elkaar uitrazen over onterechte reviews of over de (onverwachte en ongewenste) uitkomsten van onze onderzoeken. De vele gezamenlijke werkbezoeken en conferenties in het buitenland zal ik niet vergeten. Hopelijk kunnen we, ondanks dat we allemaal een andere richting hebben gekozen voor het vervolg van onze carrière, contact blijven houden.

Naast bovengenoemde personen zijn er nog talloze mensen die ik heb leren kennen en graag zou ik ze allemaal willen bedanken voor de samenwerkingen, discussies en andere gezamenlijke activiteiten. Om te beginnen zou ik graag alle coauteurs bedanken en meer specifiek Anke, Jorik, Thomas, Ivan, Heidi, Murielle en Alice. Jullie input was essentieel bij de patiëntenstudies. Thanks also to my colleagues from Münster, Seok, Felix, Umit, and Benjamin. Especially Carsten. Thank you for inviting us to your lab. We had some good discussions and I'm very proud of the papers that resulted from our collaboration.

Daarnaast wil ik ook nog graag alle onderzoekers, studenten, laboranten, artsen en andere (voormalig) medewerkers van de KNF, Hans, Mark, Angelique, bedanken voor de mooie tijd op de afdeling. Claudia, Sigrid, het was de laatste jaren ook altijd gezellig om even bij te praten.

Thanks to the colleagues from the Donders Brain Stimulation Meeting and the Transcranial Brain Stimulation Toolkit. Lennart, Til, Tom, Jim, Ian and the rest, I really liked the fruitful discussions.

Mijn promotie in het kader van het BrainGain consortium zorgde ervoor dat ik collegae van buiten het Radboud kreeg. Ik wil hen graag bedanken voor de samenwerkingen, discussies en gezelligheid, en in het bijzonder Tjitske en Edwin.

Prof. Medendorp, prof. Dössel and prof. Timmermann, members of the doctoral committee, thank you for reviewing the manuscript of my thesis.

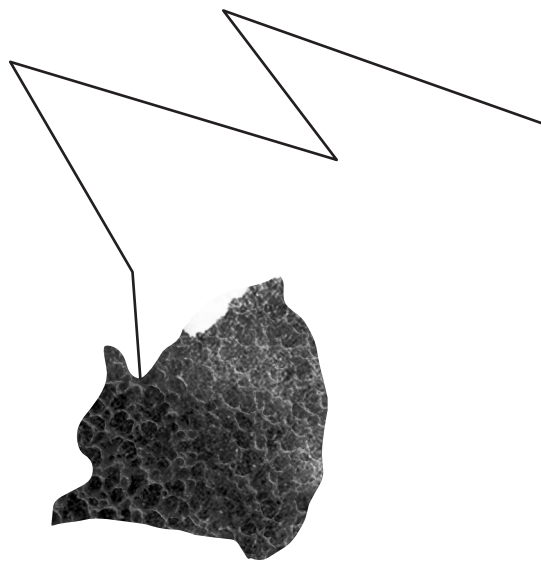
Tenslotte, lieve vrienden en (schoon)familie, dank voor jullie indirecte bijdrage aan het goed afronden van dit traject. Jullie belangstelling, maar vooral ook broodnodige afleiding was cruciaal in de afgelopen jaren. Ondanks dat jullie soms geen idee hadden wat ik nu precies aan het doen was, was jullie betrokkenheid ontzettend belangrijk. Maarten, Remco, Steef, Bart, Jur en Tim, onze borrels en jaarlijkse kerstdiner zorgden voor de gewenste ontspanning. Ook de trip naar Praag was onvergetelijk en heeft mij door een flinke dip tijdens mijn

promotie geholpen. Remco, ik ben ontzettend blij dat je mijn paranimf wil zijn. Voor mij was het een volkomen logische keus om jou te vragen. Yuri, Teun, Kevin, Ernst, Jeroen en de rest van de Oisterwijk-groep, ook al zien we elkaar niet zo vaak als we zouden willen, het is altijd weer vertrouwd als we samen komen. Deze momenten koester ik.

Hans, Tonneke, Mir, Stef en Pien, de interesse en betrokkenheid bij mijn promotie voelde altijd oprecht. Dank hiervoor.

Pap, mam en As, dank voor jullie steun en belangstelling door de jaren heen. Ook al vroegen jullie je soms af waar ik in hemelsnaam mee bezig was, de steun in het lange proces was onvoorwaardelijk.

Lieve Judith, samen promoveren wie had dat kunnen bedenken! Er is niemand die me beter begrijpt dan jij. Alweer bijna 10 jaar samen, en ik geniet nog van iedere dag samen met jou. En tenslotte lieve Sara, jij brengt zo veel plezier in mijn leven. Dankzij jou plaats ik de zaken in perspectief en relativeer ik meer. Dikke knuffel van paps.



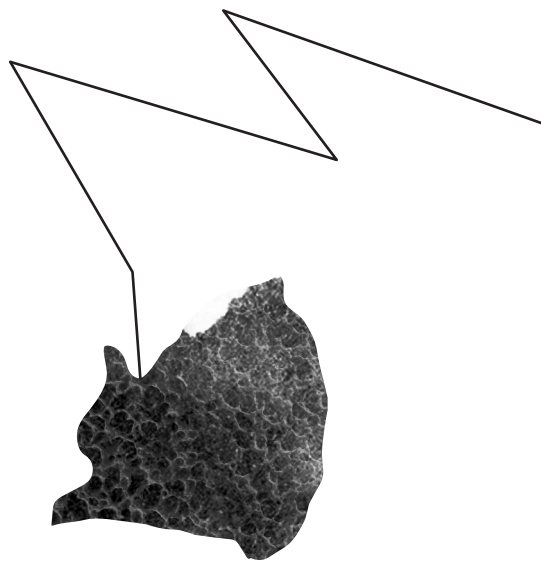
14.

BIOGRAPHY



Arno Janssen was born on July 27th 1985 in Eindhoven, the Netherlands. In 1987 his family moved to Oisterwijk, where he attended primary school. He received his secondary education at the Maurick College in Vught and graduated in 2003. In September 2003 he started with the interdisciplinary Bachelor's program Natural Sciences at the Radboud University Nijmegen. During his study he completed internships at the departments of biological psychology and cognitive neurosciences. He received his Master degree in Natural Sciences in 2009, with a specialization in Biophysics. In November 2009 he started as a PhD student at the department of Neurology/Clinical Neurophysiology on the topics of transcranial magnetic stimulation and freezing of gait in Parkinson's disease, under the supervision of prof. Dick Stegeman, prof. Bas Bloem and dr. Thom Oostendorp. In the following years he studied the effects of transcranial magnetic stimulation on freezing of gait in PD and modeled the induced electric fields with the finite element method. The results of his PhD research are described in this thesis. During his time as a PhD student he presented multiple posters and provided oral presentations at international conferences. He was part of the organizing committee of the Donders Discussions in 2010 and provided lectures in the Donders Institute Brain Stimulation Toolkits of 2013 and 2015. During his work as a PhD student he visited the University of Münster, Germany and the University of Utah in Salt Lake City, The United States of America.

After his appointment as a PhD student, he worked as a researcher at the Interdisciplinary Cardiology Institute Netherlands on the topic of inverse modeling of the human electrocardiogram. Currently, Arno works as a clinical physicist in training at the department of ENT at the Radboudumc.



15.

PUBLICATIONS



15.1 FULL PAPERS

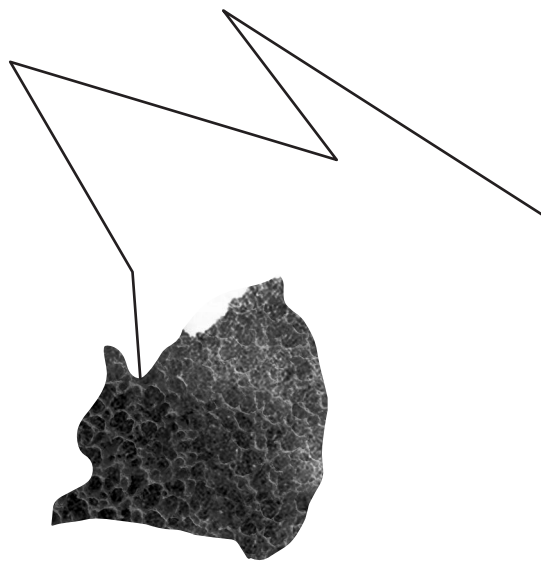
- **Janssen AM**, Rampersad SM, Lucka F, Lanfer B, Lew S, Aydin U, Wolters CH, Stegeman DF, Oostendorp TF. *The influence of sulcus width on simulated electric fields induced by transcranial magnetic stimulation*. Phys Med Biol, Vol. 58, p. 4881-4896, 2013
- Rampersad SM, **Janssen AM**, Lucka F, Aydin U, Lanfer B, Lew S, Wolters CH, Stegeman DF, Oostendorp TF. *Simulating transcranial direct current stimulation with a detailed anisotropic human head model*. IEEE Trans Neural Syst & Rehab, Vol. 22 (3), p. 441-452, 2014
- **Janssen AM**, Oostendorp TF, Stegeman DF. *The effect of local anatomy on the electric field induced by TMS: evaluation at fourteen different target sites*. Med Biol Eng Comput, Vol. 52, p. 873-883, 2014
- Nonnekes J, **Janssen AM**, Mensink SHG, Oude Nijhuis LB, Bloem BR, Snijders AH. *Short rapid steps to provoke freezing of gait in Parkinson's disease*. J Neurol, Vol. 261(9), p. 1763-1767, 2014
- Cluitmans JCA, Chokkalingam V, **Janssen AM**, Bosman GJCGM, Huck WTS, Brock R. *Alterations in red blood cell deformability during storage: a microfluidic approach*. BioMed Research International, 2014
- **Janssen AM**, Oostendorp TF, Stegeman DF. *The coil orientation dependency of the electric field induced by TMS for M1 and other brain areas*. J NeuroEng Rehab, Vol. 12(47), p. 1-13, 2015
- Zach H, **Janssen AM**, Snijders AH, Delval A, Stegeman DF, Bloem BR, Nonnekes J. *Identifying freezing of gait in Parkinson's disease during freezing provoking tasks using waist-mounted accelerometer*, Park Relat Disord, Vol. 21(11), p. 1362-1366, 2015

- **Janssen AM**, Munneke MAM, Nonnekes J, Van der Schaaf T, Nieuwboer A, Toni I, Snijders AH, Bloem BR, Stegeman DF. *Cerebellar theta burst stimulation improves gait speed in Parkinson's disease patients with freezing of gait. (submitted)*
- **Janssen AM**, Potyagaylo D, Dössel O, Oostendorp TF. *Assessment of the equivalent dipole layer source model in the reconstruction of cardiac activation times on the basis of ECGs produced by an anisotropic model of the heart. (submitted)*

15.2 CONFERENCE PRESENTATIONS

- **Janssen AM**, Rampersad SM, Hengeveld YA, Oostendorp TF, Wolters CH, Stegeman DF. *Modeling transcranial magnetic stimulation and transcranial direct current stimulation*. Poster at 18th congress of the International Society of Electrophysiology and Kinesiology (Aalborg, Denmark, 2010)
- **Janssen AM**, Rampersad SM, Hengeveld YA, Oostendorp TF, Wolters CH, Stegeman DF. *Modeling transcranial magnetic stimulation and transcranial direct current stimulation*. Poster at FENS Satellite Symposium on Motor Control (Nijmegen, the Netherlands, 2010)
- **Janssen AM**, Wolters CH, Stegeman DF, Oostendorp TF. *Modeling effects of the TMS magnetic field using precise geometries of the head and the stimulation coil*. Presentation at 3rd Dutch Biomedical Engineering Conference (Egmond aan Zee, the Netherlands, 2011)
- Rampersad SM, Oostendorp TF, **Janssen AM**, Wolters CH, Stegeman DF. *Determining the optimal electrode configuration for transcranial direct current stimulation: a model study*. Poster at 14th European Congress on Clinical Neurophysiology and 4th International Conference on Transcranial Magnetic and Direct Current Stimulation (Rome, Italy, 2011). *Reference: Clinical Neurophysiology, Vol. 122, Supplement 1, p. S142-S143, 2011*
- **Janssen AM**, Oostendorp TF, Rampersad SM, Wolters CH, Stegeman DF. *Volume conductor modeling of the effects of transcranial magnetic stimulation*. Poster at 14th European Congress on Clinical Neurophysiology and 4th International Conference on Transcranial Magnetic and Direct Current Stimulation (Rome, Italy, 2011). *Reference: Clinical Neurophysiology, Vol. 122, Supplement 1, p. S196, 2011*

- **Janssen AM**, Rampersad SM, Lucka F, Lew S, Oostendorp TF, Wolters CH, Stegeman DF. *Modeling transcranial stimulation using a realistic volume conductor model*. Poster at 2. Jahrestagung der Deutschen Gesellschaft für Hirnstimulation in der Psychiatrie (Münster, Germany, 2011)
- Stegeman DF, **Janssen AM**, Rampersad SM. *tDCS, TMS techniques to stimulate the human brain: background applications and models of tDCS and TMS*. Invited presentation at Institutscolloquium Biomagnetismus und Biosignalanalyse (Münster, Germany, 2012)
- **Janssen AM**, Rampersad SM, Wolters CH, Oostendorp TF, Stegeman DF. *The effects of cortical geometry on modeling transcranial magnetic stimulation*. Poster at Magstim Neuroscience Conference (Oxford, UK, 2012)
- **Janssen AM**, Stegeman DF, Oostendorp TF. *Simulation of the electric field induced by transcranial magnetic stimulation over multiple cortical areas using the finite element method*. Presentation at 4th Dutch Biomedical Engineering Conference (Egmond aan Zee, the Netherlands, 2013)
- **Janssen AM**, Stegeman DF, Oostendorp TF. *A comparison of TMS induced electric fields over multiple cortical areas using the finite element method*. Poster at 5th International Conference on Non-invasive Brain Stimulation 2013 (Leipzig, Germany, 2013).
Reference: Clinical Neurophysiology, Vol. 124(10), p. e79-e80, 2013



16.

DISSERTATIONS OF THE DISORDERS OF MOVEMENT RESEARCH GROUP, NIJMEGEN



Parkinson Center Nijmegen (ParC)

- Jasper E. Visser. The basal ganglia and postural control. Radboud University Nijmegen, 17 June 2008
- Maaïke Bakker. Supraspinal control of walking: lessons from motor imagery. Radboud University Nijmegen, 27 May 2009
- W. Farid Abdo. Parkinsonism: possible solutions to a diagnostic challenge. Radboud University Nijmegen, 7 October 2009
- Samyra H.J. Keus. Physiotherapy in Parkinson's disease. Towards evidence-based practice. Leiden University, 29 April 2010
- Lars B. Oude Nijhuis. Modulation of human balance reactions. Radboud University Nijmegen, 29 November 2010
- Maarten J. Nijkrake. Improving the quality of allied health care in Parkinson's disease through community-based networks: the ParkinsonNet health care concept. Radboud University Nijmegen, 29 November 2010
- Rick C.G. Helmich. Cerebral reorganization in Parkinson's disease. Radboud University Nijmegen, 24 May 2011
- Charlotte A. Haaxma. New perspectives on preclinical and early stage Parkinson's disease. Radboud University Nijmegen, 6 December 2011
- Johanna G. Kalf. Drooling and dysphagia in Parkinson's disease. Radboud University Nijmegen, 22 December 2011
- Anke H. Snijders. Tackling freezing of gait in Parkinson's disease. Radboud University Nijmegen, 4 June 2012
- Bart F.L. van Nuenen. Cerebral reorganization in premotor parkinsonism. Radboud University Nijmegen, 22 November 2012
- Wandana Nanhoe-Mahabier. Freezing of physical activity in Parkinson's disease, the challenge to change behavior. Radboud University Nijmegen, 13 February 2013
- Marlies van Nimwegen. Promotion of physical activity in Parkinson's disease, the challenge to change behavior. Radboud University Nijmegen, 6 March 2013
- Arlène D. Speelman. Promotion of physical activity in Parkinson's disease, feasibility and effectiveness. Radboud University Nijmegen, 6 March 2013
- Tjitske Boonstra. The contribution of each leg to bipedal balance control. University Twente, 6 June 2013
- Marjolein A van der Marck. The Many faces of Parkinson's disease: towards a multifaceted approach? Radboud University Nijmegen, 10 January 2014

- Katrijn Smulders. Cognitive control of gait and balance in patients with chronic stroke and Parkinson's disease. Radboud University Nijmegen, 21 May 2014
- Marjolein B. Aerts. Improving diagnostic accuracy in parkinsonism. Radboud University Nijmegen, 27 June 2014
- Maartje Louter. Sleep in Parkinson's disease. A focus on nocturnal movements. Radboud University Nijmegen, 13 February 2015
- Frederick Anton Meijer. Clinical Application of Brain MRI in Parkinsonism: From Basic to Advanced Imaging, Radboud University Nijmegen, 23 June 2015
- Jorik Nonnekes. Balance and gait in neurodegenerative disease: what startle tells us about motor control, Radboud University Nijmegen, 2 September 2015
- Martijn van der Eijk. Patient-centered care in Parkinson's disease. Radboud University Nijmegen, 1 December 2015
- Ingrid Sturkenboom. Occupational therapy for people with Parkinson's disease: towards evidence-informed care. Radboud University Nijmegen, 11 February 2016
- Merel M. van Gilst. Sleep benefit in Parkinson's disease. Radboud University Nijmegen, 13 April 2016
- Arno M. Janssen. Transcranial magnetic stimulation - measuring and modeling in health and disease. Radboud University Nijmegen, 2 June 2016

Non-Parkinsonian disorders of movement

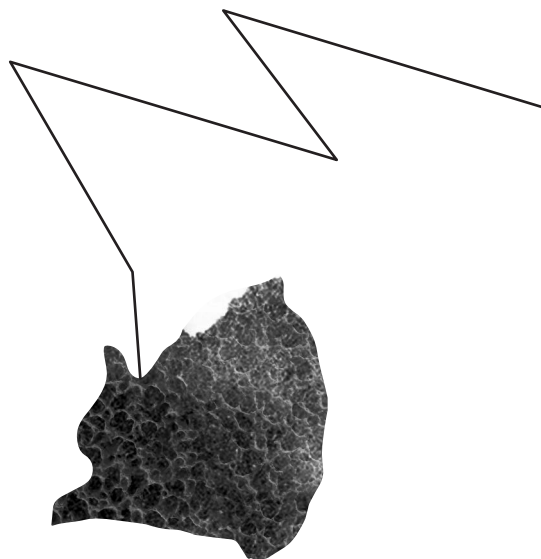
- Sacha Vermeer. Clinical and genetic characterization of autosomal recessive cerebellar ataxias. Radboud University Nijmegen, 5 April 2012
- Susanne T. de Bot. Hereditary spastic paraplegias in the Netherlands. Radboud University Nijmegen, 20 December 2013
- Catherine C.S. Delnooz. Unraveling primary focal dystonia. A treatment update and new pathophysiological insights. Radboud University Nijmegen, 7 January 2014

Vascular disorders of movement – The Radboud Stroke centre

- Liselore Snaphaan. Epidemiology of post stroke behavioral consequences. Radboud University Nijmegen, 12 March 2010
- Karlijn F. de Laat. Motor performance in individuals with cerebral small vessel disease: an MRI study. Radboud University Nijmegen, 29 November 2011
- Anouk G.W. van Norden. Cognitive function in elderly individuals with cerebral small vessel disease. An MRI study. Radboud University Nijmegen, 30 November 2011
- Rob Gons. Vascular risk factors in cerebral small vessel disease. A diffusion tensor imaging study. Radboud University Nijmegen, 10 December 2012
- Loes C.A. Rutten-Jacobs. Long-term prognosis after stroke in young adults. Radboud University Nijmegen, 14 April 2014
- Noortje A.M.M. Maaijwee. Long-term neuropsychological and social consequences after stroke in young adults. Radboud University Nijmegen, 12 June 2015

Neuromuscular disorders of movement

- Mireille van Beekvelt. Quantitative near infrared spectroscopy (NIRS) in human skeletal muscle. Radboud University Nijmegen, 24 April 2002
- Johan Hiel. Ataxia telangiectasia and Nijmegen Breakage syndrome, neurological, immunological and genetic aspects. Radboud University Nijmegen, 23 April 2004
- Gerald JD Hengstman. Myositis specific autoantibodies, specificity and clinical applications. Radboud University Nijmegen, 21 September 2005
- M. Schillings. Fatigue in neuromuscular disorders and chronic fatigue syndrome, a neurophysiological approach. Radboud University Nijmegen, 23 November 2005
- Bert de Swart. Speech therapy in patients with neuromuscular disorders and Parkinson's disease. Diagnosis and treatment of dysarthria and dysphagia. Radboud University Nijmegen, 24 march 2006
- J. Kalkman. From prevalence to predictors of fatigue in neuromuscular disorders. The building of a model. Radboud University Nijmegen, 31 October 2006
- Nens van Alfen. Neuralgicamyotrophy. Radboud University Nijmegen, 1 November 2006
- Gea Drost. High-density surface EMG, pathophysiological insights and clinical applications. Radboud University Nijmegen, 9 March 2007
- Maria Helena van der Linden. Pertubations of gait and balance: a new experimental setup applied to patients with CMT type 1a. Radboud University Nijmegen, 6 October 2009
- Jeroen Trip. Redefining the non-dystrophic myotonic syndromes. Radboud University Nijmegen, 22 January 2010
- Corinne G.C. Horlings. A weak balance: balance and falls in patients with neuromuscular disorders. Radboud University Nijmegen, 1 April 2010
- E. Cup. Occupational therapy, physical therapy and speech therapy for persons with neuromuscular diseases, an evidence based orientation. Radboud University Nijmegen, 5 July 2011
- Alide Tieleman. Myotonic dystrophy type 2, a newly diagnosed disease in the Netherlands. Radboud University Nijmegen, 15 July 2011
- Nicol Voermans. Neuromuscular features of Ehlers-Danlos syndrome and Marfan syndrome. Radboud University Nijmegen, 2 September 2011
- Allan Pieterse. Referral and indication for occupational therapy, physical therapy and speech- language therapy for persons with neuromuscular disorders. Radboud University Nijmegen, 13 February 2012
- Bart Smits. Chronic Progressive External Ophthalmoplegia more than meets the eye. Radboud University Nijmegen, 5 June 2012
- Ilse Arts. Muscle ultrasonography in ALS. Radboud University Nijmegen, 31 October 2012
- M. Minis. Sustainability of work for persons with neuromuscular diseases. Radboud University Nijmegen, 13 November 2013
- Willemijn Leen. Glucose transporter – 1 deficiency syndrome. Radboud University Nijmegen, 26 June



17.

BIBLIOGRAPHY



1. Akhtari M, Bryant HC, Mamelak AN, et al. Conductivities of three-layer live human skull. *Brain Topogr.* 2002;14(3):151-167.
2. Appel-Cresswell S, de la Fuente-Fernandez R, Galley S, McKeown MJ. Imaging of compensatory mechanisms in Parkinson's disease. *Curr Opin Neurol.* 2010;23(4):407-412.
3. Arai N, Lu M-K, Ugawa Y, Ziemann U. Effective connectivity between human supplementary motor area and primary motor cortex: a paired-coil TMS study. *Exp brain Res.* 2012;220(1):79-87.
4. Attene M. A lightweight approach to repairing digitized polygon meshes. *Vis Comput.* 2010;26(11):1393-1406.
5. Badawy RAB, Vogrin SJ, Lai A, Cook MJ. Capturing the epileptic trait: cortical excitability measures in patients and their unaffected siblings. *Brain.* 2013;136(4):1177-1191.
6. Bakker M, Lange FP De, Helmich RC, Scheeringa R, Bloem BR, Toni I. Cerebral correlates of motor imagery of normal and precision gait. *Neuroimage.* 2008;41:998-1010.
7. Balslev D, Braet W, McAllister C, Miall RC. Inter-individual variability in optimal current direction for transcranial magnetic stimulation of the motor cortex. *J Neurosci Methods.* 2007;162(1-2):309-313.
8. Barker AT, Jalinous R, Freeston IL. Non-invasive magnetic stimulation of human motor cortex. *Lancet.* 1985;325(8437):1106-1107.
9. Bartels AL, Balash Y, Gurevich T, Schaafsma J, Hausdorff JM, Giladi N. Relationship between freezing of gait (FOG) and other features of Parkinson's: FOG is not correlated with bradykinesia. *J Clin Neurosci.* 2003;10(5):584-588.
10. Bashir S, Perez JM, Horvath JC, Pascual-Leone A. Differentiation of Motor Cortical Representation of Hand Muscles by Navigated Mapping of Optimal TMS Current Directions in Healthy Subjects. *J Clin Neurophysiol.* 2013;30(4):390-395.
11. Basser PJ, Mattiello J, LeBihan D. MR diffusion tensor spectroscopy and imaging. *Biophys J.* 1994;66(1):259-267.
12. Behrens TEJ, Woolrich MW, Jenkinson M, et al. Characterization and propagation of uncertainty in diffusion-weighted MR imaging. *Magn Reson Med.* 2003;50(5):1077-1088.
13. Benninger DH, Berman BD, Houdayer E, et al. Intermittent theta-burst transcranial magnetic stimulation for treatment of Parkinson disease. *Neurology.* 2011;76(7):601-609.
14. Benninger DH, Hallett M. Non-invasive brain stimulation for Parkinson's disease: Current concepts and outlook 2015. *NeuroRehabilitation.* 2015;37(1):11-24.
15. Berardelli A, Rona S, Inghilleri M, Manfredi M. Cortical inhibition in Parkinson's disease. A study with paired magnetic stimulation. *Brain.* 1996;119:71-77.
16. Bestmann S, Ruff CC, Blankenburg F, Weiskopf N, Driver J, Rothwell JC. Mapping causal interregional influences with concurrent TMS-fMRI. *Exp brain Res.* 2008;191(4):383-402.
17. Bijsterbosch JD, Barker AT, Lee K-H, Woodruff PWR. Where does transcranial magnetic stimulation (TMS) stimulate? Modelling of induced field maps for some common cortical and cerebellar targets. *Med Biol*

Eng Comput. June 2012.

18. Birkmayer W, Hornykiewicz O. The effect of L-3,4-dihydroxyphenylalanine (=DOPA) on akinesia in parkinsonism. *Parkinsonism Relat Disord.* 1998;4(2):59-60.
19. Bloem BR, Hausdorff JM, Visser JE, Giladi N. Falls and freezing of gait in Parkinson's disease: a review of two interconnected, episodic phenomena. *Mov Disord.* 2004;19(8):871-884.
20. Bloem BR. Postural instability in Parkinson's disease. *Clin Neurol Neurosurg.* 1992;94:41-45.
21. Boroojerdi B, Battaglia F, Muellbacher W, Cohen LG. Mechanisms influencing stimulus-response properties of the human corticospinal system. *Clin Neurophysiol.* 2001;112(5):931-937.
22. Braess D. *FINITE ELEMENTS: Theory, Fast Solvers, and Applications in Elasticity Theory.* (Press CU, ed.). Cambridge: Cambridge University Press; 2007.
23. Brasil-Neto JP, Cohen LG, Panizza M, Nilsson J, Roth BJ, Hallett M. Optimal focal transcranial magnetic activation of the human cortex: Effects of coil orientation, shape of the induced current pulse, and stimulus intensity. *J Clin Neurophysiol.* 1992;9(1):132-136.
24. Browner N, Giladi N. What can we learn from freezing of gait in Parkinson's disease? *Curr Neurol Neurosci Rep.* 2010;10(5):345-351.
25. Brusa L, Ceravolo R, Kiferle L, et al. Metabolic changes induced by theta burst stimulation of the cerebellum in dyskinetic Parkinson's disease patients. *Parkinsonism Relat Disord.* 2012;18(1):59-62.
26. Brusa L, Ponzo V, Mastropasqua C, et al. Theta burst stimulation modulates cerebellar-cortical connectivity in patients with progressive supranuclear palsy. *Brain Stimul.* 2014;7(1):29-35.
27. Carrillo F, Palomar FJ, Conde V, et al. Study of cerebello-thalamocortical pathway by transcranial magnetic stimulation in parkinson's disease. *Brain Stimul.* 2013;6(4):582-589.
28. Chee R, Murphy A, Danoudis M, Georgiou-Karistianis N, Iansek R. Gait freezing in Parkinson's disease and the stride length sequence effect interaction. *Brain.* 2009;132(Pt 8):2151-2160.
29. Chen M, Mogul DJ. A structurally detailed finite element human head model for simulation of transcranial magnetic stimulation. *J Neurosci Methods.* 2009;179(1):111-120.
30. Chen R, Classen J, Gerloff C, et al. Depression of motor cortex excitability by low-frequency transcranial magnetic stimulation. *Neurology.* 1997;48:1-11.
31. Cotzias GC, Papavasiliou PS, Gellene R. Modification of parkinsonism: Chronic treatment with L-Dopa. *N Engl J Med.* 1969;280(7):337-345.
32. D'Arsonval A. Dispositifs pour la mesure des courants alternatifs de toutes frequences. *C R Soc Biol.* 1896;3:450-457.
33. Daskalakis ZJ, Paradiso GO, Christensen BK, Fitzgerald PB, Gunraj C, Chen R. Exploring the connectivity between the cerebellum and motor cortex in humans. *J Physiol.* 2004;557(Pt 2):689-700.
34. Delvaux V, Alagona G, Gerard P, De Pasqua V, Pennisi G, De Noordhout AM. Post-stroke reorganization of hand motor area: A 1-year prospective follow-up with focal transcranial magnetic stimulation. *Clin Neurophysiol.* 2003;114(7):1217-1225.
35. Deng Z-D, Lisanby SH, Peterchev A V. Electric field depth-focality tradeoff in transcranial magnetic stimulation: simulation comparison of 50 coil designs. *Brain Stimul.* 2013;6(1):1-13.
36. Devanne H, Lavoie BA, Capaday C. Input - output properties and gain changes in the human corticospinal pathway. *Exp brain Res.* 1997;114(2):329-338.
37. Djaldetti R, Ziv I, Melamed E. The mystery of motor asymmetry in Parkinson's disease. *Lancet Neurol.* 2006;5(9):796-802.
38. Dubois B, Slachevsky A, Litvan I, Pillon B. The FAB: A frontal assessment battery at bedside. *Neurology.* 2000;55(11):1621-1626.
39. Dum RP, Strick PL. An unfolded map of the cerebellar dentate nucleus and its projections to the cerebral

- cortex. *J Neurophysiol*. 2003;89(1):634-639.
40. Escudero J V, Sancho J, Bautista D, Escudero M, Lopez-Trigo J. Prognostic Value of Motor Evoked Potential Obtained by Transcranial Magnetic Brain Stimulation in Motor Function Recovery in Patients With Acute Ischemic Stroke. *Stroke*. 1998;29(9):1854-1859.
 41. Fabbri G, Brochie JM, Grandas F, Nomoto M, Goetz CG. Levodopa-induced dyskinesias. *Mov Disord*. 2007;22(10):1379-1389.
 42. Factor SA. The clinical spectrum of freezing of gait in atypical parkinsonism. *Mov Disord*. 2008;23 Suppl 2:S431-S438.
 43. Faes TJC, Van der Meij HA, De Munck JC, Heethaar RM. The electric resistivity of human tissues (100 Hz-10 MHz) a meta-analysis of review studies. *Physiol Meas*. 1999;20(4):R1-R10.
 44. Fang Q, Boas D. Tetrahedral mesh generation from volumetric binary and gray-scale images. *Int Symp Biomed Imaging*. 2009;0:7-10.
 45. Faraday M. Experimental researches in electricity. *Philos Trans R Soc London*. 1832;122:125-162.
 46. Fasano A, Herzog J, Seifert E, et al. Modulation of gait coordination by subthalamic stimulation improves freezing of gait. *Mov Disord*. 2011;26(5):844-851.
 47. Fling BW, Cohen RG, Mancini M, Nutt JG, Fair DA, Horak FB. Asymmetric pedunculopontine network connectivity in parkinsonian patients with freezing of gait. *Brain*. 2013;136(Pt 8):2405-2418.
 48. Fling BW, Cohen RG, Mancini M, et al. Functional reorganization of the locomotor network in Parkinson patients with freezing of gait. *PLoS One*. 2014;9(6):e100291.
 49. Follett KA, Weaver FM, Stern M, et al. Pallidal versus subthalamic deep-brain stimulation for Parkinson's disease. *N Engl J Med*. 2010;362(22):2077-2091.
 50. Folstein MF, Folstein SE, McHugh PR. "Mini-mental state" A practical method for grading the cognitive state of patients for the clinician*. *J Psychiatr Res*. 1975;12:189-198.
 51. Fox PT, Narayana S, Tandon N, et al. Column-based model of electric field excitation of cerebral cortex. *Hum Brain Mapp*. 2004;22(1):1-14.
 52. Fregni F, Marcondes R, Boggio PS, et al. Transient tinnitus suppression induced by repetitive transcranial magnetic stimulation and transcranial direct current stimulation. *Eur J Neurol*. 2006;13(9):996-1001.
 53. Fregni F, Santos CM, Myczkowski ML, et al. Repetitive transcranial magnetic stimulation is as effective as fluoxetine in the treatment of depression in patients with Parkinson's disease. *J Neurol Neurosurg Psychiatry*. 2004;75(8):1171-1174.
 54. Gabriel S, Lau RW, Gabriel C. The dielectric properties of biological tissues: II. Measurements in the frequency range 10 Hz to 20 GHz. *Phys Med Biol*. 1996;41(11):2251-2269.
 55. Gabriel S, Lau RW, Gabriel C. The dielectric properties of biological tissues: III. Parametric models for the dielectric spectrum of tissues. *Phys Med Biol*. 1996;41(11):2271-2293.
 56. Galea JM, Jayaram G, Ajagbe L, Celnik P. Modulation of cerebellar excitability by polarity-specific noninvasive direct current stimulation. *J Neurosci*. 2009;29(28):9115-9122.
 57. Geddes LA, Baker LE. The specific resistance of biological material-A compendium of data for the biomedical engineer and physiologist. *Med Biol Eng*. 1967;5(3):271-293.
 58. De Geeter N, Crevecoeur G, Dupré L, Van Hecke W, Leemans A. A DTI-based model for TMS using the independent impedance method with frequency-dependent tissue parameters. *Phys Med Biol*. 2012;57(8):2169-2188.
 59. George MS, Wassermann EM, Williams WA, et al. Daily repetitive transcranial magnetic stimulation (rTMS) improves mood in depression. *Neuroreport*. 1995;6:1853-1856.
 60. Gerschlag W, Siebner HR, Rothwell JC. Decreased corticospinal excitability after subthreshold 1 Hz rTMS over lateral premotor cortex. *Neuroimage*. 2001;13(6):1170.

61. Giladi N, Hausdorff JM. The role of mental function in the pathogenesis of freezing of gait in Parkinson's disease. *J Neurol Sci.* 2006;248(1-2):173-176.
62. Giladi N, Horak FB, Hausdorff JM. Classification of gait disturbances: distinguishing between continuous and episodic changes. *Mov Disord.* 2013;28(11):1469-1473.
63. Giladi N, McMahon D, Przedborski S, Flaster E, Guillory S. Motor blocks in Parkinson's disease. *Neurology.* 1992;42(2):333-339.
64. Giladi N, Nieuwboer A. Understanding and treating freezing of gait in parkinsonism, proposed working definition, and setting the stage. *Mov Disord.* 2008;23 Suppl 2:S423-S425.
65. Giladi N, Treves TA, Simon ES, et al. Freezing of gait in patients with advanced Parkinson's disease. *J Neural Transm.* 2001;108:53-61.
66. Goetz CG, Tilley BC, Shaftman SR, et al. Movement Disorder Society-sponsored revision of the Unified Parkinson's Disease Rating Scale (MDS-UPDRS): scale presentation and clinimetric testing results. *Mov Disord.* 2008;23(15):2129-2170.
67. Goodwin VA, Richards SH, Taylor RS, Taylor AH, Campbell JL. The effectiveness of exercise interventions for people with Parkinson's disease: A systematic review and meta-analysis. *Mov Disord.* 2008;23(5):631-640.
68. Grandori F, Ravazzani P. Magnetic stimulation of the motor cortex--theoretical considerations. *IEEE Trans Biomed Eng.* 1991;38(2):180-191.
69. Haaxma CA, Bloem BR, Borm GF, Horstink MWIM. Comparison of a timed motor test battery to the Unified Parkinson's Disease Rating Scale-III in Parkinson's disease. *Mov Disord.* 2008;23(12):1707-1717.
70. Haaxma CA, Bloem BR, Overeem S, Borm GF, Horstink MWIM. Timed motor tests can detect subtle motor dysfunction in early Parkinson's disease. *Mov Disord.* 2010;25(9):1150-1156.
71. Hallett M. Transcranial magnetic stimulation: a primer. *Neuron.* 2007;55(2):187-199.
72. Hamada M, Ugawa Y, Tsuji S, The Effectiveness of rTMS on Parkinson's Disease Study Group J. High-Frequency rTMS over the Supplementary Motor Area for Treatment of Parkinson's Disease. *Mov Disord.* 2008;23(11):1524-1531.
73. Hamilton R, Messing S, Chatterjee A. Rethinking the thinking cap: Ethics of neural enhancement using noninvasive brain stimulation. *Neurology.* 2011;76(2):187-193.
74. Hely MA, Reid WGJ, Adena MA, Halliday GM, Morris JGL. The Sydney multicenter study of Parkinson's disease: The inevitability of dementia at 20 years. *Mov Disord.* 2008;23(6):837-844.
75. Huang Y-Z, Edwards MJ, Rounis E, Bhatia KP, Rothwell JC. Theta burst stimulation of the human motor cortex. *Neuron.* 2005;45(2):201-206.
76. Hubel DH, Wiesel TN. Brain Mechanisms of Vision. In: *Sci Am* 241. ; 1979:150-162.
77. Hughes AJ, Daniel SE, Kilford L, Lees AJ. Accuracy of clinical diagnosis of idiopathic Parkinson's disease: a clinico-pathological study of 100 cases. *J Neurol Neurosurg Psychiatry.* 1992;55(3):181-184.
78. Hyde DE, Duffy FH, Warfield SK. Anisotropic partial volume CSF modeling for EEG source localization. *Neuroimage.* 2012;C.
79. Ilg W, Giese MA, Gizewski ER, Schoch B, Timmann D. The influence of focal cerebellar lesions on the control and adaptation of gait. *Brain.* 2008;131(Pt 11):2913-2927.
80. Jacobs J V, Lou JS, Kraakevik JA, Horak FB. The supplementary motor area contributes to the timing of the anticipatory postural adjustment during step initiation in participants with and without parkinson's disease. *Neuroscience.* 2009;164(2):877-885.
81. Jankovic J. Motor fluctuations and dyskinesias in Parkinson's disease: clinical manifestations. *Mov Disord.* 2005;20 Suppl 1:S11-S16.
82. Janssen AM, Rampersad SM, Lucka F, et al. The influence of sulcus width on simulated electric fields induced by transcranial magnetic stimulation. *Phys Med Biol.* 2013;58(14):4881-4896.
83. Jock I. The Compositiones Medicamentorum of Scribonius Largus. 2013.

84. Kerr G, Worringham CJ, Cole MH, Lacherez PF, Wood JM, Silburn PA. Predictors of future falls in Parkinson disease. *Neurology*. 2010;75(2):116-124.
85. Keus SHJ, Bloem BR, Hendriks EJM, Bredero-Cohen AB, Munneke M. Evidence-based analysis of physical therapy in Parkinson's disease with recommendations for practice and research. *Mov Disord*. 2007;22(4):451-460.
86. Klauschen F, Goldman A, Barra V, Meyer-Lindenberg A, Lundervold A. Evaluation of automated brain MR image segmentation and volumetry methods. *Hum Brain Mapp*. 2009;30(4):1310-1327.
87. Kobayashi M, Pascual-leone A. Transcranial magnetic stimulation in neurology. *Lancet Neurol*. 2003;2:145-156.
88. Koch G, Brusa L, Carrillo F, et al. Cerebellar magnetic stimulation decreases levodopa-induced dyskinesias in Parkinson disease. *Neurology*. 2009;73(2):113-119.
89. Koch G, Mori F, Marconi B, et al. Changes in intracortical circuits of the human motor cortex following theta burst stimulation of the lateral cerebellum. *Clin Neurophysiol*. 2008;119(11):2559-2569.
90. Koch G, Porcacchia P, Ponzo V, et al. Effects of Two Weeks of Cerebellar Theta Burst Stimulation in Cervical Dystonia Patients. *Brain Stimul*. 2014;7(4):564-572.
91. Krieg TD, Salinas FS, Narayana S, Fox PT, Mogul DJ. PET-Based Confirmation of Orientation Sensitivity of TMS-Induced Cortical Activation in Humans. *Brain Stimul*. 2013;6(6):898-904.
92. Kujirai T, Caramia MD, Rothwell JC, et al. Corticocortical inhibition in human motor cortex. *J Physiol*. 1993;471:501-519.
93. Laakso I, Hirata A, Ugawa Y. Effects of coil orientation on the electric field induced by TMS over the hand motor area. *Phys Med Biol*. 2014;59(1):203-218.
94. Laakso I, Hirata A. Fast multigrid-based computation of the induced electric field for transcranial magnetic stimulation. *Phys Med Biol*. 2012;57(23):7753-7765.
95. Langguth B, Eichhammer P, Zowe M, et al. Modulating cerebello-thalamocortical pathways by neuronavigated cerebellar repetitive transcranial stimulation (rTMS). *Clin Neurophysiol*. 2008;38(5):289-295.
96. de Lau LML, Breteler MMB. Epidemiology of Parkinson's disease. *Lancet Neurol*. 2006;5(6):525-535.
97. Di Lazzaro V, Profice P, Ranieri F, et al. I-wave origin and modulation. *Brain Stimul*. 2012;5(4):512-525.
98. Di Lazzaro V, Ziemann U, Lemon RN. State of the art: Physiology of transcranial motor cortex stimulation. *Brain Stimul*. 2008;1(4):345-362.
99. Di Lazzaro V. The physiological basis of transcranial motor cortex stimulation in conscious humans. *Clin Neurophysiol*. 2004;115(2):255-266.
100. Leemans A, Jones DK. The B-matrix must be rotated when correcting for subject motion in DTI data. *Magn Reson Med*. 2009;61(6):1336-1349.
101. Lefaucheur J-P. Motor cortex dysfunction revealed by cortical excitability studies in Parkinson's disease: influence of antiparkinsonian treatment and cortical stimulation. *Clin Neurophysiol*. 2005;116(2):244-253.
102. Lewis SJG, Barker RA. A pathophysiological model of freezing of gait in Parkinson's disease. *Parkinsonism Relat Disord*. 2009;15(5):333-338.
103. Lin C-H (Janice), Chiang M-C. Applying Magnetic Resonance Imaging to Structural and Functional Brain Research. *J Neurosci Neuroengineering*. 2013;2(1):29-37.
104. Lomarev MP, Kanchana S, Bara-Jimenez W, Iyer M, Wassermann EM, Hallett M. Placebo-controlled study of rTMS for the treatment of Parkinson's disease. *Mov Disord*. 2006;21(3):325-331.
105. De Lucia M, Parker GJM, Embleton K, Newton JM, Walsh V. Diffusion tensor MRI-based estimation of the influence of brain tissue anisotropy on the effects of transcranial magnetic stimulation. *Neuroimage*. 2007;36(4):1159-1170.
106. Lundin-olsson L, Nyberg L, Gustafson Y, Himbert D, Seknadji P, Karila-cohen D. "Stops walking when

- talking " as a predictor of falls in elderly people Myocardial contrast echocardiography to assess spontaneous reperfusion during myocardial infarction. *Lancet*.1997;349:617.
107. MacKinnon CD, Gilley EA, Weis-McNulty A, Simuni T. Pathways mediating abnormal intracortical inhibition in Parkinson's disease. *Ann Neurol*. 2005;58(4):516-524.
 108. Masdeu JC, Alampur U, Cavaliere R, Tavoulareas G. Astasia and gait failure with damage of the pontomesencephalic locomotor region. *Ann Neurol*. 1994;35(5):619-621.
 109. Maxwell JC. A dynamical theory of the electromagnetic field. *Philos Trans R Soc London*. 1865;155:459-512.
 110. Meijs JWH, Weier OW, Peters MJ, Oosterom A Van. Method. *IEEE Trans Biomed Eng*. 1989;36 (October):1038-1049.
 111. Merton PA, Morton HB. Stimulation of the cerebral cortex in the intact human subject. *Nature*. 1980;285:227.
 112. Meshulam RI, Moberg PJ, Mahr RN, Doty RL. Olfaction in neurodegenerative disorder A Meta-analysis of olfactory functioning in Alzheimer's and Parkinson's Diseases. *Arch Neurol*. 1998;55(1):84-90.
 113. Middleton FA, Strick PL. Basal ganglia output and cognition: evidence from anatomical, behavioral, and clinical studies. *Brain Cogn*. 2000;42(2):183-200.
 114. Mills KR, Boniface SJ, Schubert M. Magnetic brain stimulation with a double coil: the importance of coil orientation. *Electroencephalogr Clin Neurophysiol*. 1992;85:17-21.
 115. Miniussi C, Thut G. Combining TMS and EEG offers new prospects in cognitive neuroscience. *Brain Topogr*. 2010;22(4):249-256.
 116. Miranda PC, Hallett M, Basser PJ. The electric field induced in the brain by magnetic stimulation: a 3-D finite-element analysis of the effect of tissue heterogeneity and anisotropy. *IEEE Trans Biomed Eng*. 2003;50(9):1074-1085.
 117. Miranda PC, Mekonnen A, Salvador R, Ruffini G. The electric field in the cortex during transcranial current stimulation. *Neuroimage*. 2013;70:48-58.
 118. Moore O, Peretz C, Giladi N. Freezing of gait affects quality of life of peoples with Parkinson's disease beyond its relationships with mobility and gait. *Mov Disord*. 2007;22(15):2192-2195.
 119. Moore ST, Yungheer D a, Morris TR, et al. Autonomous identification of freezing of gait in Parkinson's disease from lower-body segmental accelerometry. *J Neuroeng Rehabil*. 2013;10(1):19.
 120. Moreau C, Ozsancak C, Blatt J-L, Derambure P, Destee A, Defebvre L. Oral festination in Parkinson's disease: Biomechanical analysis and correlation with festination and freezing of gait. *Mov Disord*. 2007;22(10):1503-1506.
 121. Morris TR, Cho C, Dilda V, et al. A comparison of clinical and objective measures of freezing of gait in Parkinson's disease. *Parkinsonism Relat Disord*. 2012;18(5):572-577.
 122. Morton SM, Bastian AJ. Mechanisms of cerebellar gait ataxia. *Cerebellum*. 2007;6(1):79-86.
 123. Mountcastle VB. The columnar organization of the neocortex. *Brain*. 1997;120:701-722.
 124. Mulckhuyse M, Kelley TA, Theeuwes J, Walsh V, Lavie N. Enhanced visual perception with occipital transcranial magnetic stimulation. *Eur J Neurosci*. 2011;34(8):1320-1325.
 125. Müller J, Seppi K, Stefanova N, Poewe W, Litvan I, Wenning GK. Freezing of gait in postmortem-confirmed atypical parkinsonism. *Mov Disord*. 2002;17(5):1041-1045.
 126. Munneke MAM, Rongen JJ, Overeem S, Schelhaas HJ, Zwarts MJ, Stegeman DF. Cumulative effect of 5 daily sessions of theta burst stimulation on corticospinal excitability in amyotrophic lateral sclerosis. *Muscle and Nerve*. 2013;48(5):733-738.
 127. Munneke MAM. Measuring and modulating the brain with non-invasive stimulation. 2014.
 128. Nadeem M, Thorlin T, Gandhi OP, Persson M. Computation of electric and magnetic stimulation in human head using the 3-D impedance method. *IEEE Trans Biomed Eng*. 2003;50(7):900-907.
 129. Narayana S, Laird AR, Tandon N, Franklin C, Lancaster JL, Fox PT. Electrophysiological and functional

- connectivity of the human supplementary motor area. *Neuroimage*. 2012;62(1):250-265.
130. Nicholson PW. Specific impedance of cerebral white matter. *Exp Neurol*. 1965;13(4):386-401.
 131. Nieuwboer A, Giladi N. Characterizing freezing of gait in Parkinson's disease: models of an episodic phenomenon. *Mov Disord*. 2013;28(11):1509-1519.
 132. Nieuwboer A, Rochester L, Herman T, et al. Reliability of the new freezing of gait questionnaire: agreement between patients with Parkinson's disease and their carers. *Gait Posture*. 2009;30(4):459-463.
 133. Nieuwboer A, Vercruysse S, Feys P, Levin O, Spildooren J, Swinnen SP. Upper limb movement interruptions are correlated to freezing of gait in Parkinson's disease. *Eur J Neurosci*. 2009;29(7):1422-1430.
 134. Nieuwboer A, De Weerd W, Dom R, Lesaffre E. A frequency and correlation analysis of motor deficits in Parkinson patients. *Disabil Rehabil*. 1998;20(4):142-150.
 135. Nonnekes J, Geurts ACH, Nijhuis LBO, et al. Reduced StartReact effect and freezing of gait in Parkinson's disease: two of a kind? *J Neurol*. 2014;261(5):943-950.
 136. Nonnekes J, Janssen AM, Mensink SHG, Oude Nijhuis LB, Bloem BR, Snijders AH. Short rapid steps to provoke freezing of gait in Parkinson's disease. *J Neurol*. 2014;261(9):1763-1767.
 137. Nonnekes J, Snijders AH, Nutt JG, Deuschl G, Giladi N, Bloem BR. Freezing of gait: a practical approach to management. *Lancet Neurol*. 2015;14(7):768-778.
 138. Nutt JG, Bloem BR, Giladi N, Hallett M, Horak FB, Nieuwboer A. Freezing of gait: moving forward on a mysterious clinical phenomenon. *Lancet Neurol*. 2011;10(8):734-744.
 139. Obeso JA, Rodríguez-Oroz MC, Benitez-Temino B, et al. Functional organization of the basal ganglia: Therapeutic implications for Parkinson's disease. *Mov Disord*. 2008;23(S3):S548-S559.
 140. Oliveri M, Koch G, Torriero S, Caltagirone C. Increased facilitation of the primary motor cortex following 1 Hz repetitive transcranial magnetic stimulation of the contralateral cerebellum in normal humans. *Neurosci Lett*. 2005;376(3):188-193.
 141. Ondo WG, Dat Vuong K, Khan H, Atassi F, Kwak C, Jankovic J. Daytime sleepiness and other sleep disorders in Parkinson's disease. *Neurology*. 2001;57:1392-1396.
 142. Opitz A, Legon W, Rowlands A, Bickel WK, Paulus W, Tyler WJ. Physiological observations validate finite element models for estimating subject-specific electric field distributions induced by transcranial magnetic stimulation of the human motor cortex. *Neuroimage*. 2013;81:253-264.
 143. Opitz A, Windhoff M, Heidemann RM, Turner R, Thielscher A. How the brain tissue shapes the electric field induced by transcranial magnetic stimulation. *Neuroimage*. 2011;58(3):849-859.
 144. Palmer SJ, Li J, Wang ZJ, McKeown MJ. Joint amplitude and connectivity compensatory mechanisms in Parkinson's disease. *Neuroscience*. 2010;166(4):1110-1118.
 145. Parent A. Giovanni Aldini: from animal electricity to human brain stimulation. *Can J Neurol Sci*. 2004;31(4):576-584.
 146. Parkinson James. Essay on the Shaking Palsy. Sherwood, Neely and Jones; 1817.
 147. Pascual-Leone A, Valls-Solé J, Brasil-Neto JP, Cohen LG, Hallett M. Akinesia in Parkinson's disease. I. Shortening of simple reaction time with focal, single-pulse transcranial magnetic stimulation. *Neurology*. 1994;44(5):884-891.
 148. Pascual-Leone A, Valls-Solé J, Wassermann EM, Hallett M. Responses to rapid-rate transcranial magnetic stimulation of the human motor cortex. *Brain*. 1994;117:847-858.
 149. Paviour DC, Price SL, Stevens JM, Lees AJ, Fox NC. Quantitative MRI measurement of superior cerebellar peduncle in progressive supranuclear palsy. *Neurology*. 2005;64(4):675-679.
 150. Piccolino M. Luigi Galvani and animal electricity: two centuries after the foundation of electrophysiology. *Trends Neurosci*. 1997;20:443-448.
 151. Piccolino M. The bicentennial of the Voltaic battery (1800–2000): the artificial electric organ. *Trends*

- Neurosci.* 2000;23(4):147-151.
152. Pinto AD, Chen R. Suppression of the motor cortex by magnetic stimulation of the cerebellum. *Exp brain Res.* 2001;140(4):505-510.
 153. Plonsey R. *Bioelectric Phenomena*. New York: McGraw Hill; 1969.
 154. Plotnik M, Giladi N, Hausdorff JM. Is freezing of gait in Parkinson's disease a result of multiple gait impairments? Implications for treatment. *Parkinsons Dis.* 2012;2012:459321.
 155. Pobric G, Hamilton AFDC. Action understanding requires the left inferior frontal cortex. *Curr Biol.* 2006;16(5):524-529.
 156. Polson MJ, Barker AT, Freeston IL. Stimulation of nerve trunks with time-varying magnetic fields. *Med Biol Eng Comput.* 1982;20(2):243-244.
 157. Popa T, Russo M, Meunier S. Long-lasting inhibition of cerebellar output. *Brain Stimul.* 2010;3(3):161-169.
 158. Priori A, Berardelli A, Inghilleri M, Accornero N, Manfredi M. Motor cortical inhibition and the dopaminergic system. Pharmacological changes in the silent period after transcranial brain stimulation in normal subjects, patients with Parkinson's disease and drug-induced parkinsonism. *Brain.* 1994;117:317-323.
 159. Rampersad SM, Janssen AM, Lucka F, et al. Simulating transcranial direct current stimulation with a detailed anisotropic human head model. *IEEE Trans Neural Syst Rehabil Eng.* 2014;22(3):441-452.
 160. Ranck JB. Which elements are excited in electrical stimulation of mammalian central nervous system: a review. *Brain Res.* 1975;98:417-440.
 161. Rascol O, Sabatini U, Fabre N, et al. The ipsilateral cerebellar hemisphere is overactive during hand movements in akinetic parkinsonian patients. *Brain.* 1997;120:103-110.
 162. Ravazzani P, Ruohonen J, Grandori F, Tognola G. Magnetic stimulation of the nervous system: induced electric field in unbounded, semi-infinite, spherical, and cylindrical media. *Ann Biomed Eng.* 1996;24(5):606-616.
 163. Ridding MC, Rothwell JC. Is there a future for therapeutic use of transcranial magnetic stimulation? *Nat Rev Neurosci.* 2007;8(7):559-567.
 164. Rodríguez-Oroz MC, Jahanshahi M, Krack P, et al. Initial clinical manifestations of Parkinson's disease: features and pathophysiological mechanisms. *Lancet Neurol.* 2009;8(12):1128-1139.
 165. Rosanova M, Casali A, Bellina V, Resta F, Mariotti M, Massimini M. Natural frequencies of human corticothalamic circuits. *J Neurosci.* 2009;29(24):7679-7685.
 166. Rossi S, Hallett M, Rossini PM, Pascual-Leone A. Safety, ethical considerations, and application guidelines for the use of transcranial magnetic stimulation in clinical practice and research. *Clin Neurophysiol.* 2009;120(12):2008-2039.
 167. Rossini PM, Barker AT, Berardelli A, et al. Non-invasive electrical and magnetic stimulation of the brain, spinal cord and roots: basic principles and procedures for routine clinical application. Report of an IFCN committee. *Electroencephalogr Clin Neurophysiol.* 1994;91(2):79-92.
 168. Roth BJ, Bassar PJ. A Model of the Stimulation of a Nerve fiber by Electromagnetic Induction. *IEEE Trans Biomed Eng.* 1990;37(6):588-597.
 169. Roth Y, Amir A, Levkovitz Y, Zangen A. Three-dimensional distribution of the electric field induced in the brain by transcranial magnetic stimulation using figure-8 and deep H-coils. *J Clin Neurophysiol.* 2007;24(1):31-38.
 170. Roth Y, Pell GS, Chistyakov A V, Sinai A, Zangen A, Zaaroor M. Motor cortex activation by H-coil and figure-8 coil at different depths. Combined motor threshold and electric field distribution study. *Clin Neurophysiol.* 2014;125(2):336-343.
 171. Ruthotto L, Kugel H, Olesch J, et al. Diffeomorphic Susceptibility Artefact Correction of Diffusion-Weighted Magnetic Resonance Images. *Phys Med Biol.* 2012;57(18):5715-5731

172. Sadnicka A, Hoffland BS, Bhatia KP, van de Warrenburg BP, Edwards MJ. The cerebellum in dystonia - help or hindrance? *Clin Neurophysiol.* 2012;123(1):65-70.
173. Salinas FS, Lancaster JL, Fox PT. 3D modeling of the total electric field induced by transcranial magnetic stimulation using the boundary element method. *Phys Med Biol.* 2009;54(12):3631-3647.
174. Salinas FS, Lancaster JL, Fox PT. Detailed 3D models of the induced electric field of transcranial magnetic stimulation coils. *Phys Med Biol.* 2007;52(10):2879-2892.
175. Salvador R, Silva S, Basser PJ, Miranda PC. Determining which mechanisms lead to activation in the motor cortex: a modeling study of transcranial magnetic stimulation using realistic stimulus waveforms and sulcal geometry. *Clin Neurophysiol.* 2011;122(4):748-758.
176. Schaafsma JD, Balash Y, Gurevich T, Bartels AL, Hausdorff JM, Giladi N. Characterization of freezing of gait subtypes and the response of each to levodopa in Parkinson's disease. *Eur J Neurol.* 2003;10(4):391-398.
177. Schenck JF. Physical interactions of static magnetic fields with living tissues. *Prog Biophys Mol Biol.* 2005;87(2-3 SPEC. ISS.):185-204.
178. Schepens B, Stapley P, Drew T. Neurons in the pontomedullary reticular formation signal posture and movement both as an integrated behavior and independently. *J Neurophysiol.* 2008;100(4):2235-2253.
179. Schmierer K, Niehaus L, Rörich S, Meyer BU. Conduction deficits of callosal fibres in early multiple sclerosis. *J Neurol Neurosurg Psychiatry.* 2000;68(5):633-638.
180. Schweder PM, Hansen PC, Green AL, Quaghebeur G, Stein JF, Aziz TZ. Connectivity of the pedunculo-pontine nucleus in parkinsonian freezing of gait. *Neuroreport.* 2010;21(14):914-916.
181. Shelley MW. *Frankenstein: Or, The Modern Prometheus.* Henry Colburn & Richard Bentley; 1831.
182. Shine JM, Matar E, Ward PB, et al. Exploring the cortical and subcortical functional magnetic resonance imaging changes associated with freezing in Parkinson's disease. *Brain.* 2013;136(Pt 4):1204-1215.
183. Shirvany Y, Porras AR, Kowkabzadeh K, Mahmood Q, Lui H-S, Persson M. Investigation of brain tissue segmentation error and its effect on EEG source localization. *34th Annu Int Conf IEEE Eng Med Biol Soc.* 2012:1522-1525.
184. Silva S, Basser PJ, Miranda PC. Elucidating the mechanisms and loci of neuronal excitation by transcranial magnetic stimulation using a finite element model of a cortical sulcus. *Clin Neurophysiol.* 2008;119(10):2405-2413.
185. Singh N, Pillay V, Choonara YE. Advances in the treatment of Parkinson's disease. *Prog Neurobiol.* 2007;81(1):29-44.
186. Snijders AH, Haaxma CA, Hagen YJ, Munneke M, Bloem BR. Freezer or non-freezer: clinical assessment of freezing of gait. *Parkinsonism Relat Disord.* 2012;18(2):149-154.
187. Snijders AH, Leunissen I, Bakker M, et al. Gait-related cerebral alterations in patients with Parkinson's disease with freezing of gait. *Brain.* 2011;134(Pt 1):59-72.
188. Snijders AH, Nijkrake MJ, Bakker M, Munneke M, Wind C, Bloem BR. Clinimetrics of Freezing of Gait. *Mov Disord.* 2008;23:468-474.
189. Spagnolo F, Volonté MA, Fichera M, et al. Excitatory deep repetitive transcranial magnetic stimulation with H-coil as add-on treatment of motor symptoms in Parkinson's disease: an open label, pilot study. *Brain Stimul.* 2014;7(2):297-300.
190. Stokes MG, Chambers CD, Gould IC, et al. Simple metric for scaling motor threshold based on scalp-cortex distance: application to studies using transcranial magnetic stimulation. *J Neurophysiol.* 2005;94(6):4520-4527.
191. Stolze H, Klebe S, Zechlin C, Baecker C, Friege L, Deuschl G. Falls in frequent neurological diseases--prevalence, risk factors and aetiology. *J Neurol.* 2004;251(1):79-84.
192. Taubin G, Watson IBMTJ. A Signal Processing Approach To Fair Surface Design 2 B. 1995:351-358.

193. Thevathasan W, Cole MH, Graepel CL, et al. A spatiotemporal analysis of gait freezing and the impact of pedunculopontine nucleus stimulation. *Brain*. 2012;135(Pt 5):1446-1454.
194. Thielscher A, Kammer T. Electric field properties of two commercial figure-8 coils in TMS: calculation of focality and efficiency. *Clin Neurophysiol*. 2004;115(7):1697-1708.
195. Thielscher A, Opitz A, Windhoff M. Impact of the gyral geometry on the electric field induced by transcranial magnetic stimulation. *Neuroimage*. 2011;54(1):234-243.
196. Thielscher A, Wichmann FA. Determining the cortical target of transcranial magnetic stimulation. *Neuroimage*. 2009;47(4):1319-1330.
197. Thompson SP. A Physiological Effect of an Alternating Magnetic Field. *Proc R Soc B Biol Sci*. 1910;82(557):396-398.
198. Timmann D, Brandauer B, Hermsdörfer J, et al. Lesion-symptom mapping of the human cerebellum. *Cerebellum*. 2008;7(4):602-606.
199. Toschi N, Welt T, Guerrisi M, Keck ME. A reconstruction of the conductive phenomena elicited by transcranial magnetic stimulation in heterogeneous brain tissue. *Phys medica*. 2008;24(2):80-86.
200. Trasatti S. 1799–1999: Alessandro Volta's "Electric Pile." *J Electroanal Chem*. 1999;460(1-2):1-4.
201. Trillenber P, Bremer S, Oung S, Erdmann C, Schweikard A, Richter L. Variation of stimulation intensity in transcranial magnetic stimulation with depth. *J Neurosci Methods*. 2012;211(2):185-190.
202. Tuch DS, Wedeen J Van, Dale AM, George JS, Belliveau JW. Conductivity tensor mapping of the human brain using diffusion tensor MRI. *Proc Natl Acad Sci U S A*. 2001;98(20):11697-11701.
203. Ugawa Y, Uesaka Y, Terao Y, Hanajima R, Kanazawa I. Magnetic stimulation over the cerebellum in humans. *Ann Neurol*. 1995;37(6):703-713.
204. Valls-Solé J, Pascual-Leone A, Brasil-Neto JP, Cammarota A, McShane L, Hallett M. Abnormal facilitation of the response to transcranial magnetic stimulation in patients with Parkinson's disease. *Neurology*. 1994;44:735-741.
205. Vercrusys S, Gilat M, Shine JM, Heremans E, Lewis SJG, Nieuwboer A. Freezing beyond gait in Parkinson's disease: a review of current neurobehavioral evidence. *Neurosci Biobehav Rev*. 2014;43:213-227.
206. Vercrusys S, Spildooren J, Heremans E, et al. Abnormalities and cue dependence of rhythmical upper-limb movements in Parkinson patients with freezing of gait. *Neurorehabil Neural Repair*. 2012;26(6):636-645.
207. Vercrusys S, Spildooren J, Heremans E, et al. Freezing in Parkinson's disease: a spatiotemporal motor disorder beyond gait. *Mov Disord*. 2012;27(2):254-263.
208. Vercrusys S, Spildooren J, Heremans E, et al. The Neural Correlates of Upper Limb Motor Blocks in Parkinson's Disease and Their Relation to Freezing of Gait. *Cereb Cortex*. 2014;24(12):3154-3166.
209. Vese LA, Chan TF. A Multiphase Level Set Framework for Image Segmentation Using the Mumford and Shah Model. *Int J Comput Vis*. 2002;50(3):271-293.
210. Wagner S, Rampersad SM, Aydin U, et al. Investigation of tDCS volume conduction effects in a highly realistic head model. *J Neural Eng*. 2013;11:16002.
211. Wagner TA, Eden U, Fregni F, et al. Transcranial magnetic stimulation and brain atrophy: a computer-based human brain model study. *Exp brain Res*. 2008;186(4):539-550.
212. Wagner TA, Fregni F, Eden U, et al. Transcranial magnetic stimulation and stroke: a computer-based human model study. *Neuroimage*. 2006;30(3):857-870.
213. Wagner TA, Fregni F, Fecteau S, Grodzinsky AJ, Zahn M, Pascual-Leone A. Transcranial direct current stimulation: a computer-based human model study. *Neuroimage*. 2007;35(3):1113-1124.
214. Wagner TA, Zahn M, Grodzinsky AJ, Pascual-Leone A. Three-dimensional head model simulation of transcranial magnetic stimulation. *IEEE Trans Biomed Eng*. 2004;51(9):1586-1598.

215. Walsh V, Cowey A. Transcranial magnetic stimulation and cognitive neuroscience. *Nat Rev Neurosci.* 2000;1(1):73-79.
216. Weaver FM, Follett KA, Stern M, et al. Bilateral Deep Brain Stimulation vs Best Medical Therapy for Patients With Advanced Parkinson Disease. *J Am Med Assoc.* 2009;301(1):301(1): 63-73.
217. Williams A, Gill S, Varma T, et al. Deep brain stimulation plus best medical therapy versus best medical therapy alone for advanced Parkinson's disease (PD SURG trial): a randomised, open-label trial. *Lancet Neurol.* 2010;9(6):581-591.
218. Wilson SA, Thickbroom GW, Mastaglia FL. Transcranial magnetic stimulation mapping of the motor cortex in normal subjects. The representation of two intrinsic hand muscles. *J Neurol Sci.* 1993;118(2):134-144.
219. Windhoff M, Opitz A, Thielscher A. Electric field calculations in brain stimulation based on finite elements: An optimized processing pipeline for the generation and usage of accurate individual head models. *Hum Brain Mapp.* 2013;34(4):923-935.
220. Wolters CH, Anwander A, Berti G, Hartmann U. Geometry-adapted hexahedral meshes improve accuracy of finite-element-method-based EEG source analysis. *IEEE Trans Biomed Eng.* 2007;54(8):1446-1453.
221. Wu T, Hallett M. The cerebellum in Parkinson's disease. *Brain.* 2013;136(Pt 3):696-709.
222. Wu T, Long X, Zang Y, et al. Regional Homogeneity Changes in Patients With Parkinson ' s Disease. *Hum Brain Mapp.* 2009;30:1502-1510.
223. Wu T, Wang L, Hallett M, Li K, Chan P. Neural correlates of bimanual anti-phase and in-phase movements in Parkinson's disease. *Brain.* 2010;133(Pt 8):2394-2409.
224. Yu H, Sternad D, Corcos DM, Vaillancourt DE. Role of hyperactive cerebellum and motor cortex in Parkinson's disease. *Neuroimage.* 2007;35(1):222-233.
225. Zangen A, Roth Y, Voller B, Hallett M. Transcranial magnetic stimulation of deep brain regions: Evidence for efficacy of the H-Coil. *Clin Neurophysiol.* 2005;116(4):775-779.
226. Ziemann U, Rothwell JC, Ridding MC. Interaction between intracortical inhibition and facilitation in human motor cortex. *J Physiol.* 1996;496 (Pt 3):873-881.
227. Ziv I, Avraham M, Dabby R, Zoldan J, Djaldetti R, Early- ME. Early-occurrence of manual motor blocks in Parkinson ' s disease : a quantitative assessment. *Acta Neurol Scand.* 1999;99:106-111.

